IAEA
International Atomic Energy Agency

INDC(NDS)-0574
Distr. AD, AL, e, G, IN,
SF,w

INDC International Nuclear Data Committee

Proceedings of
the IAEA Technical Meeting in collaboration with NEA
on

Specific Applications of Research Reactors: Provision of Nuclear Data

International Atomic Energy Agency
Vienna, Austria
12 - 16 October 2009

Prepared by:

Mr D. Ridikas, *International Atomic Energy Agency, Austria*

Mr D. Bernard, *Commissariat á l'Energie Atomique, France*

Mr O. Cabellos, *Universidad Politecnica de Madrid, Spain*

Mr Y.O. Lee, *Korea Atomic Energy Research Institute, Republic of Korea*

Mr S. Oberstedt, *European Commission, Joint Research Centre, EU*

Mr M. Oshima, *Japan Atomic Energy Agency, Japan*

July 2010

IAEA Nuclear Data Section, Vienna International Centre, A-1400 Vienna, Austria

Selected INDC documents may be downloaded in electronic form from
http://www-nds.iaea.org/reports-new/indc-reports/
or sent as an e-mail attachment.
Requests for hardcopy or e-mail transmittal should be directed to
services@iaeand.iaea.org
or to:
Nuclear Data Section
International Atomic Energy Agency
Vienna International Centre
PO Box 100
A-1400 Vienna
Austria

Printed by the IAEA in Austria

July 2010

INDC(NDS)-0574
Distr. AD, AL, e, G, IN, SF,w

Proceedings of
the IAEA Technical Meeting in collaboration with NEA
on

Specific Applications of Research Reactors: Provision of Nuclear Data

International Atomic Energy Agency
Vienna, Austria
12 - 16 October 2009

Prepared by:

Mr D. Ridikas, *International Atomic Energy Agency, Austria*

Mr D. Bernard, *Commissariat á l'Energie Atomique, France*

Mr O. Cabellos, *Universidad Politecnica de Madrid, Spain*

Mr Y.O. Lee, *Korea Atomic Energy Research Institute, Republic of Korea*

Mr S. Oberstedt, *European Commissio, Joint Research Centre, EU*

Mr M. Oshima, *Japan Atomic Energy Agency, Japan*

July 2010

Foreword

Yet as one means of utilizing research reactor facilities and their staff, in addition to radioisotope production, material irradiation, education and training, and other valuable services, nuclear data investigation and collection has been greatly advanced under such an environment and contains still more potential. It is, for one, an activity in which in principle a research reactor facility can participate regardless of its power and flux. Also, as evidenced in these proceedings, research reactor operators are committed to using more advanced equipment and devising innovative methods of deploying established techniques such as neutron activation analysis and mass spectrometry in order to conduct important experiments and obtain accurate measurements. These efforts can be applied not only to compiling and verifying data libraries, but also an ever expanding range of applications covering the entire nuclear fuel cycle. More in-depth elemental analysis and a broader knowledge of nuclear processes will aid in the manufacture of better dosimetry instruments, optimize production of radioisotopes, facilitate the design of future generations of reactors and improved radiation shielding, the enabling of more effective fuel burnup and more responsible operation, and the transmutation of nuclear waste for safer disposal. Finally, in accordance with the objectives of this technical meeting attended by 22 participants from 15 Member States and 2 international organizations, the research reactor community across all continents is pursuing various topics in nuclear data for a multitude of purposes, and the IAEA in close cooperation with NEA are determined to facilitate cooperation in studies, practices, and results among all researchers and facilities for accurate and useful data.

CONTENTS

1. BACKGROUND AND OBJECTIVES 9

1.1 Background 9

1.2 Objectives 9

2. WORK DONE DURING THE MEETING 10

2.1. Summaries of individual presentations 10

2.2. Results obtained 15

2.2.1. Topic 1: Capture cross section and decay data measurements using neutron beam, NAA, and other dedicated irradiation experiments 15

2.2.2. Topic 2: Fission reaction and fission fragment studies 17

2.2.3. Topic 3: Dedicated integral experiments for nuclear data and code validation 18

2.2.4. Topic 4: Efforts on code/library development and global benchmarking / validation 19

3. SUMMARY OF THE MAIN RECOMMENDATIONS 21

4. INDIVIDUAL CONTRIBUTIONS 23

Precision Neutron Cross Section Measurements at Reactor Neutron Filtered Beams 25

Neutron capture cross-section measurements by high-resolution γ-ray spectroscopy 37

The Out-of-core Neutron Irradiation Facility of HANARO for Measurement of Neutron Cross-section 48

Experimental Determination of Neutron Capture Cross Sections at a Rare Thermal Energy Using the BAEC TRIGA Reactor 55

The Use of Miniature Neutron Source Reactor Facility for the Determination of Neutron-induced Cross section Data 67

Cross Section Determination of Short-to-Medium Lived Nuclides in a Low Power Research and an Am-Be Neutron Source 72

Cross section measurements for thermal neutron-induced reactions on actinides at the ILL reactor 85

Prompt γ-ray emission in nuclear fission 95

Binary and Ternary Fission Yield Measurements at the Institut Laue-Langevin ... 104

Fast Reactor Integral Experiments at BARC for Cross-section Evaluation 114

Measurements of Nuclear Data for MA at VENUS-F and BR-1 reactors 130

Integral Experiments in MINERVE Reactor Facility for Nuclear Data Validation 139

Benchmark analysis of the 2MW TRIGA MARK II Moroccan research reactor using the MCNP code and the latest nuclear data libraries 146

Validation of the ENDF/B-VII library for the WWR-M research reactor in Ukraine 164

Improvements in the Prediction Capability of Codes Used to Design Innovative Reactors 169

The TAPIRO Fast-Neutron Source Reactor as a support to Nuclear Data Assessment 183

Research potential of the McMaster nuclear reactor 187

Provision of Nuclear Data by Experiments at the High Flux Reactor of the Institut Laue Langevin 194

The updated version of Chinese Evaluated Nuclear Data Library (CENDL-3.1) and China nuclear data evaluation activities 206

Data processing and validation needs of group-wise working cross section libraries for nuclear fission reactor shielding and radiation damage applications 218

APPENDICES

ANNEX I.: Recommended measurements of nuclear data at RR facilities 227
ANNEX II.: OECD/NEA nuclear data high priority list 229
ANNEX III.: List of RR facilities providing nuclear data measurements 230
ANNEX IV.: Monitor reactions and materials for neutron spectrum characterization 232
ANNEX V.: List of participants 234
ANNEX VI.: Meeting Agenda 238

1. BACKGROUND AND OBJECTIVES

1.1 Background

Research reactors (RRs) have played and continue to play a key role in the development of the peaceful uses of atomic energy. The main applications of most RRs continue to be radioisotope production, neutron beam applications, silicon doping and material irradiation for nuclear systems, as well as teaching and training for human resource development. What has been perceived as less important is the role of RRs to provide nuclear data, utilizing their inherent capability of integral experiments, benchmark, and validation analyses, particularly for the assessment of the safety margin and improvement of economic efficiency in the development and licensing of future nuclear power plants. In this respect, the previous International Conference on Nuclear Data for Science and Technology, held in Nice, France, from 22 to 27 April 2007, especially emphasized atomic and nuclear data needs for basic nuclear physics research, innovative power reactors and future fuel cycles (e.g., fast reactors, dedicated reactors for nuclear waste transmutation, accelerator driven systems, the Th-U fuel cycle, etc.), and the realization of fusion reactors (e.g., ITER). Other fields in which nuclear data are required relate to the testing of materials needed for such facilities, the evaluation of radioisotope production and their medical application, the simulation via computer software radiation of doses to patients and advanced cancer therapies, as well as the improvement of analytical techniques adopted for cultural heritage diagnostics and material composition analysis.

RRs continue to occupy a visibly important place in these areas of study and application along with dedicated accelerator-based neutron sources. For example, an installation like the Lohengrin Fission Fragment Separator at Institute Laue-Langevin (ILL) in Grenoble, France, remains a unique place to study fission fragments and their properties as products of thermal neutron induced fission. Equally, the importance of integral measurements performed at RRs to validate evaluated nuclear data libraries used by neutron-gamma transport and material depletion-transmutation codes is another example where the role of RRs is primordial. RRs can also provide other important experimental information such as gamma heat and material damage. In this respect, a new initiative of the Nuclear Energy Agency (NEA) Working Party on Evaluation Cooperation has been launched in order to develop methods that combine integral experimental data from RRs and various differential data to examine targeted accuracies for different reactions, isotopes and energy ranges in the interest of their effects on integral neutronic parameters used for the design of new nuclear reactors. Finally, various efforts are in progress to expand the predicting power of nuclear reaction codes for extremely unstable nuclei, where corresponding experimental data are crucial as input for the validation and further development of the reaction models associated with these codes. Some cross-section measurements for such short-lived and on-line produced radioactive target nuclei are possible only at RR facilities thanks to the high neutron fluxes available.

1.2 Objectives

This IAEA Technical Meeting (TM), held in collaboration with NEA, focused on the specific application of RRs, namely the provision of nuclear data for various purposes. The following subjects were considered with the highest priority:

- Cross-section measurements (e.g., capture, fission, branching ratios, neutron multiplicities, etc.) in thermal, epithermal and fast (fission) neutron energy regions
- Measurements of averaged cross sections in a known neutron energy spectrum
- Measurements of fission fragments (e.g., mass and charge distributions)
- Decay studies of fission fragments and activation products

- Measurements of delayed neutron yields and time characteristics
- Dedicated irradiation experiments for incineration/transmutation studies
- Dedicated integral experiments and modelling to validate evaluated nuclear data libraries

The meeting also aimed at providing a forum to exchange ideas and information through scientific presentations and brainstorming discussions, leading to the following overall objectives: 1) enhancement of RR utilization in Member States for practical applications, 2) increased cooperation between different RR centres and user communities and 3) promotion and development of specific applications of RRs.

2. WORK DONE DURING THE MEETING

The meeting was attended by 22 participants, from 15 Member States and two international organizations, namely the Joint Research Centre of the European Commission (EC JRC) and the OECD-NEA. The meeting started off with welcome, opening and introductory remarks by IAEA senior management representatives from the Physics Section and the Nuclear Data Section, both of the Department of Nuclear Sciences and Applications, Division of Physical and Chemical Sciences. Later, another welcome address was given by Mr D. Ridikas, the IAEA Scientific Secretary of the meeting. The self presentation of all meeting participants followed afterwards. Ms O. Gritzay (INR, Ukraine) was designated as the chair person and Mr S. Oberstedt (EC JRC) was appointed as the *rapporteur* of the meeting. A brief presentation by Mr D. Ridikas, the IAEA Scientific Secretary, on the specific objectives of the meeting within the ongoing IAEA project on *Enhancement of Utilization and Applications of Research Reactors* followed.

2.1. Summaries of individual presentations

The meeting then continued with individual presentations, which can be grouped into the following four main categories:

I. Capture cross section and decay data measurements using neutron beams, neutron activation analysis (NAA), and other dedicated irradiation experiments

II. Fission reaction and fission fragment studies

III. Dedicated integral experiments for cross section and code validation

IV. Efforts on code/library development and global benchmarking/validation

The subsequent brief statement on each contribution covers its major themes only, while the full individual papers are available in the 2nd part of this document. The summaries are given according to the presentation order. Copies of all presentations, papers and administrative information were distributed at the end of the meeting to all participants and may be obtained from the Scientific Secretary upon request.

D. Ridikas, IAEA, Scientific Secretary of the meeting, gave a brief introduction to the programmatic structure of RR related activities associated with the IAEA sub-programme *Research Reactors*, under which the project on *Enhancement of utilization and applications of RRs* was presented in more detail. Both recent achievements and future planned actions were reported with a major emphasis on RR utilisation issues, specific applications of RRs, networks

and coalitions, and assistance to Member States (MS) planning their first RR. Finally, the speaker detailed specific objectives of the meeting and the role RRs have played and continue to play in the field of nuclear data measurements and validation.

O. Gritzay, Institute for Nuclear Research, National Academy of Sciences of Ukraine, presented some cross section measurements obtained through the filtered neutron beam technique (FNBT) developed at Kyiv Research Reactor (KRR). She indicated there is a wide set of materials available at KRR, especially high purity isotopes that enabled the creation of neutron filters, which have been shown to provide more than ten neutron lines in the energy range from thermal energy to several hundred kilo-electron volts under a neutron beam intensity of 10^6-10^8 n/cm^2 s. The statistical accuracy of the experimental data obtained was at or below 0.1%. She noted that the development of FNBT based on natural elements as the main filter component may be useful for many research reactors. Ms Gritzay's paper also showed the merits of high-intensity high-quality neutron beams for precise measurements of neutron cross sections.

M. Oshima, Japan Atomic Energy Agency, Japan, presented the results of the development of a new method of γ-ray decay scheme analysis incorporating multi-step cascades using neutron capture reaction performed at the JRR-3 research reactor. Precise decay scheme information allows the derivation of accurate neutron capture cross sections by utilizing high resolution γ-ray spectroscopy, and is expected to be useful for the measurement of minor actinides (MAs) and long-lived fission products. Indeed, the nuclide discrimination was demonstrated as effective in removing the contribution of background γ-rays from impurities and isotopic decays. At first, the well studied ^{15}N nucleus was assessed and its 14 known levels were confirmed. Afterwards, this method was successfully applied to the analysis of excited levels in ^{63}Ni. The author also described the experimental technique and related data analysis methods for prompt γ-ray measurements as well as measurements based on NAA.

M.-S. Kim, Korea Atomic Energy Research Institute, Korea, introduced neutron cross-section measurements using a tangential beam tube of HANARO research reactor. He also presented the results of experiments using neutron transmission, the time-of-flight (TOF) method, activation and the γ-ray detection method to confirm that the out-of-core neutron irradiation facility of HANARO would be a useful facility to measure neutron induced reaction cross sections. During the design stage of the facility, the total neutron cross-sections of silicon and bismuth crystals were successfully obtained. The author also presented the thermal neutron capture cross section for ^{180}W, which was measured using NAA and the gamma-ray detection method. The ^{181}W radioisotope is used as a neutrino source for various basic neutrino experiments.

S. Hossain, Institute of Nuclear Science & Technology, Bangladesh Atomic Energy Commission, presented experiments based on the utilization of the radial piercing beam port at the 3 MW TRIGA Mark II research reactor for determination of neutron capture cross sections in the thermal region using NAA. By using a monochromator based on triple axis spectrometry, a new capability for neutron capture cross section measurements at 0.0536 eV in thermal region using NAA was implemented. The author showed that three experiments have successfully been carried out to determine the neutron capture cross section for the targets W, Ga and Sm using the reactions ^{186}W(n,γ)^{187}W, ^{71}Ga(n,γ)^{72}Ga, ^{151}Sm(n,γ)^{152}Sm and ^{153}Sm(n,γ)^{154}Sm. The results at this previously unstudied thermal energy region will be useful for observing the energy dependence of neutron capture cross sections. The obtained experimental results were critically compared with evaluated data quoted in JENDL-3.3 and ENDF/B-VII.

S. Jonah, Centre for Energy Research and Training at Ahmadu Bello University, Nigeria, discussed investigations needed to extend the experimental procedures for the determination of neutron-induced cross section data at the Miniature Neutron Source Reactors (MNSR). He also

gave the first results of fast neutron reactor spectrum-averaged cross section measurements of (n,p) reactions involving ^{27}Al, ^{28}Si, ^{29}Si, ^{47}Ti, ^{54}Fe, ^{58}Ni and (n,α) reactions involving ^{27}Al and ^{30}Si. This investigation confirmed the suitability of the MNSR for the determination of fast reactor spectrum-averaged cross-section data of threshold reactions for energies between 2 and 4.5 MeV. Additionally, thermal capture cross sections were presented for the target nuclides ^{47}Ca, ^{71}Ga, ^{75}As, ^{94}Zr and ^{238}U.

B. Nyarko, National Nuclear Research Institute, Ghana, discussed the current work on thermal, epithermal and fast neutron cross-section measurements using NAA equipment installed at the GHARR-1 research reactor and the Am-Be based neutron source. The method of foil activation was implemented using ^{55}Mn(n,γ)^{56}Mn as a reference reaction. Experimental samples with and without a cadmium cover were irradiated in the isotropic neutron field of the neutron source and the outer irradiation sites of GHARR-1. The author presented recent results on thermal and epithermal neutron cross-sections measurements for the ^{197}Au(n,γ)^{198}Au, ^{75}As (n,γ)^{76}As, ^{27}Al (n,γ)^{28}Al, ^{51}V(n,γ)^{52}V, ^{127}I(n,γ)^{128}I, ^{152}Sm(n,γ)^{153}Sm, ^{154}Sm(n,γ)^{155}Sm, ^{138}Ba(n,γ)^{139}Ba, ^{26}Mg(n,γ)^{27}Mg and ^{238}U(n,γ)^{239}U reactions. The values obtained are in good agreement with those found in literature.

A. Letourneau, CEA Saclay, France, presented the measurements performed at the High Flux Reactor of ILL in addition to the experimental set-up, methodology and summary of the obtained cross sections. In particular he talked about the current results of the Mini-INCA project designed to measure thermal neutron-induced reactions on actinides. He highlighted the experiments performed using two irradiation channels, H9 and V4. Both standard NAA and on-line fission rate measurements were adapted for high neutron fluxes available at ILL. The experiments also used high-counting rate α and γ-spectroscopy, mass spectrometry for rare isotopes and miniature fission-chambers for transmutation studies. The program is now almost completed, providing a set of new and accurate data on the capture cross sections of ^{232}Th, ^{233}Pa, ^{234}U, ^{237}Np, ^{238}Pu, ^{242}Pu, ^{241}Am, $^{242gs-m}$Am, ^{243}Am, ^{242}Cm, ^{244}Cm, ^{248}Cm, ^{249}Cf, ^{250}Cf, ^{251}Cf and the neutron-induced fission cross sections of ^{238}Np, $^{242gs-m}$Am and ^{245}Cm.

S. Oberstedt, JRC-EC, EU, introduced the recent detector suitability studies being carried out at the JRC-IRMM that are dedicated to new and accurate measurements of fission γ-ray data in response to the OECD-NEA High Priority Data Request List. He talked mainly about the use of recently developed cerium-doped lanthanum halide crystal scintillation detectors to distinguish more accurately, in terms of an improved TOF resolution, between prompt fission γ-rays and neutrons. First, prompt fission γ-ray spectra obtained from the spontaneous fission of ^{252}Cf demonstrated the superiority of the new detectors compared to the traditionally employed NaI(Tl) detector in combination with an ionization chamber. In 2010 a similar experimental set-up at the cold-neutron source of the 10 MW Budapest Research Reactor will be installed for the measurement of the prompt γ-ray emission spectrum in the ^{235}U (n,f) reaction.

O. Serot, CEA Cadarache, France, showed the results of the measurements performed at the High Flux Reactor of ILL in Grenoble. He highlighted two types of measurements: the first one concerns binary fission yields which were measured on the Lohengrin mass spectrometer, and the second concerns ternary fission yields which were measured at the PF1 cold neutron guide installed at ILL. He noted that the results were compared with those obtained from spontaneous fission process that had been measured elsewhere but with comparable experimental conditions. In particular, recently the heavy mass region of fission fragments for the reactions ^{235}U(n_{th},f), ^{239}Pu(n_{th},f) and ^{241}Pu(n_{th},f) have been investigated, where a new experimental method based on

gamma spectroscopy was introduced, reducing considerably the uncertainties. Other fissioning nuclei will be investigated in the near future.

K. Rasheed, Bhabha Atomic Research Centre, India, presented the details of the integral experiment with fast reactor materials carried out in the shielded facility of the APSARA Research Reactor. The ratios 'C/E' obtained from various reaction rates provide valuable data for nuclear data validation studies, including neutron transport codes. He reported that from the activity of irradiated gold foils on the incident face of the model, it can be concluded that the neutron flux is fairly constant. This shows the adequacy of the size of the converter assemblies and efficacy of the collimator in ensuring a uniform flux of neutrons. "C/E" values of the experiments with a cast iron model were also presented.

A. Kochetkov, SCK•CEN, Mol, Belgium, reported on the current and future possibilities of measuring nuclear data for minor actinides in integral and microscopic data experiments at the SCK•CEN research reactor installations. He stated that the results for the ^{245}Cm isotope recently have been received with a statistical uncertainty on the order of 0.9%. The measurements were performed with the well thermalized neutron beams in the large cavity of the graphite moderated BR-1 research reactor. The author also described future MA fission cross section measurements within the GUINEVERE and post-GUINEVERE experimental programmes at the VENUS-F facility.

D. Bernard, CEA Cadarache, France, presented the experimental technique and the required neutronic calculation tools based on exact perturbation theory to measure the actinide cross sections of ^{232}Th, ^{233,234}U, ^{237}Np, ^{238,239,240,241,242}Pu, ^{241,243}Am and ^{244,245}Cm in various neutron energy spectra. The measurements were performed at the 50 W pool reactor MINERVE located at CEA Cadarache. A new experimental programme on structural materials will be performed to ensure the accuracy of nuclear data involving C, H_2O, Be, Al, Zr, Pb, Mg, Fe, Cr, Ni, Mo, Cu, Ti, V, Cl, Co, Cd, Nb, Sn and Mn isotopes and elements. The author added that this ongoing research programme directly supports advanced nuclear fuel studies (e.g., actinides, plutonium), waste management, scientific and technical support of French pressurized water reactors and the European Pressurized Reactor, and future innovative systems.

B. El Bakkari, CNESTEN/CENM, Morocco, highlighted the neutronic analysis of the current core configuration of the 2 MW TRIGA MARK II research reactor in Morocco. Most of the model calculations were validated by the experimental results of a benchmarking program. The 3-D continuous energy Monte Carlo code MCNP (version 5), along with various data libraries, was used to develop a versatile and accurate full-core model of the TRIGA research reactor. The model represents a very detailed description of all components of the core with no physical approximation. The MCNP calculated values were found to be in very good agreement with the experimental and the existing data within an estimated error of 8%. Burnup calculations were also made by the newly developed burnup code BUCAL1, and the experimental programme will follow to validate its performance.

Y. Mahlers, Institute for Nuclear Research, Ukraine, discussed validation of the ENDF/B-VII library for the WWR-M Research Reactor. He concluded that for all experiments, neutronics calculation is in good agreement with the available measurements. For instance, the maximum absolute deviation of the effective multiplication factor from the results of the measurements is about 0.4% for ENDF/B-VII.0 and 0.6% for ENDF/B-VI.8. The newly developed and benchmarked model for the WWW-M reactor will be directly applicable at different stages of qualification and licensing during the core conversion process from HEU to LEU fuel.

O. Cabellos, Universidad Politécnica de Madrid, Spain, emphasized the impact of transmutation cross-section uncertainties on relevant fuel cycle parameters for a conceptual design of dedicated reactors for nuclear waste transmutation. He talked mainly about recent participation in the elaboration of a proposal entitled, "Accurate Nuclear Data for Nuclear Energy Sustainability" (ANDES), within EURATOM Call FP7-Fission-2009. One of the objectives of the ANDES proposal is to improve the inventory codes (ACAB code) to handle the complete set of uncertainty/covariance data to illustrate the potential benefit of generalizing the assessment of simulation results with full uncertainties propagation. The author concluded with recommendations for future nuclear data measurement programmes, highlighting experiments that may yield figures beyond the specific results obtained with the present nuclear data files and the limited available covariance information.

R. Rosa, ENEA, Italy, illustrated the TAPIRO research reactor's possibilities for reactor experiments with particle energies up to 1.35 MeV. The reactor is equipped with a homogeneous cylindrical core, stainless steel cladding and a cylindrical copper reflector. All components are assembled in a stainless steel tank and placed inside a nearly spherical borated concrete shielding system. Channels of various dimensions and with different neutron spectra are distributed around the core and are available for experiments, including nuclear data measurements. The author called for international cooperation to use the TAPIRO reactor in the validation of cross-section and codes in the fast neutron range, including integral experiments in different irradiation channels.

A. Buijs, McMaster University, Canada, introduced the McMaster Nuclear Reactor and its design parameters, past and current use and possible future opportunities for nuclear cross section measurements. He stated that at the moment, different codes and data libraries may be validated via comparison to integral measurements of reactor properties. Necessary investment and developments were also discussed in order to prepare for a more dedicated scientific project related to nuclear data measurements. Finally the author discussed the importance of high quality nuclear data and benchmarks of various modelling tools in the design and licensing of the Advanced CANDU Reactor.

U. Köster, ILL, France, discussed instruments for nuclear data measurements performed at the 58 MW high flux reactor of ILL. He presented a number of representative cases and the capabilities of existing instruments such as the Lohengrin mass spectrometer, crystal spectrometer GAMS, and others that use extracted neutron beams with neutron energies ranging from a few meV to about 1 eV. In particular, the author discussed how these established instruments that traditionally served specific purposes can be temporarily converted to support new applications like nuclear data measurements. Examples are the use of the fission fragment separator Lohengrin for high resolution measurements of rare (n,α) and (n,p) reactions and the use of the crystal spectrometers GAMS for (n_{th},γ) cross-section measurements on in-situ bred radioactive isotopes, also thanks to the high-neutron fluxes available at ILL.

G. Zhigang, China Institute of Atomic Energy, China, presented the updated Chinese Evaluated Nuclear Data Library (CENDL-3.1), which is based on nuclear data evaluation efforts in recent years at the China Nuclear Data Center (CNDC) in cooperation with the China Nuclear Data Coordination Network. CENDL-3.1 is a general purpose evaluated nuclear data file that contains the results of nuclear data evaluation and measurement in recent years in China. During the evaluation processes, the newest experimental information included new measurements made by Chinese scientists in China domestically are collected, evaluated carefully and corrected by using the new standard cross sections and decay data. For the most important nuclei of this library, benchmark testing and validations have been performed, including comparison with

other nuclear data libraries (ENDF, JENDL, BROND, JEFF, et al.). The new evaluated neutron data library CENDL-3.1, which contains about 210 nuclei, was released officially on 24 December 2009.

M. Pescarini, ENEA, Italy, highlighted the generation of broad-group working cross section libraries for nuclear fission reactor shielding and radiation damage applications in different spectral environments (LWR, SFR, LFR, HTR, etc.), which will allow the use of three-dimensional deterministic transport codes in data validation activities. He emphasized that it is useful not only for the data validation interests of reactor physicists and nuclear engineers, but also for nuclear safety authorities and industrial partners working in the nuclear energy field. Finally, to test new working libraries, it should be important to extend the availability of neutron shielding and radiation damage benchmark experiments with new single-material and engineering experiments dedicated to the various types of Generation III and Generation IV fission reactors. Again, in this context, use of research reactor facilities would be of great importance.

Y. Rugama of OECD-NEA and **V. Pronyaev** of NAPC-IAEA also gave overview presentations of the ongoing activities relevant to nuclear data and evaluations in their respective organizations.

2.2. Results obtained

All presentations were followed by adequate time for discussions and questions, which was widely used by the participants and chairs. Furthermore, intermediate summaries and compilations of findings and comments contributed to engage participants in the aims of the meeting and strengthening the exchange of knowledge and experience. The following text describes the outcome of the discussions, observations and conclusions relevant to the four main topics indicated in the previous section.

In addition, Annex I resumes the experiments that need to be performed at RR as the 1st priority. This list has been cross checked with the high priority data requests published by the OECD-NEA and given in Annex II. Annex III is an initial attempt to create a dedicated data base of RR facilities, where nuclear data measurements are performed. Recommended monitor reactions and materials for neutron spectrum characterization are given in Annex IV, while remaining Annexes V and VI give the list of participants of the meeting and meeting agenda respectively.

2.2.1. Topic 1: Capture cross section and decay data measurements using neutron beam, NAA, and other dedicated irradiation experiments

While there are growing demands for nuclear data at higher energy regions than keV for up-to-date scientific and technological development, accurate capture cross sections at thermal energy are still needed. The techniques to measure neutron capture cross sections are categorized into two groups: NAA and prompt gamma-ray TOF spectroscopy. In NAA, the exploitation of monoenergetic neutron beams with tunable energy as well as highly sensitive detection techniques is desirable. The neutron beams can be tuned by means of velocity filters or beam choppers, and TOF in the case of a pulsed neutron source. Notably, in prompt gamma-ray experiments at high flux neutron beam facilities, conditions of high gamma-ray background radiation are often encountered. The effective way to reduce this background is to use high-purity samples and to discriminate nuclides by high resolution gamma-ray spectroscopy utilizing germanium detectors. Thus the following three items are essential to meet the demands:

a) Preparation of physics samples

A crucial factor in the measurement of cross-sections is the availability of high quality samples. The meeting participants proposed to initiate the establishment of dedicated databases of:

- Laboratories that have a stock of sample materials potentially useful for target preparation (e.g., enriched stable and radioactive isotopes, high purity metals and special compounds, etc.)

- Laboratories that have the capability to transform materials into targets useful for nuclear data experiments (i.e., radiochemical purification, physical vapor deposition by evaporation or sputtering, electrodeposition by electrolysis or molecular plating, painting or spraypainting, ion implantation, etc.)

- Laboratories that possess the capability to characterize the quality of targets (i.e., quantification of purity, target thickness, homogeneity, stoichiometry, etc.) by various methods (e.g., low level nuclear spectrometry, Rutherford backscattering, etc.)

The above databases could be grouped according to their capability to handle stable, slightly radioactive or strongly radioactive materials. Already, the existing link to the International Nuclear Target Development Society (http://www.intds.org) should be used and common efforts with this Society should be coordinated.
The participants also recommended establishing a checklist or guidelines describing how to bring various radioactive or even fissile materials from one laboratory to another for physics experiments. In this regard, a short description of the steps to follow, including the links to access the latest procedures of specific transport regulations (e.g., ADR for road transport, IATA for air transport, and equivalents for railway and marine transport) would be very useful including share of information on good practices and lessons learned in this particular area.

b) Neutron beam design, characterization and nuclear data experiments

The contributors to the meeting gave evidence of a great variety of neutron beams, filtering devices and energy selectors. Therefore,

- A collection of guidelines dedicated to the design of neutron beams, materials of filters, energy selectors and beam characterization methods should be a great advantage for ongoing experiments and forthcoming projects. Commonly based methods and the sharing of information would facilitate experimental data inter-comparison and interpretation from complimentary measurements.

- The participants enquired about the establishment of a prioritized list, based on information collected from national laboratories and universities, of planned experiments/reactions to be studied using neutron beam techniques, which could be exchanged among interested parties

- A dedicated Technical Meeting or Workshop organized by the Agency on this topic is strongly recommended for the preparation of a specific TECDOC

c) Networking of new techniques

The following networking activities were recommended by the participants:

- Use of Accelerator Mass Spectrometry (AMS) for measuring cross-sections of long lived reaction products and establishment of a list of AMS facilities with the elements they typically handle

- Use of monochromatic neutron beams with energy tuned by neutron diffraction or with a neutron velocity selector on monochromator crystals. A list of facilities that have such

monochromatic neutron beams along with their capabilities (e.g., neutron energy range, beam size and available flux at sample position) would be very helpful

- Use of neutron interferometers for measurement of coherent scattering length, and more. Further actions could be undertaken after consulting Mr Helmuth Rauch (Atominstitut, Austria) and Mr Henry Fischer (ILL, France)

- Use of neutron beams in combination with high resolution multi-gamma-ray spectroscopy**.** Indeed, 4π geometry gamma ray spectrometers yield complete cascade information, contributing high accuracy neutron capture measurements

Again, a dedicated Technical Meeting or Workshop organized by the Agency on the above topic was strongly recommended for a preparation of a specific TECDOC.

2.2.2. Topic 2: Fission reaction and fission fragment studies

For the majority of applications based on nuclear fission, the most precise knowledge about the fission process is a prerequisite. Those data can be directly entered into nuclear models relevant for reliability and safety studies of nuclear facilities as well as nuclear waste management. The research community is particularly interested in differential fission-product yield data relevant for reactor control and calculations of decay heat from delayed gamma-ray and beta-particle emission, as well as in prompt neutron and gamma-ray emission spectra and multiplicity, to benchmark results from integral measurements.
Here, by providing high neutron fluxes, RR facilities can continue contributing intensely to the nuclear data measurement programme on a large scale, e.g., determining fission cross-sections at thermal energies, carefully verifying the 1/v dependence of fission cross-sections in the vicinity of the lowest resonance, fission-fragment yield and de-excitation for rare or highly active actinide samples. Taking into account the limited detection efficiency of neutron and gamma ray spectrometers, full correlation measurements of prompt neutron and gamma ray emission as a function of fragment mass and excitation energy explicitly require thermal neutron energy neutron beams, in which achieved fluxes and fission cross-sections are usually highest. The following sub-topics were highlighted during discussion:

a. Prompt fission neutron energy spectra
    i. Reactor calculation on the basis of new prompt neutron spectra measured at thermal energies, as performed on ^{235}U in 2008 for three different angles relative to the incident neutron beam and recently evaluated by Mr V. Maslov.
    ii. Prompt fission neutron spectral measurements are encouraged, concentrating on the energy region below 0.5 MeV, which represent the threshold of traditionally employed liquid scintillation detectors. These measurements could be performed in filtered beams providing energies in the tens of keV region and should ideally be carried out relative to ^{252}Cf under exactly the same experimental conditions.
    iii. Dedicated experimental techniques that allow measuring the entire region from low energies to beyond the distribution maximum around 1.5 MeV should be developed to avoid systematic errors due to normalisation.
    iv. (Velocity-) Filtered beam measurements might be useful to investigate the energy dependence of the spectral shape and fluctuations in multiplicity due to the influence of the spin of the first resonance, e. g., in ^{239}Pu.
    v. Reduction of uncertainty at high spectral energies is very much recommended, demanding, as a prerequisite, high fission rates provided by typical neutron fluxes at RR.

vi. A better knowledge of the spectral shape at both very low and very high neutron energies will help to select proper neutron emission models
vii. Measurements of prompt neutron spectra and multiplicity at fast reactor neutron beams

b. Prompt fission gamma ray spectrum and multiplicity
   i. Measurements of prompt fission gamma ray spectra and multiplicity in the thermal neutron energy range
   ii. Measurements of prompt fission gamma ray spectra and multiplicity using fast reactor neutron beams

c. Fission fragment characteristics for the description of neutron and gamma ray emission by means of Monte-Carlo evaporation codes
   i. Pre-neutron mass and kinetic energy distributions with high mass resolution
   ii. Correlated pre- and post-neutron mass and energy measurements
   iii. Fission fragment angular distribution as a function of fission fragment mass
   iv. Spin distribution of primary fission fragments to describe properly the competition of prompt neutron and gamma ray emission
   v. Measurements in the fast reactor neutron energy range, because no data yet exists

d. Independent and cumulated fission yields for fast reactor applications
   i. Measurement using fast fission RR beams
   ii. Design of a fast neutron spectrum by means of uranium converters placed in thermal beams at RRs (e.g., BR-1 in Belgium)
   iii. Installation of a fission fragment spectrometer

e. Fission cross-section measurements at thermal energies
   i. Isotopes accessible via (2n,f) and relevant for model normalization at thermal energies (^{232}Pa, ^{238}Np, …)
   ii. Fission cross-section measurements at thermal RRs, including measurements with (velocity-)filtered beams to test the 1/v dependence of cross-sections (Westcott-factor), e.g., ^{245}Cm complementary to previous measurements using the pure thermal beam at BR-1 and at the neutron TOF facility GELINA

In brief, the following remarks summarize the above discussion and observations:

- Need to solve the problems related to the prompt fission neutron energy spectrum
- Need for new measurements of prompt gamma ray spectra relevant for Generation IV power reactors
- Development of new measurement facilities and techniques for correlated measurements of fission fragment characteristics, in particular in the fast reactor neutron energy region

2.2.3. Topic 3: Dedicated integral experiments for nuclear data and code validation

Dedicated integral experiments in RRs are able to produce very accurate energy-integrated nuclear data. However, processing and transport codes using evaluated cross section data libraries are required to extract physical quantities. Thus, dedicated RR integral experiments are complimentary and equally important, when compared to differential measurements, to ensure the nuclear data validation.
Three main subjects were discussed within this topic: a) methodology sharing, b) experimental uncertainty assessments and c) issues related to neutron spectrum unfolding codes.

a) Methodology sharing

Both reactor technology and neutronic/photon transport calculations are concerned. First of all, RR facilities are encouraged to participate in the activities concerning the OECD ICSBEP/IRPhE databases. In particular, the experiments with detailed information on operation conditions and available experimental data with precise description such as calibration, correction factors, etc. are of the greatest importance. Numerical benchmarking to interpret such experiments is encouraged by the IRPhE database. The monitors used such as fission chambers, activation foils and other detectors should be available and easily transportable from one facility to another in order to distinguish the statistical and systematic uncertainties of a measured value. The VENUS and TAPIRO facilities are open for such collaborations in 2010. Work studies on pile oscillation technique to assess integral nuclear reaction data measurements should be encouraged, namely for cross-section measurements, determination of η and α values as well, β_{eff}, Doppler and other parameters in the fast neutron energy range. The calculation tools, such as ERANOS, and its know-how (e.g., training courses, summer schools) should be widely shared and promoted. Finally but not the least, sensitivity studies using perturbation theories are very powerful methods and therefore should be continued in order to extract and analyse physical quantities, including nuclear data.

b) The experimental uncertainty assessment

Indeed, two important components of experimental uncertainty should be provided to perform the validation of the nuclear data. A systematic and statistical covariance matrix should be given by the experimenters. Experimental benchmarking, such as using the same flux monitoring in different facilities, is encouraged, as in point a). For instance, gamma intensity in NAA or neutron kinetics parameters for residual core reactivity is the source of systematic uncertainty. Authors should then provide the exact values they used. Furthermore, technological uncertainties of the measured parameter (e.g., sample or environment impurities, geometry details, etc.) should be methodically given. All uncertainties should be considered in order to observe trends in nuclear data. Finally but not the least, the experimenters should systematically provide the average cross-section together with the corresponding neutron spectrum in numerical form and information on how the spectrum was obtained.

c) The issues related to neutron spectrum unfolding codes

A dedicated workshop or training course on this topic is requested, in particular for application and use of the SAND code applied in NAA.

2.2.4. Topic 4: Efforts on code/library development and global benchmarking / validation

The successful development of advanced nuclear systems for sustainable energy production depends on high level modelling capabilities, i.e. simulation codes and associated nuclear data files, for the reliable and cost-effective design and safety assessment of such systems. High quality nuclear data are an essential component of such modelling capabilities. For current nuclear systems, where present nuclear data are considered adequate, one can still reduce uncertainties for different applications where higher precision is required. Secondly, for the future advanced reactors and innovative fuel cycles, complete and accurate information about the nuclear reactions taking place is indispensable. In this respect, more supported work based on integral experimental data from RRs can help to improve these data. In addition, high fidelity nuclear databases with credible uncertainties will play an important role in future simulations, and uncertainty assessments. Associated sensitivity analysis will help to prioritize future research, where integral experiments performed in RR facilities will be indispensible to the evaluation and qualification process, including constraints on the covariance matrix.

The following items within this topic aimed to define the importance of basic data, codes and integral experiments for model development, evaluation/validation and error propagation issues have been discussed in more detail:.

a) Library development

The compilation and evaluation of nuclear data libraries requires complex and expensive activities. These efforts are justified on the basis of the real benefits to the end users of the data. In this respect, high quality nuclear data, including complete and accurate information, are an essential input required for cost-effective design and safety assessment of present and future nuclear systems and general and nuclear power reactors in particular.

Differential nuclear measurements in combination with nuclear models are the main source of information for nuclear data evaluators. Those experimental measurements should be preferably reported and included in the EXFOR library. The submitted experimental data must include details on sources of uncertainty and their possible correlation to improve the assessment of the associated systematic uncertainties. As one example, IRMM/AGS and CEA/CONRAD evaluation code development are encouraged to account methodically for all TOF facility uncertainties (e.g., sample homogeneity, normalization, background, etc.).

The early dissemination of the beta releases of the ENDF (e.g. ENDF/B-VII, JEFF-3.1.1, JENDL-4, etc.) data libraries to potential end users (e.g., nuclear industry, research centres, universities, etc.) and the subsequent feedback will permit the possible identification of mistakes by the evaluators.

b) Processing libraries

Quality Assurance (QA) during processing of the ENDF data libraries is an important task linking evaluators and end users. A free processing procedure including patches of processing codes, reporting bugs and updates when a new ENDF file is delivered certainly contributes to this QA process. The list below reviews how the different steps in the data processing phase can support this objective:

i) ENDF Utility Codes (e.g., CHECKR) are and should be used as pre-processing codes to guarantee format or physics checking of ENDF files. However, it can be noted that additional mistakes can be found in the next code library processing step.

ii) Processing ENDF files (e.g., NJOY, PREPRO, SCAMPI, AMPX, etc.) in PENDF/GENDF libraries is a valuable procedure to compare different ENDF files, as well as to check the algorithms used in those processing codes. Here, the messages, consisting of warning and errors, of these processing codes as well as the "human eye" can be used to spot inconsistencies and errors in the ENDF files. With those processed PENDF files, INTER code can be used with, for example, spectrum averaged cross sections, to compare experimental "standard" measurements (e.g., measurements in Maxwellian averaged neutron spectra)

iii) Besides the standard code library processing libraries (e.g., ACE, WIMS, MATXS, AMPX, etc.), the production of fine group and general-purpose cross section libraries (FGENDF) is recommended. These FGENDF files can be used to collapse problem dependent broad group coupled neutron and photon working cross section libraries for nuclear rector shielding and radiation damage applications with self-shielding neutron cross sections. These modern cross section working libraries for various spectral environments of interest (e.g., Generation III and IV reactors, ADS) would permit the use of 3D deterministic transport codes in nuclear data validation with a satisfactory treatment of neutron leakage

iv) Finally, processing of decay data (e.g. branching ratios, etc.) is also an important task to identify possible mistakes in burn-up calculations

c) Global Benchmarking and Validation Experiments

The assessment of the present accuracy of simulation tools and nuclear data can be provided by comparing the modelling results with dedicated integral experiments. This assessment is based on:

- Sufficient number of representative integral experiments
- Combination of different simulation tools (e.g., deterministic and Monte Carlo) and associated nuclear data files. This also includes preliminary work to be done by numerical code-to-code benchmarking (e.g., deterministic vs Monte Carlo, Monte Carlo vs Monte Carlo)

Well-established international databases containing a comprehensive set of experiments are available for sharing among specialists. These databases are used for international activities involving validation efforts and for testing basic nuclear data evaluations to build confidence in methods and data evaluations, assess uncertainties and define confidence bounds and associated safety margins.

Examples of such experiments can be found in

i) The *International Handbook of Evaluated Criticality Safety Benchmark Experiments* (ICSBEP)
ii) The *Shielding Integral Benchmark Experiment Data Base* (SINBAD)
iii) The *International Reactor Physics Benchmark Experiments Project* (IRPhe)
iv) The *Spent Fuel Isotopic Composition Database* (SFCOMPO)

The analysis of these and newly planned integral experiments will certainly be useful in assessing the need of new data measurements or evaluations to reach the required accuracy.

d) Error propagation

At present, the assessment of the accuracy of parameters related to core performance such as criticality value and fuel cycle parameters like the evolution and transmutation of fuel inventory, due to uncertainties in the basic nuclear data, is a critical issue. The accuracy of calculations can be performed with different *Forward Error Propagation* techniques (e.g., ASAP - *Adjoint Sensitivity Analysis Procedur*e, FSAP - *Forward Sensitivity Analysis Procedure*, GSAP - *Generalized Sensitivity Analysis Procedure* and/or using Monte Carlo approach) for the systematic introduction of uncertainty propagation in simulations.

ENDF covariance files (variance/correlations) are needed to perform this uncertainty evaluation. Consequently, an additional effort for further provision of covariance data with methodologies to evaluate the uncertainties and covariance matrices from experimental data and nuclear models is also highly recommended. In addition, the inclusion of cross-correlations for various reactions involving isotopes cannot be avoided and, therefore, certainly required.

3. SUMMARY OF THE MAIN RECOMMENDATIONS

The Tehnical Meeting was highlighted as a success by all participants at the end of the week. Furthermore, support for the meeting in terms of the number and diversity of participants as well as participating Member States, is a significant indicator of the success of the broader endeavour, which is to provide timely practical assistance and support the sharing of Research Reactor (RR) based experience related to the provision of nuclear data, fostering the development of new experimental techniques, establishment of enlarged collaborations and facilitating contacts as well as the formation of networks in nuclear data and evaluation related activities.

It was recognized that the IAEA has undertaken a number of activities through Coordinated Research Projects, Technical Meetings and Workshops, and in some cases also through Technical Cooperation (TC) projects to assist the Member States in the domain of nuclear data measurements and evaluations. Continuation and expansion, where appropriate, of such activities were desired and encouraged.
Based on the final discussions on the current status and future needs in nuclear data measurements and evaluations using RRs, the participants formulated **the following specific recommendations:**

1. Encourage and support experimental efforts based on high priority data requests (see Annexes I and II).
2. Create a database or network of RR facilities performing nuclear data measurements, with their detailed characteristics (see Annex III).
3. Create a database or network of high quality samples and targets used in nuclear data measurements and neutron beam design and facilitate and support their sharing, exchange and transportation. Initiative should be taken by one of the Member States to host a beam filter and high purity sample stock eventually supported by the IAEA.
4. Initiate and prepare a specific IAEA publication (guidelines) on the potential use of advanced neutron beam techniques and associated detection and instrumentation including data acquisition systems in the field of nuclear data measurements. Organize an IAEA TM in order to prepare such a document.
5. Use of advanced neutron beam techniques and associated detection systems possess a huge potential to provide high quality nuclear reaction and decay data. The design and implementation of a dedicated CRP is recommended illustrating the development and use of neutron beam based advanced experimental techniques and associated detection systems for the provision of nuclear data at RR facilities.
6. Promote enhanced utilization and share of RR facilities and integral measurement methodologies within the Member States for validation of nuclear data. This data are required to be provided in the form of averaged cross-sections together with the corresponding neutron spectrum in numerical form.
7. Encourage experimental and evaluation efforts on the establishment or improvement of covariance matrices relevant to reaction cross sections, propagation of associated uncertainties in reaction rates and decay data, and in particular, in material depletion/transmutation calculations. This is in support of dedicated integral measurements (cf. recommendation no. 6).

4. INDIVIDUAL CONTRIBUTIONS

Precision Neutron Cross Section Measurements at Reactor Neutron Filtered Beams

O. Gritzay, V. Kolotyi, O. Kalchenko, V. Libman

Institute for Nuclear Research of NAS of Ukraine
Prospekt Nauky, 47, Kyiv, Ukraine, 03680

Abstract. At the Kyiv Research Reactor (KRR) a neutron filtered beam technique (NFBT) has been used for more than 30 years and its development is continuing. Use of the NFBT and the new and updated facilities provide measurement of the neutron cross sections with rather high accuracy: the total neutron cross sections with accuracy 1% and better, the neutron scattering cross sections with the 3-6% accuracy, the neutron capture cross sections with the 5-6% accuracy. The ways of search new neutron filters and improving of known ones are described. Short information about the neutron measurement techniques, developed at the KRR, is presented. The main purpose of this paper is presentation of potentiality of the NFBT at research reactors, and demonstration of some experimental results obtained using these techniques at the KRR.

1. Introduction

Up-to-date level of scientific and technology development demands a high accuracy of neutron data. This high accuracy of experimental data should allow making progress in development of the nuclear simulation codes and in generation of the evaluated nuclear data libraries that are the basis for any transport calculation both for operating current and designing future reactors and for nuclear technologies in medicine, industry, etc. Now the most difficult situation with the accuracy of the neutron cross sections is in the energy range from several keV to several hundred keV. The reason is the lack of high flux installations in the mentioned energy range. Today a few of such installations have been designed and may be used (e.g., ORELA or GELINA), but they are very expensive. There is another way to get the high accuracy neutron cross sections — to use the neutron filtered beam technique at existing research reactors. We use the second way, so now we present the short characteristics of the KRR.

2. Short characteristics of the Kyiv Research Reactor

The WWR-M KRR is a light water moderated and cooled tank-type reactor with a beryllium reflector. The reactor currently uses 36 % enriched uranium-235 WWR-M2 fuel assemblies, each of which consists of an outer hexagonal tube and two inner cylindrical tubes (today replacement on the 20 % U^{235} fuel is started). The nominal thermal power is 10 MW, the neutron flux in the core is about 10^{14}n/cm^2·s. The KRR has ten Horizontal Experimental Channels (HEC), which are used for nuclear physics investigations, solid state and material structure study and applied works. Today, three of these ten HEC are employed in the experimental investigations using the neutron filtered beam technique.

3. Basic principles of the neutron filters development

The main idea of neutron filter development is the use of large quantities of matter whose nuclei have the deep interference minima in their total neutron cross sections. By transmitting reactor neutrons through thick layers of such material, one can obtain the quasi-mono-energetic neutron lines instead of white reactor spectrum.

Energy of such quasi-mono-energetic neutron line may be situated in the range from thermal to several hundreds kilo-electron-volts, and its intensity may reach 10^5-10^8n/cm^{2}s. There are essential *advantages* of the NFBT. But the NFBT is possessed of *demerits*, namely:
1) presence of the parasitic energy lines in the filtered neutron spectrum;
2) presence of the gamma-background.

To get only one quasi-mono-energetic neutron line it is possible to use the two ways:
1) to take so thick layer of this material that only neutrons, corresponding to the most deep interference minimum, would be able to pass through it;
2) to use additional materials, for which resonance maxima in their total neutron cross sections coincide with the interference minima for the filter material, with the exception of the most deep interference minimum energy.

The first way is very easy for modelling, but in general it is unacceptable in practice, as to depress all parasitic lines it is necessary to take so large quantity of the filter material, that an intensity of the main energy line becomes very low. For example, if we use as a filter material scandium with thickness about of 170 g/cm^2, we obtain the well known 2 keV filter [1]. For this filter ratio of intensities of the main neutron line and the higher energetic parasitic lines (this ratio is called a purity of filter) will be approximately equal to 75 %. To get the 95 % purity of this filter it is necessary to take scandium five times more, but the intensity of the main 2 keV line diminishes by a factor of 16.

If we use the second way, i.e. for getting of the 95% purity for the 2 keV filter, we take as additional materials Co, Ti and ^{10}B, the intensity of the main line diminishes only by a factor of 2. Selection of the suitable composite materials and their thickness by means of visual examination of the total neutron cross sections is unreal (see Fig. 1, where the total neutron cross sections for all materials of the 2 keV composite filter are presented). The selection by means of experimental investigations can demand a lot of reactor time.

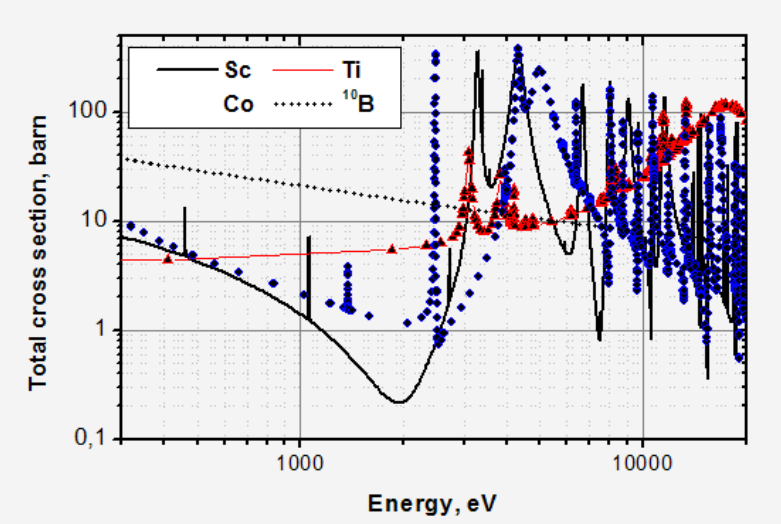

FIG.1. Total neutron cross sections for Sc, Ti, Co, and ^{10}B in the energy range from 0.3 to 20 keV (JENDL-3.3 library).

Therefore the best way to optimize a filter composition is execution of preliminary modelling calculations, with subsequent test of this calculated filter in experiment. Methods, realized for this aim in the NPD, are described below. Now, let us formulate the basic demands to neutron filters:

1. The purity of the main energy line in neutron spectrum has to be as much close to 100 % as possible.
2. Neutron intensity is to have the most possible value, sufficient to obtain the necessary accuracy in experiment.
3. Construction and composition have to provide the minimal possible gamma-background.
4. In necessary case, construction and composition have to allow increasing or reducing the width of the base line without essential worsening of the filter quality.
5. The amount of high-pure isotopes in the filter components has to be as low as possible.
6. The filter components have to provide the energy range of the filtered neutrons up to 1 MeV and more.

4. Neutron filters at the Kyiv Research Reactor

The wide set of natural elements and high-pure isotopes are used as components for the neutron filters in the Neutron Physics Department (NPD) at the KRR:
Natural elements: Si, Al, V, Sc, S, Mn, Fe, Ti, Mg, Co, Ce, Cr, Rh, Cu, B, Cd, LiF.
High-pure isotopes: ^{52}Cr (99.3%), ^{54}Fe (99.92%), ^{56}Fe (99.5%), ^{57}Fe (99.1%), ^{58}Ni (99.3%), ^{60}Ni (92.8-99.8%), ^{62}Ni (98.04%), ^{80}Se (99.2%), ^{10}B (85%), ^{7}Li (90%).

Availability of such wide set of materials, especially the high-pure isotopes, allowed to create in the NPD the unique set of the neutron filters, providing more than ten neutron lines in the energy range from thermal energy to several hundred kilo-electron volts. The intensity of these lines may reach 10^6 - 10^8 n/cm^{2}s [2], and this is much more than any other method (time of flight or others) can ensure. The wide set of the filter materials also allows us to modify the filter parameters (purity, intensity, width, etc.) subject to the given research task.

Through expensiveness of the high-pure isotopes, the natural elements or high-pure isotopes available in the NPD are usually considered as components of the new or improved filters.

The filter component optimization procedure intended for getting the most possible intensity of the main energy line at the most possible low intensity of the parasitic energy lines in filtered neutron spectrum includes the following three main steps:

1st step: modelling calculation of the neutron filtered spectra;
2nd step: creation of the filter with the calculated amount of the chosen components;
3rd step: experimental testing of the created filter.

If it is necessary, the sequence of these steps is repeated. If desired quality of the filter is attained, its characteristics are determined.

4.1. Modelling calculation of the neutron filtered spectra

For modelling calculation of the neutron spectra formed by filters, there was developed the special computer code using FORTRAN language. This code FILTER allows putting into calculation practically any material and isotope combinations, which are used to get the filtered neutron spectrum with necessary energy. This code FILTER (version 5) allows obtaining the two energy dependent values which image the filtered neutron spectrum:
1. Neutron transmission T(E) multiplied by the incident reactor neutron spectrum $\Phi(E)$:

$$F1(E) = T(E) * \Phi(E) \equiv \exp[-\sum n_i * \sigma_i(E)] * \Phi(E), \qquad (1)$$

where n_i – nuclear thickness of the i-th filter component; $\sigma_i(E)$ – total neutron cross section of the i-th nuclide.

2. Neutron transmission T(E) multiplied by the incident reactor neutron spectrum $\Phi(E)$ and multiplied by the energy dependent cross section of the reaction, which used for neutron detection $\sigma_{react}(E)$, i.e. it allows to take into account an efficiency of the used neutron detector:

$$F2(E) = T(E) * \Phi(E) * \sigma_{react}(E). \qquad (2)$$

The incident reactor neutron spectrum $\Phi(E)$ is taken as function composed of 3 parts: Maxwellian, 1/E – dependence and fission spectrum. This spectrum was normalized to unit: $\int\Phi(E)dE = 1$ in the limits from 10^{-5} eV to 20 MeV.

The total neutron cross sections for nuclides $\sigma_i(E)$ were obtained from ENDF libraries in the energy range from 10^{-5} eV to 20 MeV in point-wise form at the temperature 300K using the PREPRO2002 [3] and NJOY99 [4] codes. JENDL-3.3, ENDF/B-6 libraries were taken as the basis for forming this special library. Today it consists of 65 files, each of them includes the total neutron cross section for one nuclide.

The opportunity of using these simple expressions for determination of the neutron spectrum shape after filter is due to a strict collimation of the neutron filtration system, otherwise it would be necessary to calculate a neutron transport from core to sample place taking into account all processes (scattering, absorption, etc.). Correctness of this statement was tested by calculation of the neutron spectrum shape after the 24 keV filter using MCNP4C code [5]. The MCNP4C results were similar to those obtained by means our code FILTER.

4.2. Experimental testing of the created filter

To demonstrate the procedure of experimental testing of the created filter, let us consider the filter, main components of which are S, ^{58}Ni, V, ^{10}B, and Al. Results of the calculation with the code FILTER show that if we take ^{10}B - 0.281 g/cm^2, ^{58}Ni - 83.15 g/cm^2, V - 17.4 g/cm^2, S - 122.55 g/cm^2, Al - 5.4 g/cm^2, we can obtain the neuron filter with the energy 59 keV and the purity of this filter will be better than 99%, other additions to the main spectra will be negligible – each of lines is less than 0.2%. This filter was arranged and the neutron spectrum after them was measured by means of the proton recoil counter. The experimental results are shown in Fig. 2. On the lower part of this figure the shape of the neutron filtered beam spectrum obtained by differentiation of the previous curve is presented. As it can be seen, the contribution of the parasitic higher energy lines is negligible.

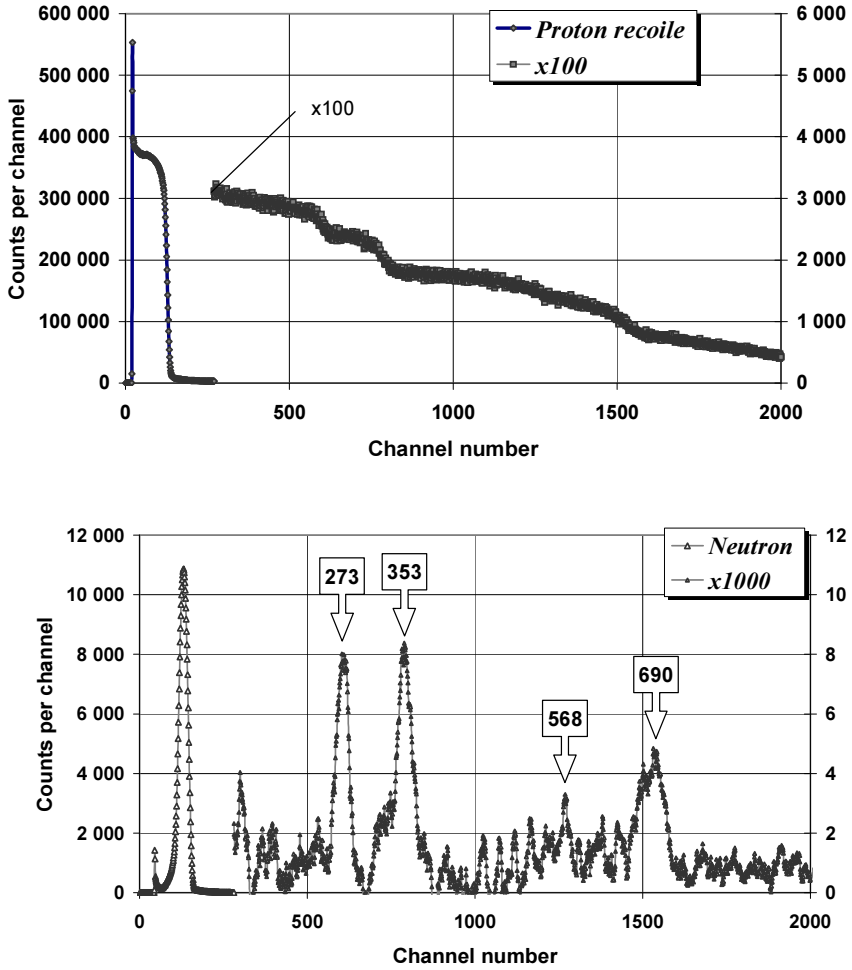

FIG.2. Instrumental spectrum from the proton recoil counter after the neutron filter with the energy 59 keV (top picture), and the shape of the neutron filtered beam spectrum obtained by differentiation of the previous curve (lower picture).

4.3. Filters used for fundamental and applied investigations in the NPD

As a result of this activity, characteristics of the whole series of the neutron filters were improved and today these filters are used for fundamental investigations, carried out in the NPD. Their energies and comparative intensities are shown in Fig. 3. The energy region, which they cover, is from thermal energy (this filter is not presented in the figure) to 149 keV.

The new filter 7.5 keV was developed; the main component of it is copper. Another filter is developing now in the NPD – the 275 keV filter. Main component of this filter is manganese. The energies of these filters are shown in Fig. 3 by red arrows. The components of some of these filters are presented in Table 1.

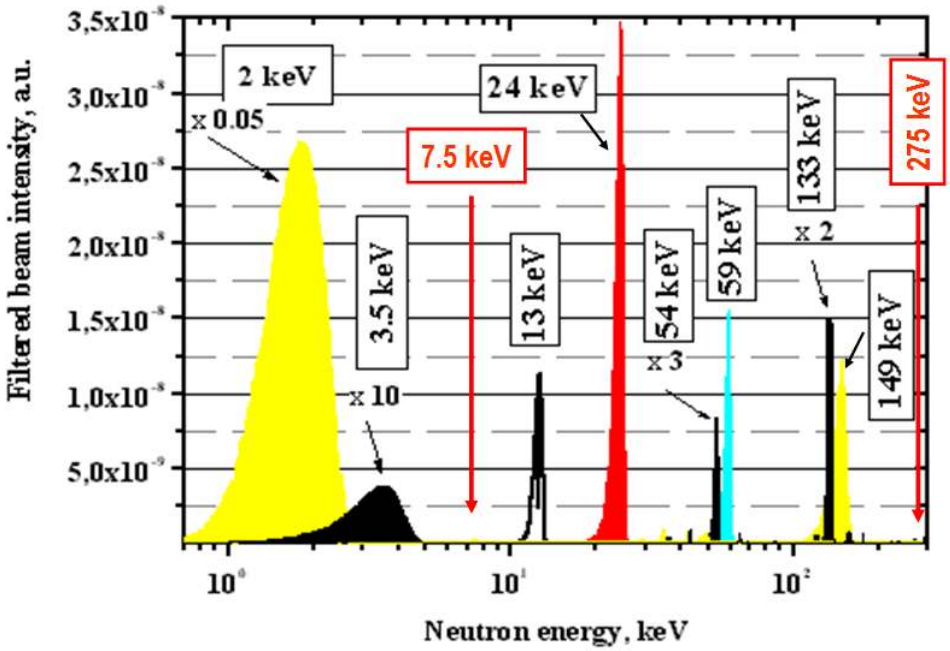

FIG.3. The neutron filters used in the NPD for fundamental investigations.

TABLE I. THE FILTER COMPONENTS (g/cm^2) USED FOR FORMING OF SOME FILTERED NEUTRON BEAMS

2 keV filter						
^{10}B	^{45}Sc	^{60}Ni	^{54}Fe	S	^{59}Co	^{27}Al
0.2	104.6	80.2	39.35	56.0	26.7	0.54
3.5 keV filter						
^{10}B	^{54}Fe	^{60}Ni	S	Cd	^{27}Al	
3.15	170.7	146.2	36.7	0.865	1.349	
24 keV filter						
^{10}B		S	Fe		^{27}Al	
0.95		16.35	236.1		99.86	
133 keV filter						
^{10}B	^{52}Cr	^{58}Ni	^{60}Ni	Si	^{27}Al	
0.2	95.94	194.06	3.1157	93.08	0.54	

5. Main tasks for scientific research, where the filtered neutron beams may be used

1. High precision measurements (better than 1 %) of the total neutron cross sections.
2. Precise measurements (to 3 %) of the neutron cross sections (σ_{el}, $\sigma_{n\gamma}$, σ_f), the getting of the averaged nuclear parameters (S_o, S_1, R_0, R_1, D, $<\Gamma_n>$, $<\Gamma_\gamma>$).
3. Measurements of the neutron capture gamma-spectra.
4. Measurements of σ_{inel} for the first exited levels of heavy nuclides.
5. Measurements of the activation cross sections.
6. Isomeric ratio investigations.
7. The use in time of flight method for precise cross section measurements of σ_{tot}, $\sigma_{n\gamma}$, σ_{inel}.
8. Research of the radiation damage energy dependence in materials.

9. Neutron radiography and tomography.
10. Neutron and boron neutron capture therapy (BNCT).
11. Prompt Gamma-ray Activation Analysis (PGAA).
12. Development of the standard fluxes for the neutron dosimetry purposes.
13. Energy calibration of proton recoil counters.

6. Investigations in the NPD

Some of these tasks are successfully solved at the KRR, where three HEC are equipped with the neutron filters. Today four neutron measurement techniques are developed in the NPD and used for fundamental investigations. There are following directions:

1) measurements of the total neutron cross sections;
2) measurements of the neutron scattering cross sections;
3) measurements of the angle distribution of scattering neutrons;
4) measurements of the neutron capture cross sections.

According to the formulated task, the filter components (even for filters with the same energy), the experimental equipment installed on the KRR horizontal channels, the shielding, etc. may be very different in configuration and size, but four main systems are always present:

1) the system for forming of the filtered neutron beams;
2) the system of the radiation shielding;
3) the sample management system;
4) the neutron detector and counting system.

As two of them – the system of the radiation shielding and the sample management system – may have a lot of engineering designs (for example, we have different systems of the radiation shielding at each HEC and several systems of the sample management), description of them is omitted in this paper. Our experience in making of the system for forming of the filtered neutron beams may be useful for users who wish to develop the neutron filtered beam technique at their installations, so there are some details about this system.

The system for forming of filtered neutron beams includes the elements of beam collimation and neutron filtration on the way from the reactor core to detector. The preliminary forming of necessary beam geometry is realized with two iron and boron carbide collimators, installed behind the shutter at the 1.5 m distance from the channel beginning. Length of the collimators is 600 mm (390 mm – iron, 210 mm - boron carbide). Further beam forming takes place in the first three discs of the shutter and in the outer collimator. Lead, textolite and a mixture of paraffin with H_3BO_3 are used as material for these collimators. The collimation system provided beam narrowing to necessary diameter. The elements of the neutron filtration system take place in the first three disks of the shutter and in the outer collimator. As a rule, the first filter component, having location on the beginning of the third beam shutter disk (the most close to core), is boron-10, to avoid an excessive activation of the rest filter components. Also, in the first three shutter disks, the main components of the filter are inserted. The filter components, which are planned to alter, are placed, if it is possible, in the outside collimator. To lighten and to quicken the procedure of the filter changing, the special containers for the filter were made. These containers are tubes from stainless steel, length of them are equal to the length of the beam shutter disks. The collimation materials and the filter components are inserted in these tubes. The typical construction of the forming system of the filtered neutron beam at the KRR is presented in Fig. 4. One of the real filters is presented in Fig. 5, as an example.

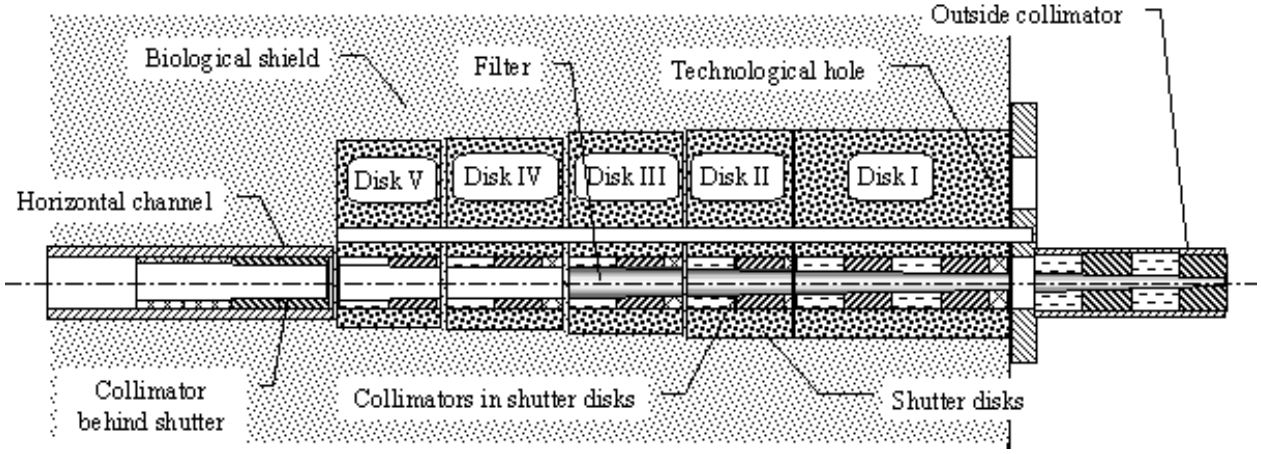

FIG.4. Typical construction of the forming system of the filtered neutron beam at the KRR.

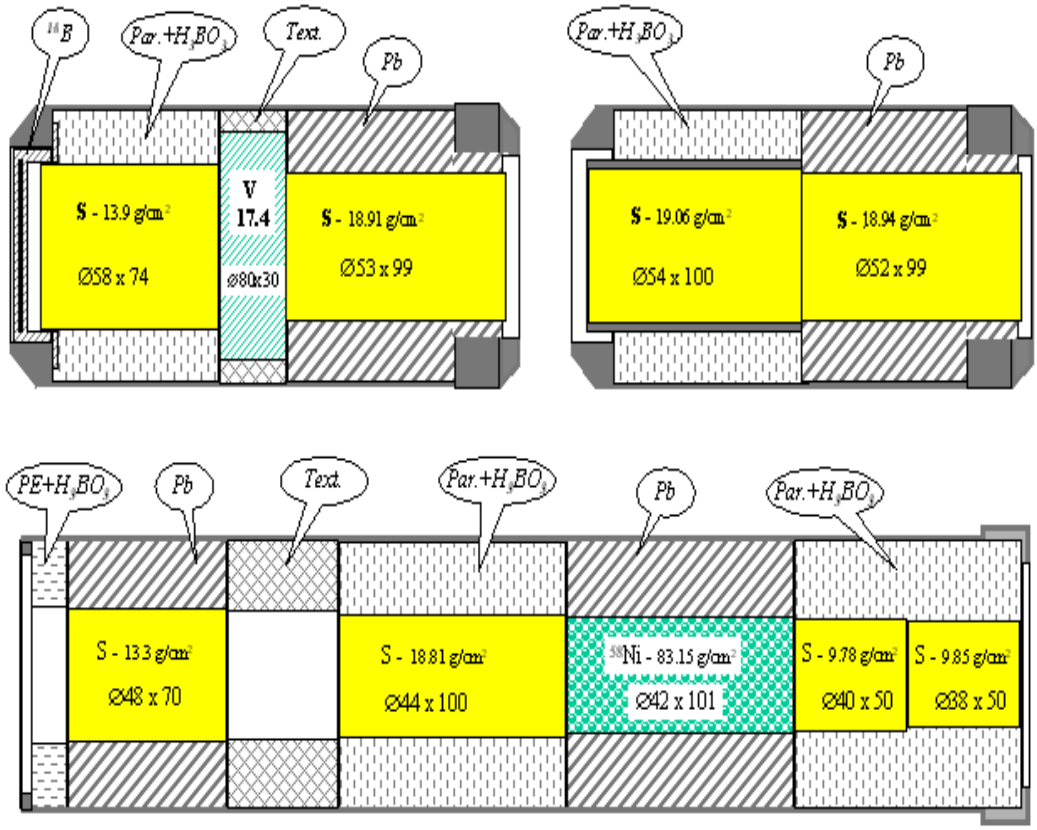

FIG.5. The 59 keV filter. Top picture– the 3rd and 2nd shutter discs (from left to right), lower picture – the 1st shutter disc.

Neutron detector and counting systems, which we use in our investigations, consist of neutron counters, electronic blocks, personal computer and communication lines about 50m long between spectrometric installation and measuring room. Type of the neutron counters depends on the given task and/or the energy of the incident filtered neutrons. List of used counters is presented in Table II.

TABLE II. LIST OF COUNTERS USED IN FUNDAMENTAL INVESTIGATIONS AT THE KRR

Measure value	Type of neutron counters
σ_{tot}	E_n <= 12 keV - helium-3 counters (CHM-37, LND 2527)
	E_n >= 12 keV - hydrogen recoil counters (CHM-38, LND 281)
σ_{el}	58 helium-3 counters placed in five layers, located just above the sample
$d\sigma/d\Omega$	Five assemblies of 7 He-3 counters CHM-17
	Set of 7 hydrogen counters LND-281
	Set of 7 helium counters LND-2527

High intensity of the neutron filterd beams and experimental methods, developed in the NPD, made it possible to carry out the following measurements:

a) High precision measurements (with accuracy better 1%) of the total neutron cross sections, *averaged* on the filter spectrum.

b) Measurements (with accuracy 3-6%) of the neutron scattering cross sections, *averaged* on the filter spectrum.

c) Measurements (with accuracy 4-6%) of the activation cross sections, *averaged* on the filter spectrum.

Rather large width of the quasi-monoenergetic filtered neutron line – the width may amount to several tens of kiloelectron-volts– is an advantage for some tasks. For instance, experimental data on the neutron cross sections, *averaged* on the filter spectrum, allow to *determine* the averaged resonance parameters. But for some tasks it is a demerit of the FNBT. We try to demonstrate it on two examples obtained in our investigations. The first of them is concerned with our measurements of the total neutron cross section on chromium at the filter energy about 55 keV [6], the second one is concerned with our measurements of the total neutron cross section on carbon at the filter energy about 148 keV [7]. Results of these measurements are presented in Figs. 6 and 7.

As it is seen in Fig. 6, our experimental value of the total neutron cross section is obtained with very good accuracy (it lays within thickness of the solid black line), but there is the cross section averaged on the large energy region (length of the solid black line corresponds to the width of the filtered neutron line). In the energy region 50 – 60 keV there are two resonances of ^{52}Cr (marked by red circles). Our measurements don't allow determination of parameters for these resonances, though they affect the cross section value.

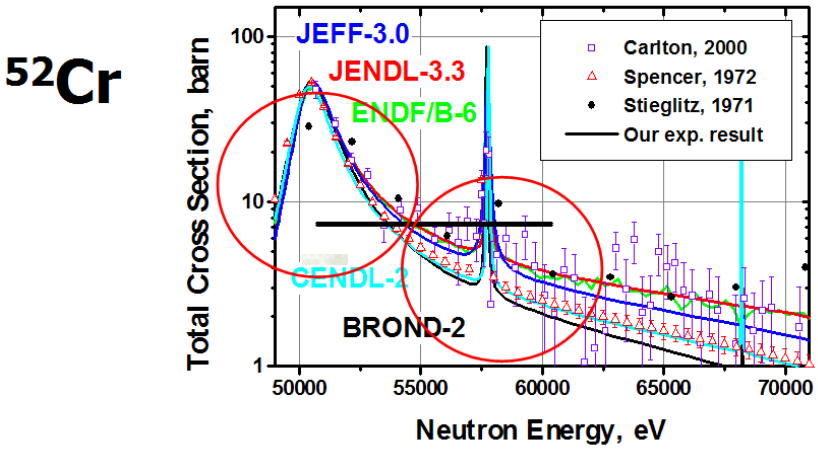

FIG.6. Comparison of the ^{52}Cr evaluated and experimental total neutron cross sections.

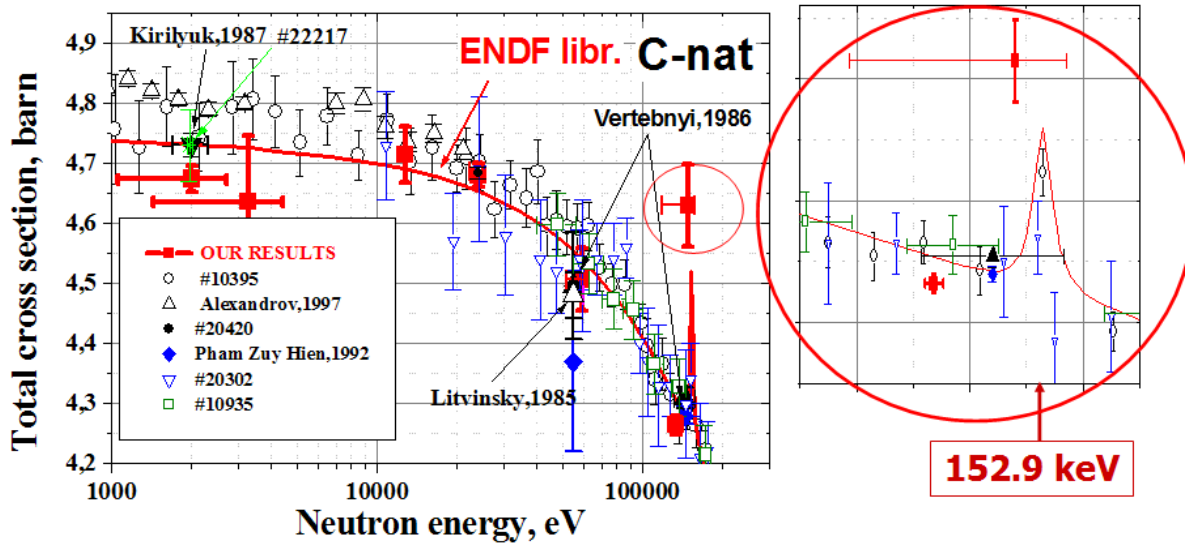

FIG.7. Our results for the C-nat. total neutron cross sections, experimental data from the database EXFOR and ENDF libraries. Right-hand picture presents the energy region in the vicinity of the 152.4 keV resonance on a large scale.

The value of the C-nat. total cross section, measured in our experiments with the neutron filter at the energy 148 keV and corrected on self-shielding effect, is considerably higher than ones, obtained by other authors.

As it follows from [8], the isotope ^{13}C, part of which in the natural carbon takes only 1.1%, has a strong p-resonance with the energy 152.9 ±1.4 keV (J=2, Γ_n=3.7 ± 0.7 keV). The value of the C-nat. total cross section, measured in our experiments with the neutron filter at the energy 148 keV and corrected on self-shielding effect, estimated by us as the averaged neutron cross section for the energy range (118.71-157.01) keV, points out that in this energy range there is a very strong resonance. Its neutron width may be much more than 3.7 keV. Later, in the theoretical work [9] it was predicted a presence of the ^{12}C resonance in the vicinity of 0.1 MeV. So, getting information about the resonance parameters in this energy region is really very important.

Can we get this information using the NFBT? Developing of new direction in the NFBT, described below, gives chase just this purpose.

7. New direction in the NFBT developing in the NPD

To get information about parameters of a single resonance it is possible, if we have **a set** of cross sections, averaged on a slightly different energy region.

There are two possibilities to modify the existing neutron filtered line: 1) to shift the main energy of the filtered spectrum; 2) to cut the main energy line of the filtered spectrum into several parts.

Shift of the filter energy may be realized owing to various processes:

1) Through reduction of the neutron energy in interaction between neutron and nuclei of the correcting sample-scatterer (see the top picture in Fig. 8);
2) Through energy dependence of the scattered neutrons from the angle of scattering (see the button picture in Fig. 8).

The second way is more preferable, as choosing different materials for the correcting sample-scatterer, we can change the energy of the neutron line in the very wide limits (see Fig. 8,

right). General idea of this approach is clearly expressed by the schemes presented in Fig. 9 for the ^{52}Cr example.

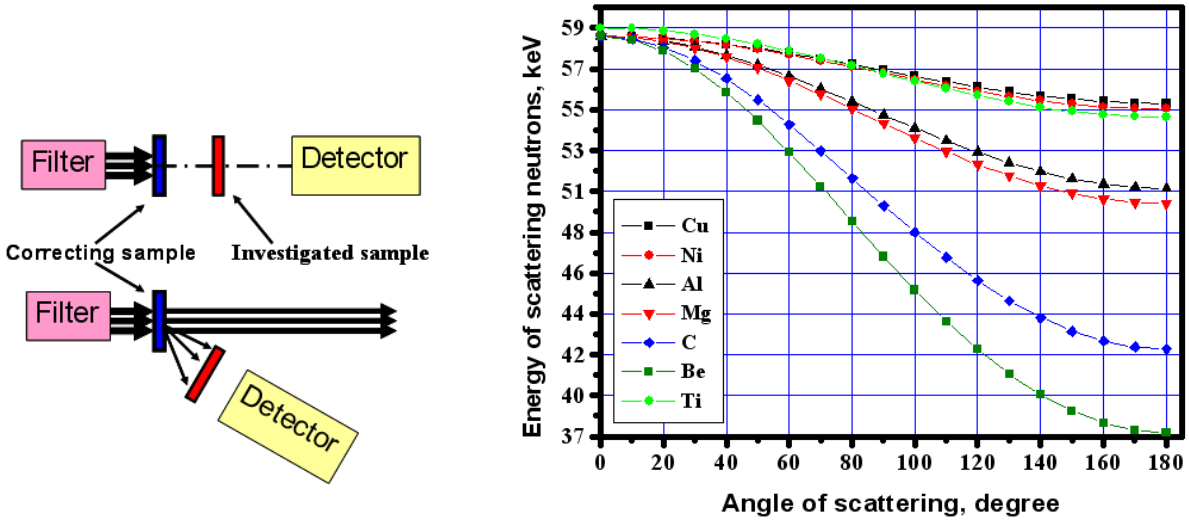

FIG.8. Schemes of measurements with the correcting sample-scatterer (left) and the scattering neutron energy against the angle of scattering for the incident energy 59 keV for different sample-scatterer (right).

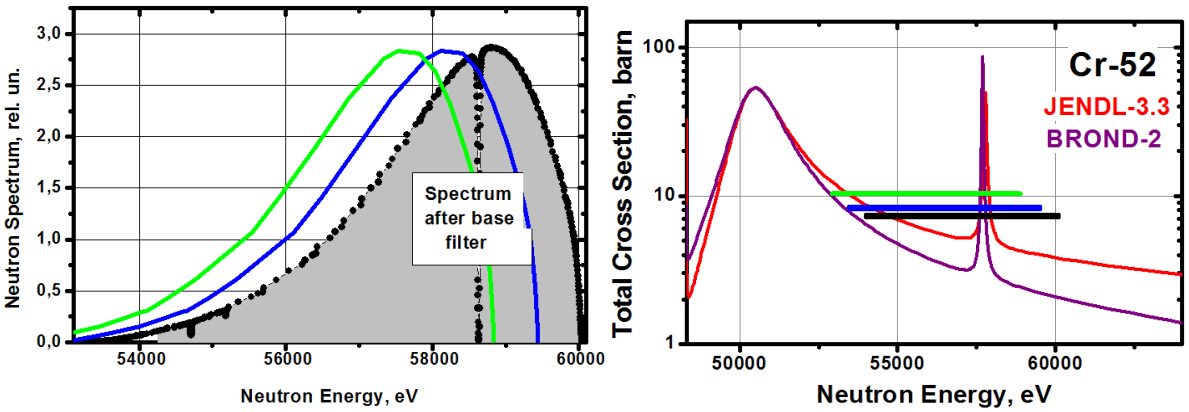

FIG.9. Shift of the spectrum and assumed set of the averaged neutron cross sections.

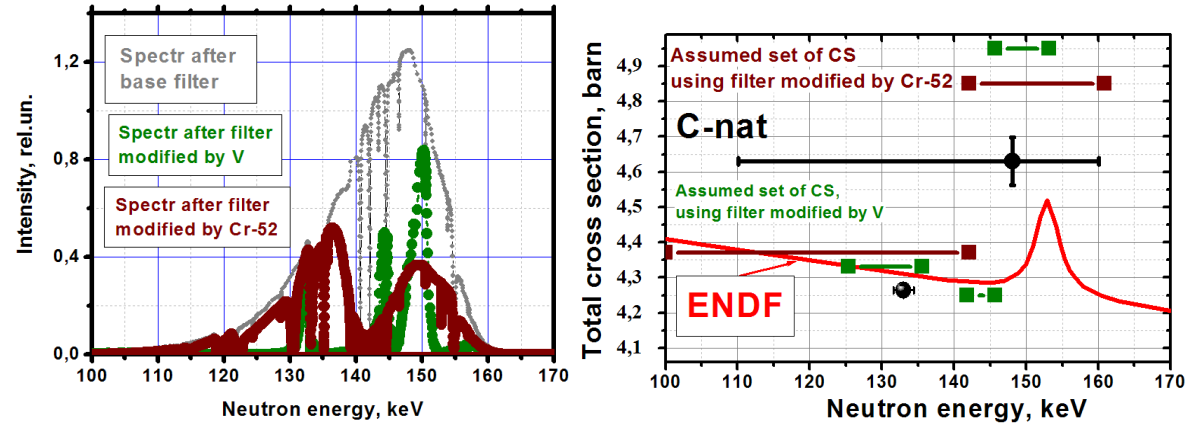

FIG.10. Two variants of cutting of the main energy line: using V – into 3 parts, using Cr-52 – into 2 parts and assumed sets of the averaged neutron cross sections.

It is possible to realize the ***cutting*** of the main energy line of the filtered spectrum into several parts, if we put into the filtered neutron beam the additional materials, which have very strong resonances in the energy range of the main filtered line. General idea of this approach is clearly expressed by schemes presented in Fig. 10 for the C-nat example.

Numerical simulation of the filter energy change for two of the existing base filters was performed and the first steps in this direction were realized in experiment. This activity will be continued in future.

Conclusion

- The NFBT at research reactors allows to get experimental data with high accuracy in energy region *from thermal energy to several hundred keV:* σ_{tot} < 1%; σ_{el} <3-4%; $d\sigma_{el}/d\Omega$ <5-6%; $\sigma_{n,\gamma}$ <4-6% .

- New directions in the NFBT (shift and cutting the main filter line) will allow to get information about the resonance parameters.

REFERENCES

[1] SIMPSON, O.D., MILLER, L.G., "A technique to measure neutron cross sections in the low keV energy region", Nucl. Instr. Meth. **61** (3) (1968) 245-250.

[2] GRITZAY, O.O., KOLOTYI, V.V., KALTCHENKO, O.I., Neutron filters at Kyiv Research reactor, Preprint KINR-01-6 (2001).

[3] CULLEN, D.E., The 1992 ENDF Pre-processing Codes, IAEA-NDS-39, Rev. 7, Feb. 1992.

[4] MACFARLANE, R.E., MUIR, D.W. The NJOY Nuclear Data Processing System, Version 91, LA-12740-M, October 1994.

[5] BRIESMEISTER, J.F. (Ed.), MCNP – A General Monte Carlo N-particle Transport Code, Version 4C, LA-13709 M (2000).

[6] GRITZAY, O., KOLOTYI, V., KLIMOVA, N., KALCHENKO, O., GNIDAK, M., KOROL', O.,VORONA, P., "Total Cross Section and Self-Shielding Effects of the Cr-52 Isotope Measured at Kyiv Research Reactor Neutron Filtered Beams", Proc. International Conference on Nuclear Data for Science and Technology , 2004, Santa Fe, NM, USA (2005) 969-972.

[7] GRITZAY, O., KOLOTYI, V., KLIMOVA, N., KALCHENKO, O., GNIDAK, M., KOROL', O.,VORONA, P., "Precision Neutron Total Cross Section Measurements for Natural Carbon at Reactor Neutron Filtered Beams", Proc. 12th International Symposium on Reactor Dosimetry, 2005, Gatlinburg, TN, USA, JAI **3** 8 (2006).

[8] MUGHABGHAB, S.F., Atlas of Neutron Resonances, Resonance Parameters and Thermal Cross Sections, 5th Edition, NNDC BNL Upton, USA.

[9] CANTON, L., AMOS, K., KARATAGLIDIS, S., PISENT, G., SVENNE, J.P., VAN DER KNIJFF, D., "Particle-unstable light nuclei with a Sturmian approach that preserves the Pauli principle", Nucl.Phys. **A790** (2007) 251-256.

Neutron capture cross-section measurements by high-resolution γ-ray spectroscopy

M. Oshima, T. Kin, S. Nakamura, K.Y. Hara, A. Kimura, Y. Toh, and M. Koizumi

Japan Atomic Energy Agency, Tokai,
Ibaraki 319-1195, Japan

Abstract. Multi-step cascades from the ^{62}Ni (n_{cold}, γ) ^{63}Ni reaction were studied via a γ-ray spectroscopy method. With a γ-ray detector arrays multiple γ-ray coincident events were accumulated. By selecting full cascade events from the capture state to the ground state, we have developed a new computer-based level construction method and it is applied to excited level assignment in ^{63}Ni.

1. Introduction

Accurate neutron reaction cross-sections of long-lived fission products and minor actinides are required for design of innovative reactor systems including fast breeder reactors (FBR) and accelerator driven systems (ADS). However, accuracy of the experimental data is not sufficient for this request at present.[1] The experimental methods are roughly categorized to either neutron activation and prompt γ-ray spectroscopic methods. The former approach has a merit of high sensitivity and is used widely, while it is limited to the case of unstable daughter nuclei only. On the contrary, the prompt γ-ray spectroscopic method can be applied to all nuclei because all the compound nuclei emit prompt γ-rays. It also is able to cover a wide energy range by combining it with a neutron time-of-flight (TOF) method. Another merit is that, by utilizing high resolution germanium (Ge) detectors, we can distinguish γ-rays from individual nuclei. Even when a sample includes large amount of impurities, one can extract cross sections accurately without their contributions. It is possible to derive neutron capture cross sections by summing all the intensities of ground-state and/or primary transitions[2,3]. In this method one needs to identify these transitions based on precise level scheme.

The method of "two-step cascade"[4] has succeeded in constructing a level scheme after neutron capture reactions. We have been developing the new method of excited level analysis incorporating multi-step cascades[5,6]. Multi-step cascades from the ^{62}Ni(n_{cold}, γ) ^{63}Ni reaction were studied via a γ-ray spectroscopy method. With the γ-ray detector array, STELLA, which consists of high-resolution Ge detectors and is installed at the Research Reactor (JRR-3) at Japan Atomic Energy Agency, multiple γ-ray coincident events were accumulated. We could determine the level scheme of ^{63}Ni up to 5.6 MeV. On the basis of the assignment of the ground-state transitions, we could derive the thermal-neutron capture cross section of ^{63}Ni.

In this report we describe at first the experimental technique and data analysis approach for the prompt γ-ray spectroscopy and neutron activation methods done at Research Reactor facilities of Kyoto University Reactor (KUR) and JRR-3. Then our new attempt of nuclear level assignment is presented including experimental apparatus, STELLA.

2. Cross-section Measurements by the Activation Method

In nuclear waste management, the major 29 fission products (FP's) shown in Table 1 are important nuclides as the targeted nuclides for transmutation. For the study of transmutation by using reactor neutrons, the accurate data are needed on the thermal-neutron capture cross-sections (σ_0) and the resonance integrals (I_0) in order to estimate the accurate reaction rates of these FP's. However, there are few cross section data on these FP's. If any, most of the data have large errors. By using the recently developed measuring equipments and the accurate -ray emission probability data, one could obtain more accurate cross-section data than that measured previously. Accordingly, we had started to measure the cross-sections of FP's to obtain the improved cross section data. In the beginning five nuclides, ^{137}Cs, ^{90}Sr, ^{99}Tc, ^{129}I and ^{135}Cs, were chosen from Table 1 because of their large fission yields and long half- lives, and then the cross sections of these nuclides were measured by the neutron activation and γ-ray spectroscopic methods. The nuclear waste usually contains a large amount of stable nuclei having the same atomic number as that of long-lived FP's. These stable nuclei absorb thermal neutrons during the neutron irradiation of the nuclear waste and affect the neutron economics; the transmutation probability of the targeted nuclei is penalised. Moreover, some of these stable nuclei breed more radioactive nuclei by the neutron capture process. It is also necessary for the transmutation study to accurately estimate these side-reactions caused by stable nuclei involved in the FP targets. Consequently, the cross sections of the stable nuclei, such as ^{127}I and ^{133}Cs, were measured.

TABLE 1. MAJOR 29 FISSION PRODUCT NUCLIDES OF HIGH IMPORTANCE FOR THE NUCLEAR WASTE MANAGEMENT

Nuclide	Half-Life (yr)	Nuclide	Half-Life (yr)	Nuclide	Half-Life (yr)
^{129}I	1.57×10^{7}	^{108m}Ag	418	^{155}Eu	4.7611
^{107}Pd	6.5×10^{6}	^{151}Sm	90	^{102}Rh	2.9
^{135}Cs	2.3×10^{6}	^{121m}Sn	55	^{125}Sb	2.7582
^{93}Zr	1.53×10^{6}	^{137}Cs	30.07	^{147}Pm	2.6234
^{99}Tc	2.1×10^{5}	^{90}Sr	28.78	^{134}Cs	2.062
^{126}Sn	1×10^{5}	^{113m}Cd	14.1	^{171}Tm	1.92
^{79}Se	6.5×10^{4}	^{152}Eu	13.542	^{109}Cd	1.270
^{94}Nb	2.03×10^{4}	^{93m}Nb	16.13	^{106}Ru	1.007
^{166m}Ho	1200	^{85}Kr	10.756	(^{14}C)	(5730)
^{158}Tb	180	^{154}Eu	8.593		
		^{146}Pm	5.53		

TABLE 2. RESULTS OF σ_0 AND I_0 FOR FP NUCLIDES

Nuclide	Half-Life	Previous Data (Author, Year)	JAEA Data
^{137}Cs	30 y	σ_{eff}＝0.11±0.03 b (Stupegia 1960) [7]	σ_0＝0.25±0.02 b I_0＝0.36±0.07 b （1990,1993,2000）[8-10]
^{90}Sr	29 y	σ_{eff}＝0.8±0.5 b (Zeisel 1966) [11]	σ_0＝15.3±1.3 /4.2 m b I_0=0.16 b (1994) [12] σ_0＝10.1±1.3 m b I_0＝104±16 m b (2001) [13]
^{99}Tc	2.1×10^{4}y	σ_0＝20±2 b I_0'＝186±16 b （Lucas 1977）[14]	σ_0＝22.9±1.3 b I_0＝398±38 b （1995）[15]
^{129}I	1.6×10^7 y	σ_0＝27±2 b I_0＝36±4 b （Eastwood 1958）[16]	σ_0＝30.3±1.2 b I_0＝33.8±1.4 b （1996）[17]
^{127}I	（stable）	σ_0＝4.7±0.2 b I_0＝109±5 b （Friedmann 1983）[18]	σ_0＝6.40±0.29 b I_0＝162±8 b （1999）[19]
^{135}Cs	3×10^6 y	σ_0＝8.7±0.5 b I_0＝61.7±2.3 b （Baerg 1958）[20]	σ_0＝8.3±0.3 b I_0＝38.1±2.6 b （1997）[21]
^{134}Cs	2 y	σ_{eff}＝134±12 b (Bayly 1958) [22]	σ_{eff}＝141±9 b (1999) [23]
^{133}Cs	(stable)	σ_0＝30.4±0.8 b I_0＝461±25 b （Baerg 1960）[24]	σ_0＝29.0±1.0 b I_0＝298±16 b （1999）[25]
^{166m}Ho	1.2×10^3 y	σ_0＝9140±650 b I_0＝1140±90 b （Masyanov 1993）[26]	σ_{eff}＝3±1 k b （2000）[27] σ_0＝3.11±0.82k b I_0＝10.0±2.7k b (2002) [28]

TABLE 3. RESULTS OF σ_0 AND I_0 FOR MA NUCLIDES

Nuclide	Half-Life	Previous Data (Author, Year)	JAEA Data
237Np	2.14×106 y	σ_0＝158±3 b I_0＝652±24 b （Kobayashi 1994）[29]	σ_0＝141.7±5.4 b I_0＝ 862±51 b （2003）[30] σ_0＝169±6 b (2006) [31]
238Np	2.1 d	No Data	σ_{eff}＝479±24 b (2004) [32]
241Am	432 y	σ_{0g}＝ 768±58 b I_{0g}＝1694±146 b （Shinohara 1997）[33]	σ_{0g}＝628±22 b I_{0g}＝3.5±2.5k b (2007) [34]
243Am	7370 y	σ_{0m}＝80 b , s0g＝4.3 σ_{0m+g}＝84.3 b （Ice 1966）[35]	σ_{eff}＝174.0±5.3 b (2006) [36]

3. Thermal-neutron capture cross-section of ^{107}Pd by prompt γ-ray spectroscopy

The long half-life (6.5×10^6 yr) and fission yield (3 % for ^{239}Pu) of ^{107}Pd make it an important fission product in studies of nuclear transmutation. In the case of ^{107}Pd, no direct measurement of the thermal-neutron capture cross-section (σ_0) has been reported. Because the ^{107}Pd (n_{th},γ) reaction leads to the stable nuclide ^{108}Pd, it is impossible to measure this cross section using an activation method. The technique of measuring intensities of prompt γ rays following thermal-neutron capture reaction can be employed to determine σ_0. Therefore, this work was undertaken to obtain σ_0 for the ^{107}Pd (nth, γ) ^{108}Pd reaction by prompt γ rays spectroscopy.

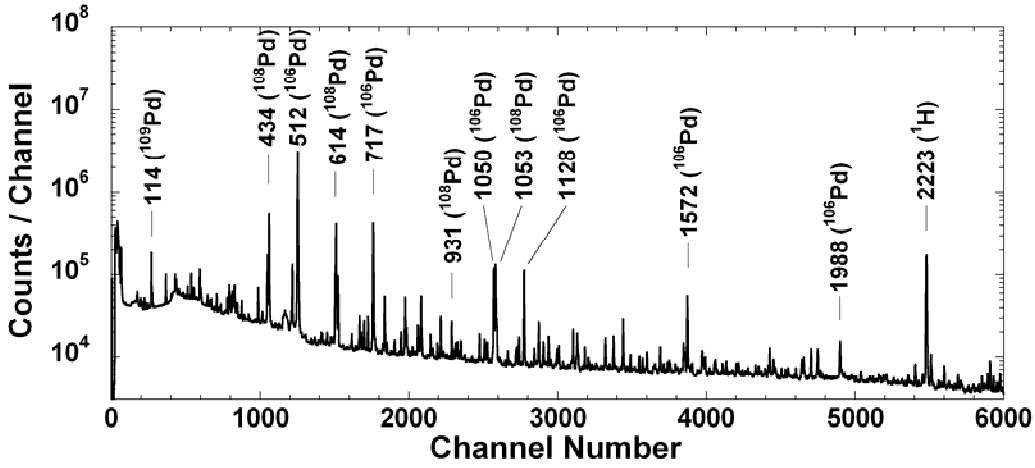

FIG.1. Prompt γ-ray spectrum from thermal-neutron capture by the ^{107}Pd sample.

The experiments were performed using the internal target facility at the 8-MW Los Alamos Omega West Reactor. The target position was at the centre of the graphite thermal column, of which thermal- neutron flux was about 6×10^{11} n/(sec cm^2) and the Cd(In) ratio was about 2×10^3. The γ rays emitted in the (*n*th,γ) reaction were measured with a 26-cm^3 coaxial Ge (Li) detector positioned inside a 20cm-outerdiameter×30cm-long NaI(Tl) annulus. The Pd sample weighed 201.4 ± 0.1 mg and contained 15.54 ± 0.05% of ^{107}Pd. A 100.0 ± 0.1 mg sample of $(CH2)_n$ was placed at the target position together with the Pd sample in the thermal column. The capture cross-sections obtained in this work are determined in the basis of standard cross-section 332.6±0.7 mb for ^{1}H. Figure 1 shows an example of the prompt -ray spectrum for the

combined Pd and $(CH2)_n$ samples. Prominent γ rays due to the $^{105, 107, 108}$Pd Pd (*n*th, γ) reactions were observed.

The γ rays feeding the ground states were identified using the known level information. Summation of their intensities yields a lower limit for σ_0, *i.e.*, $\Sigma I_\gamma(1+\alpha)= \sigma_0$. Here, the quantity α_T is an internal conversion coefficient. To test the effectiveness of the analysis method, σ_0 also was determined for ^{105}Pd. Because σ_0 for ^{105}Pd is large (20.0 ± 0.3 b), and because this isotope made up a large fraction of the Pd sample, prompt γ rays due to the ^{105}Pd (*n*th, γ) ^{106}Pd reaction were easily observed as shown in Fig.1. The present results are tabulated in Table 4 together with the previous measurement and evaluations. The thermal- neutron capture cross-section of ^{107}Pd was measured using prompt γ-ray spectroscopy. The intensities of prompt γ-ray transitions feeding the ground state of ^{108}Pd were summed to determine a lower limit of 9.16 ± 0.27 b for thermal neutron capture cross section. The present result is about five times larger than current evaluations.

TABLE 4. EXPERIMENTAL AND EVALUATED DATA FOR ^{107}Pd AND ^{105}Pd CROSS SECTIONS.

References		σ_0 (b) for ^{107}Pd	σ_0 (b) for ^{105}Pd
Mughabghab *et al*. [37]	1981	1.8 ± 0.2	21.0 ± 1.5
Table of Isotopes 8. ed.[38]	1998	1.8 ± 0.2	20.0 ± 3.0
JENDL-3.3 [39]	2002	2.0071	20.25
Firestone *et al.* [40]	2005	-	21.1 ± 1.5
Present Result [41]		9.16 ± 0.27	19.1± 0.5

* Prompt γ-ray analysis

4. Development of excited level assignments for prompt γ-ray spectroscopy

The prompt γ-ray detection method is useful for neutron capture cross section measurements of minor actinides (MA) and long lived fission products (LLFP): it may cover a wide energy range if combined with neutron time-of-flight (TOF) method. Another merit is that, by utilizing high resolution germanium (Ge) detectors, we can distinguish γ-rays from individual nuclei. Even when a sample includes large amount of impurities, it becomes possible to extract cross sections accurately for the nuclei of interest. It is useful to derive neutron capture cross sections by summing all the intensities of ground-state or primary transitions[2,3]. In this method we need to identify those transitions based on precise level scheme. Generally the capture state locates at the excitation energy of 2-10 MeV and the related levels often amount to more than 100. It is a hard task to identify them precisely.

The method of "two-step cascade"[4] seems to be successful in constructing a level scheme after neutron capture reactions. We propose a new method of excited level analysis incorporating multi-step cascades with ease and reliability. The method is based on automatic analysis utilizing a PC and can derive candidates of excited levels in a short time. In this report we describe the analysis method and how it is confirmed by auxiliary analysis method.

4.1. The method

One way to analyze a level structure is to apply the Ritz additivity rule, in which the energy of a crossover transition coincides with the sum of those for cascade transitions. The application of this method is limited under the existence of large number of cascade in general neutron capture reactions. Thus we adopt γ-ray coincidence method. Here we construct a level scheme based on the γ-ray coincidence relationships. However, we do not know the order of the coincident γ-rays because the resolving time of the Ge detectors is in the order of 10 n sec and is usually larger than the lifetimes (typically less than p sec) of the excited levels. It is crucial to decide the

location of γ-rays in a level scheme. In this section we describe the actual process of experimental and analytical procedures for the level construction.

4.2. Multiple γ-ray Coincidence Measurement with a γ-ray Detector Array

We have constructed the cold neutron beam line C2-3-2 in Japan Research Reactor, JRR-3. The neutron flux is 1.4 x 10^7 n/cm^2/sec. A γ-ray detector array, STELLA[5], is composed of eight EURYSIS 4x70x80 BC type clover Ge detectors (125% detection efficiency relative to 3"fx 3" NaI scintillator) and four coaxial Ge detectors (70-100%) coupled with surrounding BGO suppressors. The total detection efficiency amounts to 14% for single γ-ray at 1.0MeV as shown in Fig. 2.

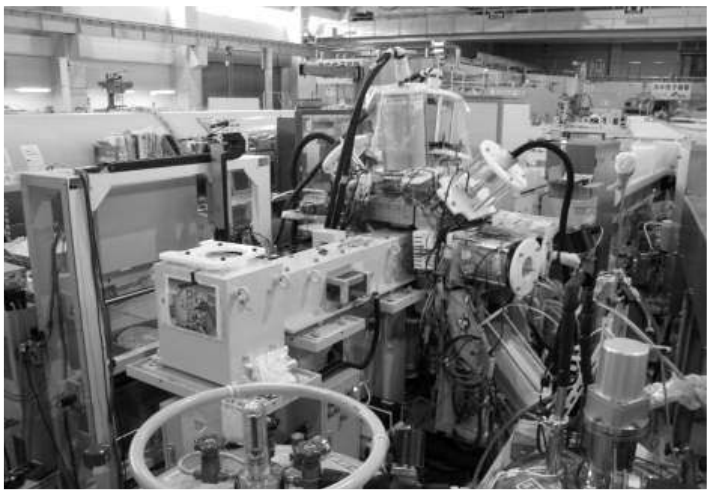

FIG.2. A γ-ray detector array, STELLA, at JRR-3 guide hall facility.

The facility is equipped with liquid nitrogen supply system, enabling the detector system operational for the whole year. The auto sampler can change 150 samples sequentially and automatically.

A melamine (C3H6N6) sample of 498 mg was irradiated with the neutron beam for three days. The Q value of ^{15}N is 10.833 MeV.

4.3. A new analysis method

4.3.1. Level spectrum construction of all combinations

After the energy calibration for the γ-ray coincidence events, a projected energy spectrum is obtained as shown in Fig. 3. We create a sum energy spectrum by adding all the γ-ray energies in each event. There appears a peak at the neutron separation energy, corresponding to the events of all the γ-rays absorbed by the detector system. By gating on this peak, we can select events with complete cascades (CC) from the capture state to the ground state.

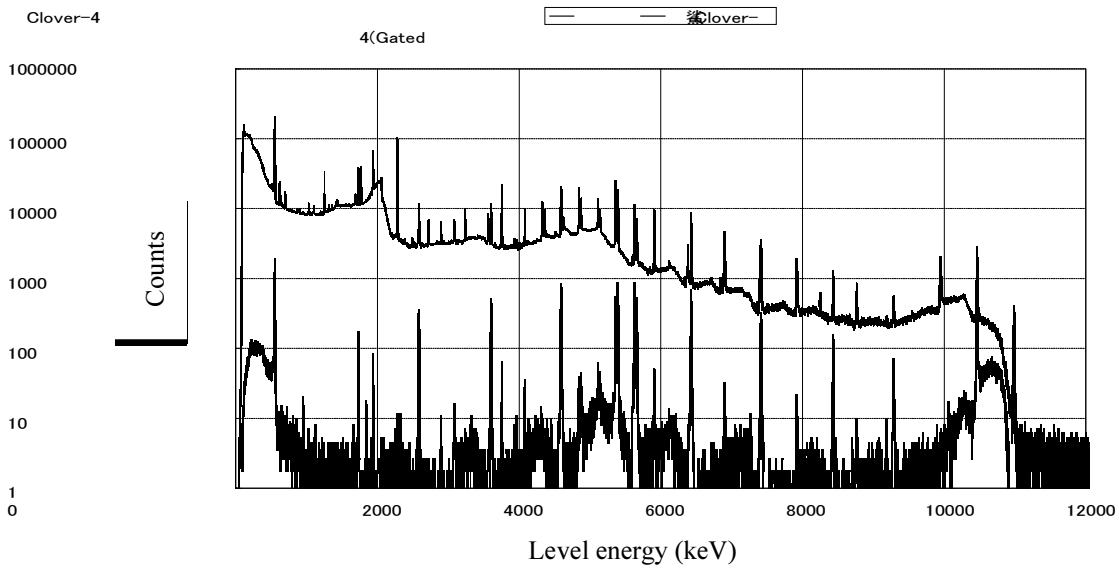

FIG.3. Upper spectrum: singles for ^{15}N, lower curve: projection of singles.

From the complete set of γ-ray cascade we can assume the excitation energies of intervening excited levels. If the γ-ray multiplicity is three, there are six combinations of cascade orders. As previously discussed we do not know the order of this cascade at this moment. We sort the CC events to create a histogram for all the possible combinations of level energies. Thus we get a level energy spectrum as shown in Fig. 4. Here we notice that there appear many peaks corresponding to real excited levels. This is due to the fact that there exist many passes traversing the real levels. Thus the level energy spectrum can be regarded as a probability distribution.

4.3.2. Probability selection and iteration

The apparent feature in Fig. 4 is that the distribution is symmetric at half the energy of neutron separation energy. This is because the inversed distribution of level energies appears with equal probability. In order to avoid such pseudo peaks, we need a selection rule in the sorting process. We select four lowest-lying well-established levels as marked in Fig. 3, and intensify the probability of those peaks by a factor of 1,000. We use it in the following sorting process as a probability distribution: in process a, we calculate a sum of probabilities for the assumed level energies; the sum is thought to stand for the probability of the assumed sequence. In the next sorting process we choose the most probable sequence and increment one count only for this sequence. After sorting for the entire event we get a modified spectrum.

The γ-rays connected to the well established levels may be placed as transitions from higher-lying levels and further selection is expected to work. We repeat this process until convergence.

4.3.3. Elimination of annihilation events related to 511 keV

There is a pair of weak peaks for each prominent peak with a separation of 511 keV. This phenomenon obviously corresponds to annihilation process of positrons produced in the pair creation in the Ge crystals. The effective method to eliminate those peaks is to discard the events including 511 keV single gamma or two gamma quanta, sum of which is equal to 511 keV. After this procedure we got the final spectrum as shown in Fig. 5.

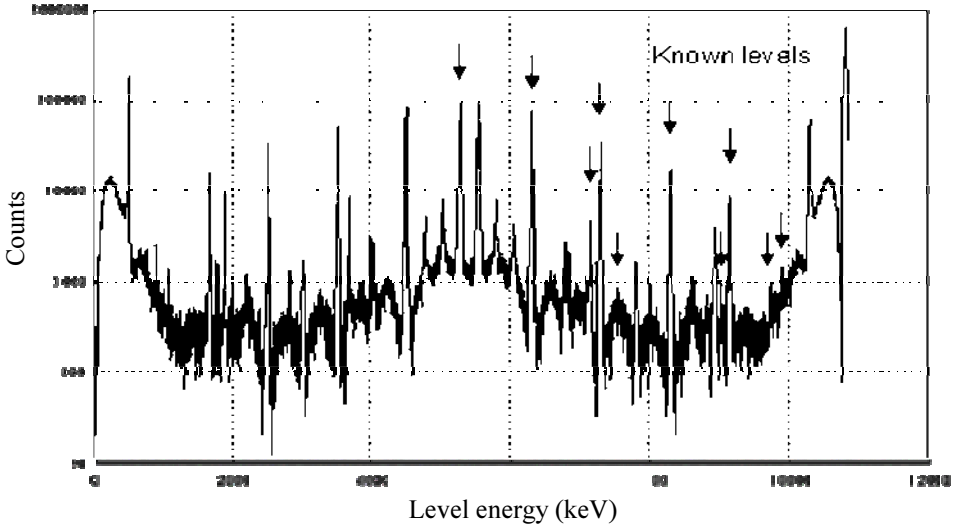

FIG.4. Level energy spectrum for ^{15}N. The arrows show the levels established before.

4.3.4. Level identification and confirmation step

Peaks appeared in the final spectrum in Fig. 5 are searched and the excited states are identified. However, it should be noted that some pseudo peaks may still appear due to the background contributions at the full energy peak in the sum energy spectrum (shown in Fig. 3) and distortions of probability distribution by Compton back ground. Those pseudo peaks can be eliminated by creating a γ-ray energy spectrum gated on each level peak and by examining whether the γ-ray peaks appeared in this spectrum are consistent with the assumed level to the known levels of the level of interest.

4.3.5. Analysis results

The observed fourteen levels in Fig. 4 are consistent with the levels reported before for ^{15}N. The intensities of ground-state transitions have been determined down to 0.1% of the total intensity. Thus the validity of this method is confirmed for ^{15}N.

Next this method is applied to the $^{62}Ni(ncold, \gamma)^{63}Ni$ reaction. A metallic ^{62}Ni sample of 120 mg was irradiated with the neutron beam for three days and the multiple γ-ray events of 1.3x109 have been accumulated by using the STELLA array. Neutron separation energy of ^{63}Ni is 6838.64 keV. Again after the same procedure as in the case of ^{15}N, we established a level scheme of ^{63}Ni as shown in Fig. 6. We could confirm previously known 14 levels of ^{63}Ni . In addition to those, candidates of 5 levels and 19 transitions have been newly derived, including 5 ground-state and 5 primary transitions.

5. Conclusion and summary

Nuclide discrimination is effective for accurate determination of neutron capture cross sections, especially for low purity MA and LLFP samples. We use a high resolution Ge spectrometer for this purpose. The prompt γ-ray spectroscopy method utilizing ground state transition or primary transition is useful to extract the capture cross sections. To identify those transitions, multiple γ-ray coincident events were accumulated by the spectrometer. By selecting full cascade events from the capture state to the ground state, we have developed a new PC-based semi-automatic level construction method. At first, the well studied ^{15}N nucleus has been studied. The known 14 levels have been derived. The detection limits of ground state transitions are 0.1%. After this method has been applied to the analysis of excited levels in ^{63}Ni. The method is expected to be useful for the neutron capture cross section measurements through the assignment of ground-state or primary transitions.

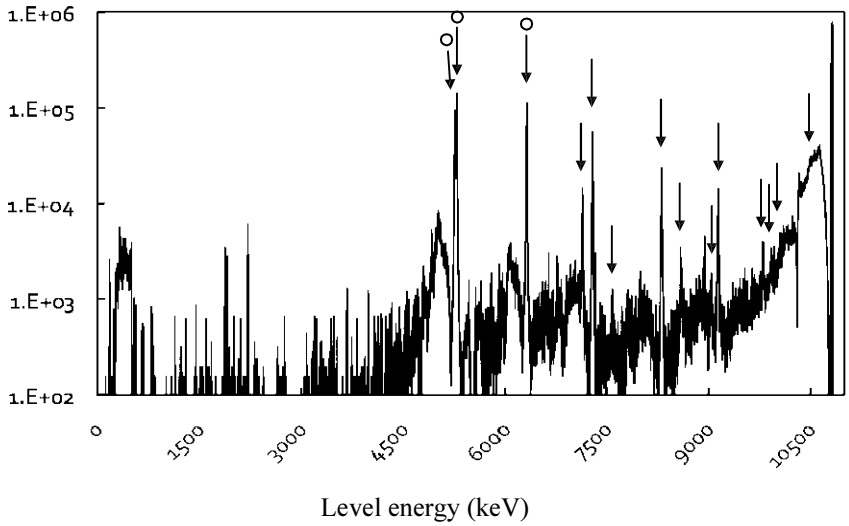

FIG.5. Level energy spectrum after process b and c. The circle indicates the well-established transitions and the arrows correspond to the known levels.

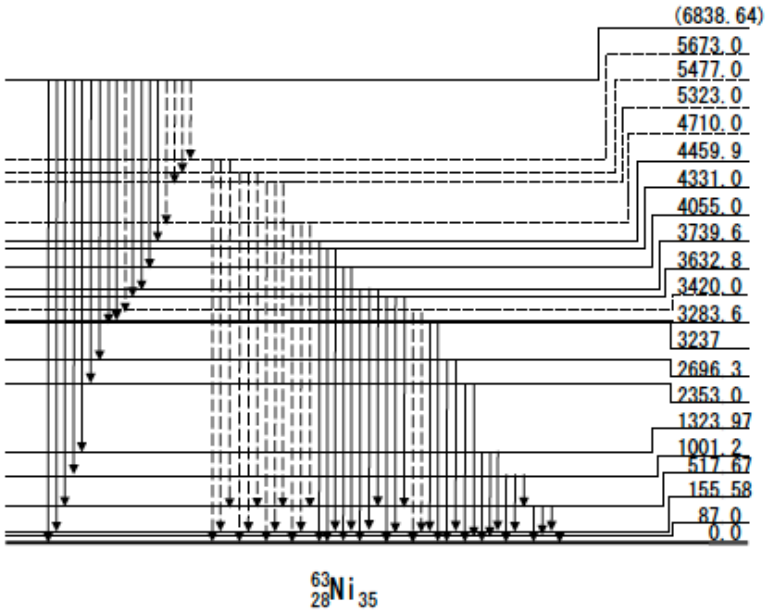

FIG.6. Excited level structure derived for ^{63}Ni. Solid lines are known levels. Dashed lines indicate the transitions and levels newly assigned in the present analysis. Dotted lines are uncertain ones. The results are preliminary.

REFERENCES

[1] See, for example, OECD/NEA Report NEA/WPEC-26 (2008).
[2] M. Oshima, *et al*., Proceedings of the 2007 International Conference on Nuclear Data for Science and Technology (2008) 603-606.
[3] K. FURUTAKA, *et al*., Nucl. Sci. Tech. **41** (2004) 1033.
[4] V. A. BONDARENKo, *et al*., Fizika **B 11** (2002) 201.
[5] T. KIN, *et al*., Proceedings of the 13th International Symposium on Capture Gamma-Ray Spectroscopy and Related Topics (AIP Conference Proceedings 1090) (2009) 575-576.
[6] M. OSHIMA, *et al*., Proceedings of the 13th International Symposium on Capture Gamma-Ray Spectroscopy and Related Topics (AIP Conference Proceedings 1090) (2009) 386-390.
[7] D.C. STUPEGIA, Nucl. Energy **A12** (1960) 16.
[8] H. HARADA *et al*., Nucl. Sci. Technol. **27** No.6 (1990) 577.
[9] T. SEKINE *et al*., Nucl. Sci. Technol. **30** No.11 (1993) 1099.
[10] H. WADA *et al*., Nucl. Sci. Technol. **37** No.10 (2000) 827.
[11] G. ZEISEl, Acta. Phys. Austr. **23** (1966) 5223.
[12] H. HARADA *et al.,* Nucl. Sci. Technol. **31** No.3 (1994) 173.
[13] S. NAKAMURa *et al*., Nucl. Sci. Technol. **38** No.12 (2001) 1029.
[14] M. LUCAS *et al*., IAEA-TC-119/14 (1977) 407.
[15] H. HARADA *et al*., Nucl. Sci. Technol. **32** No.5 (1995) 395.
[16] T.A. EASTWOOD, *et al.,* Proc. 2nd Int. Conf. Peaceful Uses of Atomic Energy, Geneva, United Nations, New York, **16** (1958) 54.
[17] S. NAKAMURA *et al*., Nucl. Sci. Technol. **33** No.4 (1996) 283.
[18] L. FRIEDMANN *et al.*, Radiochemica Acta **33** (1983) 182.
[19] S. NAKAMURA *et al.,* Nucl. Sci. Technol. **36** No.3 (1999) 223.
[20] A.P. BAERG *et al.,* Can. J. Phys. **36** (1958) 863.
[21] T. KATOH *et al*., Nucl. Sci. Technol. **34** No.5 (1997) 431.
[22] A.P. BAERG *et al.,* Can. J. Chem. **38** (1960) 2528.
[23] T. KATOH *et al*., Nucl. Sci. Technol. **36** No.8 (1999) 635.
[24] A.P. BAERG *et al.,* Can. J. Chem. **38** (1960) 2528.
[25] S. NAKAMURA *et al*., Nucl. Sci. Technol. **36** No.10 (1999) 847.
[26] S.M. MASYANOV *et al*., At. Energy **73** (1993) 673.
[27] H. HARADA *et al*., Nucl. Sci. Technol. **37** No.9 (2000) 821.
[28] T. KATOH *et al*., Nucl. Sci. Technol. **39** No.7 (2002) 705.
[29] K. KOBAYASHI *et al.,* Nucl. Sci. Technol. **31** No.12 (1994) 1239.
[30] T. KATOH *et al*., Nucl. Sci. Technol. **40** No.8 (2003) 559.
[31] H. HARADA *et al*., Nucl. Sci. Technol. **43** No.11 (2006) 1289.
[32] H. HARADA *et al.,* Nucl. Sci. Technol. **41** No.1 (2004) 1.
[33] N. SHINOHARA *et al.,* Nucl. Sci. Technol. **34** No.7 (1997) 613.
[34] S. NAKAMURA *et al*., Nucl. Sci. Technol. **44** No.12 (2007) 1500.
[35] C.H. ICE DUPONT, Savannah River Reports, **66** 69 (1966).
[36] M. OHTA *et al*., Nucl. Sci. Technol. **43** No.12 (2006) 1441.
[37] S.F. MUGHABGHAB *et al.,* Neutron Cross Section, Vol.1, Academic Press, NewYork (1981).
[38] R.B. FIRESTONE, V.S. SHIRLEY, Table of Isotopes, 8th Ed., John Wiley & Sons, New York (1996).

[39] K. SHIBATA *et al*., Nucl. Sci. Technol. **39** (2002) 1125.
[40] R.B. FIRESTONE *et al*., Proc. 12th Int. Symp. Capture Gamma-Ray Spectroscopy and Related Topics (2006) 389.
[41] S. NAKAMURA *et a*l., Nucl. Sci. Technol. **44** No.2 (2007) 103.

The Out-of-core Neutron Irradiation Facility of HANARO for Measurement of Neutron Cross-section

Myong-Seop Kim[a], Yeongduk Kim[b], Kwang-Pyo Hong[a], In-Cheol Lim[a]

[a] Korea Atomic Energy Research Institute,
1045 Daedeok-daero, Yuseong, 305-353, Daejeon,
Korea
[b] Department of Physics,
Sejong University,
Seoul 143-747,
Korea

Abstract. Neutron cross-section measurements using the out-of-core thermal neutron irradiation facility of HANARO are introduced. This facility was designed and constructed using a long beam tube and a fast neutron and gamma-ray filter composed of thick silicon and bismuth single crystals. It gives a thermal neutron field with a flux over 1×10^9 n/cm^{2}s and a Cd ratio over 150 and has a spacious irradiation room. It can be used for various experiments, and one of the applications is the measurement of the thermal neutron cross-sections for several nuclides. In the design stage of the facility, the total neutron cross-sections of the silicon and bismuth crystals were measured by using the neutron transmission and time-of-flight method. For the silicon single crystal, the measured cross-section showed good agreement with the calculated value based on the semi-empirical formula. The measurements for the bismuth crystal were much larger than those anticipated by calculation. From the result, it was confirmed that several parameters related to the Bragg scattering should be considered in the neutron transmission through the bismuth single crystal. On the other hand, the thermal neutron capture cross section for the W-180 nucleus was measured by using the activation and gamma-ray detection method. A natural tungsten foil was irradiated in this facility for 5 hours, and finally the capture cross-section was obtained at a value of 22.6±1.7 b. Measured data for the cross-section for W-180 is very rare, but the production of W-181 is very important since it is a useful radioisotope neutrino source for the various basic neutrino experiments. From the results, it was confirmed that the out-of-core neutron irradiation facility of HANARO would be useful for measuring neutron cross-sections.

1. Introduction

HANARO of the Korea Atomic Energy Research Institute (KAERI) at Daejeon is an open-tank-in-pool type research reactor with a thermal power of 30 MW and heavy water reflector. The main purposes of HANARO are material research using thermal and cold neutron beams, material irradiation tests including nuclear fuel test, neutron activation analysis, isotope production and neutron transmutation doping. It has 7 horizontal neutron beam tubes and 36 vertical irradiation holes for various experiments. At one of the horizontal tangential beam tubes, an out-of-core thermal neutron irradiation facility was designed and constructed. It gives a thermal neutron field over 1×10^9 n/cm^{2}s which can not be easily obtained using usual horizontal beam tube. Furthermore, it is possible to install various experimental setups by virtue of the spacious irradiation room with enough shielding. It can be used for various neutron beam applications which require a higher thermal neutron flux such as studies in the boron neutron capture therapy (BNCT), dynamic neutron radiography, etc. The thermal neutron cross-section measurements for several materials can also be another field of application for the facility.

In this work, two kinds of activities for the neutron cross-section measurement related to the HANARO out-of-core neutron irradiation facility are introduced.

2. Brief description of HANARO out-of-core neutron irradiation facility

The out-of-core neutron irradiation facility was installed at the end of a typical narrow tangential beam tube of HANARO. The length of the beam tube from the nose at the heavy water reflector tank is over 400 cm. This facility was originally designed and constructed for the purpose of the BNCT applications. Due to its design characteristics, a sufficient epithermal neutron flux for the BNCT cannot be obtained in HANARO. So, the thermal neutron beam facility was planned for the BNCT treatment using local irradiation after debulking and for various pre-clinical studies such as small animal irradiations. In order to prevent contamination by fast neutrons and gamma-rays and to transmit thermal neutrons as much as possible, a single crystal filter system composed of silicon and bismuth was applied. Table I shows a description of the characteristics of the facility.

TABLE I. CHARACTERISTICS OF THE HANARO OUT-OF-CORE NEUTRON IRRADIATION FACILITY [1]

Components	Specifications	Figures
Radiation filter	A silicon single crystal A bismuth single crystal	40 cm in length and 20 cm in diameter 15 cm in length and 10 cm in diameter
Water shutter	Inner diameter Axial length Volume of the inner part Time required for charging and drain of water	23.6 cm 135 cm 60 liters 2-3 minutes (compressed air and electric pump)
Beam collimator	Beam hole diameter Thickness of the cone-shaped collimator Material	10, 15 cm 1.5 cm or more Sintered mixture of $^{6}Li_2CO_3$ powder (95 % enriched in Li-6) and high density polyethylene powder
Beam monitoring	A fission chamber An ion chamber	20.3 cm in length and 2.6 cm in diameter 4.4 cm in length and 1.9 cm in diameter
Irradiation room	Height of the irradiation room Internal Bunker Space Distance from the beam exit to the wall of the room	350 cm 550 cm × 400 cm about 200 cm to 550 cm,
Neutron beam	Thermal neutron flux Cadmium ratio for Au	1.5×10^{9} n/cm^{2}s at beam exit About 150

3. Measurements of the total neutron cross-sections for Si and Bi single crystals

The out-of-core neutron irradiation facility uses a radiation filter consisting of thick silicon and bismuth single crystals in order to obtain a sufficient thermal neutron flux with low level contamination of fast neutrons and gamma-rays. In the design stage of the facility, the total neutron cross-sections of the silicon and bismuth crystals inside the radiation filter were

measured by using the neutron transmission and time-of-flight method since the cross-sections of the filter materials were the key parameters for the performance of the facility.

3.1. Experimental method

In the measurements, we used a beam tube where bismuth shielding was installed for gamma-ray attenuation. Silicon and bismuth crystals were installed next to the shielding, and the transmitted neutron beam through the crystals was measured using time-of-flight method. Fig. 1 shows the schematic diagram of the time-of-flight spectroscopy system for cross-section measurement.

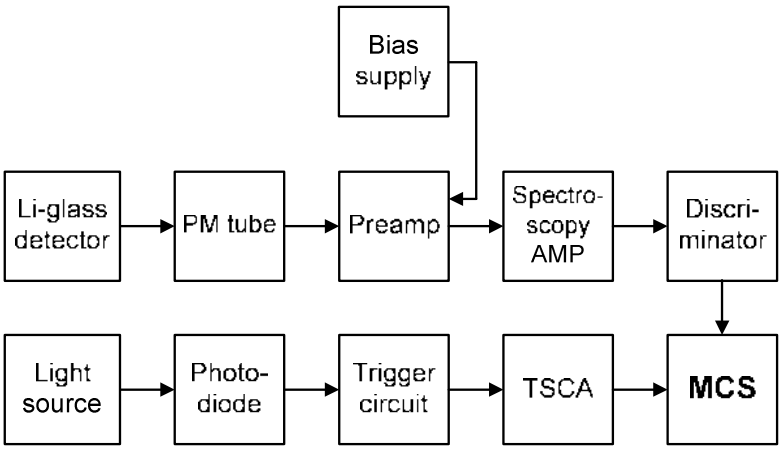

FIG.1. Schematic diagram of the time-of-flight spectroscopy system for cross-section measurement.

The neutron spectra before and after a transmission to the thick silicon and bismuth crystals were measured by using a time-of-flight spectrometer, and the neutron cross-sections were deduced from the measured spectra. The energy ranges in which the cross-sections were measured were 2~400 meV for silicon and 2~200 meV for bismuth. The silicon single crystal used in the transmission experiment was 40 cm in length and 20 cm in diameter. The bismuth crystal part was 15 cm in length and 11 cm in diameter.

The neutron was detected by a 0.32 cm thick ^{6}Li-glass scintillation detector, and the neutron flight length after the chopper to the detector was 289 cm. The time of flight was measured by a multi-channel scaler (MCS) connected to the photo collimator rotated at the same phase as that of the chopper. The dwell time of MCS was 10 μsec. The rotating speed of the chopper was set to be 3,000 rpm.

The time-of-flight spectra were taken with and without Si and Bi crystals, and, at each step, the effect of the fast neutron background was measured by installing a 3 mm cadmium plate in front of the chopper. The neutron total cross-section at the energy E_i corresponding to a channel number i was obtained from the transmission TOF spectra after background subtraction as follows,

$$\sigma(E_i) = -\left(\frac{1}{N_s t}\right)\ln\left(r\,\frac{S_{in}(E_i) - B_{in}(E_i)}{S_{out}(E_i) - B_{out}(E_i)}\right) \tag{1}$$

where

N_s is the atomic number density of a sample,
t is the transmission length in the sample,
r is the ratio of the total incident neutron intensities during data taking,
S is the signal height with sample,
B is the background signal height.

The channel-wavelength calibration was performed by the reflection experiment for the PG (Pyrolytic Graphite) using the same TOF system, and the channel-wavelength relationship was obtained as follows.

$$\lambda = 0.01326 \times C - 0.324 \tag{2}$$

where

λ is the neutron wavelength (angstrom),

C is the channel number of the MCS.

3.2. Results and discussion

Figure 2 shows the measured neutron cross-section of silicon in the thick single crystal. In the figure, the calculated value shows the semi-empirical formula obtained by fitting the previous experimental results with the fitting parameters of the material constant and the characteristic Debye temperature [2]. This formula contains the absorption cross-section due to the nuclear capture process and the thermal diffuse cross-section, but not the Bragg scattering. The statistical uncertainties of the measurements are within 10%. For the silicon single crystal, the measured neutron cross-section shows good agreement with the calculated value based on the semi-empirical formula.

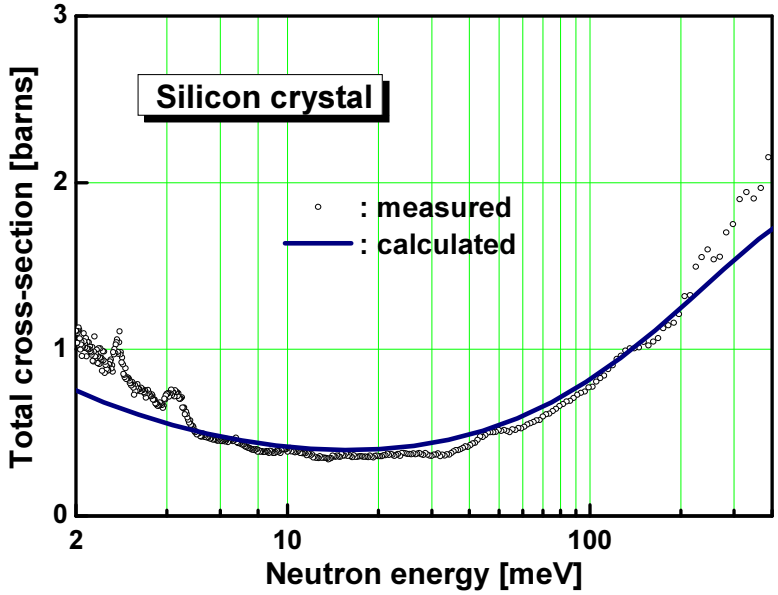

FIG.2. The total neutron cross-section of silicon in the thick single crystal.

Figure 3 shows the measured neutron cross-section of bismuth in the thick single crystal. From this figure, it is confirmed that the measured cross-section value is much larger than the calculated one. The discrepancy between the measured and the calculated values can be explained by having taken no account of the Bragg or elastic scattering. Since for the bismuth single crystal it is difficult to avoid the elastic scattering due to the large mosaic spread, the disturbance of the neutron transmission due to the Bragg scattering cannot be negligibly small [3]. Therefore, it is confirmed that several parameters related to the Bragg scattering such as the standard deviation of the mosaic spread and the cutting plane along the neutron path inside the crystal should be considered in the neutron transmission experiment through the bismuth single crystal.

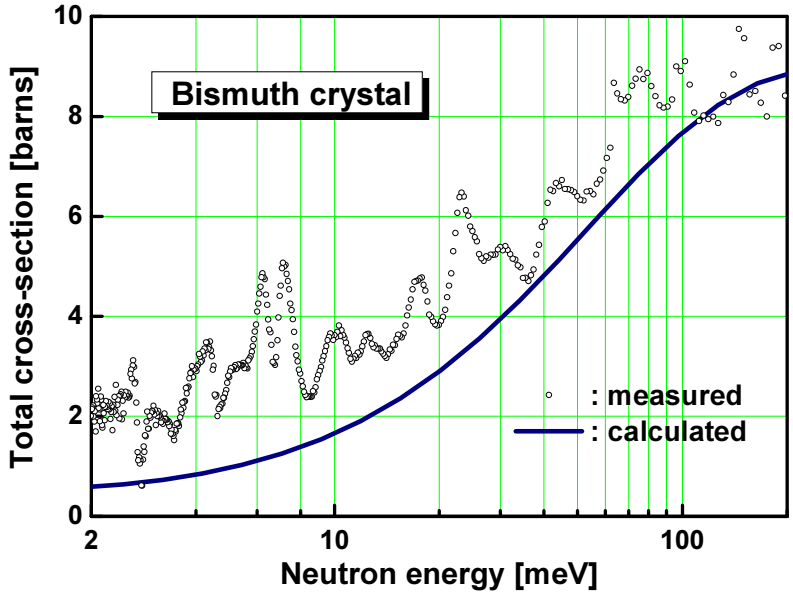

FIG.3. The total neutron cross-section of bismuth in the thick single crystal.

4. Measurement of the thermal neutron capture cross section of W-180

The artificial neutrino source (ANS) is a radioisotope which emits the neutrinos from its beta decay process. It is used for the calibration of a neutrino detector and for the study of several neutrino properties. There are several candidate isotopes for the ANS such as Cr-51, Ar-37, W-181, Tm-170 and Pm-147. Among them, W-181 has good properties for an artificial neutrino source, but the production cost is relatively high due to the low abundance of W-180 at a level of 0.12%. Therefore, the thermal neutron capture cross section of W-180 is an important parameter in the aspect of the W-181 production. However, there are very few measurements with regard to the thermal neutron capture cross section for this nucleus. And the uncertainty of this value is very large. So, the thermal neutron capture cross section of the W-180 nucleus was measured using the activation experiments at the HANARO out-of-core irradiation facility and the gamma-ray detection method.

In these measurements, natural tungsten foils were irradiated at the out-of-core irradiation facility, and the gamma-rays from the W-181 decay were measured. The W-180 capture cross section was obtained by a comparison of the measured activities of W-185 and W-187, i.e., the capture cross section of W-180 with respect to the capture cross sections of W-184 and W-186 was obtained in order to avoid the potential systematic effects caused by various irradiation and sample conditions. Details of the experimental setup for W-180 cross-section measurement are shown in Table II. The contribution of the non-thermal neutron to the measurements is negligible since the cadmium ratio for W-187 is very high as shown in the same table. The 136.3 keV peak area of W-181 was obtained 81 days after irradiation to eliminate the contribution of the 134.2 keV gamma-rays from W-187.

The thermal neutron flux at the sample position was obtained using the known cross-sections of W-185 and W-187: its value is $(6.84 \pm 0.28)\times10^{8}$ n/cm^{2}s. The capture cross section of W-180 was calculated using the known cross sections of 1.76 ± 0.09 b for W-184 and 39.5 ± 2.3 b for W-186. The final W-180 capture cross section thus obtained was 22.6 ± 1.7 b. This value is about 25% smaller than that of Pomerance [5], and the uncertainty was much less.

TABLE II. DETAILS OF THE EXPERIMENTAL SETUP FOR W-180 CROSS-SECTION MEASUREMENT [4]

Components	Specifications	Figures
Sample	Tungsten foils (99.9% pure)	50.1×50.1×0.138 mm (6.644 g)
Irradiation condition	Irradiation time Decay time at irradiation room Measured Cd ratio for W-187 Flux variation for irradiation Thermal neutron flux at sample position	5 hours 12 days 245 Less than 1% About 7×10^8 n/cm^{2}s
Gamma-ray detection	Decay time for W-181 Detector	81 days Low-background 100% efficiency high-purity germanium (HPGe) detector located underground at a depth of 700 m in the Yangyang laboratory of the Dark Matter Research Center (DMRC) in Korea
Detector calibtation		by comparing the measurements from a calibrated multi-gamma source with GEANT4 simulations [20] and deduction for relative efficiencies of W-180 gamma-rays to W-185 and W-187 gamma-rays

5. Conclusion

The two kinds of neutron cross-section measurement activities using out-of-core neutron irradiation facility of HANARO are introduced in this work. The facility gives a thermal neutron field with a flux over 1×10^9 n/cm^{2}s and a Cd ratio over 150. The shielded irradiation room is spacious enough for various experiments such as studies in the boron neutron capture therapy (BNCT), dynamic neutron radiography, etc. So far, two collimators with neutron beam diameters of 10 and 15 cm have been used. One of the applications of this facility is the measurement of the thermal neutron cross-sections for several nuclides. In the design stage of the facility, the total neutron cross-sections of the silicon and bismuth crystals were measured by using the neutron transmission and time-of-flight method since the cross-sections of the filter materials were the key parameters for the performance of the facility. The thermal neutron capture cross section for the W-180 nucleus was measured by using the activation and gamma-ray detection method. The capture cross-section was obtained at a value of 22.6±1.7 b. Measured data for the cross-section for W-180 is very rare, but the production of W-181 is very important since it is a useful radioisotope neutrino source for the various basic neutrino experiments. From the results, it was confirmed that the out-of-core neutron irradiation facility of HANARO would be a useful facility for measuring the neutron cross-sections.

REFERENCES

[1] KIM, M.S., LEE, B.C., HWANG, S.Y., KIM, H., JUN, B.J., Development and characteristics of the HANARO neutron irradiation facility for applications in the boron neutron capture therapy field, Phys. Med. Biol. **52** (2007) 2553.

[2] FREUND, A.K., Cross-Sections of Materials Used as Neutron Monochromators and Filters, Nucl. Intstr. Meth. **213** (1983) 495.

[3] ADIB, M., KILANY, M., On the use of bismuth as a neutron filter, Rad. Phys. Chem. **66** (2003) 81.

[4] KANG, W.G., KIM, Y.D, LEE, J.I., HAHN, I.S., KIM, A.R., KIM, H.J., Measurement of the thermal neutron capture cross section of ^{180}W, Phys. Rev. **C76** (2007) 067602.

[5] POMERANCE, H., Thermal Neutron Capture Cross Sections, Phys. Rev. **88** (1952) 412.

Experimental Determination of Neutron Capture Cross Sections at a Rare Thermal Energy Using the BAEC TRIGA Reactor

S.M. Hossain and M.S. Uddin

Institute of Nuclear Science & Technology, Atomic Energy Research Establishment, G.P.O. Box No.-3787, Savar, Dhaka-1000, Bangladesh

Abstract. Since the installation of theTriple Axis Spectrometer (TAS) in the radial piercing beam port of the 3 MW TRIGA Mark-II research reactor of Bangladesh Atomic Energy Commission (BAEC), it has been utilized for material research using neutron scattering technique. Recently, we have opened a new arena by utilizing the same beam port for determination of neutron capture cross sections at a rare energy in thermal region using the neutron activation analysis (NAA) technique. Three experiments have successfully been carried out in determining the neutron capture cross section for the targets W, Ga and Sm using the reactions $^{186}W(n,\gamma)^{187}W$, $^{71}Ga(n,\gamma)^{72}Ga$, $^{151}Sm(n,\gamma)^{152}Sm$ and $^{153}Sm(n,\gamma)^{154}Sm$ at the thermal energy of 0.0536 eV. Recent extensive literature review insisted us to claim that there are no experimental neutron capture cross-section data available at our investigated energy. So far, we carried out experiments at 0.0536 eV neutrons for cross section measurements for the first time. Our experimental results were critically compared with the evaluated data quoted in JENDL-3.3 and ENDF/B-VII. The results at this particular thermal energy will be useful to observe energy dependence of neutron capture cross sections.

1. Introduction

The BAEC 3 MW TRIGA is the only nuclear research reactor in the country. It is a pool type research reactor achieved its first criticality in the morning of September 14, 1986. For proper utilization, the reactor is equipped with a number of irradiation facilities. Recently, we have opened a new arena by utilizing the radial piercing beam port (where a Triple Axis Spectrometer has been installed for material research using neutron scattering technique) for determination of neutron capture cross sections at a rare energy in thermal region using NAA technique. The term 'rare' means that there are no experimental neutron cross section data available in the literature [1-13] at our investigated energy. In those references the neutron capture cross sections were determined for various targets using the Cd cut-off technique at the average thermal energy 0.025 eV that is quite complex and possibility of inclusion large uncertainty.

Three targets initially, namely tungsten, gallium and samarium were selected for this purpose. The neutron capture cross sections in thermal energy range for all three targets have importance. Tungsten is a structural material used in various parts of fusion reactors. To meet the requirements of compactness and high temperature operation, tungsten has been suggested for use both as a fuel-element material and as a shielding material. To evaluate the merits of tungsten for these applications, accurate and complete nuclear data are required, particularly the thermal neutron induced activation cross section for the $^{186}W(n,\gamma)^{187}W$ reaction is of great importance. On the other hand, Gallium is an important semiconductor material. The thermal neutron cross-section on gallium (Ga) is important for the development of Ga-radiation detectors, activation analysis, radiation safety, improvement of model calculation etc. Samarium is a rare earth element mainly uses as control material in nuclear reactor. In particular, ^{149}Sm and ^{152}Sm is used as a neutron absorber in nuclear reactors. The ^{153}Sm isotope is a β emitting therapeutic radioisotope uses in nuclear medicine. So far three

experiments have successfully been carried out in determining the neutron capture cross section for the reactions $^{186}W(n,\gamma)^{187}W$, $^{71}Ga(n,\gamma)^{72}Ga$, $^{152}Sm(n,\gamma)^{153}Sm$ and $^{154}Sm(n,\gamma)^{155}Sm$ at the thermal energy of 0.0536 eV. Our experimental results were critically compared with the evaluated data quoted in JENDL-3.3 [15] and ENDF/B-VII [16]. The results published in the reputed journal [17-20] are a testimony of our claim. The results at new thermal energy will be useful to observe energy dependence of neutron capture cross section.

2. Materials and methods

2.1. Choice of neutron source

The neutrons coming out of the reactor are of various wavelengths. They are monochromized before sending them to the target for irradiation. They can effectively be done by Bragg reflection from a Cu(200) monochromator using a suitable single crystal. The plane of Cu(200) single crystal ($5\times15\times1.2$ cm^3)was inclined in a position that neutron beam of single wavelength $\lambda = 1.236$ A^0 was obtained, which is corresponded to 0.0536 eV neutron energy. A schematic cross sectional view of the arrangement for monochromatization of reactor neutrons and experimental setup is shown in Fig.1. The monochromatic neutrons are reflected through a solar collimator and then pass through another collimator and finally hit the target.

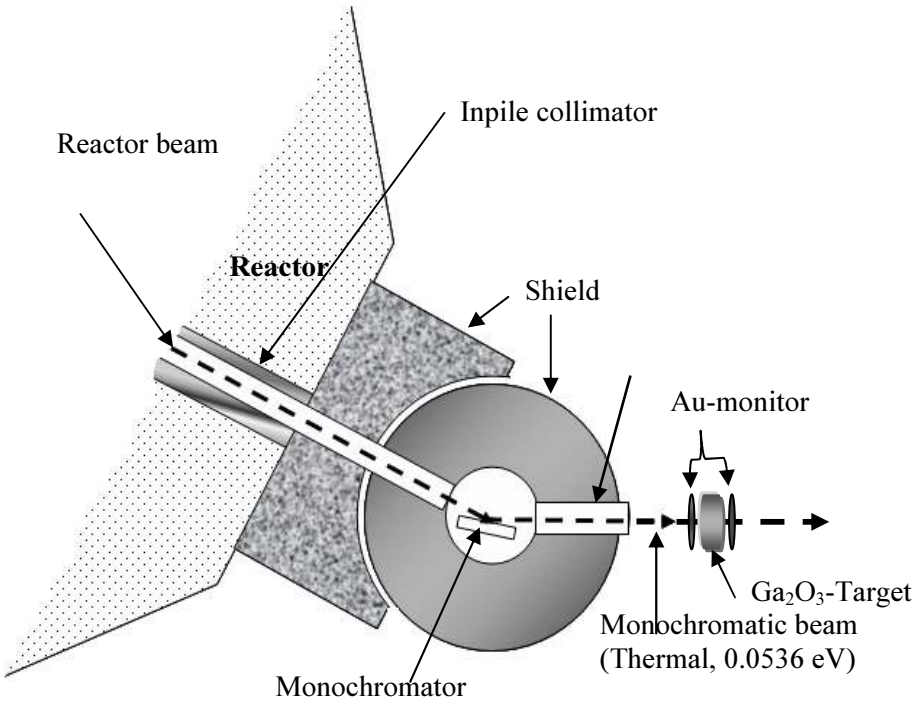

FIG.1. A schematic cross sectional view of the arrangement for monochromatization of reactor neutrons and experimental setup.

2.2. Sample preparation and irradiation

The tungsten foil of 796 mg (99.99% purity, 10 mm dia, 200μm thick) was sandwiched with two gold foils (each ~60 mg, 10 mm dia and 25 μm thick). For Ga and Sm targets, the powder samples of gallium oxide (Ga_2O_3; 99.99% purity; 1.27g) and samarium oxide (Sm_2O_3; 99.99 % purity; 0.82g) were used. The powder sample was pressed with a pressure of 5 tons per cm^2 using a hydraulic press to prepare pellet of about 1.2 cm diameter and 0.13 cm thickness. Each of the pellets was also sandwiched with two gold foils of approximately same size and weight. Two gold foils were attached at the front and back of the target to check the difference in neutron beam intensity between entrance and exit of target. Gold foils were used

to measure the effective neutron flux using the $^{197}Au(n,\gamma)^{198}Au$ reaction. In case of tungsten and gallium targets irradiations were performed for 5 hrs and in case of samarium for 2 hrs with 0.0536 eV neutron beam with the power of 3 MW. The Cd-covered gold foil and bare aluminum foil were also irradiated to check the presence of epithermal and fast neutrons.

2.3. Gamma ray counting and peak analysis

The activities of the radioisotopes produced in the targets and the monitor foils were measured using high-purity germanium (HPGe) gamma-ray spectroscopy (Canberra, 15% relative efficiency, 1.8 keV resolution at 1332.5 keV of ^{60}Co) coupled with digital gamma spectrometry system (ORTEC DSPEC jr ^{TM}) and Maestro data acquisition software. The gamma peak analysis was done using the software Hypermet PC Version 5.12. The gamma spectrometry of the irradiated targets was performed several times depending on the half-lives of product radionuclides of investigated reactions. Each target was counted 3 times giving enough intervals to avoid disturbance by overlapping gamma-lines from undesired sources. The gamma ray spectrum for tungsten target is shown in Fig.2.

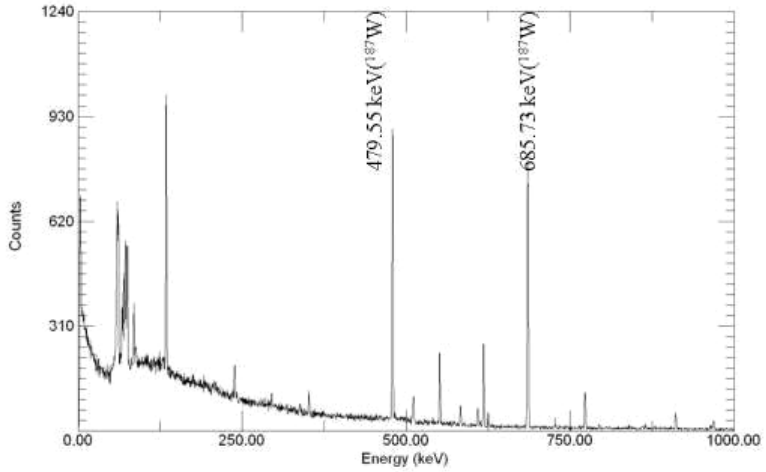

FIG.2. Gamma spectrum of irradiated tungsten target.

2.4. Construction of efficiency curve

The ε_p curve ($\log\varepsilon_p$ versus $\log E\gamma$) was constructed at 30 cm distance from the detector surface based on Moen et al. [21]. The curve was constructed by measuring the absolutely calibrated multi- and single-gamma point sources ^{22}Na, ^{57}Co, $^{60}C0$, ^{54}Mn, ^{133}Ba, ^{137}Cs and ^{152}Eu, covering the energy range 80.9 – 1408 keV, as shown in Fig 3. Once the efficiency curve is constructed at the reference position it can easily be converted to the required counting geometry. This conversion can be done by measuring single gamma emitting (coincidence free) point source (^{137}Cs emits 661.6 keV gamma or ^{54}Mn emits 834 keV gamma) at the reference position and at the required geometry. From the ratio of these two measurements, the efficiency curve can easily be constructed at the geometry where the sample is counted.

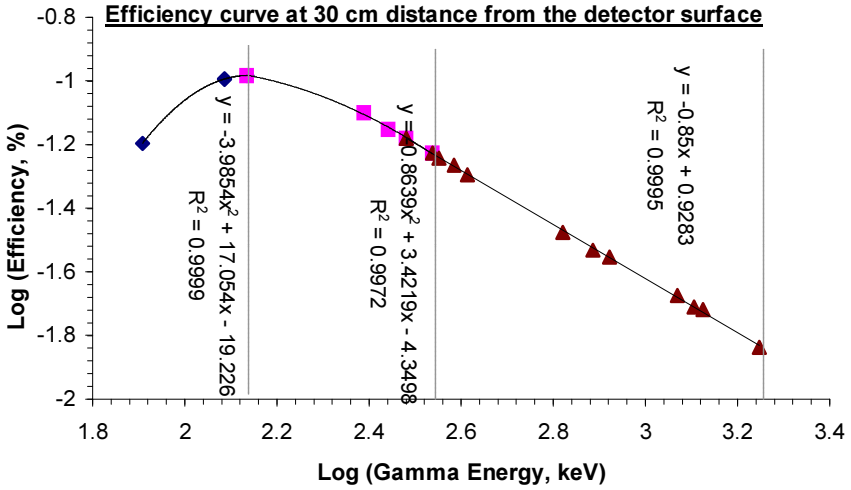

FIG.3. Experimental determination of the full energy peak detection efficiency curve at 30 cm distance from the surface of the HPGe detector.

2.5. Determination of neutron flux

The neutrons coming out through the radial piercing beam port are monochromized by the plane of a Cu(200) single crystal before sending them on the sample for irradiation, we can assume that only the mono-energetic thermal neutrons of 0.0536 eV hit the sample. In this case the neutron flux ϕ(E) can simply be obtained as (assuming the self attenuation factor for gold foil at 0.0536 eV is negligible)

$$\phi(E) = \frac{A_{sat}}{\sigma(E_{peak})} \qquad (1)$$

A_{sat} is the saturated activity of gold foil, γ(E_{peak}) is the cross section of gold at the peak neutron energy. A_{sat} can be derived as:

$$A = N\phi\sigma(1 - e^{-\lambda t_i}) \times e^{-\lambda t_d} \times \frac{1 - e^{-\lambda t_c}}{\lambda t_c} \qquad (2)$$

Where A is the observed activity of the target at time t_c, N is the number of nuclei in the target, λ is the decay constant, $(1 - e^{-\lambda t_i})$ is the irradiation factor, $e^{-\lambda t_d}$ is the decay factor and $\frac{1-e^{-\lambda t_c}}{\lambda t_c}$ is the counting factor. From eq. (2) the saturated activity per atom can be derived as:

$$A_{sat} = \frac{A\lambda t_c}{N(1-e^{-\lambda t_i})\times e^{-\lambda t_d} \times (1-e^{-\lambda t_c})}$$

where, $A = \frac{N_p}{\frac{t_c}{\varepsilon \times I_\gamma}}$; N_p = net peak area, ε = peak detection efficiency, I_γ = gamma intensity

$N = \frac{N_{av} \times w \times \theta}{A_{wt}}$; N_{av} = Avogadro's number, w = mass of the target, θ = isotopic abundance, A_{wt} = Atomic weight

$$A_{sat} = \frac{N_p \times \lambda . e^{+\lambda t_d}}{\varepsilon \times I_\gamma \times \frac{6.02 \times 10^{23} \times w \times \theta}{A_{wt}} \times (1 - e^{-\lambda t_i}) \times (1 - e^{-\lambda t_c})} \qquad (3)$$

From equations 1 and 3, the neutron flux can be obtained. It was determined from the measured activities induced in gold monitor foils using the $^{197}Au(n,\gamma)^{198}Au$ monitor reaction. The monitor foils were measured with the same detector and in a comparable geometry as the targets. The cross section of the monitor reaction, 68.5 ±1.7 b at 0.0536 eV, was evaluated from the trend line of experimental data reported by Yamamoto et al. [22], Pavlenko *et al*. [23] and Haddad *et al*. [24].

2.6. Cross section calculation

As the neutrons have a pure mono-energetic spectrum, the cross-section at the peak neutron energy $\gamma(E_{peak})$ can simply be obtained by

$$\sigma(E_{peak}) = \frac{A_{sat}}{\phi(E) \times F_g} \qquad (4)$$

Where F_g is the correction factor for gamma-ray attenuation in the sample at a given gamma-ray energy at a fixed cylindrical geometry, coaxially positioned with the detector. All other terms in equation (4) have already been explained above. The F_g can be determined by the following relation:

$$F_g = \frac{\mu x}{1 - e^{-\mu x}} \qquad (5)$$

where μ is the linear attenuation coefficient (cm^{-1}); μ/ρ is the total mass attenuation coefficient (cm^2/g) for the compounds used, ρ is the density of sample (g/cm^3) and x is the sample thickness (in cm). The correction factors for gamma-ray attenuation along the gallium oxide pellet were found to be 1.0311 and 1.0356 for the 834.03 and 629.96 keV gamma-rays, respectively. In case of tungsten the correction factors for both gamma energies of 479.55 and 685.73 keV are very close to one. In case of samarium, the F_g value was found to be very large, F_g = 1.8, viz.

3. Results and discussion

Thermal neutron capture cross sections of the $^{186}W(n,\gamma)^{187}W$, $^{71}Ga(n,\gamma)^{72}Ga$, $^{152}Sm(n,\gamma)^{153}Sm$ and $^{154}Sm(n,\gamma)^{155}Sm$ reactions were measured by activation technique at 0.0536 eV neutron energy using the radial piercing beam port of the TRIGA reactor. The decay data of the radioactive products were taken from the NUDAT database (*National Nuclear Data Centre, information extracted from the NuDat database, http://www.nndc.bnl.gov/nudat2*) are quoted in Table 1. The results with uncertainties for the $^{186}W(n,\gamma)^{187}W$ and $^{71}Ga(n,\gamma)^{72}Ga$ reactions are quoted in Table 2 and Table 3 and for $^{152}Sm(n,\gamma)^{153}Sm$ and $^{154}Sm(n,\gamma)^{155}Sm$ reactions in Table 4, respectively together with reference values. They are also shown in Figs. 4-7. The

quoted uncertainties (1γ) were calculated based on the total uncertainty budget considering: statistical uncertainty of γ-ray counting, uncertainty in the monitor flux, uncertainty in the decay branching ratio, uncertainty in isotopic abundance and the uncertainty in efficiency calibration of the gamma ray detector. The overall uncertainty in the cross section is found to be 9%, 5%, 6% and 5% for tungsten, gallium and samarium reactions, respectively. For each reaction the radionuclide was identified by individual gamma-lines. The values determined individually for these gamma-lines are consistent to each other for all investigated reactions.

Up to now, a number of authors reported thermal neutron capture cross section for the those reactions and recently evaluated data are also reported in the ENDF/B-VI [25] and JENDL-3.3 libraries. In these references a mixed neutron beam of thermal and epithermal energies was used for activation. They corrected the activation due to the epithermal neutrons by the Cd cut-off energy technique that is rather complex, and and risks to carry large uncertainties to the results. The existing experimental reference values determined using this technique are reported at 0.0253 eV neutron energy.

3.1. $^{186}W(n,\gamma)^{187}W$

The evaluation value of ENDF/B-VI for the reaction $^{186}W(n,\gamma)^{187}W$ is about 5% lower than that of JENDL-3.3. The data reported by Gillette [26], Pomerance [12] and Seren *et al.* [27], which are very old, are significantly lower than from other experiments and there is no explanation for the discrepancy. On the other hand, recently published data of Mustafa Karadag [10] and De Corte [28] are larger than from this work due to the effect of neutron energy on cross section. Mustafa Karadag reported cross section measured by the activation method using ^{55}Mn as a single monitor. Friesenhahn *et al.* [3] have shown the energy dependence of the capture cross section over the appreciable energy interval 0.01 to 10 eV. A large difference between the values at 0.0253 and 0.0536 eV was found from their reported excitation curve, which is consistent with this work. Neutron capture cross sections in the thermal region ordinarily obey the 1/v law, where v is the speed of incident neutron. On the other hand, the ratios of the capture cross sections of the $^{197}Au(n,\gamma)^{198}Au$ monitor reaction at 0.0536 eV to that at 0.0253 eV is 0.7. The ratios of the result obtained in this work to the reported values at 0.0253 eV are in the range 0.6 to 0.8. The present and the previous values at 0.0253 eV are in agreement within analytical uncertainty. Obviously, our result from the $^{186}W(n,\gamma)^{187}W$ reaction cross section is reliable.

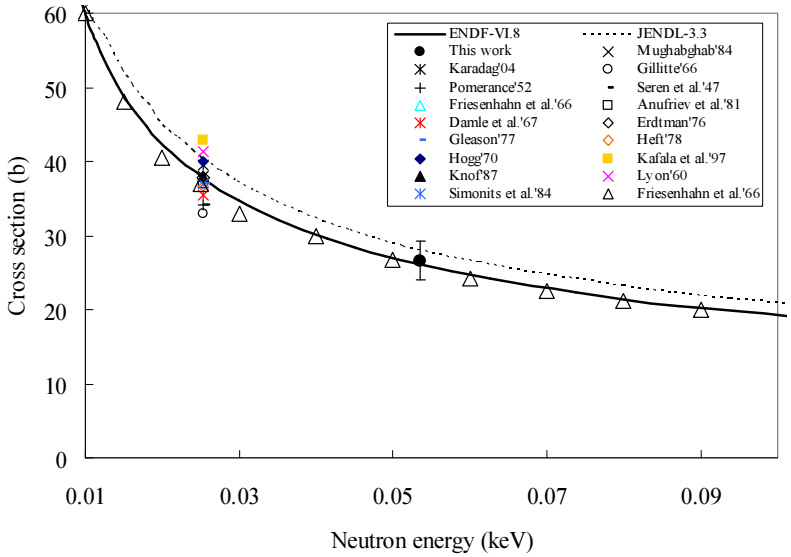

FIG.4. Neutron capture cross sections for the $^{186}W(n,\gamma)^{187}W$ reaction: a) Solid circle-this work at 0.0536 eV and b) other references at 0.0253 eV.

3.2. $^{71}Ga(n,\gamma)^{72}Ga$

A number of authors [6, 11, 13, 29] have reported experimental thermal-neutron capture cross section values for the $^{71}Ga(n,\gamma)^{72}Ga$ reaction determined at 0.0253 eV using the Cd cut-off energy technique. Data reported in both the ENDF/B-VII and the JENDL-3.3 library are evaluated. In these libraries the value at 0.0536 eV is calculated from the thermal cross section at 0.0253 eV using the 1/v relationship. This is very accurate. The calculated value of ENDF/B-VII at 0.0536 eV is about 27% higher than that of JENDL-3.3. It can be explained by the fact that ENDF/B-VII used γ_0 (0.0253 eV) = 4.73 b but this has been replaced by 3.709 b in JENDL-3.3. As shown in Fig. 5, the cross section values at 0.0253 eV are reported in the range of 3.36 – 4.9 b. Assuming a 1/v cross section dependence JENDL-3.3 gives a neutron capture cross section 2.55 b at 0.0536 eV and agrees precisely with the value in this paper.

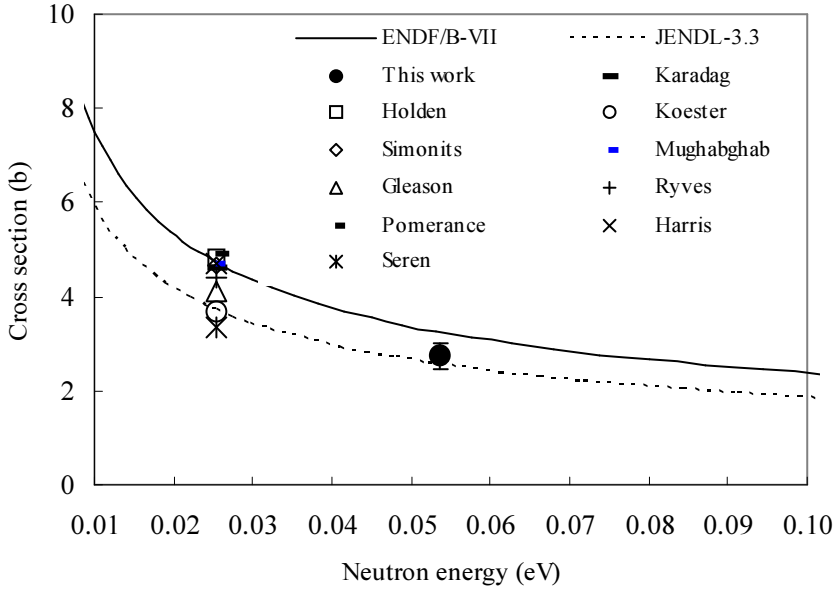

FIG.5. Neutron capture cross sections for the $^{71}Ga(n,\gamma)^{72}Ga$ reaction: a) Solid circle-this work at 0.0536 eV and b) other references at 0.0253 eV.

3.3. $^{152}Sm(n,\gamma)^{153}Sm$ and $^{154}Sm(n,\gamma)^{155}Sm$

Few authors have also reported the experimental thermal neutron capture cross section data for $^{152}Sm(n,\gamma)^{153}Sm$ and $^{154}Sm(n,\gamma)^{155}Sm$ reactions at average thermal energy (0.0253 eV) using the Cd-cut off technique [7, 27, 30-35]. The reported data are in the range of 138-250 b for the $^{152}Sm(n,\gamma)^{153}Sm$ reaction and present large discrepancies as shown in Figs. 6-7 and Table 4. In view of our available literature survey [7, 27, 30-35], only Seren [27] and Heft [7] reported the experimental values for the $^{154}Sm(n,\gamma)^{155}Sm$ reaction at 0.0253 eV neutron energy amounting to 8.5 b and 1.1 b. Their results deviate about 87% from each other. In this work careful measurements have been carried out at 0.0536 eV for $^{152}Sm(n,\gamma)^{153}Sm$ and $^{154}Sm(n,\gamma)^{155}Sm$ reactions and the obtained values are 144.6±8.6 b and 5.9±2.9 b, respectively. Data reported both in the ENDF/B-VII and JENDL-3.3 libraries are evaluated and no measurements have been made at 0.0536 eV using the 1/v relationship. The evaluated value of ENDF-VII at 0.0536 eV is about 2% higher than that of JENDL-3.3. It can be explained by the fact that ENDF/B-VII used a base cross section, γ_0 (at 0.0253 eV) = 210.34 b, but this has been replaced by 207.92 b in JENDL-3.3 giving a neutron capture cross sections of 147 b and 144 b at 0.0536 eV, respectively, which are in excellent agreement with the value of this work. The present cross section value of $^{154}Sm(n,\gamma)^{155}Sm$ reaction is about

3% and 2.3% higher than the evaluated value of ENDF-VII and JENDL-3.3 at 0.0536 eV, respectively.

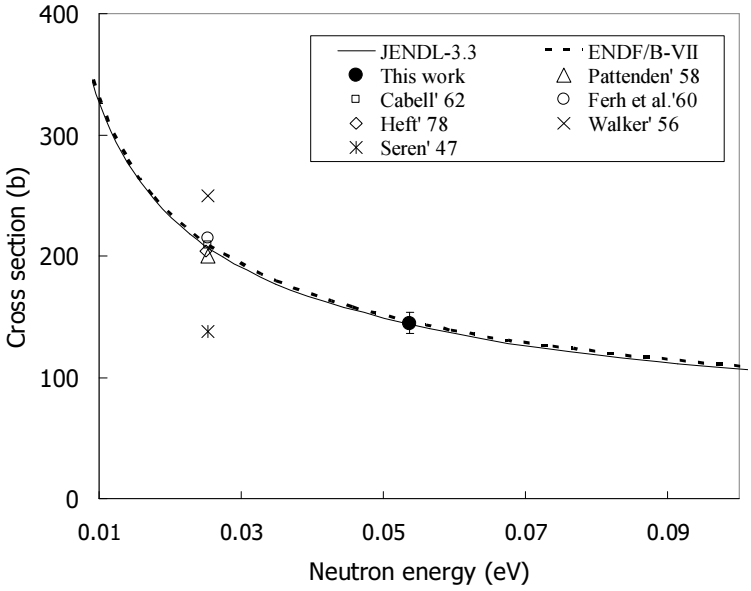

FIG.6. Neutron capture cross sections for the $^{152}Sm(n,\gamma)^{153}Sm$ reaction: a) Solid circle-this work at 0.0536 eV and b) others for references at 0.0253 eV.

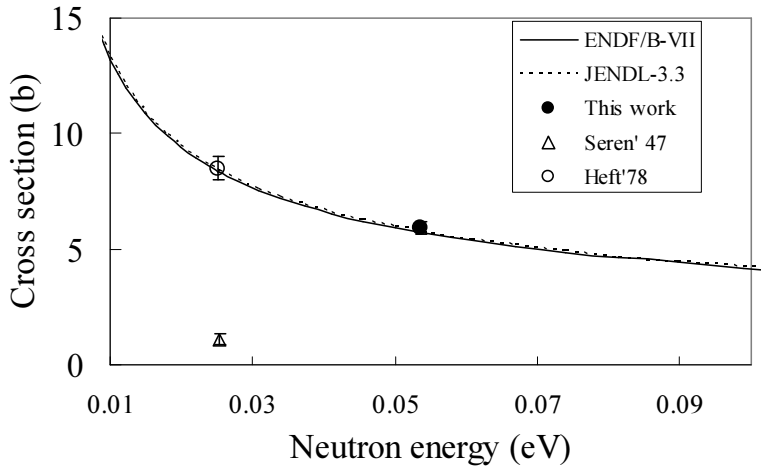

FIG.7. Neutron capture cross sections for the $^{154}Sm(n,\gamma)^{155}Sm$ reaction: a) Solid circle-this work at 0.0536 eV and b) others for references at 0.0253 eV.

TABLE 1. DECAY DATA OF THE INVESTIGATED NUCLIDES AND THE CONTRIBUTING REACTIONS

Nuclear Reaction	Half-life	Gamma ray Energy (keV)	Branching Ratio (%)
$^{186}W(n,\gamma)^{187}W$	23.72 h	479.55	21.8
		685.73	27.3
$^{71}Ga(n,\gamma)^{72}Ga$	14.1 h	834.03	95.63
		629.96	24.8
$^{152}Sm(n,\gamma)^{153}Sm$	46.5 h	103.17	28.3
$^{154}Sm(n,\gamma)^{155}Sm$	22.2 min	104.32	73.0
$^{197}Au(n,\gamma)^{198}Au$	2.695 d	411.8	95.5

TABLE 2. NEUTRON CAPTURE CROSS SECTION FOR THE $^{186}W(N,\gamma)^{187}W$ REACTION

Year	References	Neutron capture cross section (b)
2007	This work	26.6±1.6
2004	Karadag *et al.*	39.5±2.3
2003	Garland *et al.*	36.5±4.2
2003	De Corte	41.8±2.9
1999	Holden	37±2
1997	Kafala *et al.*	42.8±0.8
1989	De Corte *et al.*	38. 7±1.9
1987	Knopf *et al.*	38.5±0.8
1984	Simonits *et al.*	37±1.8
1984	Mughabghab	37.9±0.6
1981	Anufriev *et al.*	37±3
1978	Heft	36.6±0.8
1977	Gleason	37±1.5
1976	Erdtmann	37.8±1.5
1970	Hogg *et al.*	40±1.5
1967	Damle *et al.*	35.4±0.8
1966	Gillette	33
1966	Friesenhahn *et al.*	37.8±1.2
1960	Lyon	41.3
1952	Pomerance	34.1±2.7
1947	Seren *et al.*	34.2±6.8

TABLE 3. NEUTRON CAPTURE CROSS SECTION FOR THE $^{71}Ga(N,\gamma)^{72}Ga$ REACTION

Year	References	Neutron energy (eV)	Neutron capture cross section (b)
2007	This work	0.0536	2.75±0.14
2006	ENDF/B-VII	0.0253	4.73
2003	Karadag *et al.*	0.0253	4.41±0.18
2002	JENDL-3.3	0.0253	3.709
1999	Holden	0.0253	4.85±0.20
1984	Simonits et al.	0.0253	4.67±0.23
1984	Koester et at.	0.0253	3.67±0.10
1981	Mughabghab *et al.*	0.0253	4.71±0.23
1975	Gleason	0.0253	4.40±0.2
1971	Ryves *et al.*	0.0253	4.71±0.23
1952	Pomerance	0.0253	4.9±0.40
1950	Harris *et al.*	0.0253	4.71±0.23
1947	Seren, *et al.*	0.0253	3.36±0.67

TABLE 4. NEUTRON CAPTURE CROSS SECTION FOR THE ^{152}Sm(N,γ), ^{153}Sm AND ^{154}Sm(N,γ)^{155}Sm REACTIONS

Year	Reference	Neutron energy (eV)	Neutron capture cross section (b)	
			^{152}Sm(n,γ)^{153}Sm	^{154}Sm(n,γ)^{155}Sm
2008	This work	0.0536	144.6 ± 8.6	5.9 ± 0.29
2007	Karadag *et al.* [31]	0.0253	204.8 ± 7.9	
1978	Heft [36]	0.0253	204 ± 9	8.5 ± 0.5
1962	Cabell [34]	0.0253	209 ± 9	
1960	Fehr *et al.* [35]	0.0253	215 ± 10	
1960	Tattersall *et al.[*37]	0.0253	224 ± 7	
1956	Walker [38]	0.0253	250 ± 56	
1947	Seren *et al.* [32]	0.0253	138 ± 27.6	1.1 ± 0.22

4. Conclusion

We have opened a new arena by utilizing the Triple Axis Spectrometer (TAS) irradiation facility in the radial piercing beam port of the BAEC TRIGA reactor for determining neutron capture cross sections at a rare thermal energy (0.0536 eV) using NAA technique. Our method is simple and straight forward. We could avoid the use of the complex Cd cut-off energy technique. We report new cross sections for ^{186}W(n,γ)^{187}W, ^{71}Ga(n,γ)^{72}Ga, ^{152}Sm(n,γ)^{153}Sm and ^{154}Sm(n,γ)^{155}Sm reactions amount to 26.6±2.5b, 2.75±0.14b, 144.6±8.6b and 5.9±0.29b, respectively, which are the first experimental values at 0.0536 eV neutron energy for the tungsten, gallium and samarium targets. Our experimental results were critically compared with the evaluated data quoted in JENDL-3.3 and ENDF/B-VII. In these libraries the value at 0.0536 eV is calculated from the thermal cross section at 0.0253 eV using the 1/v relationship. As discussed in the results and discussion part, in most of the cases our results are comparable with the evaluated data. Some discrepancies observed from library to library are due to inconsistent nuclear data. The established method can be used for other targets.

Acknowledgement

Grateful acknowledgement is made to the members of Reactor Operation and Maintenance Unit (ROMU) for their nice cooperation, encouragement and operation of reactor. Neutron Scattering Group deserves special thanks for allowing us to use their irradiation facilities.

REFERENCES

[1] ANUFRIEV, V.A., *et al.*, Neutron resonances of ^{186}W in the energy range up to 300 eV, At Energy **50** 1 (1981) 67.

[2] DAMLE, P.P., *et al.*, Study of the reaction ^{186}W(n,γ)^{187}W, Report from Euratom-countries +Euratom to EANDC-76, **107** 2 (1967).

[3] FRIESENHAHN, S.J., *et al*., The neutron capture cross section of the tungsten isotopes from 0.01 to 10 electron volts, Nucl. Sci. Eng. **26** (1966) 487.

[4] GARLAND, M.A., *et al*., Neutron flux characterization of a peripheral target position in the high flux isotope reactor, Appl. Radiat. Isot. **59** 1 (2003) 63.

[5] GLEASON. G., Thermal neutron (n,γ) cross sections and resonance integrals –part 2, Private Communication to NEA-Data Bank, ORL, USA (1977).

[6] GLEASON, G., Thermal neutron cross sections and (n,γ) resonance integrals, Part I. Radiochem, Radioanal. Lett. **23** (1975) 317.
[7] HEFT, R.E., A consistent set of nuclear parameter values for absolute INAA, In: Conference on Computers in Activation Analysis and Gamma ray Spectroscopy, vol. 495, Mayaguez, Puerto Rico (1978).
[8] HOGG, C.H., WILSON, W.L., Reactor thermal-neutron cross sections of ^{64}Zn, ^{68}Zn, ^{121}Sb, ^{123}Sb, ^{55}Mn, and ^{186}W, Idaho Nuclear Corp. Reports: 1317 (1970) 53.
[9] KAFALA, S.L., *et al.*, Neutron activation for precise nuclear data, J. Radioanal. Nucl. Chem. **215** 2 (1997) 193.
[10] KARADAG, M., YUCEL, H., Measurement of thermal neutron cross-section and resonance integral for ^{186}W(n,γ)^{187}W reaction by the activation method using a single monitor, Ann. Nucl. Eng. **31** (2004) 1285.
[11] KARADAG, M., *et al*., Measurement of thermal neutron cross-sections and resonance integrals for ^{71}Ga(n,γ)^{72}Ga and ^{75}As(n,γ)^{76}As by using ^{241}Am–Be isotopic neutron source, Nucl. Instrum. Methods Phys. Res. A **501** (2003) 524.
[12] POMERANCE, H., Thermal neutron capture cross sections, Phys. Rev. **88** 2 (1952) 412.
[13] SIMONITS, A., *et a*l., Comparative study of measured and critically evaluated resonance integral of thermal cross-section ratios, II. J. Radioanal. Nucl. Chem. **81** 2 (1984) 397.
[14] SHOOK, D.F., BOGART, D., Effective resonance integrals of separated tungsten isotopes from reactivity measurements, Nucl. Sci. Eng. **31** (1968) 415.
[15] JENDL-3.3. Japan Atomic Energy Research Institute, Nuclear Data Center. Copyright, JAERI (2002).
[16] ENDF/B-VII Library, Database Version of 30 October (2007).
[17] UDDIN M.S., *et al*., Neutron capture cross-section measurement for the ^{186}W(n,γ)^{187}W reaction at 0.0536 eV energy, Appl. Radiat. Isot. **66** (2008) 1235-1239.
[18] UDDIN M.S., *et al*., Measurement of neutron capture cross section of the ^{171}Ga(n,γ)^{172}Ga reaction at 0.0536 eV energy, Nucl. Instrum. Methods Phys. Res. B **266** (2008) 3341-3345.
[19] UDDIN M.S., *et al.*, Thermal neutron cross sections for the ^{152}Sm(n,γ)^{153}Sm and ^{154}Sm(n,γ)^{155}Sm reactions at 0.0536 eV energy", Nucl. Instrum. Methods Phys. Res. B, 266 (2008) 4855-4861.
[20] HOSSAIN S.M., Utilization of radial piercing beam port of TRIGA reactor for nuclear cross section measurements, INST Internal Report, INST–115/RNPD-27, April (2008).
[21] MOENS L. *et al*., Calculation of the absolute peak efficiency of gamma-ray detectors for different counting geometries, Nucl. Instrum. Methods **187** (1981) 451-472.
[22] YAMAMOTO, S., *et al*., Application of BGO scintillators to absolute measurements of neutron capture cross sections between 0.01 eV and 10 eV, J. Nucl. Sci. Technol. **33** (1996) 815.
[23] PAVLENKO, E.A., GNIDAK, N.L., Neutron capture cross section measurement for hafnium and vanadium isotopes, All Union Conf. on Neutron Phys., 3 (1975) 171.
[24] HADDAD, E., *et al*., High efficiency detector for neutron capture cross section measurements, Nucl. Instrum. Methods Phys. Res. **31** (1964) 125.
[25] ENDF/B-VI library, Database version of 15 December (2006).
[26] GILLETTE, J.H., Preprint: ORNL-4013, vol. 5, Oak Ridge National Laboratory (1966).
[27] SEREN, L., *et al*., Thermal neutron activation cross sections, Phys. Rev. **72** 10 (1947) 888.

[28] DE CORTE, F., 2003. The updated NAA nuclear data library derived from the Y2K k_o-database, J. Radioanal. Nucl. Chem. **257** 3 (2003) 493.
[29] KOESTER, L., *et al*., Interactions of neutrons with gallium and its isotopes, Z. Phys. A, **318** 3 (1984) 347.
[30] KARADAG, M., *et al*., Measurement of thermal neutron cross section and resonance integral for (n,γ) reaction in ^{152}Sm, Ann. Nucl. Eng. **34** (2007) 188.
[31] PATTENDEN, N.J., Some neutron cross sections of importance to reactors Tc^{99}, Nd^{143}, Nd^{145}, Sm^{149}, Sm^{152}, Eu^{153}, Gd^{155}, Gd^{157}, Pu^{240}, Proceedings of the 2nd International Conference in Peaceful Uses of Atomic Energy, Geneva, Vol.16 (1958) 44.
[32] CABELL, M.J., Neutron capture cross-section data for Sm-152, J. Inorg. Nucl. Chem., 24 (1962) 749.
[33] FEHR, E., HANSEN, E., Fission-product cross-section measurements, Knolls Atomic Power Lab, Report Series No. 2000, 12, 1 (1960).
[34] TATTERSALL, R.B., *et al*., Pile Oscillator measurements of resonance absorption integrals, J. Nucl. Energy, Part A: Reactor Sci. 12 (1960) 32.
[35] WALKER, W.H., The relative abundances and Pile Neutron Capture Cross Sections of the isotopes of samarium, gadolinium, dysprosium, and ytterbium, Thesis, McMaster University, Hamilton, Ontario (1956).
[36] DE CORTE, F., Simonits, A., k_0-measurements and related nuclear data compilation for (n,γ) reactor activation analysis IIIb: tabulation, J. Radioanal. Nucl. Chem. **133** (1989) 43.
[37] HARRIS, S.P., Muehlhause, C.O., Thomas, G.E., Low energy neutron resonance scattering and absorption, Phys. Rev. **79** (1950) 11.
[38] HOLDEN, N.E., Neutron scattering and absorption properties (Revised 1996). In: Lide, D.R. (Ed.), CRC Handbook of Chemistry and Physics, 79th ed. CRC Press, New York (1999).
[39] KNOPF, K., Waschkowski W., Interaction of neutrons with tungsten and its isotopes (in German). Z. Naturforsch. A **42** (9) (1987) 909.
[40] LYON, W.S.,. Reactor neutron activation cross sections for a number of elements. Nucl. Sci. Eng. **8** (1960) 78.
[41] MUGHABGHAB, S.F., Neutron Cross Sections. Neutron Resonance Parameters and Thermal Cross Sections, Part B, Z=61-100, vol. 1, Academic press, New York.
[42] MUGHABGHAB, S.F. et al., 1981. Neutron cross sections from neutron resonance parameters and thermal cross sections, Academic press, New York (1984).
[43] RYVES, T.B., PERKINS, D.R., Further activation thermal neutron capture cross sections and resonance integrals, J. Nucl. Ener. **25** (1971) 129.

The Use of Miniature Neutron Source Reactor Facility for the Determination of Neutron-induced Cross section Data

S.A. Jonah[1], U. Sadiq[2]

[1] Reactor Engineering Section, Centre for Energy Research and Training, Ahmadu Bello University, Zaria
[2] Department of Physics, Ahmadu Bello University, Zaria

Abstract. Miniature Neutron Source Reactors are compact low-power nuclear research reactor designed mainly for neutron activation analysis and limited radioisotope production. These facilities have stable neutron flux distribution as a function of operating time as well as a high neutron flux relative to power. Because of proximity of the irradiation channels to the core, the neutron spectral distribution is made up of fast, thermal and epithermal components and therefore careful investigations are needed to evolve experimental procedures for the determination of neutron-induced cross section data. Specifically using an inner irradiation channel, a comparator method relative to the resonance integral of $^{197}Au(n,\gamma)^{198}Au$ reaction was found to be appropriate for the determination of reactor neutron spectrum averaged cross section data for some low and medium mass nuclei. Furthermore, thermal neutron capture cross section data were determined on the basis of Cadmium ratio measured in one of the outer irradiation channel. Results of spectrum averaged cross sections are presented for the (n,p) reaction on ^{27}Al, ^{28}Si, ^{29}Si, ^{47}Ti, ^{54}Fe, ^{58}Ni and (n,α) reactions on ^{27}Al and ^{30}Si. Additionally, thermal capture cross sections are presented for the target nuclides ^{47}Ca, ^{71}Ga, ^{75}As, ^{94}Zr and ^{238}U.

1. Introduction

The knowledge of the neutron-induced cross section data is of great importance in reactor dosimetry and NAA, especially for elemental analysis using semi-absolute and absolute methods. Low-power nuclear research reactors such as the miniature neutron source reactor (MNSR) and SLOWPOKE facilities have relatively higher component of fast neutrons in the inner irradiation channels due to their compact nature and the proximity of the inner irradiation channels to the core. Therefore, primary nuclear interferences due to fast neutron-induced reactions in these facilities are significant for NAA by the neutron capture reaction [1, 2]. Fast neutron-induced threshold reactions of the type (n,p) and (n,α) on a number of low- and medium-mass nuclei are suitable for elemental analysis and are widely used in dosimetry for in-pile neutron spectra and fast neutron flux measurements. With regards to the reactor technology, these reactions are very important as they provide information on hydrogen and helium gas production in structural materials of nuclear reactors. A survey of the literature reveals that the measured reactor neutron spectrum-averaged cross-section data of interest in NAA are scanty and inconsistent, therefore recommended data are themselves discrepant. Consequently, in this work, a comparator method, which is based on epithermal neutron flux monitored by the $^{197}Au(n,\gamma)^{198}Au$ reaction and well known neutron spectrum parameters of the irradiation channel was developed for the determination of the fast neutron spectrum-averaged cross-section data in an irradiation channel of MNSR facilities. The objective was to establish the suitability of MNSR for the determination of neutron-induced cross-section data, especially the fast neutron spectrum-averaged cross-sections. Furthermore, thermal neutron capture cross section data were determined on the basis of Cadmium ratio measured in one of the outer irradiation channel. Measurements were performed in the frame work of the IAEA CRP “Development of database for NAA” for which some of the thermal

capture cross section data were identified as discrepant. Results of the spectrum averaged cross section are compared with data obtained by the absolute method, which is based on the reactor fast spectrum-averaged cross section of $^{27}Al(n,p)^{27}Mg$ reaction. Results of the thermal captured cross section are compared with literature data.

2. Materials and Method

2.1. *Reactor neutron spectrum averaged cross section data*

The comparator and appropriate materials in form of foils and powder were prepared from high-purity metals/alloys and pure oxides, respectively. They were packed inside a Cd box of 1mm thickness and heat sealed in a 7cm^3 polyethylene vial for the irradiation. The irradiation was performed for 1 h in an inner irradiation channel (i.e.B2) of NIRR-1 due to the relatively higher fast-to-thermal flux ratio. The use of Al–0.1%Au foil (IRMM-530) as the comparator and irradiation under Cd-cover permits the monitoring of the fast neutron flux via the $^{27}Al(n,p)^{27}Mg$ reaction and the epithermal neutron flux via the $^{197}Au(n,\gamma)^{198}Au$ reaction simultaneously.

Detailed descriptions of the irradiation channels and the characteristic data of the reactor are given elsewhere [3, 4]. The description of the target materials and nuclear data of the reactions of interest are given in Table 1. Furthermore, experimental procedures including gamma ray spectrometry of product radio nuclides have been published in Reference [5].

2.2. *Thermal capture cross section data*

Target materials of low and medium mass nuclei, which are of interest and made up of high-purity foils and metallic oxides were prepared for irradiation in the irradiation channels of NIRR-1. Irradiation was performed with and without a one mm thick Cd box in an outer irradiation channel, where the neutron spectrum has been found to be soft [3]. All irradiations were performed at a thermal power level of 15.5 kW, which corresponds to a thermal neutron flux value of 5.0 x 10^{11} n/(cm^2 s) preset on the control console. After the irradiation, induced radioactivity in detector foils were counted on a HPGe coaxial detector (ORTEC), which has a relative efficiency of 10% and resolution of 1.95 keV, at 1.33 MeV, ^{60}Co. The gamma-ray acquisition system consists of MAESTRO multi-channel analyzer (MCA) emulation software card, coupled to the detector via electronic modules, which are all manufactured by ORTEC. The multi-purpose gamma-ray analysis software, WINSPAN-2004 [6] was used for peak identification and peak area analysis. The thermal neutron capture cross section data were calculated based on measured Cd ratios (R_{cd}) of nuclides of interest using the expression given in eq. 1.

$$Q_O(\alpha) = \frac{f}{(F_{Cd}.R_{Cd} - 1).\dfrac{G_{e,i}}{G_{th},i}} \tag{1}$$

With,

$$R_{Cd} = \frac{A_{sp,bare}}{A_{sp,Cd}} \tag{2}$$ and

$$A_{sp} = \left[\frac{N_p / t_m}{wSDC}\right] \tag{3}$$

where,

f is the ratio of thermal to epithermal neutron flux

α is a measure of the deviation of epithermal neutrons from the ideal *1/E* distribution

N_p = the number of counts in the full-energy peak

w = mass of monitor
M = atomic mass of target nucleus
ϑ = isotopic abundance of target nucleus
γ = gamma-ray abundance of residual radionuclide
ϕ_{th} = sub-cadmium (thermal) neutron flux
$S = (1 - e^{-\lambda t_{irr}})$, saturation factor
$D = e^{-\lambda t_d}$, decay factor
$C = (1 - e^{-\lambda t_m}) / \lambda t_m$, counting factor
t_{irr} = irradiation time
t_d = decay time
t_m = measuring time
λ = decay constant
i denotes the i[th] monitor, N the number of monitors used and
$\overline{E}_{r,i}$ is the effective resonance energy of the i[th] monitor
F_{Cd} is the Cd-transmission factor for epithermal neutrons
$G_{e,i}$ is the epithermal neutron self-shielding factor for the i[th] monitor
$G_{th,i}$ is the thermal neutron self-shielding factor for the i[th] monitor
$R_{Cd,i}$ is the ratio of the specific activity of the i[th] monitor irradiated without the Cd ($A_{sp,bare}$) to that with the Cd cover ($A_{sp,\,Cd}$)
$Q_{0,i} = I_0/\gamma_0$ is the ratio of resonance integral to thermal neutron capture cross section at a neutron velocity of 2200 m/s for the i[th] monitor

In order to validate the measured neutron spectrum parameters, a comprehensive MCNP model of NIRR-1 was established and used to determine the neutron energy spectrum in the experimental channels in 640 energy group [7].

3. Results and Discussion

A comparison of the results of reactor spectrum averaged cross section data obtained in this work with literature data is given in Table 1. The well known dosimetry reactions ^{27}Al(n,p)^{27}Mg, ^{58}Ni(n,p)$^{58m+g}$ Co, ^{47}Ti(n,p)^{47}Sc, and ^{54}Fe(n,p)^{54}Mn were used to determine the fast neutron flux in the reference channel. Results show that the average fast neutron flux in the inner channel of NIRR-1 at a power level of 15.5kW is (1.047±0.08) x 10^{11}cm^{-2}s^{-1}, which approximates to a thermal-to-fast neutron flux ratio of 5 for the inner channels of MNSR facilities. This value is consistent with the calculated value obtained by Monte Carlo simulation of neutronics parameters of NIRR-1 [7]. The reactor fast neutron spectrum-averaged cross-sections for the dosimetry reactions are the recommended data taken from Reference [8]. Results of (n, p) reaction on ^{27}Al, ^{28}Si, ^{29}Si, ^{46}Ti, ^{47}Ti, ^{56}Fe, ^{58}Ni and (n,α) reaction on ^{30}Si were found to be in good agreement with recommended data within standard deviation. However, data obtained for the ^{27}Al(n,α)^{24}Na reaction using the Al-0.1%Au foil as the flux monitor for both the comparator approach and the conventional method are higher than recommended data from the literature by over 25%. The ^{27}Al(n,α)^{24}Na reaction cross section for reactor fast neutrons is very small due to the high Coulomb barrier for a-particle emission. This may be the reason for the large spread of existing experimental data as well as discrepancies in the recommended data. Full discussions on the results are provided in Reference [5]. The thermal capture cross section data for the target nuclides ^{47}Ca, ^{71}Ga, ^{75}As, ^{94}Zr and ^{238}U reactions are presented in Table 2. The measured R_{CD} data were used to calculate Q_O values based on equation 1. The deduced Q_O values are compared with data from reference 9, while the γ_O data are compared with data from reference 10. For completeness

and to validate the experimental procedures, data for the ultimate monitor reaction, $^{197}Au(n,\gamma)^{198}Au$ were also determined and are presented in Table 2.

4. Conclusions

A comparator method based on the resonance integral of $^{197}Au(n,\gamma)^{198}Au$ reaction has been used to determine reactor fast neutron spectrum-averaged cross-section data in an inner irradiation channel of MNSR facility. Results agree well with literature data, except for $^{27}Al(n,\alpha)^{24}Na$ and $^{64}Zn(n,p)^{64}Cu$ reactions, which deviate by over 25%. This investigation confirms the suitability of the MNSR for the determination of reactor fast spectrum-averaged cross-section data of threshold reactions of energy between 2 and 4.5 MeV.

Acknowledgement

This work is part of the IAEA Coordinated Research Project: ‘‘Development of Reference Database for NAA’’ through contract no. NIR/13278.

REFERENCES

[1] ZIKOVSKY, L., GALINER, J.L., Calculation of primary nuclear interferences occurring in neutron activation analysis with a SLOWPOKE reactor. J. Radioanal. Nucl. Chem. **67** (1981) 193–203.

[2] JONAH, S.A., Fission neutron-induced analytical sensitivities and interference factors in NAA with MNS reactors. Acta Phys. Chim. Debrecina **38–39** (2005) 207–216.

[3] JONAH, S.A., BALOGUN, G.I., UMAR, I.M., MAYAKI, M.C., Neutron spectrum parameters in irradiation channels of the Nigeria Research Reactor-1 (NIRR-1) for the k0-NAA standardization. J. Radiaonal. Nucl. Chem. **266** (2005) 83–88.

[4] JONAH, S.A., UMAR, I.M., OLADIPO, M.O.A., BALOGUN, G.I., ADEYEMO, D.J., Standardization of NIRR-1 irradiation and counting facilities for instrumental neutron activation analysis, Appl. Radiat. Isot. **64** (2006) 818–822.

[5] JONAH, S.A., IBRAHIM YV., AKAHO, E.H.K., The determination of reactor-averaged cross-sections miniature neutron source reactor facility. Appl. Radiat. Isot. **66** (2008) 1377–1380.

[6] WANG, LIYU, WINSPAN 2004 A Multi-Purpose Gamma-Ray Spectrum Analysis Software, CIAE, Beijing, China (2004).

[7] JONAH, S.A., LIAW, J.R., MATOS, J.E., Monte Carlo simulation of core physics parameters of the Nigeria research reactor-1 (NIRR-1), Ann. Nucl. Energy **34** (2007) 953–957.

[8] JENDL-3.3, Japan Evaluated Nuclear Data Library, Version 3.3. Nuclear Data Center, Japan Atomic Energy Research Institute, Japan (2002).

[9] DE CORTE, F., SIMONITS, A., Recommended nuclear data for use in the *k*0 standardization of neutron activation analysis, Atomic Data and Nuclear Data Tables **85** (2003) 47-67.

[10] MUGHABGHAB S., Thermal Neutron Cross Sections and Resonance Integrals, IAEA INDC (NDS)-440.

TABLE 1. A COMPARISON OF SPECTRUM AVERAGED CROSS SECTION OBTAINED IN THIS WORK WITH LITERATURE DATA

Reaction	This work		Ref. 11	Ref.8
	γ_f (mb) rel. to γ_f $^{27}Al(n,p)$ reaction	γ_f (mb) rel. to Io(α) $^{197}Au(n,\gamma)$ reaction		
$^{27}Al(n,p)^{27}Mg$	4.20±0.20	4.45±0.25	3.84±0.18	4.28
$^{27}Al(n,\alpha)^{24}Na$	0.93±0.05	0.98±0.06	0.72±0.03	0.69
$^{28}Si(n,p)^{28}Al$	6.83±0.22	6.85±0.21	5.68±0.25	6.13
$^{29}Si(n,p)^{29}Al$	3.98±0.16	3.98±0.16	3.02±0.15	2.99
$^{30}Si(n,\alpha)^{27}Mg$	0.16±0.01	0.15±0.01	0.14±0.01	0.13
$^{46}Ti(n,p)^{46}Sc$	12.5±0.7	13.4±0.9	-	13.10
$^{47}Ti(n,p)^{47}Sc$	16.6±1.1	17.8±1.5	-	17.75
$^{54}Fe(n,p)^{54}Mn$	85.5±4.9	91.4±5.2	-	81.85
$^{58}Ni(n,p)^{58}Co$	120.0±5.9	128.0±8.8	-	107.2
$^{64}Zn(n,p)^{64}Cu$	49.7±2.1	53.1±4.0	-	-

TABLE 2. A COMPARISON OF MEASURED THERMAL CAPTURE CROSS SECTION OBTAINED IN THIS WORK WITH LITERATURE DATA

Reaction	Q_O		γ_O (b)	
	This work	Ref. 9	This work	Ref.
$^{47}Ca(n,\gamma)^{48}Ca$	1.21 ±0.05	1.3	0.85±0.24	1.09±0.07
$^{71}Ga(n,\gamma)^{72}Ga$	6.52±0.66	6.69	4.79±1.1	4.73±1.8
$^{75}As(n,\gamma)^{76}As$	13.9±0.4	13.6	4.38±0.33	4.23±0.08
$^{94}Zr(n,\gamma)^{95}Zr$	5.31±0.11	5.31	0.043±0.007	0.0499±0.0024
$^{238}U(n,\gamma)^{239}U$	101.6±2.5	103.4	2.73±0.03	2.68±0.019
$^{197}Au(n,\gamma)^{198}Au$	15.6±0.3	15.7	98.7±0.1	98.65±0.09

Cross Section Determination of Short-to-Medium Lived Nuclides in a Low Power Research and an Am-Be Neutron Source

B.J.B. Nyarko[1], R.B.M. Sogbadji[2], E.H.K. Akaho[1], S.E. Agbemava[1]

1) University of Ghana, School of Nuclear and Allied Science, P.O. Box AE1, Atomic Energy, Accra, Ghana.
2) National Nuclear Research Institute, P.O. Box LG80, Legon, Ghana.

Abstract. Thermal and epithermal neutron cross-sections for the $^{197}Au(n,\gamma)^{198}Au$, $^{75}As(n,\gamma)^{76}As$, $^{27}Al(n,\gamma)^{28}Al$, $^{51}V(n,\gamma)^{52}V$, $^{127}I(n,\gamma)^{128}I$, $^{152}Sm(n,\gamma)^{153}Sm$, $^{154}Sm(n,\gamma)^{155}Sm$, $^{138}Ba(n,\gamma)^{139}Ba$, $^{26}Mg(n,\gamma)^{27}Mg$ and $^{238}U(n,\gamma)^{239}U$ reactions were determined by the method of foil activation using $^{55}Mn(n,\gamma)^{56}Mn$ as a reference reaction. The experimental samples with and without a cadmium cover of 1 mm wall thickness were irradiated in the isotropic neutron field of the ^{241}Am-Be neutron source and the irradiation sites of the Ghana Research Reactor-1 facility. The epithermal neutron shaping neutron factor (α) of the irradiation channels used were measured using a thin Au wire and a Zr foil. The induced activities in the sample were measured using a gamma ray spectrometry with a high purity germanium detector. The necessary correction for gamma attenuation, thermal neutrons and resonance neutron self shielding effects were taken into account during the experimental analysis. By defining cadmium cut-off energy of 0.55eV, samples in the form of wire of negligible thickness and standard solutions of known mass were irradiated in both irradiation channels of the ^{241}Am-Be neutron source and the miniature neutron source reactor operating at 3 kW and 15 kW to determine the resonance integral for the (n,γ) reactions. The values obtained are in good agreement with those found in literature.

1. Introduction

The use of radioisotopes as tracers is well established all over the world. In general, thermal cross-sections for thermal neutrons and the resonance integrals for epithermal neutrons (from cadmium cut off energy 0.5eV to 0.1MeV) can be determined experimentally by two methods, which are the oscillation and activation methods [1]. In this work, the cross-sections of the elements were measured using the activation method. The miniature neutron source reactor, which has not been used extensively in the measurement of such microscopic parameters and Am-Be neutron source were used. This work is to ascertain the ability of the miniature neutron source reactor produced by China to measure such parameters since it is extensively been used for NAA, and also to use a low neutron source such the Am-Be neutron source to measure cross sections of some short-lived elements. Karadag et al, 2003[2] measured the cross-sections of Arsenic and Gallium using 3 x 592 GBq Am-Be source which is non-fissionable source. Measurement of the cross-sections of element using both an Am-Be source and a fissionable source needs to be investigated. This is because neutron flux parameters can be regulated in fissionable sources. This is to observe the effect of the changes in the nuclear data due to the neutron source. It is important to verify these data because the knowledge of thermal neutron cross-sections and resonance integral cross-sections for elements has become important in recent years due to research and development of radiation detectors for activation analysis and other theoretical and experimental studies concerning interaction of neutrons with matter [2].

1.1. Design Considerations of Ghana Research Reactor-1 (GHARR-1)

The Ghana Research Reactor-1 (GHARR-1) which was used for the measurements is a 30kW tank-in-pool reactor, which uses 90.2% enriched uranium-Al alloy as fuel. The cross-sectional diagrams of Ghana Research Reactor-1 (GHARR-1) are shown in fig.1 and fig.2. The detailed description of the facility has been published by Y.A. Ahmed et al in 2006[3].

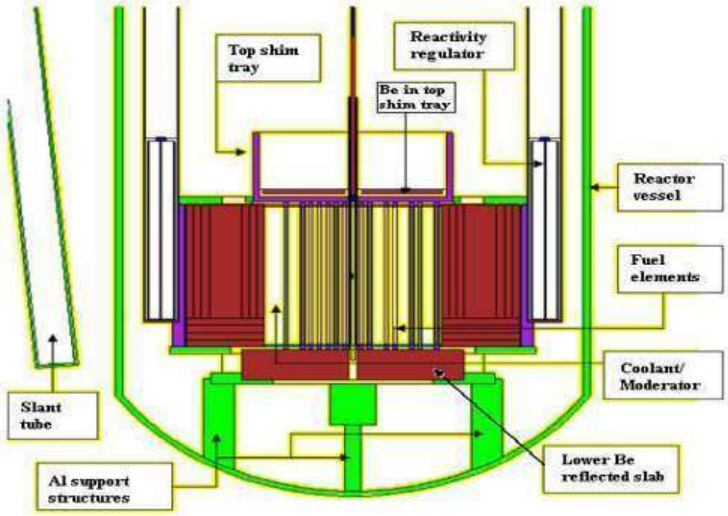

FIG.1. MCNP plot of vertical cross section of GHARR-1 reactor (control rod in full withdrawn position) showing structural supports.

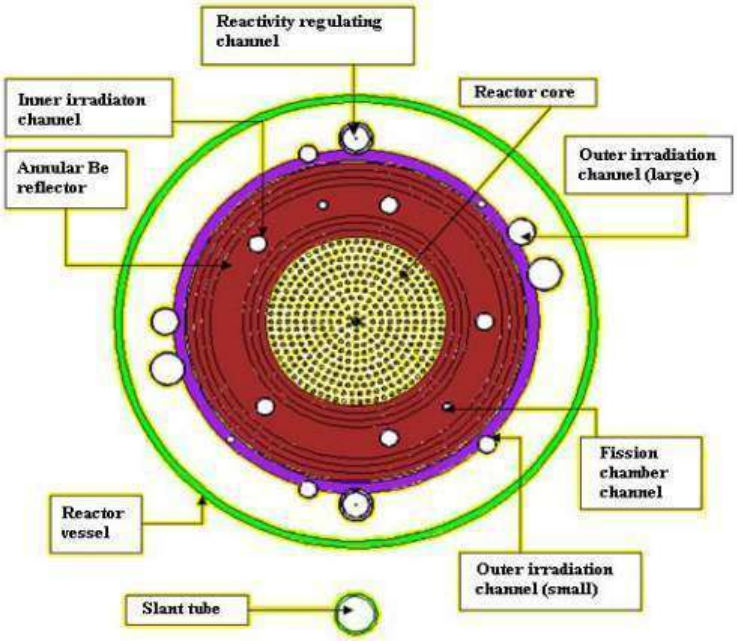

FIG.2. MCNP5 plot of GHARR-1 core configuration showing fuel region (reactor core), channels for irradiation, fission chamber, regulating, slant and annular beryllium reflector.

1.2. Design Considerations of the Americium-Beryllium (Am-Be) Neutron Source

Isotopic neutron sources of ^{241}Am-Be type have found many applications in industry, scientific research, science education and as calibration sources all over the world. They have been applied with great success to prompt gamma-ray neutron activation analysis (PGNAA) because they are relatively inexpensive, easy to shield and portable. ^{241}Am is an intense α particle emitter and it produces neutrons through the ^{9}Be (α,n) ^{12}C reaction. The Americium-Beryllium Neutron Source at Ghana Atomic Energy Commission is a 20 Ci Am-Be neutron

source which is moderated with water, and contained in a cylindrical plastic container which is shielded with concrete blocks. The neutron emission is quoted as 2.2×10^{6} $ns^{-1}Ci^{-1}$ [4].

FIG.3. A picture of the 20 Ci Americium-Beryllium neutron source.

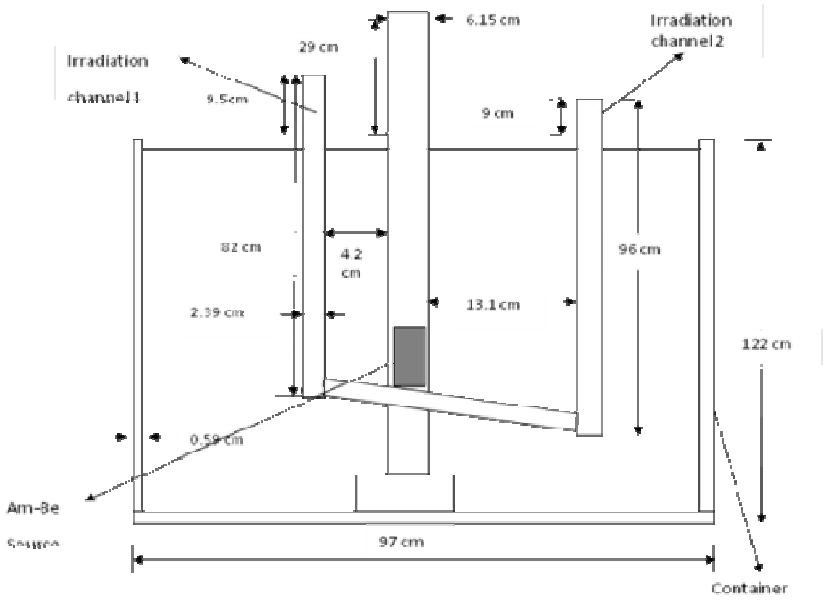

FIG.4. Cross sectional view of the 20 Ci Am-Be neutron source.

2. Theory

The theoretical make up of this work has been well defined by Karadag et al, 2003 in their work to measured the cross-sections of Arsenic and Gallium using 3 x 592 GBq Am-Be source. The theory behind the cross-section measurement adopted from Karadag et al, 2003 is presented below.

2.1. Thermal neutron cross-section determination

In the present work, the thermal neutron cross-section for the reactions for the isotopic reactions was determined relative to that for ^{55}Mn $(n,\gamma)^{56}Mn$ reaction. The thermal neutron cross-section, $\sigma_{o,x}$ for the (n,γ) reaction of interest, is calculated as

$$\sigma_{o,As} = \frac{(R_s - R_{s,Cd})_x}{(R_s - R_{s,Cd})_{Mn}} \frac{(G_{th})_{Mn}}{(G_{th})_x} \frac{g_{Mn}}{g_x} \sigma_{o,Mn} \quad (1)$$

where $R_s R_s$ and $R_{s,Cd}$ are the reaction rate per atom of bare and Cd-covered isotope irradiation, g_{Mn} and g_x are the correction for departure from $1/v 1/v 1/v$ cross-section behavior for Mn and any isotope in this work respectively but the ratio is approximately unity, G_{th} $G_{th}$the self-shielding factor for thermal neutrons, $\sigma_o \sigma_o \sigma_o$ the thermal neutron cross-section, and $F_{cd} F_{cd}$ the cadmium correction factors are unity for the studied reaction; R_s and $R_{s,cd} R_{s,Cd}$ $R_{s,cd}$are determined by

$$R_s \text{ or } R_{s,Cd} = \frac{(A_{sp} \text{ or } A_{sp,s}) F_g M}{\theta N_A \gamma \varepsilon_p} \quad (2)$$

with

$$A_{sp} \text{ or } A_{sp,s} = \frac{N_p / t_m}{w S D C} \quad (3)$$

where $A_{sp} A_{sp}$, $A_{sp,s}$ $A_{sp,s}$ are the specific activities obtained after a bare and cadmium covered isotope irradiation, N_p $N_p$the net number of counts under the full-energy peak collected during measuring time, $t_m t_m$, w the weight of irradiated element, $S = 1 - e^{-\lambda t_{irr}}$ the saturation factor with λ being the decay constant, $t_{irr} t_{irr}$ the irradiation time, $D = e^{-\lambda t_d}$ the decay factor with $t_d t_d t_d$ being the decay time, $C = (1 - e^{-\lambda t_{irr}}) / \lambda t_m$ $C = (1 - e^{-\lambda t_m}) / \lambda t_m$ $C = (1 - e^{-\lambda t_m}) / \lambda t_m$ $C = (1 - e^{-\lambda t_{irr}}) / \lambda t_m$ the measurement factor correcting for decay during the measuring time $t_m t_m t_m$, M the atomic weight ,θ the isotopic abundance, N_A the Avogadro's number, γ he absolute gamma-ray emission probability, ε_p the full-energy peak detection efficiency, and F_g the correction factor for gamma-ray attenuation (Karadag *et al.,* 2003*).*

The correction factor for gamma-ray attenuation in the sample at a given gamma-ray energy at a fixed geometry for the case a cylinder, coaxially positioned with the detector, is given by

$$F_g = \frac{\mu x}{1 - e^{-\mu x}} \quad (4)$$

Where μ is the linear attenuation coefficient (cm^{-1}), μ / ρ is the total mass attenuation coefficient ($cm^2 g^{-1}$ cm^2/g cm^2/g) $cm^2/g$for the compounds used, which are taken from the

XCOM database of Berger and Hubble, (Berger *et al., 1999*) ρ is the density of sample (gcm^{-3}) and x is the sample thickness (cm) (Karadag *et al., 2003).* The sample size was small as compared to the detector.

2.2. Resonance integral cross-section determination

In an ideal 1/E epithermal neutron spectrum, the resonance integral cross section, I_o including $1/v$ tail of thermal neutron spectrum, which is defined by the following relation;

$$I_o = \int_{E_{Cd}}^{\infty} \frac{\sigma(E)}{E} dE, \tag{5}$$

where $\sigma(E)$ the cross section as a function of energy E and E_{Cd} is the cadmium cut-off energy. It has been shown by De Corte *et al*., (De Corte, F., *et al.,* 1989) that the resonance integral definition I_o according to equation (5) is not valid in a real epithermal neutron spectrum and that such a deviating epithermal neutron fluence distribution can be in most cases approximated by $\phi_e(E) \sim 1/E^{1+\alpha}$ $\Phi_e(E) \sim 1/E^{1+\alpha}$, which is epithermal neutron fluence rate per unit $\left(E^{-\alpha}/\alpha\right) 1eV^{\alpha}$ of neutron energy interval. Accordingly, a resonance integral $I_o(\alpha)$ replaced by equation (5) for a $1/E^{1+\alpha}$ real epithermal neutron spectrum is defined as. (De Corte, F., *et al., 1979,* De Corte F., *et al.,* 1981*)*

$$I_o(\alpha) = \int_{E_{Cd}}^{\infty} \frac{\sigma(E) 1eV^{\alpha}}{E^{1+\alpha}} dE \tag{6}$$

where $I_o(\alpha)$ is the resonance integral, which should be used in the calculation of the epithermal activation in a particular irradiation position, characterized by α and the term $1eV^{\alpha} \equiv 1$ is omitted (Karadag *et al.,* 2003*)*. It has also been shown by De Corte *et al*., (De Corte F., *et al.,* 1981*)* that the relationship between I_o , and $I_o(\alpha)$ for the conversion is given by

$$I_o(\alpha) = (1eV)^{\alpha} \left[\frac{I_o - 0.429\sigma_o}{(\bar{E}_r)^{\alpha}} + \frac{0.429\sigma_o}{(2\alpha+1)(E_{Cd})^{\alpha}} \right] \tag{7}$$

Where the term $(I_o - 0.426\sigma_o)$ represents the reduced resonance integral, i.e.; with the 1/v tail subtracted. Equation (7) is only valid for E_{Cd} = 0.55eV, since $0.429 = 2(E_o/E_{Cd})^{1/2}$ with E_o= 0.025eV and E_{Cd} = 0.55eV. The literature values of $\bar{E}_r$ in equation (7) are 5.47eV for ^{197}Au, 468eV for ^{55}Mn and 105eV for ^{75}As. The measured $I_o(\alpha)$ value for the $^{75}\mathrm{As}(n,\gamma)^{76}\mathrm{As}$ reaction is determined relatively $^{55}\mathrm{Mn}(n,\gamma)^{56}\mathrm{Mn}$ reaction as a standard by the following relation: (Karadag *et al.,* 2003*)*.

$$I_o(\alpha)_x = I_o(\alpha)_{Mn} \frac{\sigma_{o,x}}{\sigma_{o,Mn}} \frac{(R-1)_{Mn}}{(R-1)_x} \left(\frac{G_{epi}}{G_{th}} \right)_{Mn} \times \left(\frac{G_{th}}{G_{epi}} \right)_x \tag{8}$$

In the determination of the resonance integral $I_o(\alpha)_x$ for the isotopes under study, the obtained $I_o(\alpha)$ values are converted to I_o by using equation (7), and the results for ^{97}Au and ^{75}As are evaluated.

2.3. Spectrum parameter (α)

For non-ideal reactor situation, the resonance integral, I_o, needs to be modified with an α-dependent term because the I_o values, which are valid only for ideal spectra, is not true for a deviating spectra *(*Moen *et al.,* 1979). For the non-ideal conditions $I_o(\alpha)$ values ought to be used instead of I_o. The conversion of I_o to α-dependent terms takes the form*: (*Jovanovic *et al.,* 1989):

$$I_o(\alpha) = \left[\frac{I_o - 0.429\sigma_o}{(\bar{E}_r)^{\alpha}} + \frac{0.429\sigma_o}{(2\alpha+1)(E_{Cd})^{\alpha}} \right] E_{\alpha}^{\alpha} = \int_{E_{Cd}}^{\infty} \alpha(E) \frac{E_{\alpha}^{\alpha}}{E^{1+\alpha}} dE \tag{9}$$

where E_r^{α} =effective resonance energy, E_a^{α} = leV -arbitrary energy, E_{cd}^{α} = 0.55eV-effective cadmium cut-off energy, σ_o = 2200ms^{-1} (n,γ) = cross section and α = an experimentally determinable characteristics of the reactor channel.

Although the epithermal neutrons represent only a small fraction of the total reactor neutrons, they are sometimes useful in NAA for several elements (e.g. Br, Kb, Sr, Mo, Ba, Ta and U) that have higher relative reaction rates for epithermal neutrons than for thermal neutrons. The technique of taking advantage of those (n,γ) reactions with high resonance integrals through the irradiation of samples under a cadmium cover to shield out the thermal neutrons is commonly known as Epithermal Neutron Activation Analysis (ENAA).

The large number of resonance peaks for most nuclides makes a calculation of effective cross sections for the epithermal neutrons slightly complicated. In order to avoid these resonances, a gold standard is used (Nisle, R.G., 1963) because the reaction ^{197}Au (n,γ) ^{198}Au reaction cross section has a dominant resonance at 4.8eV which has been well investigated (Kennedy *et al.,* 2000, De Corte *et al.,* 1987) and found to be 1550 barns. The activity ratio for an infinitely thin gold foil or alloy irradiated with and without cadmium covers (Cadmium ratio method) is used for measuring spectral parameter and thermal to epithermal flux ratio. This method is also used as a calibration standard to measure the resonance integrals for (n,γ) reactions (Jovanovic *et al*., 1989).

If the single comparator technique is adopted for routine NAA, the effect of the non-ideal epithermal spectrum should not be neglected. Thus, to be accurate in all relevant expressions, Q_0 should be replaced by $Q_0(\alpha)$ [where $Q_0(\alpha)$ is the α-corrected Q_0 to take care of the non-ideality of the epithermal spectrum]

$$Q_o(\alpha) = \frac{I_o(\alpha)}{\sigma_{th}} = \left(\frac{Q_o - 0.429}{E_r^{\alpha}} + \frac{0.429}{(2\alpha + 1) E_{cd}^{\alpha}} \right) \tag{10}$$

where Q_o is the ratio of resonance integral to thermal cross-section is given as $Q_o = \frac{I_o}{\sigma_{th}}$

which is related to flux ratio,

$$f \text{ as } f = (R_{cd} - 1) Q_o \tag{11}$$

Experimental determination of α, using the cadmium ratio method involves irradiating two or more monitors (e.g. Au, Zr, Co) with and without cadmium alternately at the same irradiation channel. When monitors such as ^{197}Au and ^{94}Zr are irradiated under uniform neutron flux, equation (11) transforms to:

$$(R_{cd,1} - 1) Q_o(\alpha)_1 = (R_{cd,2} - 1) Q_o(\alpha)_2 \tag{12}$$

The epithermal deviation factor is obtained from equation (12) using iteration method by using a computer program.

3. Experimental

3.1. Cross Section Determination by the Activation Method

In the determination of the thermal and epithermal cross-section of the isotopes, where manganese is used as a comparator, the irradiation of the samples was done in 30kW research reactor and a 20 Ci Am-Be neutron source at the national nuclear research institute, GHARR-1 center. Standard solution of the elements which contained 10% nitric acid was used for the

cross-sections measurement of the isotopes. The comparator isotope which is manganese was also a standard solution which contained 10% nitric acid.

The irradiation times of the (n,γ) reactions of the manganese and the other standard solutions were carefully chosen yielding enough activity to be measured in γ-ray counting system. The suitable waiting times were employed to minimize dead time losses.

Irradiations of samples using the reactor were performed at a thermal power level of 3kW and 15kW and irradiation using the Am-Be were at a stable flux of 4.2×10^{4} $ns^{-1}cm^{-2}$. After the irradiation, induced radioactivity in the detector foils and solutions were counted on a HPGe coaxial detector (ORTEC), which has a relative efficiency of 25% and energy resolution of 1.8keV at 1332.5KeV gamma-ray of ^{60}Co. The thermal and epithermal neutron cross-sections were calculated using equations (1) and (7) respectively.

TABLE 1: SOME PROPERTIES OF THE ISOTOPES USED DURING THE EXPERIMENTAL MEASUREMENT AGAINST THEIR NUCLEAR CONSTANTS (DE CORTE *et al*., 2003), (IAEA, 1990).

Samples	**Target nuclides**	**Nuclides formed**	**Mode of production**	**Gamma energy** Eγ /(KeV)	**Half-life** $T_{1/2}$	**Isotopic abundance** (%)	**Thermal cross section** (σ/b)	**Epithermal cross section** (I_o/b)	$Q_0 = I_o/\sigma_o$	**Resonance energy** Er/eV	**Absolute gamma intensity** $\gamma(\%)$
Al-0.1%Au foil	^{197}Au	^{198}Au	^{197}Au(n,γ)^{198}Au	411.80	2.70 days	100.00	98.65	1549.79	15.71	5.65	95.56
Arsenic Standard Solution	^{75}As	^{76}As	^{75}As(n,γ)^{76}As	559.10	26.32 hrs.	100.00	3.86	52.50	13.60	106	45
Manganese Standard Solution	^{55}Mn	^{56}Mn	^{55}Mn(n,γ)^{56}Mn	1810.70	2.58 hrs.	100.00	13.20	13.90	1.053	468	27.2
Al-0.1%Au wire	^{27}Al	^{27}Mg	^{27}Al(n,p)^{27}Mg	843.76	9.46 min.	100.00	1.53	0.98	0.64	25700	71.4
Zirconium foil	^{95}Zr	^{96}Zr	^{95}Zr(n,γ)^{96}Zr	756.70	16.74 hrs.	2.80	0.0213	0.1148	5.39	6260	99
Samarium Standard Solution	^{152}Sm	^{153}Sm	^{152}Sm(n,γ)^{153}Sm	103.20	46.27 hrs.	26.70	220.00	3168.00	14.40	8.53	28.3
Magnesium Standard Solution	^{26}Mg	^{27}Mg	^{26}Mg(n,γ)^{27}Mg	1014.40	9.46 min.	11.01	0.0372	0.0238	0.64	25700	28
Barium Standard Solution	^{138}Ba	^{139}Ba	^{138}Ba(n,γ)^{139}Ba	165.80	84.63 min.	71.70	0.405	0.9856	0.88	15700	23.76
Calcium Standard Solution	^{48}Ca	^{49}Ca	^{48}Ca(n,γ)^{49}Ca	3084.50	8.72 min.	0.19	1.12	0.504	0.45	133000	92.1
Aluminium Standard solution	^{27}Al	^{28}Al	^{27}Al(n,γ)^{28}Al	1779.00	2.24 min.	100.00	0.226	0.1605	0.71	11800	100
Vanadium Standard Solution	^{51}V	^{52}V	^{51}V(n,γ)^{52}V	1434.10	3.75 min.	99.75	4.79	2.6345	0.55	7230	100
Iodine Standard Solution	^{127}I	^{128}I	^{127}I(n,γ)^{128}I	442.90	24.99 min.	100.00	4.04	100.192	24.8	57.6	16.9
Samarium Standard Solution	^{154}Sm	^{155}Sm	^{154}Sm(n,γ)^{155}Sm	104.40	22.3 min.	22.70	7.74	33.282	4.3	142	….
Uranium Standard Solution	^{238}U	^{239}U	^{238}U(n,γ)^{239}U	74.70	23.47 min.	99.27	2.75	284.35	103.4	16.9	….

4. Results and Discussion

The results of the measurements of the epithermal neutron shaping factor (α) and, the thermal and resonance integral of the isotopes carried out in this study and the ones reported earlier by other authors are presented and discussed below.

4.1. Epithermal Neutron Shaping Factor (α) in the Irradiation Channels

Among the various experimental methods available for determining the epithermal neutron shaping factor (α), the cadmium ratio method is known to yield the most accurate results.

Determination of the shaping factor in this study was carried out using the cadmium ratio method.

TABLE 2. MEASURED EPITHERMAL NEUTRON SHAPING FACTOR (A) OF THE OUTER IRRADIATION CHANNELS 7 AND INNER IRRADIATION CHANNELS 2.

	Cadmium Ratio (R_{cd})				**Epithermal Neutron Shaping Factor (α)**	
	^{94}Zr		**^{197}Au**			
Channels	**This Work**	**Other Works**	**This Work**	**Other Works**	**This Work**	**Other Works**
Inner irradiation channel 2	3.47±0.07	3.33 [15]	2.36±0.01	2.36 [16]	-0.961±0.034	-1.104 [16]
Outer irradiation channel 7	11.28±0.40	12.65 [15]	3.78±0.01	3.92 [16]	0.037±0.001	0.029 [15]

TABLE 3. MEASURED EPITHERMAL NEUTRON SHAPING FACTOR (A) OF CHANNELS 1 AND 2 OF THE AM-BE NEUTRON SOURCE.

Channels	**Flux ratios** $\frac{\Phi_0}{\Phi_e}$	**Epithermal Neutron Shaping Factor (α)**
Irradiation Channel 1	20.2	0.134±0.001
Irradiation Channel 2	29.7	-0.239±0.003

In general, the neutron spectrum parameters α obtained in this work for the irradiation channels of GHARR-1 being considered compares very well with the α values obtained by Akaho et al on the same reactor in 2002 [15].

The measured α value for the outer irradiation channel of GHARR-1 used compares very well with the Nigeria Research Reactor-1 (NIRR-1) which is also an MNSR similar to GHARR-1, but α values for the outer irradiation channel of GHARR-1 used deviates significantly when compared with that of NIRR-1. In order to ascertain the source of the deviation, the values of the cadmium ratios, $R_{Cd,}$ of the isotopes used (^{94}Zr and ^{197}Au) were considered since that of NIRR-1

could be found in other journals. This was done because both reactors with similar fuel are believed to have identical neutron spectra. It was discovered that the uncertainty may be due to the cadmium ratio value of ^{197}Au, R_{Cd} (Au), which is 2.36 determined in the work and is comparable to the work by Akaho et al on the same reactor in 2002 [15], who had a cadmium ratio value of ^{197}Au, R_{Cd} (Au) for 2.36, which is quite different from a result of 2.12 for NIRR-1 [16].

For that of the Am-Be there wasn't any reference to compare with, but the values obtained were incorporated in the calculation of the epithermal neutron flux of the Am-Be source, the epithermal neutron flux obtained for both channels were comparable to that of an MCNP run.

4.2. Thermal and Epithermal (n,γ) Reaction Neutron Cross-Sections

All factors were experimentally determined and calculated relative to the 846.76 keV - line ^{56}Mn. This comparator isotope has to be considered as the ultimate standard for the evaluations preformed in this work. The nuclear data of interest, which are required for the calculations according to equations (1) and (7), are listed in Table 1. The complete α-mapping of the Ghana Research Reactor-1 irradiation channels 7 and 2 has been found in this work and tabulated in Table 2. The results obtained for this work and for similar work performed on the same isotopes are presented. That of the Am-Be source are presented in Table 3.

TABLE 4. MEASURED THERMAL NEUTRON CROSS-SECTIONS AND RESONANCE INTEGRALS OF ISOTOPES USING THE IRRADIATION CHANNELS OF THE NUCLEAR REACTOR AND THE ^{20}Cl Am-Be SOURCE.

(n,γ) REACTIONS	Thermal Neutron Cross -Section σ_o/b				RESONANCE INTEGRAL I_o/b		
			Other Works			Other Works	
	This Work		IAEA-TECDOC -564, 1990 [14]	De Corte, *et al*., 1988 [17]	This Work	IAEA-TECDOC -564, 1990 [14]	De Corte, *et al*., 1988 [17]
	MNSR	Am-Be			MNSR		
^{75}As (n,γ) ^{76}As	4.28± 0.19	---	4.29	3.86	61.88 ±1.07	63.50	63.50
^{197}Au(n,γ) ^{198}Au	97.47 ± 0.64	---	98.66	98.65	1549 ± 174	1560	1546
^{152}Sm(n,γ)^{153}Sm	238.93± 19.11	---	220	220	3121.48± 249	3168	3038
^{26}Mg(n,γ)^{27}Mg	0.032± 0.001	---	0.037	0.037	0.260± 0.004	0.024	0.024
^{138}Ba(n,γ)^{139}Ba	0.58± 0.01	---	0.41	0.405	0.380± 0.005	0.36	0.35
^{48}Ca(n,γ)^{49}Ca	1.14± 0.02	---	1.12	1.12	0.89± 0.01	0.50	0.53
^{27}Al (n,γ) ^{28}Al	----	0.20 ± 0.02	0.23	0.226	---	---	---
^{51}V(n,γ)^{52}V	----	5.66± 0.36	4.79	4.79	---	--	---
^{127}I(n,γ)^{128}I	----	4.63 ± 0.60	4.04	4.04	---	---	---
^{154}Sm(n,γ)^{155}Sm	7.77± 0.46	7.06 ± 0.53	7.74	7.74	---	---	---
^{238}U(n,γ)^{239}U	----	3.12 ± 0.51	2.75	2.75	---	---	

The present results for thermal neutron cross-sections and the resonance integral for (n,γ) reactions were compared to other works as shown in table 4, and the results did not differ much from the ones compared with.

5. Conclusion and Recommendation

In this work, the shaping factor (α) was measured using the cadmium ratios of ^{95}Zr and ^{198}Au coupled with an iterative computer program written in Fortran 90 for equation (10). This parameter, (α), could also be measured using the graphical method [15]. Using ^{56}Mn as a comparator, most of the measured thermal and epithermal neutron cross-sections of the isotopes were in good comparison with neutron cross-section data published in other journals. Since nuclear data are of great importance in neutron activation analysis (NAA), further experiments should be performed to measure the cross-sections of these and other isotopes using other methods, such as the $K_{o,e}$ comparator method. This will help to improve current nuclear data libraries, which will also improve experimental results in neutron activation analysis (NAA) for the miniature neutron source reactors designed by China as well as for the Am-Be neutron sources.

REFERENCES

[1] MOTEFF, J., *et al*., Neutron fluence measurement, Technical report series No. 107, IAEA, Vienna, 1970.

[2] KARADAG M., YüCEL H., TAN M., ÖZMEN A., Measurement of thermal neutrons and resonance integral for ^{71}Ga(n,γ) ^{72}Ga and ^{75}As (n,γ)^{76}As by using ^{241}Am-Be isotopic neutron source, Nucl. Instr. Methods A **501** (2003) 524-527.

[3] AHMED Y.A., EWA I.O.B., UMAR I.M., BEZBORAH T., JOHRI M., AKAHO E.H.K., The low power miniature neutron source reactors: Design, Safety and Applications, Nigerian J. Phys. **14** (1) (2006) 82-85.

[4] OSEA, E.K., AMOH, G.K., Determination of the thermal neutron flux of an Am-Be neutron source, J. University of Science and Technology, Kumasi,**16** (3) (1996) 108-114.

[5] BERGER M.J., HUBBELL J.H., SELTZER S.M., COURSEY J.S., ZUCKER D.S., XCOM: Photon cross sections database (version 1.2), National Institute of Standards and Technology, Gaithersburg, MD. 1999. Available from http://physics.nist.gov/xcom.

[6] De CORTE F., SIMONITS A., k_o-Measurements and related nuclear data compilation for (n,γ) reactor activation analysis IIIb:tabulation, J. Radioanal. Chem. **133** (1989) 43.

[7] De CORTE F., MOEN L., SORDO-EL H., SIMONITS A., HOSTE J., The effective resonance energy E_r as a parameter for the correction of resonance integrals, $1/E^{(1+\alpha)}$ epithermal neutron spectra: tabulation of E_r for 96 isotopes, J. Radioanal. Chem. **52** (2) (1979) 379-387.

[8] De CORTE F., HAMMAMI K.S., MOENS L., SIMONITS A., De WISPELAERE A., HOSTE J., The accuracy of the experimental alpha-determination in the epithermal reactor neutron spectrum, J. Radioanal. Chem. **62** (1981) 209-255.

[9] JOVANOVIC S., VUKOTIC P., JACIMOVIC R., MIHALJEVIC N., STEGNAR P., Epithermal neutron flux characterization of the TRIGA II Reactor, Ljubljana, Yugoslavia for use in NAA, J. Radioanal. Chem. **113** (1) (1989) 177-185.

[10] NISLE R.G., A unified formulation of the specification of neutron flux spectra in reactors, Neutron Dosimetry, IAEA-TECH REPORT 1 (1963) 111-152.

[11] KENNEDY G., St. PIERRE J., WANG K., ZANG Y., PRESTON J., GRANT C., VUTCHOV, Activation constant of SLOWPOKE and MNSR reactors calculated from the neutron spectrum and K_o and Q_o values, J. Radioanal. Chem. **245** (1) (2000) 167-172.

[12] De CORTE F., De WISPELAERE A., HOSTE L., Accuracy and applicability of k_o method, J. Radioanal. Chem. **113** (1987) 145-161.
[13] De CORTE F., The updated NAA nuclear data library derived from the Y2K k_o-database, J. Radioanal. Nucl. Chem. **257** (3) (2003) 493-499.
[14] INTERNATIONAL ATOMIC ENERGY AGENCY, Practical aspects of operating a neutron activation analysis laboratory, IAEA-TECDOC-564, Vienna (1990).
[15] AKAHO E.H.K., NYARKO B.J.B., Characterization of neutron flux spectra in irradiation sites of MNSR reactor using the Westcott-formalism for the K_o neutron activation analysis method, Appl. Radiat. Isot. **57** (2002) 268.
[16] JONAH S.A., BALOGUN G.I., UMAR I.M., MAYAKI M.C., Neutron spectrum parameters in irradiation channels of the Nigeria Research Reactor-1 (NIRR-1) for the k_0-NAA standardization, J. Radioanal. Nucl. Chem. **266** (1) (2005) 82-85.
[17] De CORTE F., SIMONITS A., A compilation of accurately measured 2200 ms^{-1} cross sections for 101 (n,γ) reactions of interest in activation analysis; a critical comparison with literature, Nuclear data for Science and Technology, (1988) 583 - 586.
[18] INTERNATIONAL ATOMIC ENERGY AGENCY NUCLEAR DATA SERVICE 1998-2008, EXFOR-CINDA DATABASE AND RETRIEVAL SYSTEM VERSION 1.98, July 2008.

Cross section measurements for thermal neutron-induced reactions on actinides at the ILL reactor

A. Letourneau[a], E Dupont[a], P. Mutti[b], S. Panebianco, Ch. Veyssière[a]

[a] Irfu, CEA-Saclay, 91191 Gif-sur-Yvette, France
[b] Institut Laue-Langevin, ILL, 38042 Grenoble Cedex 9, France

Abstract. In the framework of the Mini-INCA project we use the High Flux Reactor of the Laue-Langevin Institut to measure thermal neutron-induced reactions on actinides. Experiments are performed using two irradiation channels: the H9 and the V4 channels. These two channels offer a diversity of neutron fluxes ranging from pure thermal neutrons to about 15% epithermal neutrons with intensities as high as 1 10^{15} n/cm^2/s. The analysis of irradiated samples is based on standard activation techniques and on-line fission rate measurements. All these techniques have been adapted for high neutron fluxes: high-counting rate and - spectroscopy, mass spectrometry for rare isotopes, and miniature fission-chambers for transmutation studies. Thanks to the high neutron fluxes and such techniques it is possible to form short-live isotopes (such as ^{242gs}Am or ^{244m}Am) and to study their decay or their neutron-induced reactions. The program is now almost completed providing a set of new and accurate data on the capture cross sections of ^{232}Th, ^{233}Pa, ^{234}U, ^{237}Np, ^{238}Pu, ^{242}Pu, ^{241}Am, $^{242gs-m}$Am, ^{243}Am, ^{242}Cm, ^{244}Cm, ^{248}Cm, ^{249}Cf, ^{250}Cf, ^{251}Cf and the neutron-induced fission cross sections of ^{238}Np, $^{242gs-m}$Am and ^{245}Cm.

Introduction

Faced with a probable increase of the world demands in energy, the nuclear power option seems to be a conceivable solution for energy production without using remaining limited fossil fuel resources which contribute to the alarming global warming effect. However, public opinion still expresses major concerns about this energy source, mainly due to the residual long-term highly radioactive wastes. In this context, even if the creation of a long-term geological repository seems to be unavoidable, research and development about partitioning and transmutation are essentials. In particular, the reduction of uncertainties on nuclear data is one of the fundamental aspects of these researches for systems considered as possible transmuters of transuranic elements or even simply for systems which have to respond to high-level requirements as waste minimization, sustainability, safety and non-proliferation. Most of the nuclear data are available in modern data files, but their accuracies and validation are still a major concern, especially for Minor Actinides (MA).

In the framework of the Mini-INCA project [1], we took benefit of the high neutron fluxes provided by the High Flux Reactor (HFR) of the Institut Laue-Langevin (Grenoble, France) to provide new and accurate data for slow neutron-induced reaction on MA and β-decay parameters such as decay half-lives or γ-ray intensities for short-lived isotopes or isomers. High fluxes are very useful to study the transmutation chain of minor actinides and to form short-lived isotopes or isomers by double neutron capture. Furthermore mass samples of few micrograms or tens of micrograms are sufficient in the experiments leading to lower costs and an easier way to handle the samples, especially for neutron emitters like ^{244}Cm or α-emitters like ^{238}Pu. On the other hand, they require adapted measurement techniques able to withstand the huge activity of the samples and to develop accurate analysis tools. In this paper, we present the experimental approach and detail a few measurements to illustrate the analysis technique.

The High flux reactor of ILL

Description

The High Flux Reactor of the Laue-Langevin Institut is the most intense continuous source of neutrons in the world. It went critical on August 31 of 1971 and since delivers neutrons for different instruments and experiments. The top view of the core is shown in *FIG.1*, where we see the different tubes allowing neutrons to escape from the core.

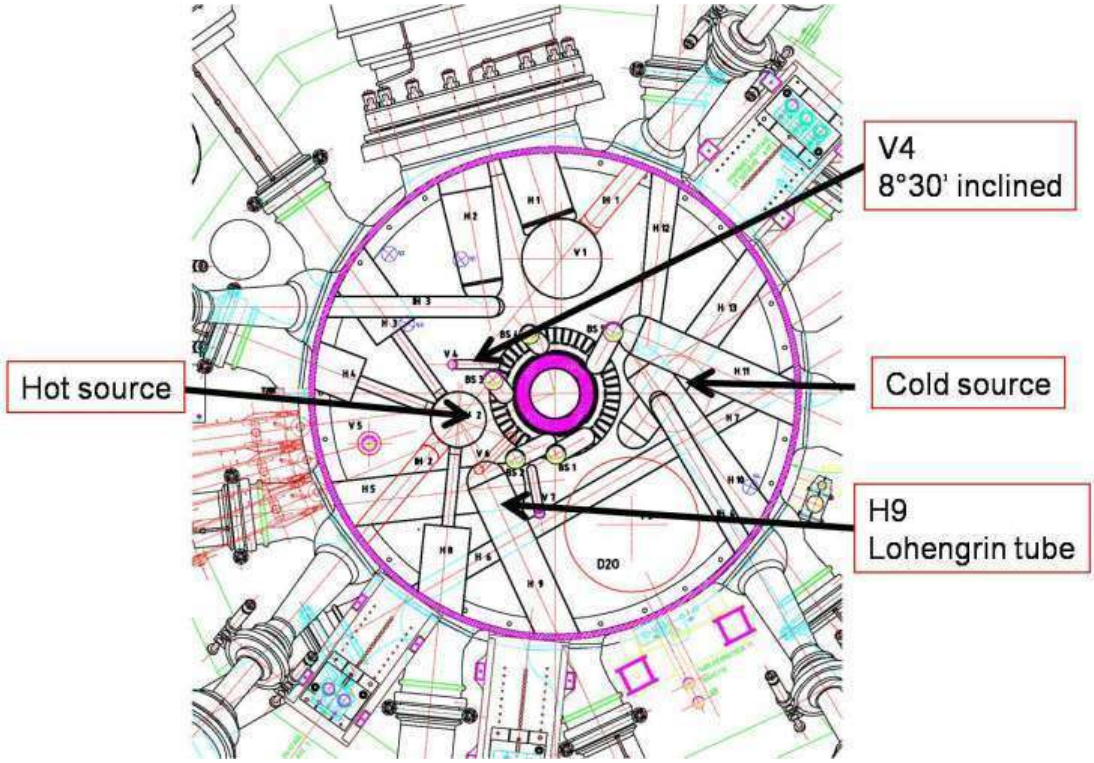

FIG.1. Top view of the HFR core, where we see the V4 and the H9 channels used for our experiments together with the other channel tubes. Also are indicated the hot and cold sources which can locally modify the neutron energy spectra. The fuel element is located in the centre.

We use the V4 and the H9 channels for our measurements. The V4 channel is located very close to the fuel element and provides the highest thermal neutron flux in the world accounting for 10^{15} n/cm^2/s in its lowest position. Due to its inclination of 8°30' with respect to the vertical axis it is possible to irradiate samples into either pure thermal neutron fluxes or with a small component of about 10% of epithermal neutrons (neutrons with energy greater than 1 eV). The H9 channel is used by the Lohengrin spectrometer and is located at about 50 cm from the fuel element and offers a neutron flux with about 2% of epithermal neutrons.

Monte Carlo simulations

The reactor core was simulated using a precise geometry description of the core including all the beam channels, the hot and the cold sources. The first simulation was performed with the MCNP2.5 code [2]. Calculations were done for the moderator temperature of 50°C. Results of the calculated neutron fluxes for different positions of irradiation in the V4 and H9 channels are shown on FIG.2 (left). A recent simulation using TRIPOLI4 code coupled with the evolution code APOLLO2 was also done [14]. The evolution of the neutron flux deduced from this simulation is shown on FIG.2 (right).

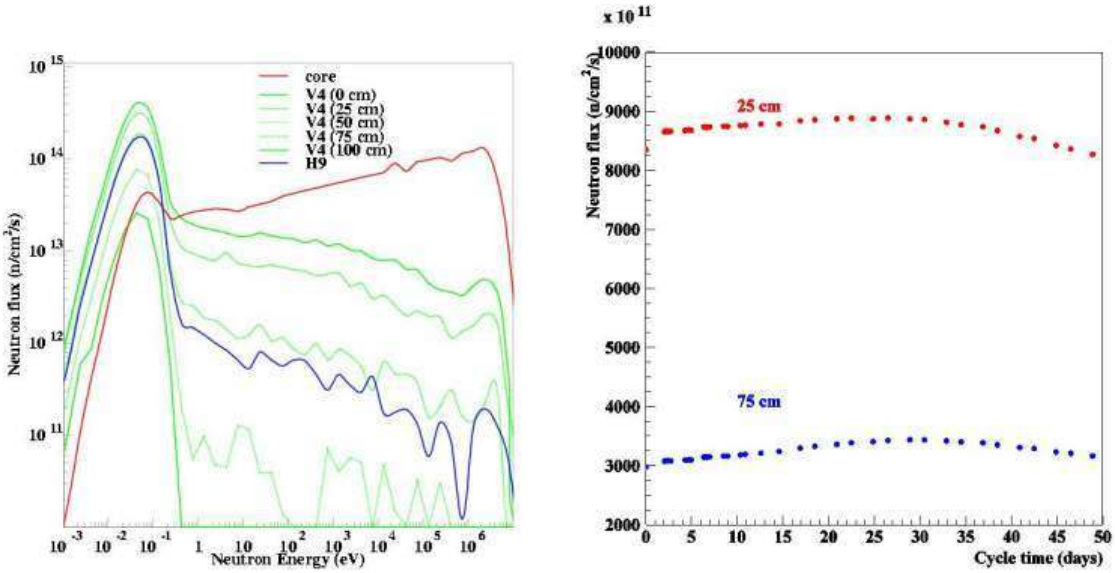

FIG.2. Left: Neutron energy spectra simulated with MCNP2.5 at different positions of irradiation at the HFR [2]. Right: Neutron flux evolution for two of these irradiation positions [14].

In TABLE 1 are given the mean neutron flux values measured at different positions of irradiation of the V4 and H9 channels [3]. The calculated thermal contribution is also given showing a strong contribution even in the lowest position of the V4 channel. For comparison with other experiments we also expressed the neutron flux features in terms of the Westcott convention. In this convention the effective cross section is expressed as:

$$\hat{\sigma} = \sigma_0 (g + r\sqrt{\frac{T}{293.53}} s_0) \qquad (1)$$

where σ_0 is the reaction cross section for 2200 m/s neutrons, g the Westcott factor and s_0 is defined by $s_0 = \frac{2}{\sqrt{\pi}} . \frac{I_0^{'}}{\sigma_0}$ and $I_0^{'} = I_0 - 0.484\sigma_0$ is the reduced resonance integral, i.e., the resonance integral above 0.5 eV after subtracting the 1/v component. From the $^{59}Co(n,\gamma)^{60}Co$ and $^{197}Au(n,\gamma)^{198}Au$ reactions we calculated the epithermal index $r\sqrt{T/T_0}$ at different irradiation positions of the V4 channel (see TABLE 1).

TABLE 1. NEUTRON FLUX CHARACTERISTICS AND EFFECTIVE CROSS SECTIONS (IN BARN) FOR THE TWO STANDARD REACTIONS USED FOR THE NORMALISATION ($\sigma_0(^{59}Co)$=37.18±0.06 b, $\sigma_0(^{235}U)$=582.6±1.1 b [13]).
ϕ is the mean neutron flux value as measured in [3] and ϕ_{th} is the calculated thermal component defined with a cut at 1 eV. The $r\sqrt{323/T_0}$ is the epithermal index defined in Eq.1.

Positions	ϕ (n/cm^2/s)	ϕ_{th}/ϕ	$r\sqrt{323/T_0}$	$^{59}Co(n,\gamma)^{60}Co$	$^{235}U(n,f)$
25 cm	8. 10^{14}	0.898	0.0144	28.33	424.68
50 cm	7.96 10^{14}	0.966	0.0039	30.74	466.83
75 cm	4.3 10^{14}	0.997	0.00061	31.66	484.17
100 cm	5.5 10^{13}	1.000	<0.0006	31.84	487.29
H9	6 10^{14}	0.981	0.0021	31.10	473.93

Integral measurements and corrected cross sections

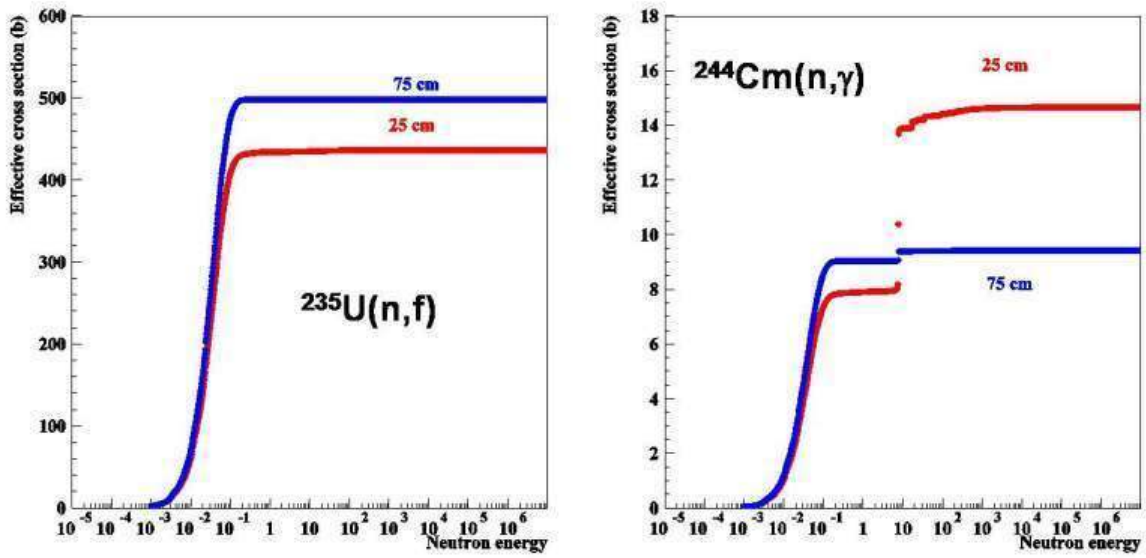

FIG.3. Effective cross sections defined by Eq.2 as a function of the neutron energy for $^{235}U(n,f)$ (left) and $^{244}Cm(n,\gamma)^{245}Cm$ (right) reactions at two irradiation positions in the V4 channel.

In-core measurements provide integral quantities. The reaction rate which is measured is proportional to the integral of the cross section times the neutron flux density and the averaged cross section deduced from the measurement is then expressed as:

$$<\sigma>=\frac{\int_0^\infty \sigma(E).\phi(E)dE}{\int_0^\infty \phi(E)dE} \qquad (2)$$

where $\sigma(E)$ is the cross section as a function of the neutron energy and $\phi(E)$ is the neutron energy distribution at the irradiation position.

Instead of using the standard cadmium ratio technique to determine the thermal cross section, we oriented our analysis towards the use of Monte Carlo simulations. We use evaluated resonance parameters to calculate the effective cross section at the irradiation position [4] and to extract the 25.3 meV value (σ_0) from the calculated ratio $\sigma_0/<\sigma>$. On FIG.3 are shown the effects of resonances on the effective cross sections for two reactions. Regarding the $^{244}Cm(n,\gamma)^{245}Cm$ reaction, about half of the effective cross section measured at 25 cm is due to the huge resonance located at 7.67 eV. This effect is less pronounced in Maxwellian fluxes corresponding to the positions 75 or 100 cm. Then by measuring the reaction rate in different positions the contribution of such resonance to the total cross section can be estimated. On the other hand such effects are not seen for the $^{235}U(n,f)$ reaction. Thus for reactions behaving like $^{235}U(n,f)$ the correction procedure does not introduce significant errors especially if resonances are well characterised, whereas for reactions behaving like $^{244}Cm(n,\gamma)$ added errors have to be introduced. Nevertheless, the uncertainties on resonance parameters and on neutron flux distribution are fully propagated through the extraction procedure.

Off-line analysis by α- and γ-spectroscopy

Description of the instrumentation

The α and γ-spectroscopic techniques are largely used for neutron capture cross section measurements but often they are used separately. As a consequence discrepancies could exist between data measured only by γ-spectroscopy and data obtained only by α-spectroscopy. This is mainly due to the fact that the γ-ray emission probabilities could have wrong values whereas for actinides the α-ray emission probabilities are better known. That is the reason why we decided to use both techniques in order to measure either separately the α or the γ activities of the irradiated sample or to follow the α versus the γ activities of the sample. We use the latter technique to measure the γ-ray emission probabilities for rare isotopes.

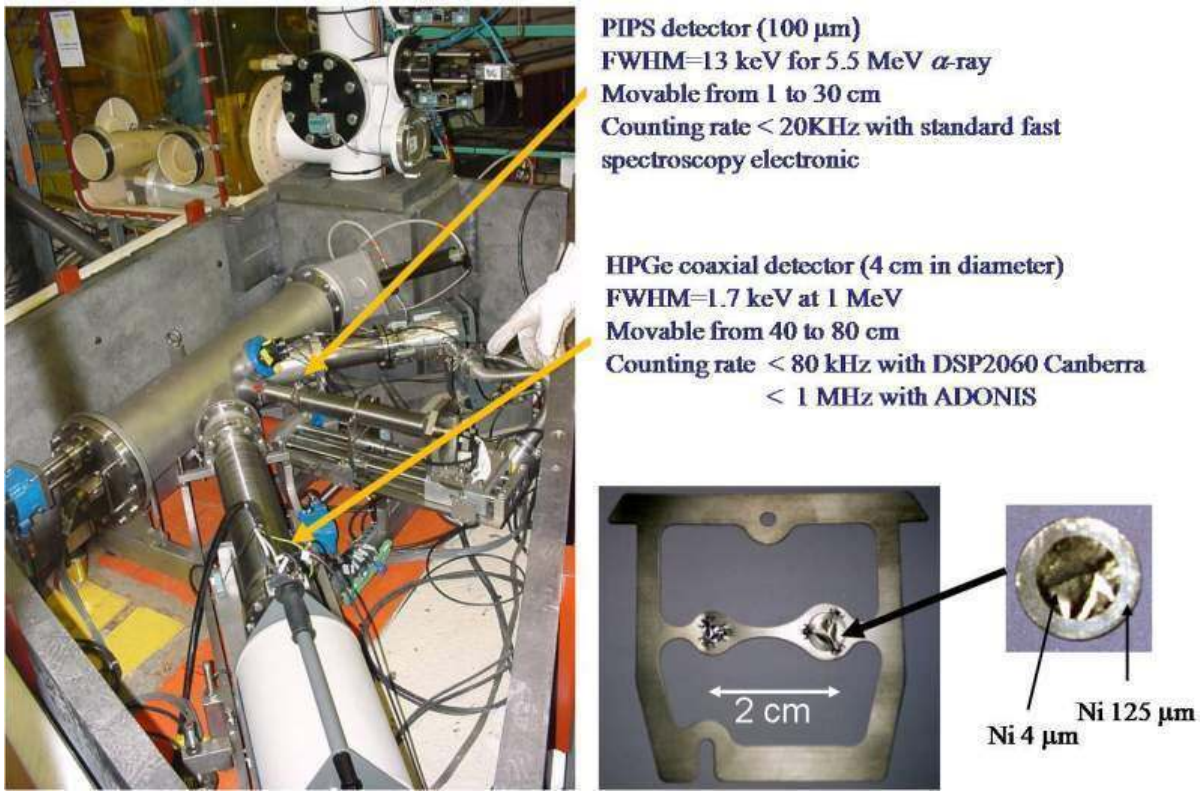

FIG.4. Left: α and γ-spectroscopy bench connected to the H9 target source exchanger. Right: Target holder used to irradiate the samples. The Al-Co monitor (6 mm in diameter) is located to the left and the sample (12 mm in diameter) to the right.

Connected to the target exchanger of the Lohengrin spectrometer (H9 channel) we have installed an α and γ spectroscopy bench [5] (see FIG.4) which allows a quasi-on-line characterization of the irradiated samples as well as a repeated sequence of irradiation/measurement operations. The γ-rays are recorded using a high purity coaxial Germanium detector and the α-rays with a Passivated Implanted Planar Silicon detector. The Si- and Ge-detector electronics are able to manage high counting rates (up to 80 kHz for Ge-detector and up to 20 kHz for Si-detector). The sample is electrodeposited on the centre of a 4 µm Ni backing and mounted on a Ti target holder together with an Al-Co foil to measure the neutron fluence during the irradiation (see FIG.4).

This set-up is used for (n,γ) cross section measurements but also to measure the life of short-lived isotopes or isomers and the absolute emission probabilities of the γ-rays.

The ^{237}Np(n,γ)^{238}Np reaction cross section

The ^{237}Np(n, γ)^{238}Np cross section was measured by α and γ-spectroscopy in the H9 channel. The ^{237}Np sample (13.52±0.14 μg) was electrodeposited on the centre of the Ni backing and was irradiated for 2.733 hours in the H9 channel [9]. The sample was analysed before and after irradiation (see FIG.5). From the analysis before irradiation we could deduce the isotopic composition of the sample and the quantity of ^{237}Np.

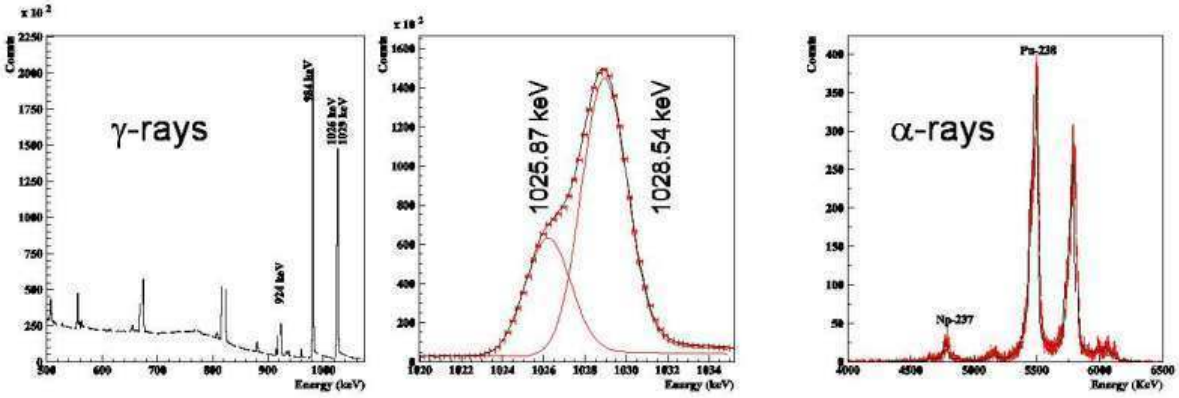

FIG.5. Recorded γ-ray (left) and α-ray (right) energy spectra. The figure in the center is a zoom of the γ-ray energy spectra to show the good resolution of the measurement.

From the analysis after irradiation we could measure the α- and γ-activities and their evolution as a function of time. From these measurements we deduced the absolute γ-ray emission probabilities for the ^{238}Np β-decay. By normalising the α and γ activities with the standard ^{59}Co(n,γ)^{60}Co reaction we deduced the ^{237}Np(n, γ)^{238}Np reaction cross section. The obtained values are listed in TABLE 3.

The ^{243}Am (n,γ)$^{244gs-m}$Am cross sections and the β-decay half-life of ^{244m}Am.

We used the H9 instrumentation to measure the ^{243}Am(n,γ)$^{244gs-m}$Am cross sections and the β-decay half-lives of ^{244m}Am and ^{244gs}Am. The ^{243}Am (10.926±0.14 μg) was electrodeposited on the Ni backing and was irradiated for (3.277±0.002) hours to determine the total capture cross section by measuring the α-activity of ^{244}Cm. Then the sample was irradiated for (24.00±0.02) min more to measure the decay half-lives of ^{244m}Am and ^{244gs}Am isotopes and the branching ratio. Due to the high counting rate in the γ-detector, we used the ADONIS system [15] which allows for counting rates as high as 1 MHz. We deduced a new half-life for ^{244m}Am of (28.25±1.3) min and (10.65±0.12) h for ^{244gs}Am and a branching ratio of (0.0474±0.0001) [10]. The total capture cross section we obtain is (73.8±2.3) b in agreement with the previous measured value [7].

Off-line analysis by mass spectrometry

Description

The standard Thermal Ionisation and Inductive Coupled Plasma mass spectrometry analysis techniques are also used to characterise the sample before and after irradiation. For some measurements, these methods have been developed to measure low mass samples and rare actinides as protactinium [8] and more recently to measure berkelium and californium isotopes. Generally, samples are irradiated for one cycle and then analysed by mass spectrometry.

We had to develop analysis software, named MERCS [12], able to calculate the evolution of the isotopes under irradiation and to properly propagate the uncertainties taking into account the correlations. It is based on the ROOT shared libraries and solved numerically the Bateman equations for one-energy group cross sections. Its originality lies in its capacity to compute the sensitivity of the experimental observables to the nuclear parameters.

^{232}Th(n,γ)^{233}Th and ^{233}Pa(n,γ)^{234}Pa reaction cross sections

The ^{232}Th(n,γ)^{233}Th and ^{233}Pa(n,γ)^{234}Pa reaction cross sections were measured by means of a precise mass spectrometry analysis [8]. The analysis was performed few months after 43 days of irradiation in V4. The irradiated sample was a pure 100 µg ^{232}Th sample canned in a quartz container. The irradiation position was chosen to get a significant evolution by multiple captures (i.e. intense flux) and to reduce corrections due to the contribution of resonances (i.e. thermal flux). The neutron fluency, over which thorium evolved, was measured thanks to an Al-0.1%^{59}Co monitor.

TABLE 2. EFFECTIVE CROSS SECTIONS (<σ>) MEASURED, CORRECTED VALUES TO 25.3 MEV (σ_0) AND CALCULATED OVER EXPERIMENTAL RATIO (C/E) FOR THE MAIN DATA LIBRARIES.

Reactions	<σ> (b)	σ_0 (b)	$C/E_{JEFF3.1}$	$C/E_{ENDF-B7}$	$C/E_{JENDL3.3}$
^{232}Th(n,γ)^{233}Th	6.27±0.18	7.34±0.21	1.008±0.029	1.003±0.029	1.008±0.029
^{233}Pa(n,γ)^{234}Pa	34.16±1.54	38.34±1.78	1.085±0.05	1.114±0.05	1.081±0.05
^{234}U(n, γ)^{235}U	87.34±2.75	106.12±3.34	0.94±0.03	0.955±0.03	0.97±0.03
^{235}U(n, γ)^{236}U	79.01±9.05	98±11	1.006±0.11	1.006±0.11	1.006±0.11

Experimental uranium and thorium isotopic ratios were fitted using the MERCS code with the effective cross section values listed in TABLE 2 as free parameters. The fit procedure was repeated several times. At each step, all other nuclear parameters (included neutron flux for which we have used the experimental value) were randomly sampled within their Gaussian error distribution. Furthermore, for each cross section the best combination of measured isotopic ratio for which the cross section is the most sensitive was chosen. By this means, the covariance matrix is close to a diagonal one and calculated errors could be considered as independent. Resulting cross sections are given in TABLE 2**.**

On-line monitoring with fission chambers

Fission chambers are largely used in power plants either as in-core or out-core instrumentation to control the neutron flux. We develop a concept of compensated fission chambers to follow on-line the fission rate evolution of an irradiated sample. This evolution is done in reference to the evolution of ^{235}U. The detector, referred in the following as Triple-Deposit Fission-Chamber (TDFC), is composed of three microscopic fission-chambers[1] mechanically coupled but electrically isolated and sharing the same gas (see FIG.6). They operate in current mode [6]. Parasitic currents induced by γ-rays and neutron activation are subtracted thanks to the third chamber without deposit. Each fission chamber is 2 cm long, has a diameter of 4 mm, and is filled with pure Argon gas. Therefore, these small detectors could be placed one very close to the other, thus reducing systematic errors due to distance. We measured this effect by rotating TDFC to be less than 2%.

[1] Fabricated by Photonis company, France

In high neutron fluxes the main problem is the accumulation of charges within the inter-electrode gap due to the high fission rates. This effect is considerably reduced thanks to the thin gap between anode and cathode. Nevertheless we performed a lot of theoretical studies and developments to reduce this accumulation. A review, including their functioning, can be found in [7].

FIG.6. Picture of a TDFC, where we see the three independent fission chambers of 4 mm in diameter.

The ^{238}Np(n,f) and ^{238}Pu(n,γ)^{239}Pu reaction cross sections

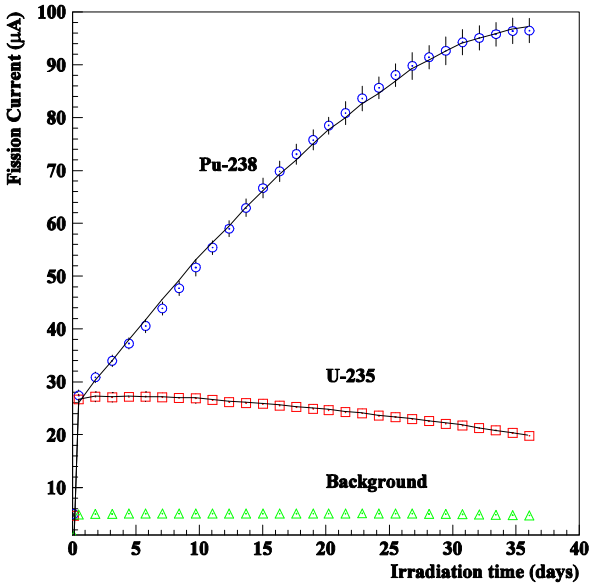

FIG.7. Measured fission currents (symbols) as a function of time for the ^{238}Pu TDFC. Data were fitted using the MERCS code (lines).

The ^{238}Np(n,f) and ^{238}Pu(n, γ)^{239}Pu cross sections were measured in the V4 channel using two TDFCs [16]: one containing (42±1.3) μg of pure ^{237}Np and the other one containing (42.6±1.6) μg of ^{238}Pu with 4.978% of ^{239}Pu. The two detectors were containing also (2.64±0.01) μg and (4.48±0.01) μg of ^{235}U, respectively. The TDFCs were irradiated separately during one cycle. The nuclear parameters were fitted to the measured currents using the MERCS code (see FIG.7). The obtained cross sections in all these experiments are

shown in TABLE 3. The ^{238}Np and ^{238}Pu is still in analysis so that the values are still preliminary.

TABLE 3. EFFECTIVE CROSS SECTIONS (<σ>) MEASURED, CORRECTED VALUES TO 25.3 MEV (σ_0) AND CALCULATED OVER EXPERIMENTAL RATIO (C/E) FOR THE MAIN DATA LIBRARIES. (*) IS FOR PRELIMINARY RESULTS.

Reactions	<σ> (b)	σ_0 (b)	$C/E_{JEFF3.1}$	$C/E_{ENDF-B7}$	$C/E_{JENDL3-3}$
^{237}Np(n, γ)^{238}Np	151±4	182±4.5	0.99±0.03	0.89±0.03	0.89±0.03
^{238}Np(n,f)	1611±100*	2050±110*	0.925±0.06	0.955±0.06	0.955±0.06
^{238}Pu(n, γ)^{239}Pu	411±20*	514±21*	1.05±0.04	1.09±0.04	1.05±0.04

The ^{244}Cm(n, γ)^{245}Cm and ^{245}Cm(n,f) reaction cross sections

The ^{244}Cm(n, γ) and ^{245}Cm(n,f) cross sections were measured very recently by means of TDFC in the V4 channel. A (39.46 ±0.4) µg sample of curium containing 66.9% of ^{244}Cm, 3.8% of ^{245}Cm and 23.6% of ^{240}Pu was irradiated. The isotopic concentration was determined before irradiation by mass spectrometry with a precision better than 1%. The ^{245}Cm(n,f) cross section was measured during the start-up phase of the reactor [16]. Then measured currents were fitted with the MERCS code taking into account the evolution of ^{240}Pu and propagating the associated errors (see *FIG.8*). ^{240}Pu isotope is the main responsible for the bump in the curium fission current between 10 and 30 days. Preliminary results are given in TABLE 4 [12].

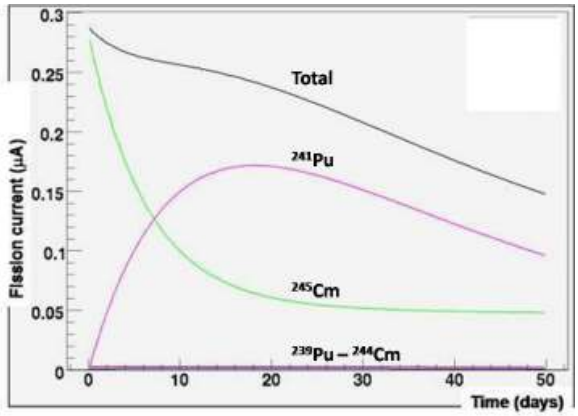

FIG.8. Measured fission current (black line) of the ^{244}Cm TDFC and calculated contributions of the listed isotopes to the fission current.

TABLE 4. EFFECTIVE CROSS SECTIONS (<σ>) MEASURED, CORRECTED VALUES TO 25.3 MEV (σ_0) AND CALCULATED OVER EXPERIMENTAL RATIO (C/E) FOR THE MAIN DATA LIBRARIES. (*) IS FOR PRELIMINARY RESULTS.

Reactions	<σ> (b)	σ_0 (b)	$C/E_{JEFF3.1}$	$C/E_{ENDF-B7}$	$C/E_{JENDL3-3}$
^{244}Cm(n, γ)^{245}Cm	19.11±2.67*	15.81±3*	0.74±0.1	0.96±0.13	0.96±0.13
^{245}Cm(n,f)	1352±23	1979±65*	1.086±0.019	1.086±0.019	1.083±0.019

Conclusions

Within the Mini-INCA project, we took benefit of the high neutron flux of the ILL reactor to provide new accurate data on slow neutron-induced reaction cross sections for minor actinides. High-flux research reactors seem to be well suited for such studies as they allow

measurements on isotopes for which it is difficult to produce targets due to their short half-life. In return, strong efforts have to be made on the development of the instrumentation for high counting rates and to extract properly the signal from a large background due to activation. On the other hand as neutrons have a strong Maxwellian component, we have seen that for most of the actinides, resonances do not contribute too much to the thermal cross section. In consequence measured cross sections can be considered as differential cross sections at thermal energy. Finally, the capture and fission cross sections we measured show good agreements with the most recent measurements. However, large discrepancies with evaluated data libraries have been observed in few cases.

Acknowledgements

Authors are grateful to ILL technicians for their great help in the preparation of the experiments. This work was partially supported by the GDR GEDEPEON (France).

REFERENCES

[1] FIONI, G., *et al*., J. Nucl. Sci. Technol., Supplement, **2** (2) (2002) 876.
[2] RIDIKAS, D., *et al*., Proceedings of the 6th OECD/NEA Information Exchange Meeting on Actinide and Fission Partitioning and Transmutation, 11-13 December 2000, Madrid, Spain.
[3] FADIL, M., Ph.D. thesis, INP Grenoble, 2003 (in French).
[4] LETOURNEAU, A., *et al*., CEA/DSM/SPhN-03-243 report, 2003 (unpublished).
[5] MARIE, F., *et al*., Nucl. Inst. Meth. **A556** (2006) 547.
[6] CHABOD, S., *et al*., Nucl. Inst. Meth. **A566** (2006) 633.
[7] LETOURNEAU, A., *et al*., Proceeding of ANIMMA 2009, IEEE Trans. Nucl. Science (in press).
[8] BRINGER, O., *et al*., Nucl. Instr. Meth **A59** (2008) 510-516.
[9] LETOURNEAU, A., *et al*., submitted to Appl. Rad. Isot. (2009).
[10] LETOURNEAU, A., *et al*., to be submitted to Appl. Rad. Isot. (2009).
[11] FIONI, G., *et al*., Nucl. Phys. **A693** (2001) 546.
[12] BRINGER, O., Ph. D. thesis, INP Grenoble (2007).
[13] MUGHABGHAB, S.F., Atlas of neutron resonances, 5th Ed., Elsevier.
[14] CAMPIONI, G., *et al*., Proceedings of the International Conference on the Physics of Reactors Physor, 14-19 September 2008, Interlaken, Switzerland; G. Campioni, private communication.
[15] BARAT, E., *et al*., IEEE Nucl. Scien. Sympo. Conf. Record N30-6, 955 (2006).
[16] LETOURNEAU, A., *et al*., Proceedings of Seminar on fission, 18-21 September 2007, Corsendonk, Belgium, 63.

Prompt γ-ray emission in nuclear fission

S. Oberstedt[a], R. Billnert[b], R. Borcea[a], F.-J. Hambscha, J. Karlsson[b], A. Oberstedt[b]

[a] European Commission Joint Research Centre IRMM
Retieseweg 111
2440 Geel
Belgium

[b] Akademin för Naturvetenskap och Teknik
Örebro Universitet
70182 Örebro
Sweden

Abstract. A challenging task within the modelling of new generation reactor neutron kinetics is the calculation of the γ-heat deposition e. g. in steel and ceramics reflectors without UO_2 blankets, which is required to be known with an uncertainty as low as 7.5%. A major difficulty in measuring prompt γ-ray emission in fission is the competition between γ-ray emission and prompt neutron evaporation during fission-fragment de-excitation and the suppression of background γ-rays induced by those neutrons in the γ-ray detector. A common method is to distinguish between γ-rays and neutrons by their different times of flight, which however is limited by the timing resolution of the detector (not better than 5 ns for sodium-iodine detectors). A promising experimental approach seems to be the use of recently developed cerium-doped lanthanum halide crystal scintillation detectors in conjunction with an ultra-fast fission event trigger based on artificial diamonds. This is the report on recent detector suitability studies being carried out at the European Commission Joint Research Centre IRMM, which are dedicated to new and accurate measurements of fission γ-ray data.

1. Introduction

In the core of a standard nuclear reactor about 10% of the total energy release is accounted for by the γ-ray energy released in fission. 40% or 8 MeV result from the prompt γ-decay of fission fragments [1]. Although the characteristics of γ-ray emission, e.g. multiplicity, total energy and energy distribution, are fairly well known for neutron capture and inelastic neutron scattering, fission γ-rays are the major source of uncertainty in the modelling of γ-ray heating. Since four out of six nuclear systems identified by the Generation-IV international forum are fast reactors, a very innovative core design is required in order to respond to the high performance expected of those future systems.

A particular challenge for the modelling of new generation reactor neutron kinetics is the calculation of the γ-heat deposition e.g. in steel and ceramics reflectors without UO_2 blankets, which is required to be known with an uncertainty as low as 7.5% [2]. The comparison of various benchmark experiments with calculated γ-heating shows a systematic underestimate ranging from 10 to 28% for the main fuel isotopes ^{235}U and ^{239}Pu. This is attributed to deficiencies in γ-ray production data in evaluated nuclear data files [3]. Data found in modern nuclear-data libraries all date back to experiments performed in the early 1970's [4-6]. In those experiments sodium-iodine (NaI) scintillation detectors were used as γ-ray spectrometer with an ionisation chamber as fission trigger, which today are inferior with respect to both energy and timing resolution.

Therefore, the Nuclear Energy Agency (NEA) has formulated requests for new measurements on prompt γ-ray emission in the reactions ^{235}U(n,f) and ^{239}Pu(n,f) and included into the Nuclear Data High Priority Request List (NEA, Req. ID: H.3, H.4) [7]. In a recent modelling exercise of neutron emission from fission fragments by means of a Monte-Carlo approach [8] the authors achieve a reasonably good description of the average γ-energy released in fission, but they are unable to reproduce the experimentally obtained dependence as a function of the fission-fragment mass. They recommend putting more work in clarifying the competition between neutron and γ-ray emission during fission-fragment de-excitation.

A major difficulty in measuring prompt γ-ray emission in fission is the competition between γ-ray emission and prompt neutron evaporation during fission-fragment de-excitation and the suppression of background γ-rays induced by those neutrons in the γ-ray detector. A common method is to distinguish between γ-rays and neutrons by their respective time-of-flight, which however is limited by the timing resolution of the detector (not better than 5 ns for NaI detectors). A promising step towards better data seems to be the use of recently developed cerium-doped lanthanum halide crystal scintillation detectors. They have a light output larger than NaI and provide a timing resolution as good as 500 ps [9, 10] together with a 40% improved pulse-height resolution compared to traditional crystal scintillation detectors [11].

In order to fully profit from the excellent characteristics of this type of scintillation material for γ-ray measurements a new fission event-trigger is needed with similar timing capabilities. Recently, artificial diamond material became available for designing charged-particle detectors. In nuclear physics diamond detectors are used mainly in high-energy experiments as beam monitors and tracking devices, replacing traditionally employed silicon detectors, because they survive in high radiation environments, have low leakage current and do not need cooling [12-15]. In particular, the timing properties of artificial diamonds are remarkable and an intrinsic timing resolution better than 30 ps has been achieved for a mono-energetic ^{52}Cr-beam at incident energy of 650 MeV/u [16]. In view of the properties of this surprising material it is tempting to see, whether a similar timing resolution may be obtained with low energy fission fragments with energies typically between 0.5 and 2.0 MeV/u.

In this work we will present results of the characterization of $LaCl_3$:Ce detectors in terms of energy conversion and resolution, linearity, intrinsic efficiency, timing resolution and intrinsic radioactivity in the relevant dynamical range [17]. Additionally, we will discuss a new experimental set-up for fission γ-ray measurements and present the design of a first fission experiment to be carried out at thermal neutron energies.

2. Experiment

In a first step we will report about our study on the capability of lanthanum-chloride detectors with respect to prompt fission γ-ray studies. The study was carried out with three coaxial 1.5" × 1.5" $LaCl_3$:Ce detectors with a 5% concentration of cerium [18]. Next, we will present the characterization of artificial diamond detectors with respect to their response to low-energy heavy ions, i.e. fission fragments.

2.1. Characterisation of lanthanum chloride detectors

The cylindrical $LaCl_3$ crystals are mounted on photomultiplier tubes (PMT) of type Photonis XP2500/FB. Only one signal output is connected to its base, in addition to the connector for applying the high voltage. Therefore, the output signal had to be split for a simultaneous measurement of time and energy. During the study of the detector performances the bias

voltage, amplification of the signals and the shaping time were varied. Different radioactive sources (^{22}Na, ^{54}Mn, ^{57}Co, ^{60}Co, ^{133}Ba, ^{137}Cs and ^{232}Th) as well as γ-rays from the reaction ^{19}F(n,α)^{16}O* were used to determine detector characteristics at γ-ray energies from 81 keV to 6919 keV.

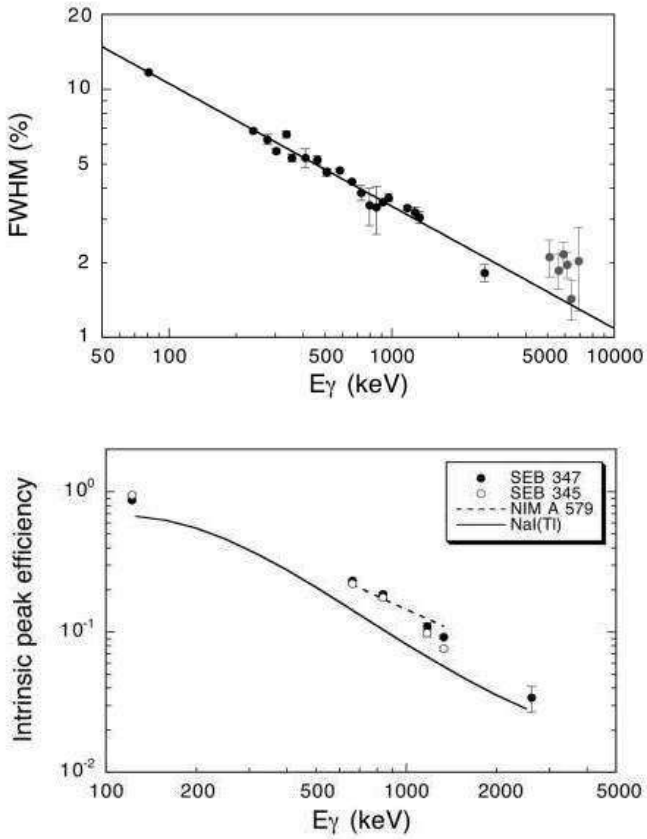

FIG.1. Upper part: measured energy resolution for γ-rays in the energy range between 81 and 6919 keV. The full drawn line describes the expected $E^{-1/2}$ behavior; Lower part: intrinsic peak efficiency vs. γ-energy from this work (full and open circles for two different detectors) together with estimates (dashed line) from values in Ref. [13]. For comparison corresponding values for NaI:Tl detectors of same size [14] are shown as full drawn line.

The well-known intrinsic activity arising basically from the radioactive ^{138}La (0.09% relative abundance in naturally occurring lanthanum) and from contamination with the chemically similar actinium isotope ^{227}Ac (and the daughters from its α-decay chain) amounts to about 1.3 Bq/cm^3 in reasonable agreement with previously reported values of about 0.9 Bq/cm^3 [19, 20]. This background activity may be tackled by imposing a coincidence condition with a fission fragment.

In terms of both energy resolution and intrinsic efficiency the superiority of $LaCl_3$:Ce over NaI:Tl detectors was confirmed, in this work with about 40% and 50% better, respectively. The energy resolution was determined from spectra taken for different radioactive sources. From a fit of Gaussians to the γ-peaks the widths of the peaks were determined. Experimentally, the energy resolution at 662 keV was found to be between 3.8 and 4.2% for the three investigated detectors, which is in accordance with information from the manufacturer. Figure 1 (upper part) shows the measured energy resolution as a function of energy.

The intrinsic full peak efficiency of the detectors were determined for different point sources at a distance of (25.0±0.3) cm between source and detector. The number of detected photons was obtained from the spectra by fitting with a Gaussian and a linear background function. Our results are in good agreement with efficiency values for $LaCl_3$ detectors of size 1"×1" and 2"×2" [21], respectively, obtained by interpolation to the size of our detectors. Our results are shown in the lower part of Fig. 1 together with corresponding values for a NaI: Tl of the same size [22].

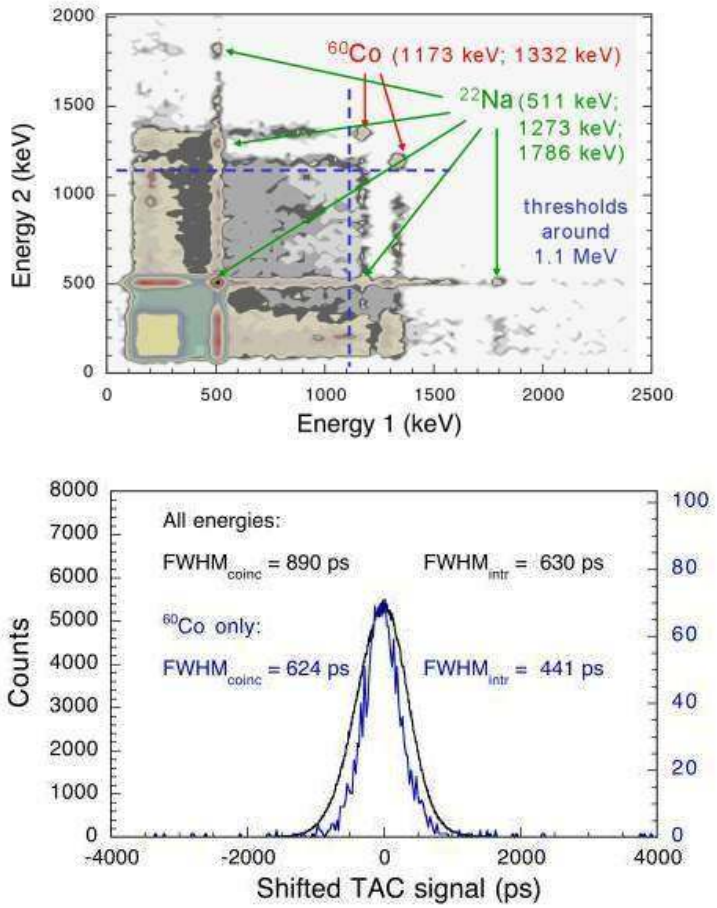

FIG.2. Upper part: energy of detector 2 vs. energy of detector 1 as obtained from the coincident measurement of γ-rays from a ^{22}Na and ^{60}Co source. Indicated are the full energy peaks and the threshold (dashed line) set just below the ^{60}Co peak energy of 1173 keV. Lower part: TAC spectra obtained in coincident measurement of two γ-rays from ^{22}Na and ^{60}Co sources with two virtually identical $LaCl_3$:Ce detectors. The intrinsic timing resolution is given for both the entire energy region and for the ^{60}Co γ-rays only.

The timing resolution of $LaCl_3$:Ce detectors was determined by exposing two detectors to a ^{22}Na and ^{60}Co source at the same time. As a result, a two-dimensional representation of the energy signals from both detectors was obtained, as shown in the upper part of Fig. 2. Best coincidence timing resolution over the entire energy range was found to be about 890 ps (FWHM), which corresponds to an intrinsic timing resolution of 630 ps (cf. Figure 2, lower part). This result is not as good as published previously for lanthanum halide detectors [9]. However, those results were obtained for much smaller detectors, i.e. 1 cm^3 compared to the 43 cm^3 in this study. By putting a threshold just below the ^{60}Co-peaks, i.e. around 1000 keV, an intrinsic timing resolution of 441 ps was achieved as indicated in Fig. 2.

Further experiments have been performed to investigate the neutron sensitivity of the scintillation material and the risk of long-term activation when used in a high intensity neutron field. For that purpose we installed the detectors at the Van-de-Graff driven pulsed neutron source at CEA DAM at Bruyères-le-Châtel and exposed them to neutrons at E_n = 5 MeV. In contrast to experimental results obtained by another group investigating $LaBr_3$ detectors [23] no long-term activation could be observed. However, different prompt reactions with fast neutrons on the scintillation material are visible (for details we refer to Ref. [24]).

2.2. Diamonds as fission event triggers

As detector material for the fission event trigger an artificial polycrystalline chemical vapour deposited (pcCVD) diamond film was chosen. Its thickness is 100 μm and its active area is 10 mm × 10 mm. Electrical contact is made by 150 nm thick gold layers deposited on the diamond film. Polycrystalline diamond material has a very limited charge collection efficiency, typically around 30% [14], which deteriorates further when irradiated with strongly ionizing particles with a stopping range much smaller than the film thickness. This is due to polarisation caused by electric charges trapped within a layer characteristic for the range of the particles. Experimentally, it was observed, that the charge collection efficiency may be stabilized and even slightly improved, if the material is irradiated with long-ranging electrons prior to use. This procedure is called "priming" [25, 26]. The priming effect is due to an increase of carrier lifetime caused by saturation of deep traps with electrons (holes) produced by radiation. This saturation has been demonstrated to be very effective and very stable in time under irradiation with α-particles [26], provided the sample is not exposed to ambient light.

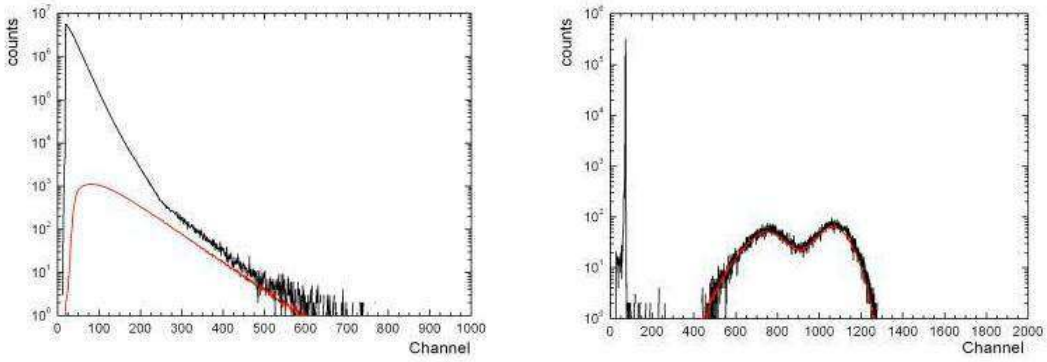

FIG.3. Left part: pulse height spectra of fission fragments plus α-particles (black) and fission fragments only (red), when coincidence with the silicon detector is required; Right part: typical pulse height spectra from fission fragments are shown, taken with (red) and without (black) coincidence required with the diamond detector

In a first step we investigated, whether such diamond detectors could distinguish between fission fragments and α-particles possibly emitted by the target isotope under investigation. For this exercise a ^{252}Cf spontaneous fission source, deposited on 250 nm thick Al-backing, was mounted practically on top of a diamond detector, which was biased to +180V. A silicon detector was placed opposite to the diamond detector. In the right part of Fig. 3 a typical pulse height spectra from fission fragments are shown, taken with (light) and without (black) coincidence with the diamond detector required. The α-particles, being about 30 times more abundant than the fission fragments, are well suppressed when a coincidence condition between two detectors is set (left part of Fig. 3). In a next step the timing properties of a pcCVD diamond detector was investigated. For that a symmetric configuration with two identical diamond detectors has been set up, again with the spontaneous fission source placed

on top of one detector. Using pre-amplifiers built at the Technical University of Darmstadt [27] and standard timing filter amplifiers and constant fraction discriminators time-of-flight was registered event by event. The time-of-flight spectrum is shown in the left part Fig. 4.

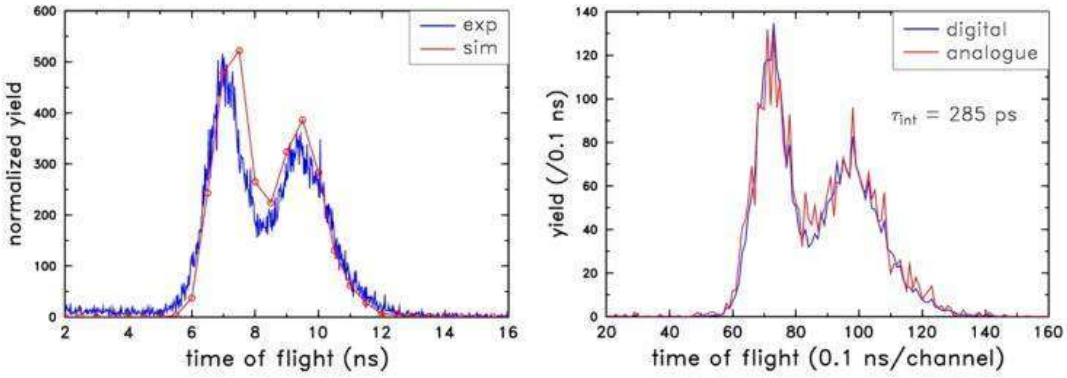

FIG.4. Left part: experimental time-of-flight distribution of fission fragments from the reaction ^{252}Cf (SF), which is shown as full line. The simulated spectrum is given by open circles interconnected with a solid line; Right part: time-of-flight spectrum taken with both analogue and digital electronics. Improvement by using wave-form digitization is little. The intrinsic timing resolution of a pcCVD diamond detector, as deduced from simulations (see text) is well below 300 ps

Since the time-of-flight spectrum is composed of a large variety of particles, with different energies and masses, timing properties had to be deduced from simulations. For that purpose Monte-Carlo simulations have been performed on the bases of experimental mass and kinetic energy yield data [28-30] and taking the geometry of the set-up into account. The free parameter in such a simulation is the width of the total resolution function, which was varied until the best description was achieved. The result of those simulations is shown in the left part of Fig. 4 as open circles (connected with a solid line). The intrinsic timing resolution of a single pcCVD diamond detector is then obtained from the resolution parameter divided by $\sqrt{2}$. In this way the intrinsic timing resolution of a 100 μm thick and 1 cm^2 large pcCVD diamond detector was determined to (285±15) ps.

This result appears to be considerably worse than what might be expected from high-energy heavy-ion experiments. However, one should not forget that here we are dealing with a mixed "particle beam", leading to a great variety of pulse heights and rise times. Considering that the timing resolution is well below or comparable with that of a lanthanum halide detector, and about 4 to 5 times smaller than for an ionization chamber, artificial polycrystalline CVD diamond detectors appear to be the ideal fission event trigger for the measurement of prompt fission γ-rays in conjunction with the above discussed $LaCl_3$:Ce scintillation detectors

The same experiment has been repeated using wave-form digitization techniques, which led to only little improvement of the timing resolution, as depicted in the right part of Fig. 4.

3. Fission γ-ray spectra from the reaction ^{252}Cf(SF) – a first test

Next to the characterisation of the detectors a first feasibility test was performed by measuring prompt γ-ray emission in the spontaneous fission of ^{252}Cf. A source with about 6000 fissions/s was placed on top of a well-characterised pcCVD diamond detector. The $LaCl_3$:Ce detector

was mounted at 39 cm distance. For comparison a fast plastic scintillation detector (pilot U) was installed, too.

From first spectra we can see already, that prompt fission γ-rays may be well separated from prompt fission neutrons. The achieved total timing resolution of about 1.2 ns may well be subject to further optimization. However, also fission neutrons with energies up to 20 MeV are well separated with the presently achieved timing resolution. The fact that $LaCl_3$:Cl detectors provide energy resolution, the neutron component in the spectra might be attributed to specific reaction channels in the detector housing and the scintillation crystal as indicated in the upper spectrum in Fig. 5 by an arrow commented with "neutrons!".

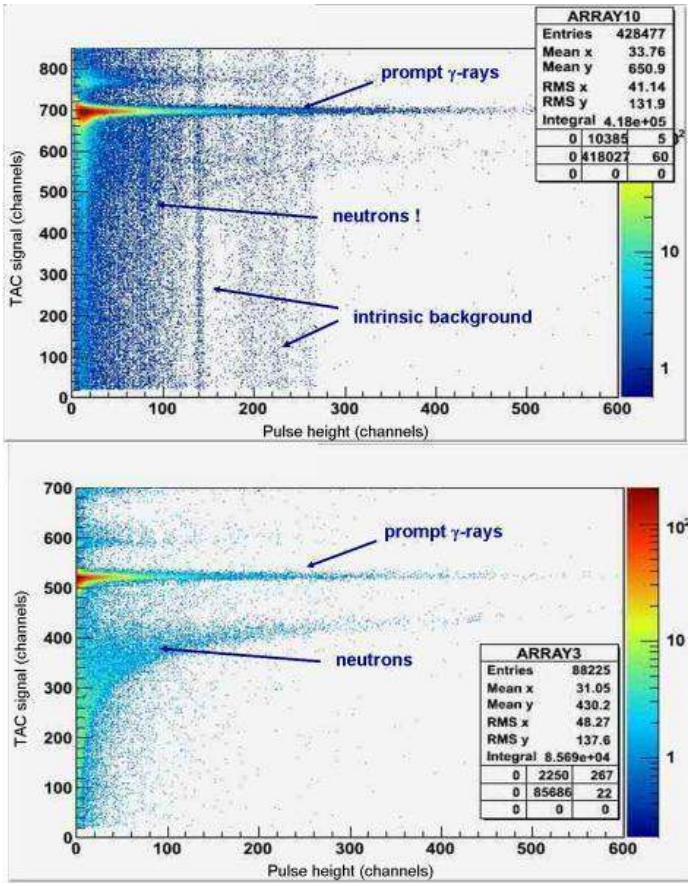

FIG.5. Examples of prompt fission γ-ray and neutron emission spectra taken with both a 1.5" × 1.5" $LaCl_3$:Ce (upper part) and a 1" × 1" plastic scintillation detector (pilot U, lower part). The respective positions of prompt γ-rays and neutrons are indicated in the spectra (see text for details).

4. Summary

In this paper we have presented the results of suitability studies of recently developed scintillation detectors and artificial diamond-based charged particle detectors for the accurate investigation of prompt γ-ray emission in fission.

In terms of both energy resolution and intrinsic peak efficiency the superiority of $LaCl_3$:Ce over NaI:Tl detectors was confirmed, being in this work 40% and 50% better, respectively. Within an energy range up to E_γ = 7 MeV an excellent linearity was observed, the dynamical range was estimated to 17 MeV for γ-rays. The observed timing resolution was 630 ps and

441 ps, depending on the applied γ-energy threshold. With an ultra-fast fission fragment trigger, built from artificial poly-crystalline CVD diamond, prompt fission γ-rays may be measured with a timing resolution around 1 ns. In addition, the good energy resolution of $LaCl_3$:Ce permits identification of neutron-induced reactions, e.g. inelastic neutron scattering on ^{27}Al present in the detector housing, opening up further means for n/γ separation. First prompt fission γ-ray spectra obtained from spontaneous fission of ^{252}Cf demonstrate the superiority of the new detectors compared to the traditionally employed NaI:Tl detector in combination with an ionization chamber.

In early 2010 we will install the same experimental set-up at the cold-neutron source of the 10 MW Budapest Research Reactor measuring the prompt γ-ray emission spectrum in the reaction ^{235}U (n, f).

A next step should be to replace pcCVD diamond material by single crystal diamonds. This would allow performing compact double-energy measurements permitting the investigation of prompt γ-ray emission as a function of fragment mass and TKE. However, the production of such single crystal diamonds is still limited to very small sizes and remains a challenging task for the future.

Acknowledgements

The authors would like to gratefully acknowledge the support for this project, obtained within the EFNUDAT programme of the European Commission (agreement number 31027).

REFERENCES

[1] K. S. KRANE, Introductory Nuclear Physics, John Wiley & Sons, ISBN 0-471-80553-X

[2] G. RIMPAULT, Proc. Workshop on Nuclear Data Needs for Generation IV, April 2005 (Editor: P. Rullhusen) Antwerp, Belgium, World Scientific, ISBN 981-256-830-1 (2006)

[3] G. RIMPAULT, A. COURCELLE, and D. BLANCHET, Nuclear Data High Priority Request List of the NEA (Req. ID: H3, H4; explanatory note)

[4] R. W. PEELLE and F. C. MAIENSCHEIN, *Spectrum of Photons Emitted in Coincidence with Fission of ^{235}U by Thermal Neutrons,* Phys. Rev. **C3** (1971) 373

[5] F. PLEASONTON, R. L. FERGUSON and H. W. SCHMITT, *Prompt Gamma Rays Emitted in the Thermal-Neutron Induced Fission of ^{235}U*, Phys. Rev. **C6** (1972) 1023

[6] V. V. VERBINSKI, H. WEBER and R. E. SUND, *Prompt Gamma Rays from $^{235}U(n,f)$, $^{239}Pu(n,f)$ and Spontaneous Fission of ^{252}Cf*, Phys. Rev. **C7** (1973) 1173

[7] Nuclear Data High Priority Request List of the NEA (Req. ID: H.3, H.4), http://www.nea.fr/html/dbdata/hprl/hprlview.pl?ID=421 and http://www.nea.fr/html/dbdata/hprl/hprlview.pl?ID=422

[8] S. LEMAIRE, P. TALOU, T. KAWANO, M. B. CHADWICK and D. G. MADLAND, *Monte Carlo approach to sequential neutron emission from fission fragments*, Phys. Rev. **C72** 024601 (2005)

[9] K. S. SHAH, J. GLODO, M. KLUGERMAN, L. CIRIGNANO W. W. MOSES, S. E. DERENZO, M. J. WEBER, Nucl. Inst. Meth. **A 505** (2003) 76

[10] A. ILTIS, M. R. MAYHUGH, P. MENGE, C. M. ROZSA, O. SELLES, V. SOLOVYEV, Nucl. Inst. Meth. **A 563** (2006) 359

[11] B. D. MILBRATH, B. J. CHOATE, J. E. FAST, W. K. HENSLEY, R. T. KOUZES, J. E. SCHWEPPE, Nucl. Inst. Meth **A 572** (2007) 774
[12] P. WEILHAMMER *et al*., Nucl. Inst. Meth. **A 409** (1998) 264
[13] D. MEIER et al., Nuc. Inst. Meth. **A 426** (1999) 173
[14] E. BERDERMANN, K. BLASCHE, P. MORITZ, H. STELZER, "Diamond Detectors for Heavy-Ion Measurements", XXXVI Int. Winter Meeting on Nuclear Physics, Bormio (1998).
[15] E. BERDERMANN, K. BLASCHE, P. MORITZ, H. STELZER, B. VOSS, F. ZEYTOUNI, Nucl. Phys. B (Proc. Suppl.) **78** (1999) 533-539.
[16] E. BERDERMANN, K. BLASCHE, P. MORITZ, H. STELZER, B. VOSS, Diamond and Related Materials **10** (2001) 1770-1777.
[17] A. OBERSTEDT, S. OBERSTEDT, W. GEERTS and F.-J. HAMBSCH, *Capability of lanthanum-chloride detectors with respect to prompt fission γ-ray studies*, submitted to NIM A
[18] SCIONIX Holland bv, P.O. Box 143, 3980 CC Bunnik, The Netherlands.
[19] M. BALCERZYK, M.MOSZYNSKI, M. KAPUSTA, Nucl. Instr. Meth. A 537, 50 (2005).
[20] R. NICOLINI, F. CAMERA, N. BLASI, S. BRAMBILLA, R. BASSINI, C. BOIANO, A. BRACCO, F. C. L. CRESPI, O. WIELAND, G. BENZONI, S. LEONI, B. MILLION, D. MONTANATI, A. ZALITE, Nucl. Instr. Meth. A 582, 554 (2007).
[21] B. AYAZ-MAIERHAFER and T. A. DEVOl, Nucl. Instr. Meth. **A 579** (2007) 410.
[22] G. GILMORE, Practical Gamma-ray Spectroscopy, John Wiley & Sons, ISBN 978-0-470-86196-7 (2008)
[23] J.-M. LABORIE, private communication.
[24] Progress report to the EFNUDAT programme of the European Commission (agreement number 31027), in preparation.
[25] M. MARINELLI, E. MILANI, A. PAOLETTI, A. TUCCIARONE and G. VERONA RINATI, App. Phys. Lett. **75** (1999) 3216-3218.
[26] M. MARINELLI, E. MILANI, A. PAOLETTI, A. TUCCIARONE, G. VERONA RINATI, M. ANGELONE, M. PILLON, Nucl. Inst. Meth. **A 476** (2002) 701-705.
[27] U. BONNES and M. MUTTERER (1999) private communication.
[28] F.-J. HAMBSCH and S. OBERSTEDT, Nucl. Phys. **A 617** (1997) 347-355.
[29] F.-J. HAMBSCH, 2004, private communication.
[30] E. BIRGERSSON, S. OBERSTEDT, A. OBERSTEDT, F.-J. HAMBSCH, D. ROCHMAN, I. TSEKHANOVICH, S. RAMAN, Nucl. Phys. **A 791** (2007) 1-23.

Binary and Ternary Fission Yield Measurements at the Institut Laue-Langevin

O. Serot[a], A. Bail[a], O. Litaize[a], L. Mathieu[a], H. Faust[b], U. Koester[b], T. Materna[b], E. Dupont[c], A. Letourneau[c], S. Panebianco[c], S. Vermote[d], C. Wagemans[d]

[a] CEA Cadarache, F-13108 Saint Paul Lez Durance, France
[b] Institut Laue Langevin, F-38042 Grenoble Cedex 9, France
[c] CEA Saclay, F-91191 Gif-Sur-Yvette, France
[d] University of Gent, B-9000 Gent, Belgium

Abstract. In spite of the huge amount of fission yield data available in the different evaluated nuclear data libraries, such as JEFF3.1, ENDF/B-VII, JENDL3.3 and others, more accurate data are still needed for both nuclear energy applications and for the understanding of the fission process itself. Hence, various campaigns of measurements of fission yields were performed at the High Flux Reactor of the Institut Laue-Langevin (ILL) in Grenoble, France. Two types of measurements were carried. The first one concerns the binary fission yields which were measured on the Lohengrin mass spectrometer. Up to now, this mass spectrometer coupled to a high-resolution ionization chamber has been used to investigate the mass and isotopic yields of the light mass region for fissioning nuclei from Th to Cf. To complete these measurements, the heavy mass region for the reactions $^{235}U(n_{th},f)$, $^{239}Pu(n_{th},f)$ and $^{241}Pu(n_{th},f)$ have been investigated. For these higher masses, isotopic separation is no longer possible, so a new experimental method based on gamma spectroscopy was introduced with the reaction $^{239}Pu(n_{th},f)$ to determine isotopic yields. These experiments have permitted to reduce considerably the uncertainties. The second type of measurements concerns the ternary fission yields which were measured at the PF1b cold neutron guide installed at ILL. In the frame of a systematic investigation of ^{4}He, ^{6}He and ^{3}H ternary particles, various neutron induced fission reactions were measured covering target nuclei between ^{229}Th and ^{251}Cf. A ΔE-E telescope was used to identify ternary particles and determine both their energy distribution and their emission probability. These results are compared with those obtained from spontaneous fission decays which were measured elsewhere within the same experimental conditions.

1. Introduction

This paper deals with the experimental work on binary and ternary fission yield measurements which have been performed at the research reactor of the Institute Laue Langevin (ILL/ Grenoble / France). It is mainly based on refs. [1-4].

2. Binary fission yield Measurements

The fission yield data are of importance in several nuclear energy applications (reactivity or decay heat in nuclear power, fission rate of a fuel …). Despite the fact that nuclear fission has been intensively investigated during the last decades, the evaluated nuclear data libraries (JEFF-3.1, ENDF/B-VII.0, JENDL-3.3 …) which contain already a huge amount of fission yield data need to be improved. In particular, strong efforts are still needed to reduce the uncertainties of the fission yields and to understand the differences which can be sometimes observed between the various evaluated nuclear data libraries [5]. For systems which undergo fission in a thermal neutron flux, detailed results for kinetic energy, nuclear mass and nuclear charge have been measured at the Lohengrin mass spectrometer, in particular for the target nuclei ^{229}Th, ^{233}U, ^{235}U, ^{238}Np, ^{239}Np, ^{239}Pu, ^{241}Pu, ^{245}Cm, ^{249}Cf and ^{251}Cf (see Ref. [1] and references therein). However, only the light fission yields for these actinides have been

investigated so far at Lohengrin (except for ^{245}Cm [6], where mass yields were measured for both the light and the heavy region). In order to study fission product characteristics in the heavy mass region, a new experimental setup has been installed and will be briefly described here. The first results obtained in this way will be also presented.

2.1. The Lohengrin mass spectrometer

The experiments were performed at the Lohengrin recoil mass spectrometer [7, 8] located at the Institut Laue-Langevin (Grenoble, France). It uses low-energy fission reactions for the production of fission products (Figure 1). Investigation of the fission product distributions is then possible for thermal neutron induced fission with a very high resolution. The Lohengrin fission source is typically a thin layer of a fissile material placed close to the core of ILL's research reactor in a high thermal-neutron flux of 5.3×10^{14} n/cm²/s. High energetic fission products are leaving the target with high ionic charge states. Fission products emerging from the target are selected by a combination of a magnetic and electric sector field. They are separated according to their A/q and E_k/q values, with A the mass number, q the ionic charge state and E_k the kinetic energy of the ion. The flight path for the fission products is 23 m and the separation time is of the order of 2 μs so that fission products reach the detection system before undergoing β-decay. Different equipment may be installed next to the exit slit of Lohengrin according to the aim of the experiment.

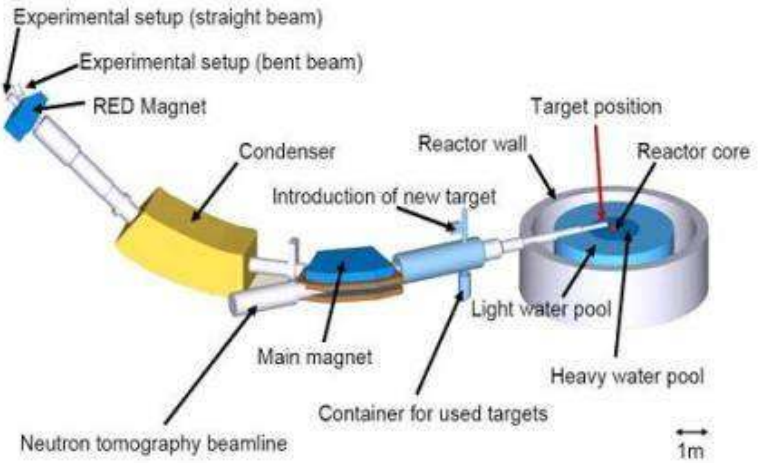

FIG.1. Schematic view of the Lohengrin recoil mass spectrometer

2.2. Mass Yields

Our aim here was the determination of mass yield and kinetic energy for heavy fission fragments. For that, we used at the exit slit of the spectrometer an ionization chamber which allows to determine the kinetic energy (E_k) value of the separated fragments, giving thus the mass (A) and ionic charge state (q) values.

The ionization chamber is filled with isobutene at P=40 mbar pressure. The high voltage applied between the anode and the Frisch grid is 400V, and the same voltage is applied between the Frisch grid and the cathode. This set-up allows us to obtain the complete mass yields of a fissioning nucleus by integration over kinetic energy and ionic charge distributions for every mass.

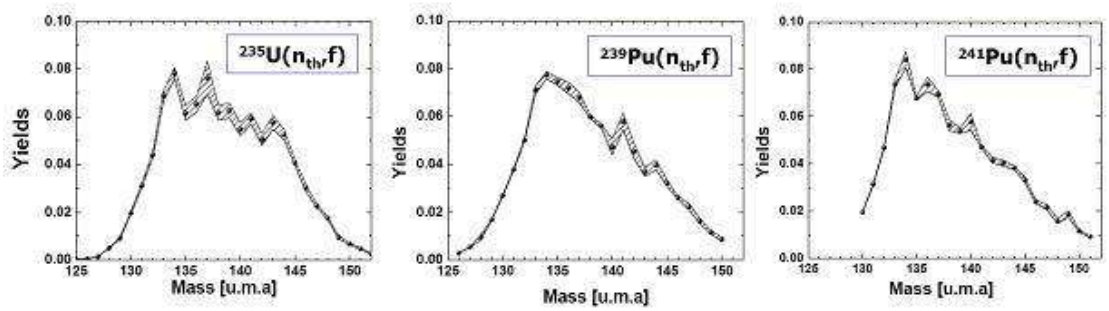

FIG.2. Mass yields measured recently in the heavy mass region using an ionization chamber at the exit slit of the Lohengrin mass spectrometer [1].

The $^{235}U(n_{th},f)$, $^{239}Pu(n_{th},f)$ and $^{241}Pu(n_{th},f)$ reactions were studied. Results of the mass yields are plotted in Fig. 2. The vertical bars correspond to the statistical uncertainties, while the systematic uncertainties are represented by the dashed zones. A comparison between our results and the European nuclear data library JEFF3.1 shows a nice agreement, but with a significant reduction of the uncertainties.

2.3. Isotopic Yields

As already said, using a high resolution ionization chamber as detection system, the mass and isotopic yields of the light fission products for a lot of actinides were measured. Unfortunately, this method is no longer applicable for nuclei with nuclear charges higher than 42 [6]. Therefore, in order to determine heavy isotopic yields, a new setup was installed, which is based on gamma spectrometry for the isotopic identification. Indeed, as the beta-decays of fission products are often followed by gamma de-excitation, and because these decays occur after leaving the spectrometer, beta-gamma coincidences can be used to determine isotopic yields.

For this purpose the fission products are implanted in a moving tape which is coupled to a vacuum chamber at the focal point of the spectrometer. Two germanium clover detectors are used to measure the gamma-decay with high efficiency, whereas the beta disintegration process is detected by a proportional gas counter or a scintillator. The tape system is used to remove long-lived activity. Note that the isotopic yield can be determined only if the branching ratios and decay constants of the different isotopes are known. The analysis of the data is then based on the integration of the Bateman equations. All the details of the analysis can be found in Ref. [1].

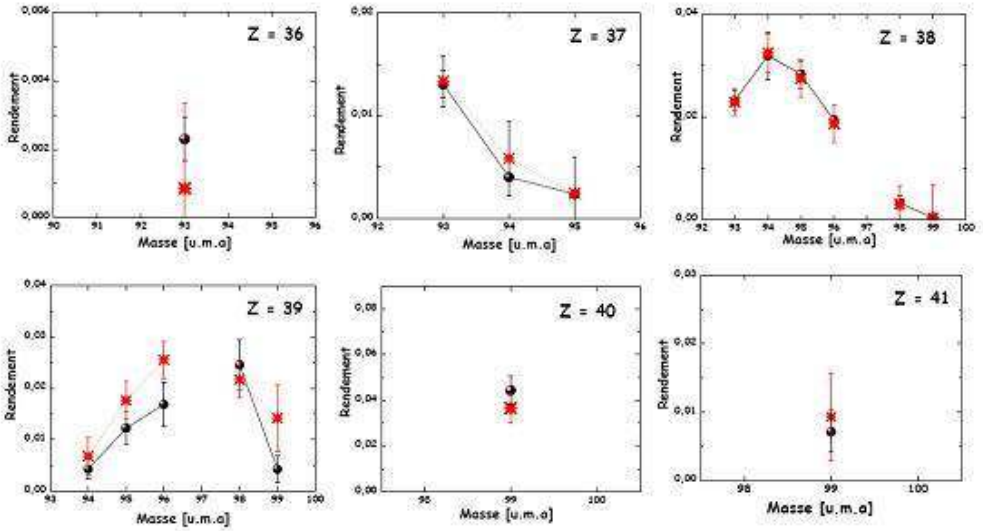

FIG.3. Comparison of the isotopic yields measured in the light mass region on $^{239}Pu(n_{th},f)$ with an ionization chamber (red stars [9]) and by gamma spectroscopy (black circles [1]).

In order to test the good functioning of our new experimental setup, some isotopic fission product yields from $^{239}Pu(n_{th},f)$ were measured in the light mass region and compared with the results obtained by Schmitt [9] with a completely different experimental setup, i.e. an ionisation chamber. As shown in Fig. 3, a good agreement was reached.

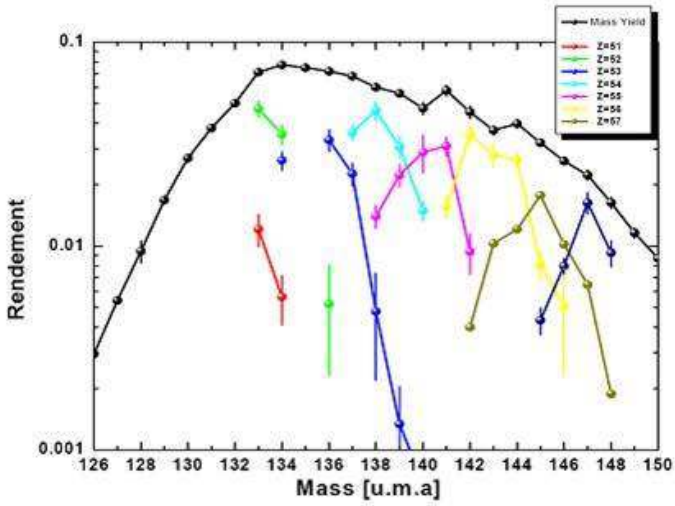

FIG.4. Isotopic yields measured recently by gamma spectroscopy in the heavy mass region on $^{239}Pu(n_{th},f)$ [1, 10].

Data of our measured isotopic fission product yields in the heavy mass region are given in Fig. 4, for Z=51 up to Z=57 [10]. Again, a nice agreement between our results and the JEFF3.1 library was seen (not shown in Fig. 4). In addition, the uncertainties could be significantly reduced, except for nuclei where gamma branching ratios are poorly known.

Using this gamma spectroscopy technique, other neutron induced fission reactions ($^{233}U(n_{th},f)$, $^{241}Pu(n_{th},f)$…) are planned to be investigated.

3. Ternary fission yield Measurements

Nuclear fission is essentially a binary process, but roughly 2 to 4 times every thousand fission events, the two heavy fragments are accompanied by a light charged particle. In this so-called ternary fission process, the emission yields for α particles, tritons and ^{6}He particles are the most important [11]. The ternary fission process is therefore an important source of helium and tritium gas in nuclear reactors and also in used fuel elements due to spontaneous fission. So, accurate ternary fission yields mainly for ^{4}He and tritons are requested by nuclear industry. Furthermore, ternary fission data are of interest for nuclear physics in order to improve our understanding of the ternary particle emission mechanism and to provide information on the fission process itself.

Since several years, our group has been involved in a systematic study of the characteristics of ternary α particles, tritons and ^{6}He particles emitted during spontaneous fission decays and from thermal neutron induced fission [12-16]. The spontaneous fission decays have been studied at the Institute for Reference Materials and Measurements (IRMM) in Geel, Belgium, while the neutron induced measurements were carried out at the Institut Laue-Langevin (ILL) in Grenoble, France.

3.1. Experimental setup

The measurements of the yield and energy distributions of ternary particles emitted from thermal-neutron induced fission have been performed at the PF1B cold neutron guide of the ILL in Grenoble (France), where the neutron flux at sample position is about 3.5×10^{9} neutrons/s/cm^{2}. The sample was placed in the centre of a vacuum chamber at an angle of 45° with the incident neutron beam as shown in Fig. 5. Two ΔE-E telescopes, each consisting of a thin ΔE and a thick E silicon surface barrier detector, were placed on both sides of the sample and perpendicular to the beam.

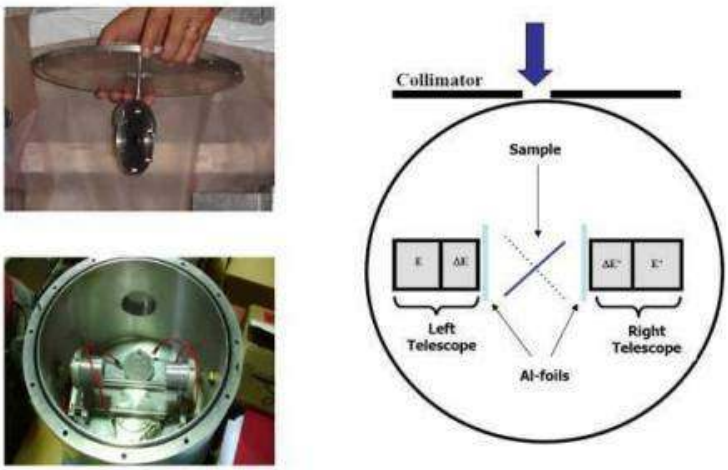

FIG.5. Vacuum chamber used for the ternary fission measurements. The two pictures on the left represent respectively the top (under which the sample is fixed) and the inside (where the two telescopes can be seen) of the chamber. A schematic top view of the chamber is also drawn on the right part of this figure.

The measurement was performed in 3 steps:

- The first step consists in the determination of the fission counting rate. For that, the sample was placed to face the ΔE-E telescope as shown by the straight line in Fig. 5. The Al foil is removed and the ΔE detector is replaced by an empty dummy (with exactly the same dimensions as the ΔE detector). Heavy fission fragments are detected by the E detector and the fission counting rate (N_F) can then be determined.

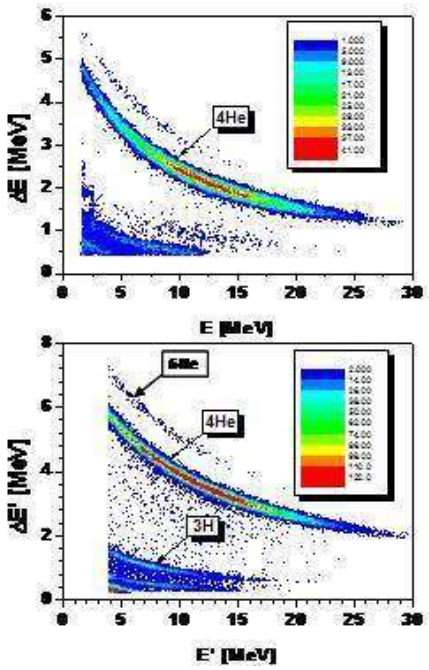

FIG.6. ΔE-E spectra obtained with two different telescopes.

- The second step consists in the measurement of the ternary alpha particles (also called Long Range Alpha particles (LRA)). It is done using the ΔE-E telescope. A 30 µm Al foil is put in front of the telescope to stop the heavy fission fragments and the alpha particles coming from radioactivity of the sample. A 29.8 µm ΔE and 500 µm E telescope allows a good separation between LRA particles and the background as can be seen in the top of Fig. 6. After the selection of the ternary alpha's, their energy (given by ΔE+E) is corrected for the energy loss in the sample and in the Al foil as well. Performing a Gaussian fit on this corrected spectrum allows the determination of the average energy and the Full Width of Half Maximum (FWHM) of the energy distribution. The area of the fit gives the ternary alpha counting rate (noted N_{LRA}). The ternary alpha emission probability (which is usually noted in the literature by LRA/B) is then given by: LRA/B= N_{LRA}/N_F.

- For the third step, the sample was turned over an angle of 90° in order to place it in front of the ΔE'-E' telescope (dashed line in Fig. 5). Again, a 30 µm Al foil covered the telescope. A 49.8 µm ΔE' and 1500 µm E' telescope was used to measure the ^{6}He, ^{4}He and ^{3}H yields simultaneously. The use of a thicker ΔE' detector (compared to the ΔE detector) allows a better separation between the ternary particles, but has the disadvantage of raising the energy threshold at which particles reach the E' detector (see bottom of Fig. 6). As in the second step, the ternary particle energy distributions can be determined and their counting rate can then be deduced (N'_{LRA}, N'_{6He}, N'_{3H}). Combining results from the two last steps, the ternary triton and ternary ^{6}He emission probabilities (respectively noted by t/B and ^{6}He/B) can be deduced from:

$$t/B = \frac{N'_{3H}/N'_{LRA}}{N_{LRA}/N_F} \quad \text{and} \quad {}^{6}He/B = \frac{N'_{6He}/N'_{LRA}}{N_{LRA}/N_F}$$

Typical example of the ^{4}He, ^{3}H and ^{6}He energy distributions are given in Fig. 7. These spectra come from the ^{245}Cm(n_{th},f) reaction and are corrected for the energy loss in the sample and in

the Al foil. For LRA particles, a Gaussian fit was performed to experimental data with energy above 12.5 MeV. In the case of ^{6}He particles the fit started at 13 MeV. For tritons, the fit was performed starting at 7 MeV.

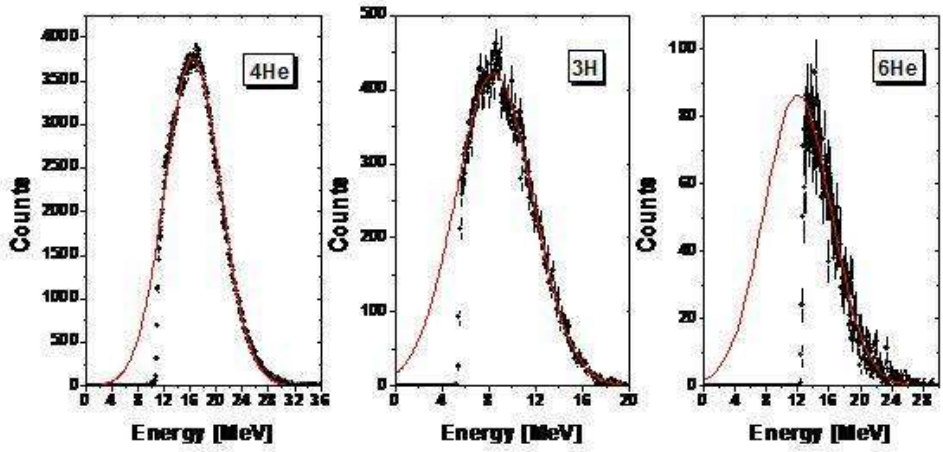

FIG.7. Energy distributions for LRA (left), ^{3}H(middle) and ^{6}He (right) ternary particles measured for the ^{245}Cm(n,f) reaction. Gaussian fits (red curves) were performed on each spectra.

3.2. Energy distributions

By making a weighted average of all the average energies for the different isotopes for a certain ternary particle, we can conclude that this average energy remains constant within the uncertainties for a certain ternary particle. For LRA particles a value of (16.0 ± 0.1) MeV is obtained (left part of Fig. 8), for tritons (8.4 ± 0.1) MeV (right part of Fig. 8) and for ^{6}He particles an average energy of (10.8 ± 0.2) MeV is found. This is a consequence of the stability of the heavy fragment peak in the fission fragment mass distribution as explained in Ref [11].

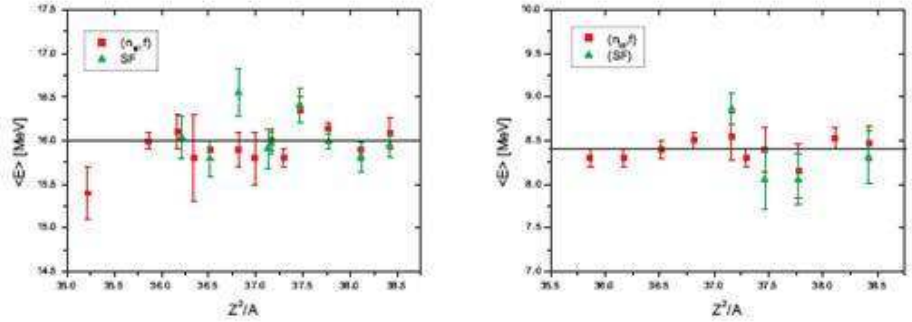

FIG.8. Average energy for LRA (left) and triton (right) particles as a function of Z^2/A of the fissioning nucleus. The red squares correspond to the (n_{th},f) reactions and the green triangles to the (sf) decays (from S. Vermote [3, 4]).

Another striking observation, illustrated in Fig. 9, is that for the same compound nucleus, the FWHM for the ternary α energy distribution is systematically 0.3 MeV smaller for spontaneous fission than for neutron induced fission. It is the first time that this phenomenon could be demonstrated, thanks to our systematic study involving 9 spontaneously fissioning nuclides and 13 neutron induced fission reactions. Furthermore, the FWHM of a certain ternary particle linearly increases with increasing fissility parameter Z^2/A which can be seen too in Fig. 9.

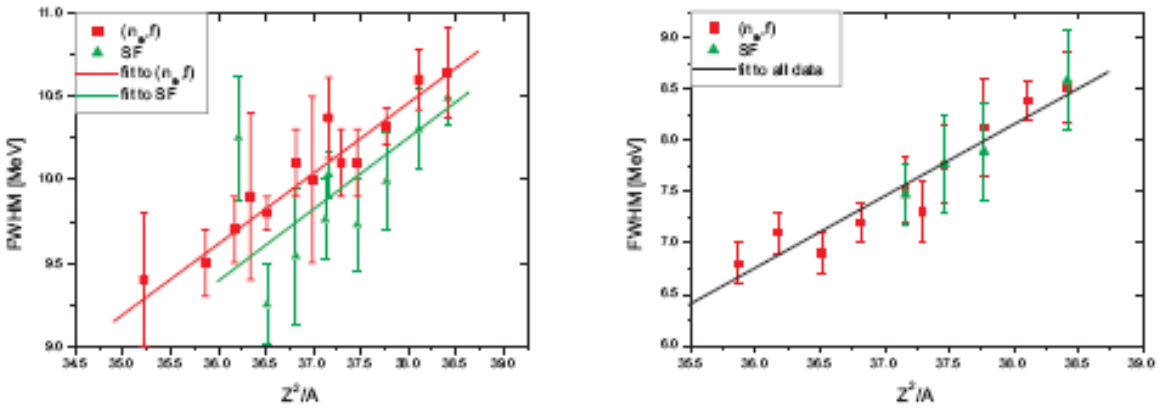

FIG.9. Full Width at Half Maximum for LRA (left) and triton (right) particles as a function of Z^2/A of the fissioning nucleus. The red squares correspond to the (n_{th},f) reactions and the green triangles to the (sf) decays (from S. Vermote [3, 4]).

3.3. Emission probability

In order to study the impact of the excitation energy (brought by capture of a neutron) on the ternary emission probability, we have compared this probability for the same fissioning nucleus at zero excitation energy (spontaneous fission) and at an energy corresponding to the neutron binding energy (thermal neutron induced fission). With the new available database, the comparison was possible for 7 compound nuclei for LRA particles (^{240}Pu, ^{242}Pu, ^{244}Cm; ^{246}Cm; ^{248}Cm; ^{250}Cf and ^{252}Cf); 5 compound nuclei for ^{3}H particles (^{244}Cm; ^{246}Cm; ^{248}Cm; ^{250}Cf and ^{252}Cf), and, lastly, 3 compound nuclei for ^{6}He particles (^{244}Cm; ^{250}Cf and ^{252}Cf). In Fig. 10, the ratios between the emission probabilities measured for the same compound nucleus from (n_{th},f) and from (sf) are plotted as a function of the excitation energy, for the three investigated ternary particles (LRA, ^{3}H, ^{6}He). This ratio is described by the following law:

$$\text{Ratio} = \frac{\text{Proba}\left(A_{CN}, E_{EXC} = Bn\right)}{\text{Proba}\left(A_{CN}, E_{EXC} = 0\right)} = 1 + a_{EXC}\, E_{EXC} \qquad (1)$$

The parameter a_{EXC} is assumed to be independent of the mass of the fissioning nucleus. From linear fits performed on the experimental data (see Fig. 10), we have found:

$a_{EXC}(^{4}He)$ = - (0.030 ± 0.003) MeV^{-1},
$a_{EXC}(^{3}H)$ = - (0.002 ± 0.012) MeV^{-1},
$a_{EXC}(^{6}He)$ = - (0.022 ± 0.010) MeV^{-1}.

Various comments can be made about the a_{EXC}-values:

- For LRA particles, the a_{EXC}-value means for instance that the ternary alpha emission probability is about 20% lower for a fissioning nucleus at 6.5 MeV excitation energy than for the same nucleus at zero excitation energy. This strange fact has been already observed more than 40 years ago [17] and is now confirmed for 7 fissioning nuclei.
- For the triton, the behavior is totally different, since the excitation energy of the fissioning nucleus has a negligible influence on the emission probability. A similar result has been reported for the first time by our group on the ^{248}Cm compound nucleus [18] and is confirmed now for four new nuclei.
- For the ^{6}He particles, data on only three nuclei are available with large uncertainties due to poor statistics. Nevertheless, the extracted new $a_{EXC}(^{6}He)$-value shows a similar behavior for ^{6}He and ^{4}He-particles.

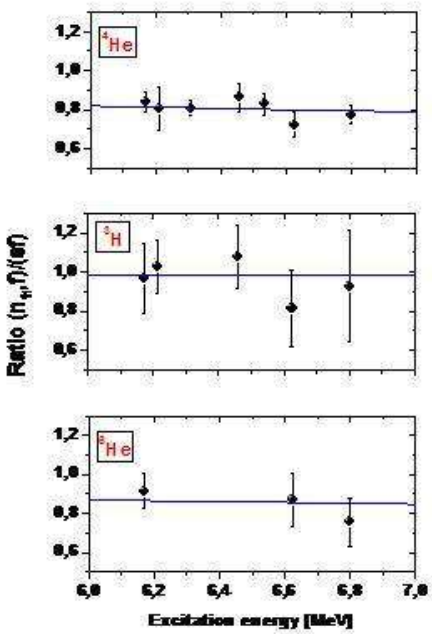

FIG.10. Ratios between the emission probabilities measured for the same compound nucleus obtained from (n_{th},f) and from (sf) as a function of the excitation energy. Three ternary particles were considered: ^{4}He (top), ^{3}H (middle) and ^{6}He (bottom). Straight lines correspond to the fit performed on the experimental data using Eq. (1).

All these results indicate that the ternary emission process seems to be different for H and for He isotopes. This difference could be explained by the fact that the ^{4}He or ^{6}He ternary emission process is governed by the cluster preformation probability factor (S_{4He} or S_{6He}), which is not the case for the ternary triton particles. The strong impact of the cluster preformation on LRA emission process has been suggested by Carjan in Ref. [19].

Conclusion

For the binary fission yield measurements, a new experimental setup has been installed on the Lohengrin mass spectrometer which is based on γ spectrometry for the identification of the fission products. In this way, and for the first time on the Lohengrin facility, mass and isotopic fission product yields of ^{239}Pu(n_{th},f) could be investigated in the heavy mass region. Other fissioning nuclei (^{242}Pu, ^{234}U …) will be measured in a near future.
For the ternary particle yields, we have reported in the present paper new results for the main characteristics (energy distribution and emission probability) of ^{4}He (also called LRA), tritons and ^{6}He particles. Since several years, our group has been involved in a systematic study of these characteristics. So, the database has been considerably enlarged, since for spontaneous fission, results on ^{244}Cm up to ^{256}Fm nuclides are now available, while the neutron induced fission data cover target nuclei between ^{229}Th and ^{251}Cf. Our systematic investigation of fissioning systems in the ground state (=spontaneous fission) and at an excited state (=neutron induced fission) permitted to put into evidence the strong impact of particle preformation on the ternary-particle emission probability.

REFERENCES

[1] A. BAIL, Ph.D. Thesis, University of Bordeaux (France) (2009).
[2] A. BAIL *et al*., in Proc. of the Int. Conf. on Nuclear Data for Science and Technology, April 22-27, 2007, Nice, France, Eds O.Bersillon et al., EDP Sciences, 2008, p.100.
[3] S. VERMOTE, Ph.D. Thesis, University of Gent (Belgium) (2009).
[4] S. VERMOTE *et al*., in Proc. of the 4th Int. Workshop on Nuclear Fission and Fission Product Spectroscopy, Cadarache (France), May 13-16, 2009 (in press).
[5] O. SEROT, R. MILLS, JEF-doc 1078 (2005) http://www.nea.fr/html/dbdata/projects/jeffdoc.html
[6] D. ROCHMAN *et al*., Nucl. Phys. **A710** (2002) 3.
[7] P. ARMBRUSTER *et al*. Nucl. Instr. Meth. **139** (1976) 213.
[8] G. FIONI *et al*., Nucl. Instr. Meth. **A335** (1993) 175-180.
[9] C. SCHMITT *et al*., Nucl. Phys. **A430** (1984) 21-60.
[10] A. BAIL *et al*., in Proc. of the 4th Int. Workshop on Nuclear Fission and Fission Product Spectroscopy, Cadarache (France), May 13-16, 2009 (in press).
[11] C. WAGEMANS, *The Nuclear Fisson Process,* CRC Press, Boca Raton, USA, 1991.
[12] O. SEROT *et al*., Nucl. Phys. **A641** (1998) 34.
[13] S. VERMOTE, C. WAGEMANS, O. SEROT *et al*., Nucl. Phys. **A806** (2008) 1-14.
[14] O. SEROT *et al*., Proc. of Int. Conf. on Nuclear Data for Science and Technology April 22-27, 2007, Nice, France, Eds. O. Bersillon *et al.*, EDP Sciences, 2008, p. 128.
[15] O. SEROT *et al*., Proc. of Int. Conference on Nuclear Data for Science and Technology (ND2004), Santa Fe (USA), Eds. Haight *et al*., AIP Conference proceedings, vol. 769, p.857.
[16] C. WAGEMANS, J. HEYSE, P. JANSSENS *et al*., Nucl. Phys. **A742** (2004) 291-302.
[17] I. HALPERN, Annu. Rev. Nucl. Sci. **21** (1971) 245.
[18] O. SEROT and C. WAGEMANS, Proc. 3rd Int. Conf. on Fission and Properties of Neutron Rich Nuclei, Sanibel Island, USA, Nov. 2002, World Scientific, p. 543.
[19] N. CARJAN, J. Phys. (Paris) **37** (1976) 1279.

Fast Reactor Integral Experiments at BARC for Cross-section Evaluation

K.K.Rasheed[1], R.N.Jindal[1], Rajeev Kumar[1], R.Indira[2], D. Sunilkumar[3], Vimal Kumar[4], R.V.Kolekar[5]

[1]Reactor Physics Design Division, [5]Radiation Safety Systems Division
Bhabha Atomic Research Centre,
Mumbai, India
[2]Radiation Safety Division, [3]Reactor Physics Division, [4]Technical Coordination & Quality Control Section,
Indira Gandhi Centre for Atomic Research,
Kalpakkam, India

Abstract. Neutron and gamma transport through single shield materials were experimentally studied and compared with theoretical calculations and bias factors (C/E) obtained for large size 1000 MWe fast reactor shield materials. The shield materials studied were: Carbon steel, Stainless Steel (SS-316), Cast Iron, Nickel, Graphite, Sodium, Boron carbide and Borated graphite. With the experimental data of neutron transmission through different materials and thickness, the computational capabilities of Codes with various libraries can be assessed with respect to anisotropy, self-shielding, group structure etc. The experiments were carried out in the Shielding corner of Apsara reactor, BARC, India. The leakage thermal spectrum of Apsara was converted to a fast reactor leakage spectrum by using 0.65 % U-235 depleted Uranium Converter Assemblies (CA). The space between Apsara reactor core and the shielding corner being light water, the neutron flux available for the shielding experiments was attenuated by a factor of 10^{-3} to about 10^{7} n/cm^{2}s. The flux was increased to 10^{10} n/(cm^{2}s) by displacing the water between the core edge and the stainless steel lining of Apsara pool on the shielding corner side by an air-filled aluminium box. The scattered neutron contribution from the surroundings was prevented by use of a collimator on the incident face and surrounding the model by borated concrete blocks of 25 cm thickness on all sides except front and back. Theoretical calculations of the experimental configurations were carried out using 2D Transport theory Code DORT in X-Y geometry with S8P3 approximation. Hundred-group multi-group neutron cross-section Library DLC-37 (based on ENDF B-VI) was used. A large number of bare and cadmium covered activation detectors and solid state track detectors were used for obtaining the reaction rates which covered the entire energy range from thermal to fast. $CaSO_4$:Dy thermoluminescent dosimeters were used for absorbed gamma dose measurements. The measured reaction rates (E) were then compared with the calculated values (C) and 'C/E' values obtained for the reaction rates as well as the attenuation along the model length.

1. Introduction

Bulk shielding experiments have been carried out in the shielding corner of APSARA reactor [1] for optimizing the in-vessel radial and axial shield of the Prototype Fast Breeder Reactor (PFBR) [2] being built at Kalpakkam, Tamil Nadu, India. Shield models with various combinations of steel, sodium, graphite and boron carbide, which simulate the radial shielding in the PFBR, have been studied [3]. These experiments pertain to specific design configuration in PFBR and based on the analyses of these experiments with available calculation tools, bias factors for design have been obtained [4]. To extrapolate the bias factor to any further design change or for the design of future FBR-500 and larger size 1000 MWe fast reactors, it is essential to study the neutron transport through single shield materials. From

nuclear data requirement viewpoint, it is seen that data for iron, chromium and nickel are poorly represented in the 25-group set used for core design analysis. In this set, it has been established in earlier critical assembly analyses, that Ni cross-sections are inadequate. Fe cross-sections do not have self-shielding. With respect to cross-sections, this old data set shows large deviations from the newer evaluations**.**

For the shield design, finer neutron structure is needed, but still the group structure practically chosen, say 100 groups as in DLC-37 [5], is not fine enough to ignore self-shielding effects, especially for thick materials. Neither the DLC-37 (American), nor the indigenous IGC-S2 (based on ENDF/B-VI) coupled set can account for self-shielding effects. The task of creating such a set with self-shielding involves a large data processing and writing a new code for mixture cross-section preparation and will take time. Hence at present, the errors due to ignoring self-shielding effects are not known.

The basic data of evaluations on Fe, Cr, Ni have uncertainties in the range of 10 to 25 %, specially in the keV ranges, important for shielding. Spread across different evaluations also is significant. Data adjustment of shielding is not feasible, because individual error information along with the covariance data are not available, and also because it is laborious with large number of groups. Hence the reliability of a multi-group data derived from basic data, under several assumptions, is generally established based on C/E values only, and not on the error estimates derived from the errors of the basic data. Hence experimental validation is essential. The present validations are based on analysis of a few shielding experiments done elsewhere. Indigenous experiments with all details known, is surely preferable. With experiments involving neutron transmissions through varying thickness and directions, the prediction capabilities could be assessed with respect to anisotropy, self-shielding, group structure etc.

Presently cross section data are being generated from various libraries such as ENDFB/VI, JENDL (Japanese) and JEF (Joint European) libraries. These experiments can serve as validation data for inter-comparison of the multi-group data obtained from these libraries and will lead to choice of the best data set for different materials. The self-shielded cross section set being developed can also be tested using these measurements as benchmark data. To meet the above requirements, experiments were conducted to study the neutron transport through single shield materials, in the shielding corner of APSARA. The following shield materials were studied: Carbon Steel, SS-316, Graphite, Boron Carbide, Sodium, Borated Graphite, Nickel and Cast Iron.

2. Experimental Facility

The experiments are best done in a fast reactor environment. Since such suitable experimental locations are not available in India, the experiments were carried out at APSARA reactor, a swimming pool light water thermal reactor. The APSARA shielding corner consists of three trolleys (with concrete shields) mounted on wheels, which can be moved on rails (Fig.1). The trolleys A, B and $A^{/}$ constitute the Block-1, Block-2 and Block-3 of shielding corner. The measurements are carried out in the cave of Block-3. Fig 2 shows the plan view of the experimental arrangement in the shielding corner. In order to increase the neutron flux at shielding corner, water from the gap between the core and the SS liner towards block-3 is removed by using an aluminium box. The APSARA core edge neutron spectrum is converted to a typical hard PFBR neutron spectrum using converter assemblies mounted on a trolley. The trolleys are positioned outside the aluminium panel in the cave of block-3. The length of the CA is such that the neutron beam from the CA fully covers the model. The activation of

CA and consequent dose rates at the time of handling were evaluated and found to be acceptable. The scattered neutrons from the concrete walls of shielding corner were contributing significantly to the measured reaction rates on incident face. To reduce this contribution, a collimated beam of incident neutrons is used in these experiments, by placing a collimator block of borated heavy density concrete between CA and shield models. Lateral size of all shield models were reduced to 500 mm X 500 mm. This was done to reduce cost of shield models. However to prevent neutrons from entering from sides, a 25 cm borated concrete shield was provided on all the four sides of shield models (except front and back sides).

3. Shield Model Arrangement

The measurements of reaction rates were carried out only along the central line of the model. Hence, to reduce the cost of shield models, shield model dimensions were restricted to 500 mm x 500 mm. The thickness of the model varied for the different models. The shield models have ducts for placing foil holder at various distances along the shield model thickness. It is necessary to prevent the effect of neutrons scattered by the walls of shielding corner, by surrounding it with a shield model concrete block. The variation of reaction rates as a function of thickness were calculated for four types of concrete, namely, ordinary concrete, heavy density concrete, borated concrete and borated heavy density concrete. It was found that 250 mm of borated heavy density concrete was sufficient to minimize the scattered neutron contribution from outside the model.

3.1. Shield Model Concrete Blocks

The shield models are placed at the centre of a borated heavy density concrete block of 1098 mm x 1000 mm x 1200 mm. The concrete blocks are made in two parts and the bottom block (848 mm high) has a 500 mm x 500 mm cavity at the centre. The upper block is a concrete block of 250 mm height. The upper block has ducts for inserting foil holders at locations, corresponding to the ducts in shield models. Sectional plan and elevation of the shield model concrete blocks are shown in Figs.3 & 4.

3.2. Shield Models

Eight single material shield models were fabricated for these experiments. The materials are: Carbon Steel, SS-316, Graphite, Boron Carbide, Sodium, Borated Graphite, Nickel and Cast Iron. The shield model thickness and locations of the foil holders was based on the attenuation characteristics of the shield material. Measurements were carried out to study attenuation of the order of 10^{-4}. Based on these, shield model design has been carried out. The cast iron model has density 7.2 g/cm^3. The composition of this model is given in Table I. Fig.5 gives details of this shield model. The shield thickness is chosen as 1200 mm, with foil holders positioned at 200 mm, 350 mm, 450mm, 600mm, 750 mm and 1000 mm.

TABLE I. NUMBER DENSITIES (ATOM/B-CM) OF NUCLIDES IN CAST IRON MODEL.

Element	Number density
C	1.22766E-02
Mn	5.13062E-04
S	1.35264E-04
P	4.20074E-04
Fe	7.41930E-02

3.3 Foil Holder

The foil holder is made of Aluminium. The total height of the foil holder is 575 mm. The height inside shield model is 525 mm. An aluminium plate with a central hole of 30 mm diameter is welded to two aluminium strips of 450 mm length, 10 mm width and 5 mm thick. At the bottom end a rectangular plate of 50 mm x 60 mm x 3 mm thick is welded. The foils are fixed on this plate (on the side facing the core) with the help of cellophane tape. On inserting foil holder, the centre of the bottom plate, where foils are loaded, is in line with the centre of shield model. Details of the foil holder are given in Fig.6. Foils are retrieved using a tool with a telescopic arm.

4. Biological Shielding

Biological shielding was provided around the shielding corner to ensure accessibility to the surrounding areas in the reactor hall. Adequate shielding was provided for reactor operation with core at C' position at 200 kW reactor power. It was also noted that the dose rates are lesser when CA are present. Hence, the arrangement of biological shielding was adequate, for the proposed experiments. This was confirmed by dose mapping at low power operation.

5. Experimental Details

The activation foils used are given in Table II along with their nuclear parameters and typical masses. The measurements are carried out only along the central line of shield model and are hence free from boundary effects.

TABLE II. ACTIVATION DETECTORS AND SSNTDS.

Reaction	Isotopic Abundance	Mass (g)	Half-life	Resonance Energy	Threshold Energy	Gamma Energy
$^{23}Na(n,\gamma)^{24}Na$ (as NaF)	100.0	0.43	15.0 h	2.85 kev	-	1.37 Mev
$^{63}Cu(n,\gamma)^{64}Cu$	69.17	0.28	12.7 h	0.580 kev	-	0.511 Mev
$^{197}Au(n,\gamma)^{198}Au$	100.0	0.05	2.7 d	0.0049 kev	-	0.412 Mev
$^{237}Np(n,f)$ SSNTD	-	200 to 800 (dpm)	-	-	0.6 Mev	-
$^{232}Th(n,f)$ SSNTD	-	0.12	-	-	1.4 Mev	-
$^{115}In(n,n')^{115m}In$	95.7	0.46	4.49 h	-	1.3 Mev	0.336 Mev
$^{32}S(n,p)^{32}P$	95.2	0.86	14.3 d	-	2.7 Mev	β emmiter

The experimental campaign for each experiment consists of two irradiations: (1) 40 kW reactor operation for 8 hours and (2) 200 kW reactor operation for 12 hours. In the 40 kW operation Au, Au/Cd, Cu, Cu/Cd, Th/Cd, SSNTD with Np and TLDs for gamma dose measurements are irradiated and these are retrieved after 8 hours of cooling. In the 200 kW operation Na, Na/Cd, In and S activation foils were irradiated and the foils are retrieved after 12 hours cooling. There are five/six foil holder locations in each shield model. Incident neutron flux measurement is done using foil holder in the collimator block.

6. 2-D Transport Calculations

Calculations for the various shield configurations have been done using 2D transport theory code DORT [6]. Calculations have been carried out in X-Y geometry. S8-P3 approximations have been used. For the purpose of calculations, the fuel elements have been homogenised over each fuel box region. Graphite and BeO reflectors at the peripheral positions of the core

are also homogenised over the square region. Apsara reactor is surrounded by pool water on all sides. The converter assemblies have been modelled as homogeneous assemblies. The hexagonal outline has been modelled as close as possible in 2D X-Y representation. The pointwise group flux convergence criterion use is 10^{-4}. This convergence was obtained in all the groups for all the spatial mesh points, but for a few corner points in the first two groups and thermal group. Energy dependent activation / fission cross sections for the reaction rate calculations have been taken from SAND II library [7]. The 620 group cross sections have been collapsed to 100 group cross sections using a flat weighting function. The total neutron flux at the core centre was normalised to the total flux obtained using the 3D transport code TRITAC [8].

7. Results of Measurements

Gamma activities of the irradiated detectors were measured in a standard high purity germanium detector coupled to a multi-channel analyzer. The high purity germanium detector was calibrated using ^{152}Eu source. The counting set-up consists of slots at various distances from the detector. The counting time was chosen so as to keep the error in photo-peak counts acceptable. The measured count rates (in Counts per second) are converted into saturation activation integral per atom, using the following formula:

$$\int \gamma(E)\phi(E)\,dE = A / (N \varepsilon_1 \varepsilon_2 \varepsilon_3 G(\tau)(1-\exp(-\lambda t))\exp.(-\lambda T))$$

where
A = photo-peak counting rate for the detector
N = total number of target atoms
ε_1 = isotopic abundance
ε_2 = yield of gamma ray
ε_3 = photo-peak counting efficiency
T = time elapsed between end of irradiation and start of counting
t = duration of irradiation
λ = Decay constant for the isotope
G (τ) = self shielding factor for the detector
γ (E) = Activation cross-section at energy E
ϕ(E) = Neutron flux at energy E

In-order to check the uniformity of neutron flux on the incident face of shield model, large number of bare gold foils were fixed horizontally and vertically on the emergent face of collimator, which corresponds to the incident face of the model. Table III shows variation of bare gold foil activity on the incident face of shield model. Inner values (columns 3, 4 & 5 in the rows 5-9) correspond to the incident face of shield model and other values correspond to the surrounding concrete. Incident neutron flux is fairly constant on incident face (variation from central value is ≈5%). The bold numbers in the Table III corresponds to top half of incident face of shield models.

The measured reaction rates on the incident face changes from model to model since the scattering contribution is different in different models. The ratios of bare to Cadmium-covered foil activities (cadmium ratios) are given in Table IV indicate that the contribution to the neutron spectrum in low energy region is significantly less with the present CA configuration, thus closely simulating the FBR blanket exit spectrum.

TABLE III. RELATIVE VARIATION OF NEUTRON FLUX ON INCIDENT FACE.

Axial distance from center	Plane 40 cm away from cent	End plane of model (Cave side)	Center of model	End Plane of model (control room side)	Plane 40 cm away from center
50	1.43	1.62	1.81	1.81	1.91
40	0.32	0.37	0.49	0.45	0.41
30	0.27	0.58	0.73	0.62	0.33
25	0.30	0.72	0.86	0.86	0.40
20	0.35	**0.97**	**0.98**	**0.86**	0.42
15	0.41	**0.97**	**0.96**	**1.01**	0.42
10	0.41	**0.96**	**0.99**	**0.96**	0.46
5	0.40	**0.97**	**0.97**	**1.07**	0.45
0	0.44	**0.99**	**1.00**	**1.03**	0.44

For cast iron model, the ratio of calculated to measured reaction rates (C/E values) with various activation detectors is given in Tables V-XIV. The normalized C/E values are also given in the Tables. The data for other models are not given as the same would be too voluminous. Table XV gives measured gamma dose using thermoluminescent dosimeter. The attenuation values are shown plotted in Fig.7. All reaction rates have been normalized to 200 kW reactor power. The absorbed gamma dose values are given at 40 kW reactor operation for 8 hours.

TABLE IV. CADMIUM RATIOS ON THE INCIDENT FACE.

Detector	Earlier experimental geometry without collimator/ outer shield	New experimental geometry with collimator/shield
$^{197}Au(n,\gamma)^{198}Au$	1.43-1.66	1.03-1.24
$^{23}Na(n,\gamma)^{24}Na$	1.85-2.58	1.14-1.54
$^{63}Cu(n,\gamma)^{64}Cu$	1.62-2.33	1.07-1.39

TABLE V. CAST IRON MODEL - BARE $^{23}Na(n,\gamma)^{24}Na$.REACTION RATES COMPARISON.

Distance from incident face (cm)	C/E	Normalized C/E
0	0.460	1.000
20	0.555	1.208
35	0.377	0.824
45	0.461	1.000
60	0.378	0.825
75	0.324	0.704
100	0.638	1.385

TABLE VI. CAST IRON MODEL - CADMIUM COVERED $^{23}Na(n,\gamma)^{24}Na$. REACTION RATES COMPARISON

Distance from incident face (cm)	C/E	Normalized C/E
0	0.390	1.000
20	0.569	1.460
35	0.525	1.347
45	0.471	1.203
60	0.378	0.970
75	0.323	0.828
100	0.659	1.693

TABLE VII. CAST IRON MODEL - BARE $^{197}Au(n,\gamma)^{198}Au$. REACTION RATES COMPARISON.

Distance from incident face (cm)	C/E	Normalized C/E
0	0.183	1.000
20	0.295	1.612
35	0.335	1.829
45	0.325	1.775
60	0.280	1.527
75	0.248	1.355
100	0.452	2.471

TABLE VIII. CAST IRON MODEL - CADMIUM COVERED $^{197}Au(n,\gamma)^{198}Au$. REACTION RATES COMPARISON.

Distance from incident face (cm)	C/E	Normalized C/E
0	0.214	1.000
20	0.320	1.494
35	0.347	1.641
45	0.306	1.426
60	0.261	1.216
75	0.231	1.077
100	0.478	2.225

TABLE IX. CAST IRON MODEL - BARE $^{63}Cu(n,\gamma)^{64}Cu$. REACTION RATES COMPARISON.

Distance from incident face (cm)	C/E	Normalized C/E
0	0.568	1.000
20	0.693	1.220
35	0.660	1.159
45	0.576	1.015
60	0.478	0.840
75	0.426	0.750
100	0.927	1.627

TABLE X. CAST IRON MODEL - CADMIUM COVERED $^{63}Cu(n,\gamma)^{64}Cu$. REACTION RATES COMPARISON

Distance from incident face (cm)	C/E	Normalized C/E
0	0.586	1.000
20	0.714	1.223
35	0.687	1.713
45	0.602	1.028
60	0.482	0.825
75	0.424	0.728
100	0.889	1.517

TABLE XI. CAST IRON MODEL - $^{115}In(n,n')^{115m}In$ CADMIUM COVERED. REACTION RATES COMPARISON

Distance from incident face (cm)	C/E	Normalized C/E
0	0.601	1.000
20	0.449	0.746
35	0.358	0.595
45	0.313	0.522
60	---	---
75	---	---
100	---	---

TABLE XII. CAST IRON MODEL - $^{232}Th(n,f)$ CADMIUM COVERED. REACTION RATES COMPARISON

Distance from incident face (cm)	C/E	Normalized C/E
0	1.030	1.000
20	0.468	0.455
35	0.294	0.286
45	0.297	0.288
60	0.285	0.277
75	0.333	0.323
100	1.020	0.990

TABLE XIII. CAST IRON MODEL - $^{237}Np(n,f)$ CADMIUM COVERED. REACTION RATES COMPARISON.

Distance from incident face (cm)	C/E	Normalized C/E
0	0.947	1.000
20	0.551	0.581
35	0.339	0.359
45	0.231	0.245
60	0.178	0.188
75	0.188	0.200
100	0.674	0.713

TABLE XIV. CAST IRON MODEL - $^{32}S(n, p)^{32}P$ CADMIUM COVERED. REACTION RATES COMPARISON.

Distance from incident face (cm)	C/E	Normalized C/E
0	0.331	1.000
20	0.154	0.464
35	---	---
45	---	---
60	---	---
75	---	---
100	---	---

TABLE XV. CAST IRON MODEL - ABSORBED GAMMA DOSE.

Distance from incident face (cm)	Measured Gamma dose (Gray)
0	1.271E+01
20	2.760E+00
35	1.090E+00
45	6.135E-01
60	1.481E-01
75	6.176E-02
100	5.486E-02

8. Conclusions

The ratios 'C/E' obtained from various reaction rates provide valuable data for nuclear data validation studies. From the activity of irradiated gold foils on the incident face of the model, we see that the neutron flux is fairly constant. This shows the adequacy of the size of the converter assemblies and efficacy of the collimator in ensuring a uniform flux of neutrons.

From the plots of the reaction rates v/s distance from the incident face of the model, we see that the effect of backscattering is seen in only at the last data point, towards the end of the model. At all other points, the data is free from backscattering contribution. This is due to the use of borated concrete around the model, large length of the model and the use of collimator block. Because of this improvement, the attenuation values are very reliable except the last data point.

The activities of bare sodium, copper and gold foils (a measure of the thermal flux) show attenuation factors of 0.012, 0.01 and 0.014 respectively in the cast iron model. The activities of cadmium-covered sodium, copper and gold foils (a measure of the epi-thermal flux) show attenuation factors of 0.013, 0.011 and 0.016 respectively in the cast iron model.

The activities of threshold detectors sulphur and indium were too low to be measured inside the model. The activities of neptunium and thorium (a measure of the fast flux) show attenuation factors of 0.0019 and 0.0004 respectively in the cast iron model.

Most of the C/E values are less than 1 indicating that the fluxes are under-predicted. It is to be noted that the various activation foils are sensitive to different parts of the neutron spectrum and hence show different C/E along the shield model. A comparison of C/E

obtained with other codes and cross section sets only will bring out the full impact of these experiments.

In order to reduce the bias used in the present calculations, it is felt that problem dependent multigroup cross section set with a large number of groups should be generated. More number of groups must be considered in the thermal (< 0.415 eV) region. It is also recommended that there should be a concerted effort to identify and generate suitable activation cross-section set for activity calculations. These need to be compatible with the problem dependent cross section sets used in the transport calculations.

The measured gamma dose values are due to contributions from prompt fission, inelastic capture and activation gammas. Since capture gamma contribution is significant, the measured doses vary considerably from model to model. No attempt has been made to separate the various contributions to the total dose.

REFERENCES

[1] 50 Glorious Years of APSARA (2006-2007), Government of India, BARC, Trombay-40085.

[2] CHETAL, S.C, *et al*., "The Design of Prototype Fast Breeder Reactor", Nuclear Engineering and Design, Vol. 236, Issue 7-8, Pages 852-860 (2006).

[3] H.K. DRAVID, R. INDIRA, *et al*., "PFBR Bulk Shielding Experiments at APSARA", BARC NEWSLETTER, No.216, January 2002.

[4] R. INDIRA, H.K. DRAVID, *et al*., IGC NEWSLETTER, Volume 50, October 2001.

[5] D.M. PLASTER, et al., "Coupled 100 Group Neutron and 21 Group Gamma-ray Cross Section for EPR Calculation", ORNL-TM-4872 (1975).

[6] RHOADES, W.A. and CHILDS, R.L, The DORT-Two dimensional discrete ordinates transport code, Nucl. Sci. Eng. **99** (1988) 88.

[7] W.N. MCELROY, S. BERG *et al*., "A Computer-automated Iterative Method for Neutron Flux Spectra Determination by Foil Activation", AFWL-TR-67-41, Vol. I to IV (1967)

[8] BANDO, M., YAMAMOTO, T., SAITO, Y. and TAKEDA, T., J. Nucl. Sci. Technol. **22** (10) (1985) 841.

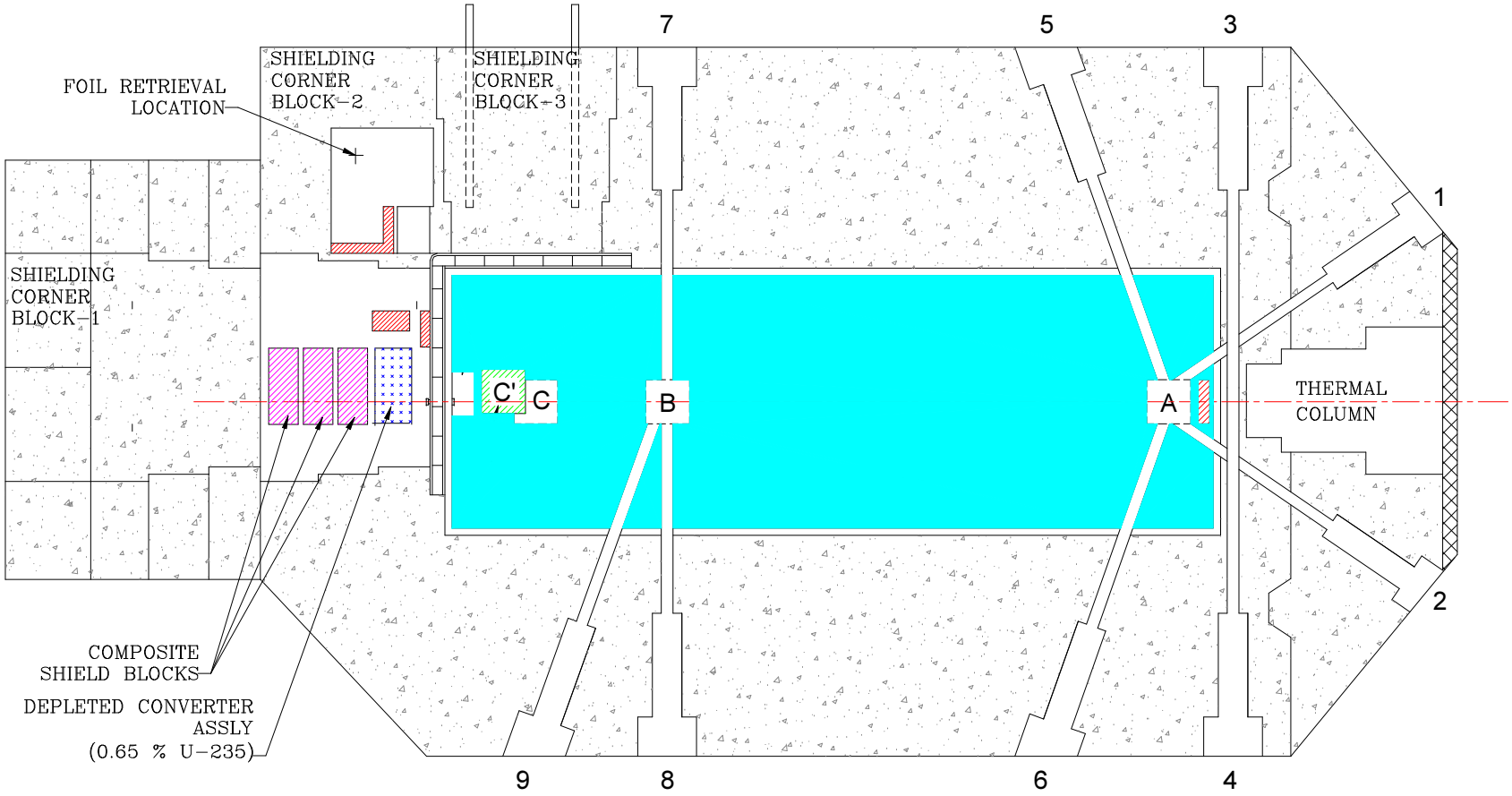

FIG.1 APSARA SECTIONAL PLAN ARRANGEMENT FOR PFBR SHIELD EXPERIMENT

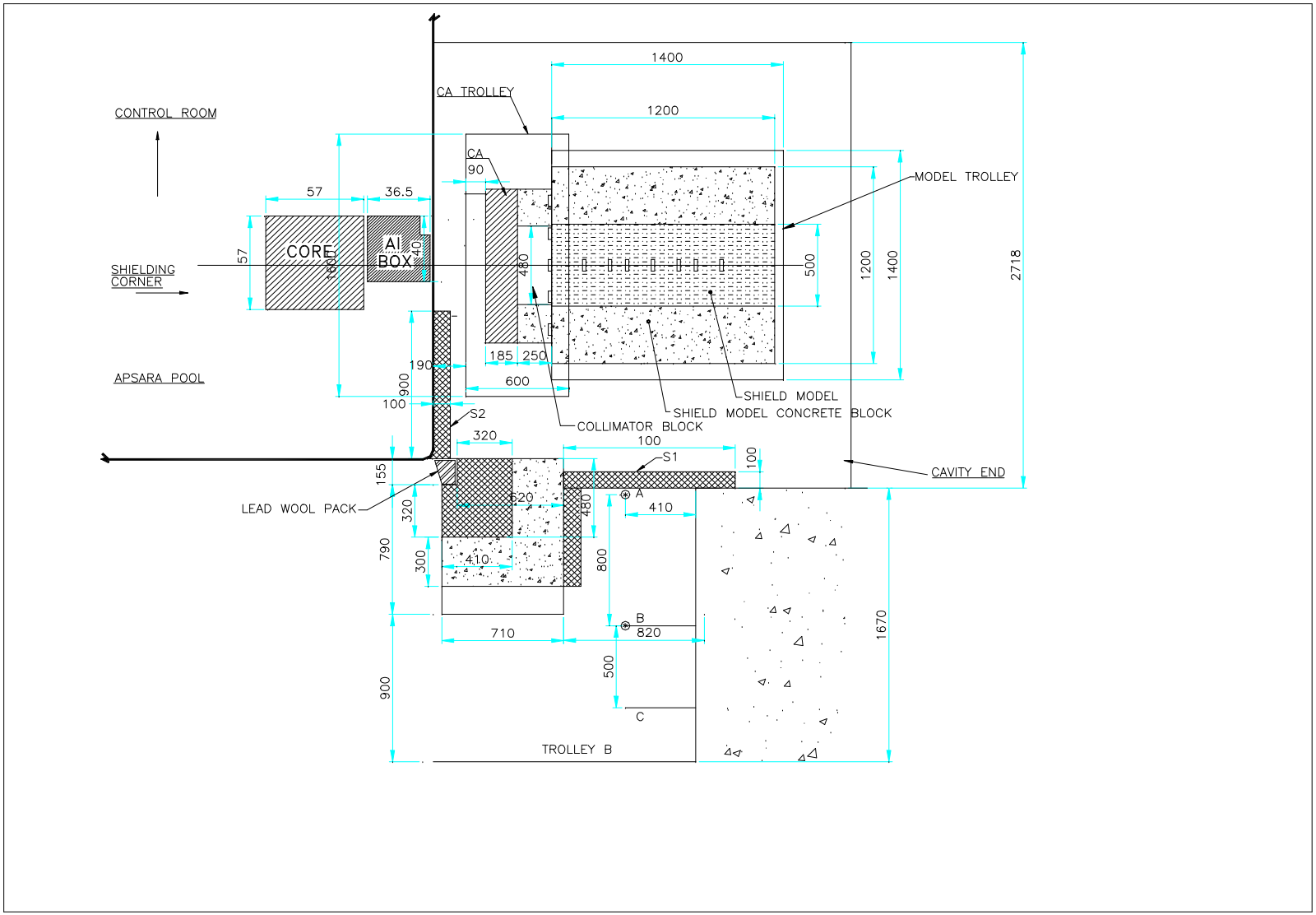

FIG.2. Sectional plan of experimental arrangement.

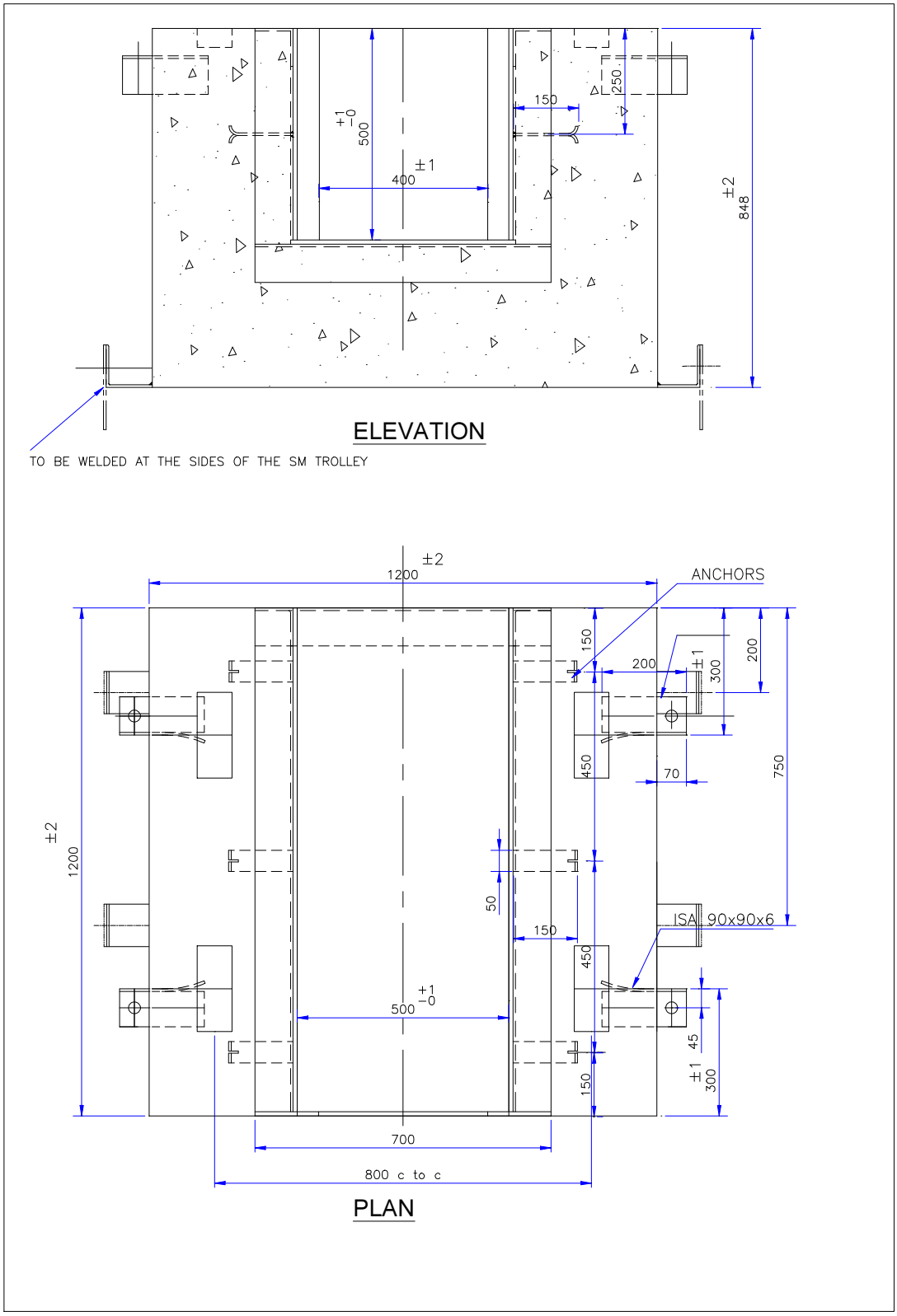

FIG.3. Lower concrete block.

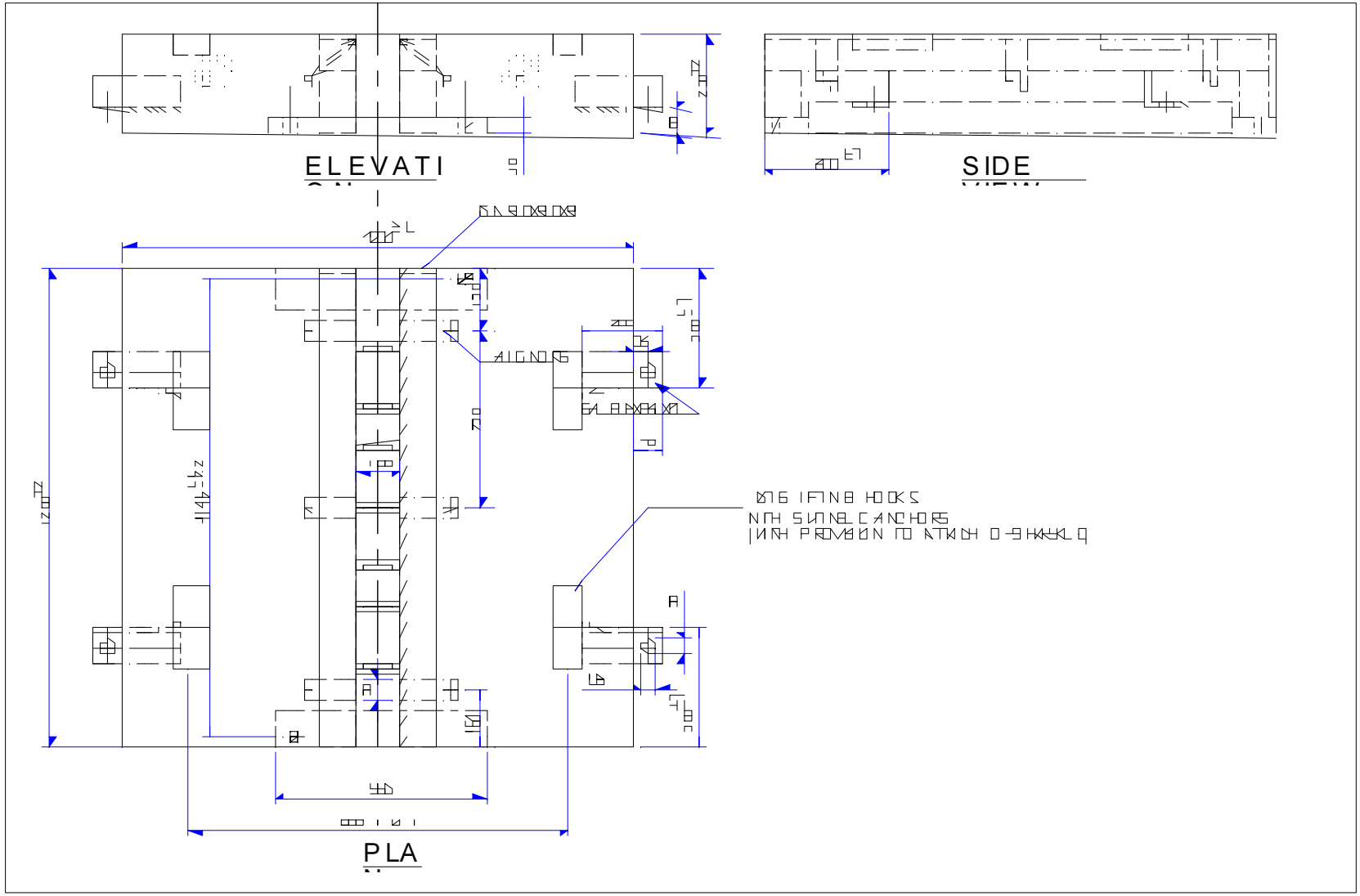

FIG.4. Upper concrete block.

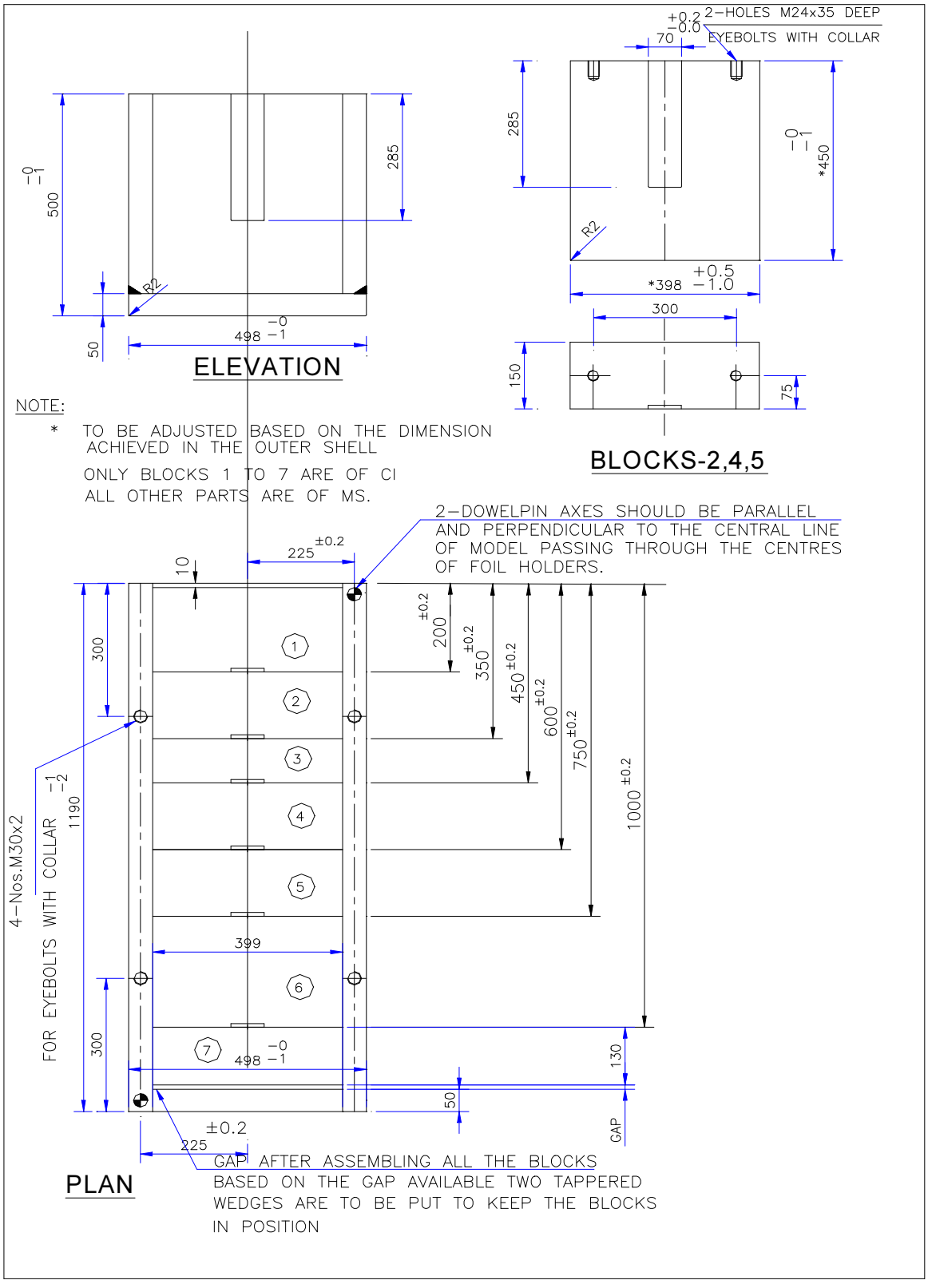

FIG.5. Shield model (Cast iron).

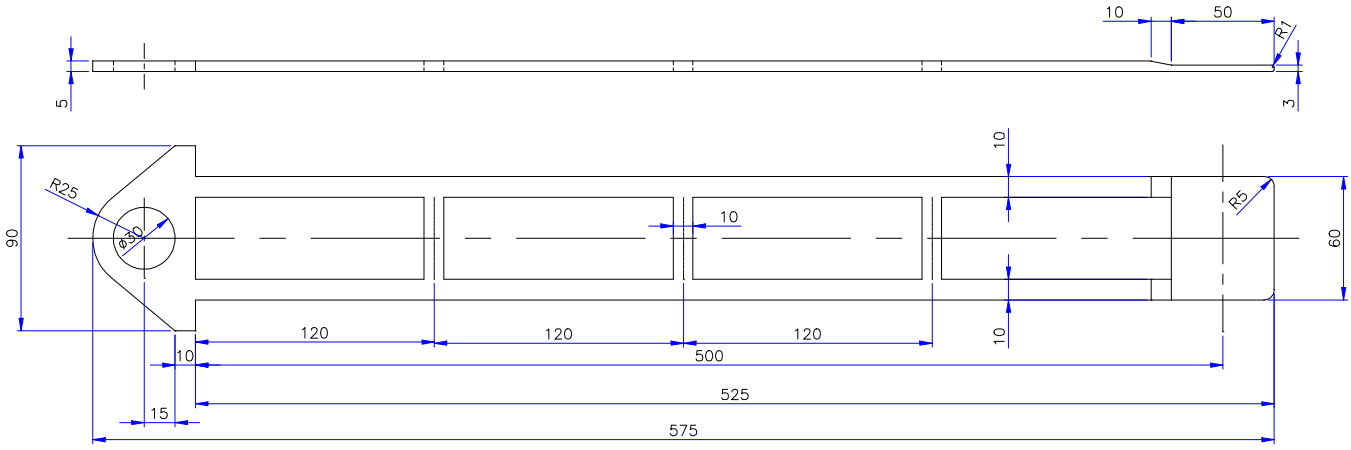

FIG.6. Foil holders.

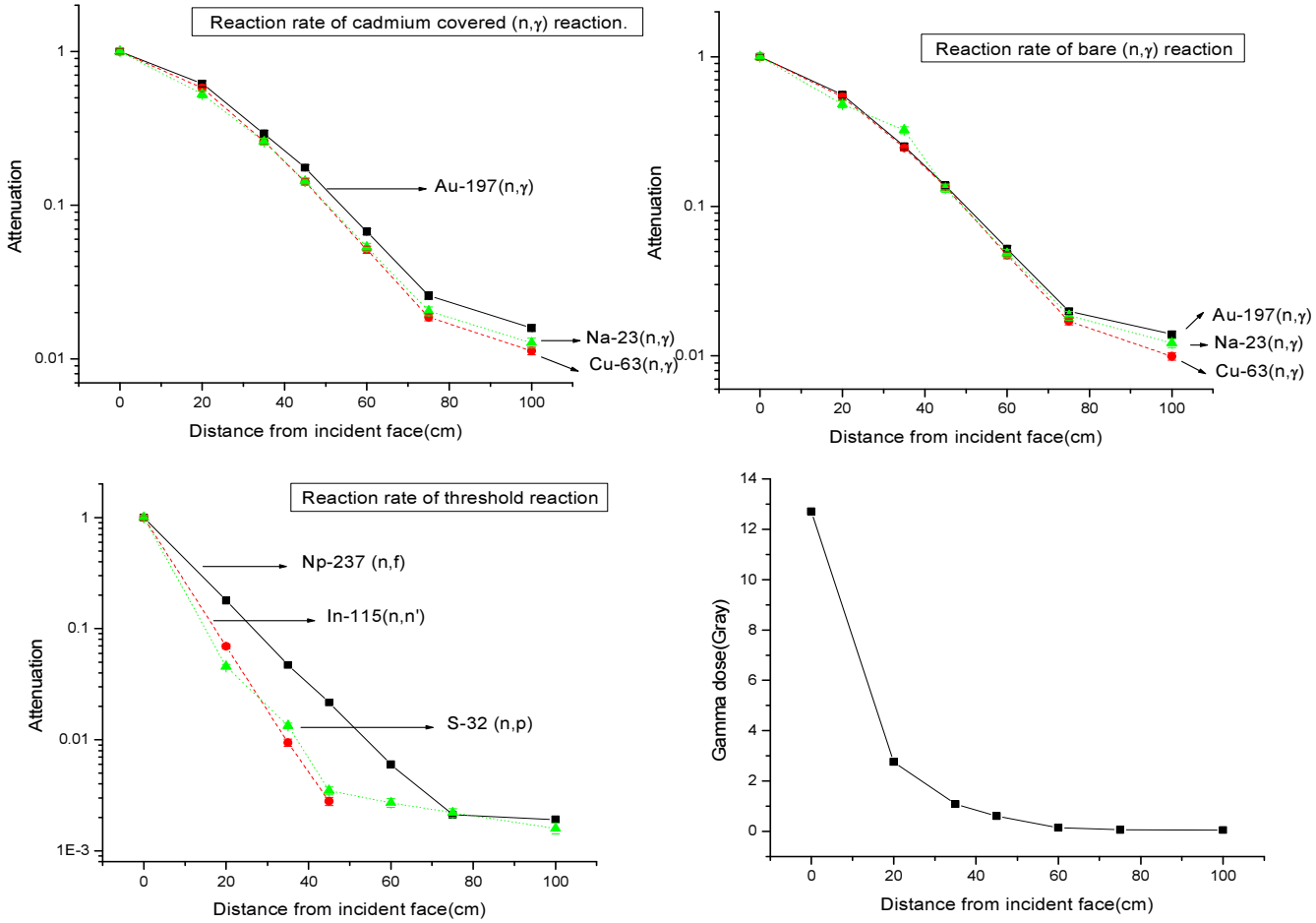

FIG.7. Attenuation of neutron flux and Gamma dose in Cast iron.

Measurements of Nuclear Data for MA at VENUS-F and BR-1 reactors

P. Baeten, A. Kochetkov, G. Vittiglio, J. Vagemans

SCK•CEN, Boeretang 200, 2400 Mol, Belgium

Abstract. One of the declared advantages of the perspective systems as ADS and Gen.IV fast reactors is the transmutation of the minor actinides (MA) such as neptunium, americium and curium. From the viewpoint of reactor neutronic design, the loading of MA in the core generally affects the physics parameters. The detailed core designs of these advanced systems are difficult so as the reliability of nuclear data of MA, especially for the leads cooled facilities, is not sufficient. The current and future possibilities of measuring of nuclear data (ND) for MA in integral and micro data experiments at the SCK•CEN (Mol, Belgium) reactor installations are presented.

1. Introduction

So as the uncertainties of ND for MA can result in the significant impact in multiplication coefficient [1] and other ADS transmutation reactors parameters, calculated on the basis of different evaluated nuclear data files, and since their uncertainties are several times more then it is required [2], at present there are no possibilities to decrease the real errors in calculated parameters down to acceptable level without new measurements with minor actinides. Two types of experiment are necessary: new micro data measurements and integral experiments.
In SCK•CEN the GUINEVERE (Generator of Uninterrupted Intense NEutrons at the lead VEnus REactor) project has been lunched. The project consists in coupling a subcritical zero power fast lead core, at the VENUS-F reactor, with a GENEPI external 14 MeV neutron source has to be operated in pulsed and in continuous mode. This project aims to investigate the feasibility of ADS on the steps of loading and reactivity monitoring of the subcritical and critical cores. So as an experimental programme dedicated to a critical operation of heavy liquid metal cooled fast reactors can serve both for the LMFR development and for the critical mode operation of ADS. MA fission rates cross sections ratios so as spectral indexes will be measured at 30% enriched uranium lead VENUS-F benchmark core, by means of fission chambers and foils. The measurements will be accompanied with deterministic and Monte Carlo calculations.

The measurements of the thermal neutron-induced fission cross section of a number of Cm isotopes was set up at SCK•CEN in the well thermalized neutron beams provided by the Maxwellian Thermal Spectrum Reference Field in the large cavity of the graphite moderated BR1 reactor. The results for the ^{245}Cm isotope recently have been received with statistical uncertainty of the order of 0.9%. These results were presented at FISSION 2009 Conference in May. This work is on the way. The coming future and current experiments at SCK•CEN in support of the improvement of the uncertainties of MA data, so as the designs of the reactors in use are discussed in the paper.

2. VENUS-F fast zero power facility for MA nuclear data integral experiments

The GUINEVERE project takes part of the European EUROTRANS FP6 project, and aims to investigate on-line subcriticality measurement methods for Accelerator Driven Systems (ADS) with a fast neutron spectrum. Therefore the VENUS reactor at the SCK•CEN site has started to modify towards a system with a fast spectrum: the fuel pins actually surrounded by water will be replaced by fuel pins surrounded by lead. The deuteron accelerator GENEPI, previously used in the MUSE project, will be modified in order to provide a continuous

neutron source.

2.1. The modification of the VENUS installation for the GUINEVERE Project

The VENUS reactor was built in 1963-1964 and is a water moderated reactor ("zero-power critical facility"). The VENUS reactor is made critical by increasing the water level in the reactor. In case of an emergency stop, the water can be evacuated in a very short time by opening safety valves to so-called dump tanks. The execution of the GUINEVERE project has activated two major modifications at the SCK•CEN site:

-The adaptation of the VENUS critical facility to host a fast lead core, further on referred to as VENUS-F,

-The modifications which are connected to the installation of the new GENEPI-3C accelerator at the VENUS critical facility and its coupling to the core.

To implement the vertical penetration option, the accelerator has to be put in a technical room to be constructed on top of the VENUS bunker (see Fig. 1).To change the water-moderated thermal reactor into a fast lead reactor, two main modifications are necessary:

- Full in-core modification, including removing all existing components and the construction of fuel assemblies with lead blocks and uranium fuel for the core and large lead blocks for the reflector,
- Installation of a shut-down system based on shut-down rods suspended by electro-magnets.

The basic features of the core design are as follows:

-The core is a fast lead one, consisting of a fuel zone surrounded by a lead reflector, arranged within the existing vessel of the VENUS facility (160 cm in diameter),

-The fissile material in fuel sub-assemblies (FA's) is 30% ^{235}U enriched metallic uranium bars of cylindrical shape are ½ inch in diameter (1.27 cm), 8 inches in length (20.32 cm), and covered with a nickel deposit about 70 μm in thickness. They are provided by the CEA (France). Three uranium bars are placed on the assembly height,

-For the subcritical case, at the core centre, a channel is arranged in order to allow the crossing of the neutron generator glove finger. This channel has the same cross section as one sub-assembly,

-The supporting structure of the vessel itself will be reinforced to support the added weight of the lead components.

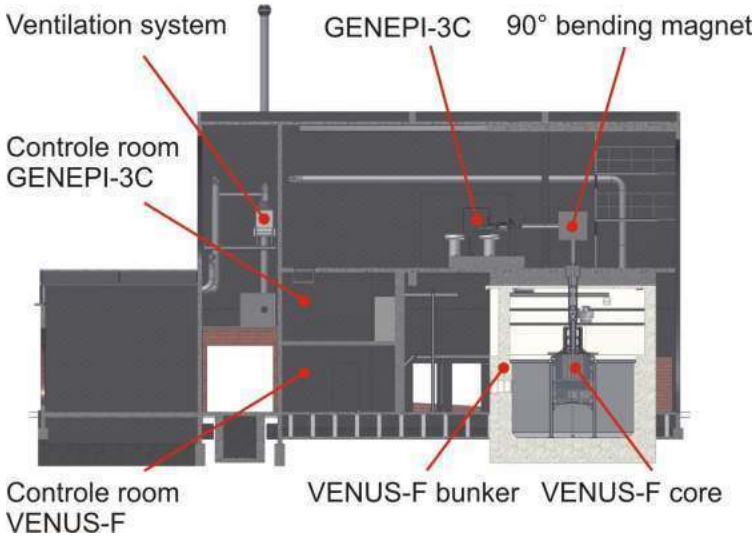

FIG.1. Side view of the modified VENUS facility

In the FA's the arrangement “5 x 5 with lead plates” (9 fuel stacks vs. 16 lead stacks) was chosen allows to receive homogeneous, symmetrical view of the FA layout (see Fig. 2).

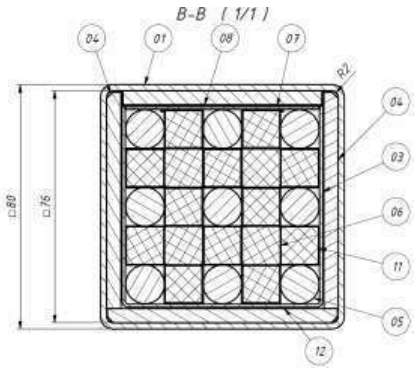

1 : Weld-assembly tube (stainless steel)
3, 7 : Steel casing
4, 8, 12 : Lead plate (Pb 99,9)
5 : Uranium metallic bar
6 : Bare lead bar (Pb 99,9)
11 : Lead bars with SS lining

FIG.2 Cross-section of a fuel sub-assembly in the fuel part.

A new shut down system had to be implemented for the new fast neutron VENUS-F. The standard philosophy of safety rods (SR) which fall in the core by gravity upon receiving the signal for de-energizing of the electro-magnets was chosen. The SR's consist of an absorbing material (B_4C with natural boron), 60 cm long, with a fuel follower (with the same pattern as shown in Fig. 2). When a safety rod is up, its fuel follower is at the same height as regular FA’s in the core, thereby eliminating most of the core perturbations. This way, an anti-reactivity is inserted when a rod drops, due to replacement of the fuel by the absorber material. The control rods (CR) simply consist of an absorbing part that placed inside a wrapper tube, and their position is flexible. During the reactivity piloting the CR's are inserted in the core by replacing the empty space. In total six Safety Rods and two Control Rods are foreseen. Fig. 3 shows the current location for these rods, and their reactivity worth is given in the following section.

Every component of the new FA structure have been already manufactured and preassembled. Currently the most of the VENUS to VENUS-F modifications have been realized and we will be ready to launch the experimental programme at the beginning of the next year. The VENUS-F system will provide a unique facility in Europe (except Russian BFS in Obninsk) for fast sub-critical and critical reactor physics investigations.

2.2. GUINEVERE critical configuration at VENUS-F

The first GUINEVERE core will be the critical “reference” core (called CR0) without central hole for the accelerator. This core will be built to assess the reactivity scale by the rod drop and multiplication method through the entire programme, and this pure benchmark core will be used for the spectral indexes and MA fission ratios measurements. The core will consist of 88 FA’s (when the SR are up). The CR0 core is shown in Fig. 3 and 4. Main parameters of this core have been calculated with MCNPX 2.5.0 code [3], and with the ZZ LEPH-LIB-JEFF3.1 nuclear data library, a continuous energy multi-temperature library created at SCK•CEN [4, 5, 6]. Results are summed-up in Table I.

Compared calculations performed with the same code but different data libraries (ENDFB-VI.6, JEFF3.1), the results for k_{eff} values remain in agreement within 500 pcm.

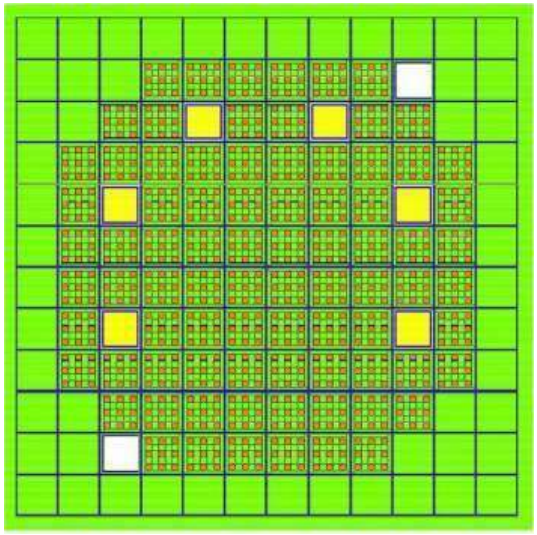

*FIG.3. Critical (CR0) configuration when SR's down: safety (yellow) and control (*white*) rod locations are shown.*

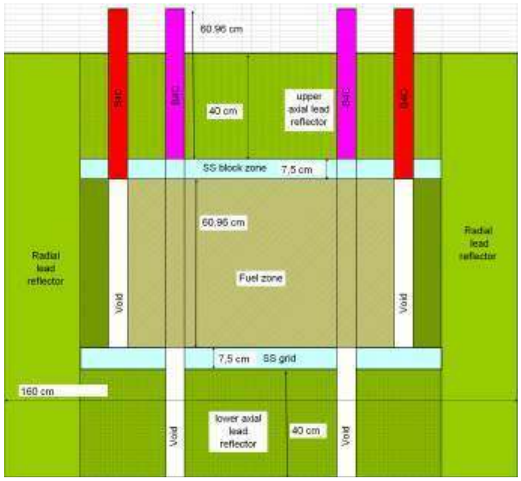

FIG.4. Critical (CR0) configuration vertical cut: all SR's / CR's up.

TABLE I. MAIN NEUTRONIC PARAMETERS OF THE CR0 CRITICAL CORE

Parameter	Indicative value
Core height / diameter, cm	60.96 / 85.42
Fuel enrichment / volume content	30 / 17 (%)
Critical mass	88 FA's
k_{eff}	1.01031 ± 0.00029
Peripheral FA reactivity worth (pcm)	232±42
β_{eff}	748 pcm ± 17
Safety rod reactivity worth	14 $
Control/pilot rod reactivity worth	1.1 $

2.3. Experimental program CR0 critical configuration

The experimental programme foreseen in the scope of the GUINEVERE project activity within the EUROTRANS FP6 will concern the critical CR0 and subcritical configurations. More sub-critical (k_{eff} = 0.85, 0.95, 0.99) and critical configurations are expected to be investigated beyond this period, inside next EUROTRANS FP7. We limit here the description

of the experiments have planned in the CR0 configuration.

First of all in the CR0 phase core characterization measurements will be done and validation of reactivity measurement techniques will be carry out. Radial and axial traverses will be executed by foil activation and with fission chambers (FC) respectively and a number of spectral indices will be performed in the core center. Control rod worth will be calibrated by means of the stable period measurement and rod-drop measurements will be used to determine the sub-critical reactivity scale and allow the implementation of a reference technique for validation of sub-critical reactivity measurements. Measurements of βeff are also planned by Cross Power Spectral Density (CPSD) and Rossi-α techniques.

The following MA fission rate ratios to the ^{235}U fission rate will be measured by 4 and 8mm fission chambers, arranged in the special hole in experimental FA (see Fig.5): $^{237}Np/^{235}U$, $^{238}Pu/^{235}U$, $^{240}Pu/^{235}U$, $^{242}Pu/^{235}U$, $^{241}Am/^{235}U$.

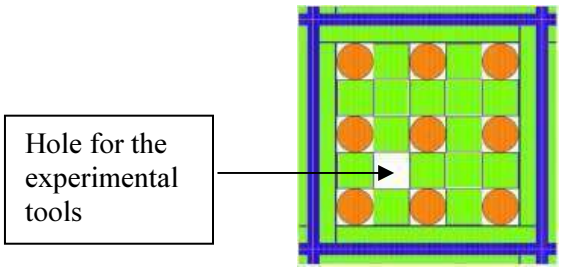

FIG.5. Experimental fuel assembly.

The results of MA measurements will be compared with calculational ones received by ERANOS and MCNP5 codes and different data sets to conclude the current data level reliability on the base of the c/e comparisons.

Before the experiments in VENUS-F fission chambers with MA deposits will be calibrated in BR-1 reactor.

2.4. VENUS-F for MYRRHA/FASTEF critical operation

It has been declared that Fast Spectrum Transmutation Experimental Facility MYRRHA/FASTEF will be operated as a subcritical facility and a critical facility. Therefore, an experimental programme in support of the operation of the critical phase is needed. Such an experimental programme with regard to the critical mode operation of MYRRHA/FASTEF can be sufficiently generic to be also valid for the needed validation of reactor codes for LFR development.

After finalization of the GUINEVERE programme dedicated different subcritical VENUS-F configurations, the application of the VENUS-F facility for the mock-up investigations of MYRRHA/FASTEF critical operation have been discussed.
As the result, an experimental programme for code validation in support of Lead Fast Reactor development can be easily implemented. The necessary measurements will be performed to validate the code performances and nuclear data reliability. Nuclear data of minor actinides are the candidate number one in the list of the investigations due to their participation in fast neutron designs transmutation process and their current uncertainties. This programme is foreseen in the framework of EUROTRANS FP7 project. The proposal is under discussion and welcome to contribute for all participants.

3. BR-1 reactor for MA nuclear micro data measurements

The BR1 reactor is a research reactor of the "natural uranium – graphite – air" type which has been in operation since May 1956 (Fig. 6). The reactor is mainly used as a neutron reference source for reactor physics experiments, neutron activation analysis, and calibration of nuclear detectors and instruments.

3.1. BR-1 Reactor design

The reactor core consists of a matrix of 14500 graphite blocks (moderator) with a total volume of 6.7 * 6.8 * 6.8 m^3. In this volume, there are 829 horizontal channels; 569 of these channels are loaded with natural uranium (0.7 % U5). The core loading is approximately cylindrical with a radius of about 2.4 m.

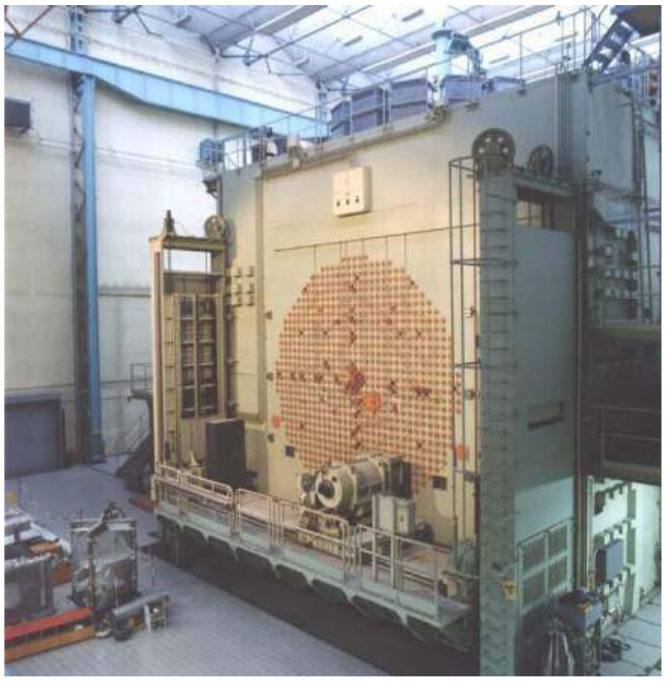

FIG.6. View of the BR1 reactor

Each fuel channel contains 23 uranium rods. The geometry of a fuel rod is given in Fig. 7 and consists of a natural uranium rod in an aluminium cladding. The fuel channels have a square section of 50 mm * 50 mm, with a lattice pitch of 180 mm (Fig. 8). The total length of the core loading is 214 mm * 23 = 4.920 m. The total number of fuel rods is 569*23 = 13 087 which gives approximately 25 tons of natural uranium. The shielding of the reactor consists of heavy concrete with a thickness of 2.1 m.

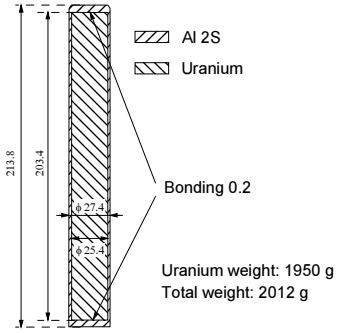

FIG.7. Fuel rod BR1 reactor

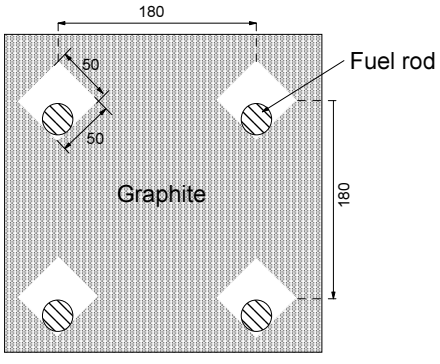

FIG.8. Partial view of the BR1 matrix

The burn-up of the fuel is very small, so as the initial loaded fuel is still in use. The main parameters of BR-1 reactor are shown in the Table II.

TABLE II: MAIN CHARACTERISTICS OF THE BR1-REACTOR

	Operation with 2 main fans	Operation with auxiliary fan
Reactor power (MW)	4	1
Electrical power of fans (kW)	1640	25
Total air flow (m^3/s)	60	10
Air speed (m/s)	90	15
Max. uranium temp. (°C)	250	200
Max. graphite temp. (°C)	90	104
Air outlet temp. (°C)	60	90
Operation	Continuous	8h/day

3.2 BR-1 Irradiation Facilities

About 50 channels (with cylindrical sections of 80 mm in diameter or square sections of 100 mm * 100 mm) are penetrating the reactor core, parallel or perpendicular to the axis of the fuel channels (see Fig. 9). The neutron fluxes in these channels are very thermalised and come up to $3.5 \cdot 10^{11}$ $cm^{-2}s^{-1}$. These irradiation channels can be used for exposure of samples of various sizes, for example for neutron activation analysis. Two thermal columns (large cavities), with a well characterized thermal neutron flux, which serves as a reference source, are used for specific experiments. The vertical one is 1m sphere with Maxwellian flux (T = 20°C) and has isotropic thermal flux in the cavity centre $7 \cdot 10^8$ $cm^{-2}s^{-1}$ at 700kW power. Using different types of converters mounted in the cavity it is possible to receive: ^{235}U fission spectrum field, prompt capture γ-ray fields, mixed n- γ fields (see Fig.10). These fields are used for the detectors calibration (fission chambers, foils), integral and data measurements.

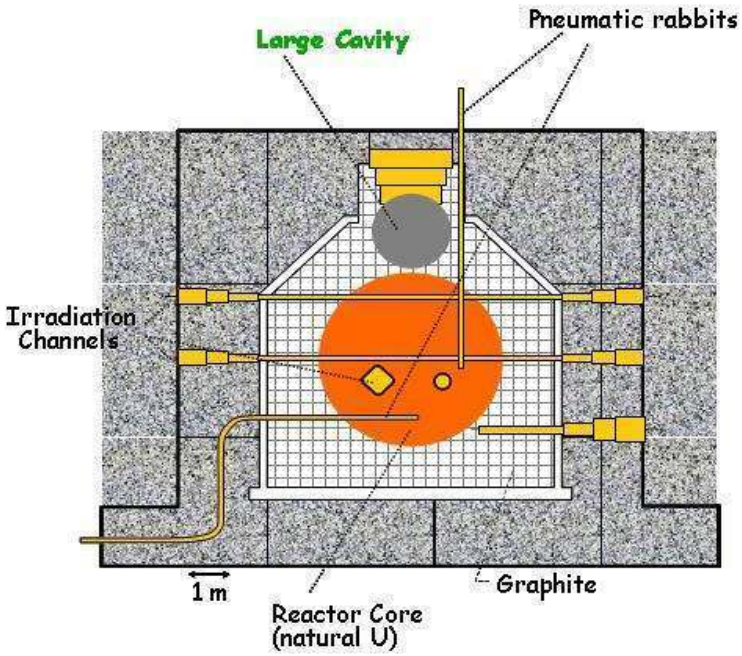

FIG.9. BR1 irradiation channels and columns.

Pneumatic rabbits are available as well for short time activation of small samples during the reactor operation.

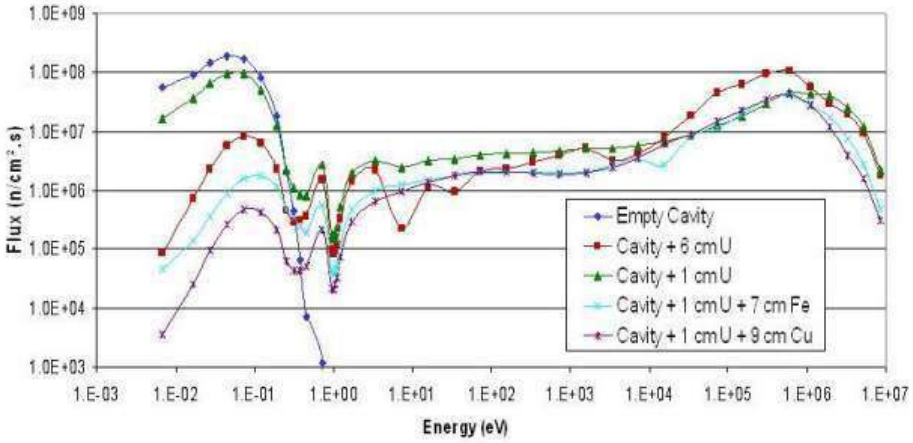

FIG.10. Neutron spectrum for large cavity.

3.3 Thermal neutron-induced fission cross sections of Cm isotopes at BR-1

As the sample of standard neutron fields utilization for micro data measurements are the measurements of the thermal neutron-induced fission cross section of a number of Cm isotopes was set up in the well thermalized neutron beams provided by the Maxwellian Thermal Spectrum Reference Field in the large cavity of the graphite moderated BR1 reactor.

For the ^{245}Cm(n,f) measurement, the Cm-oxide sample of (141±3) μg was used (^{245}Cm isotope content 98.685 at.%) , which was deposited on the 30 μm thick Al backing. The measured ^{245}Cm(n,f) fission fragments pulse height spectrum is plotted in Fig. 11.

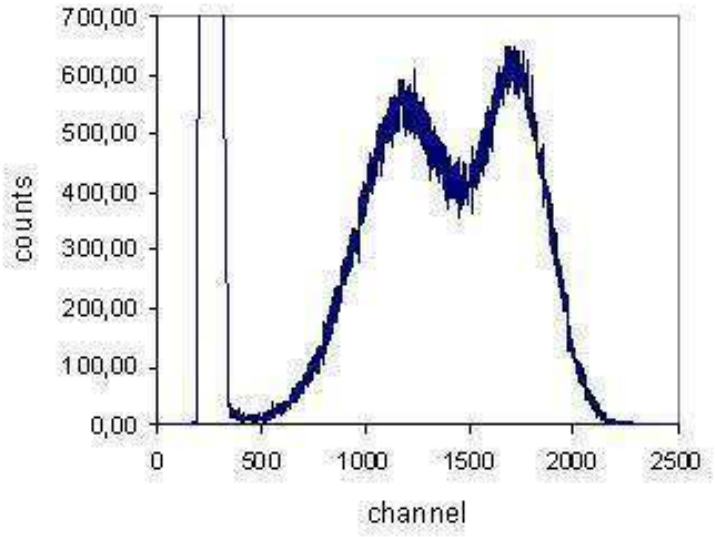

FIG.11. Fission fragments pulse height spectrum of ^{245}Cm sample.

It was founded 1.6% contribution from spontaneous fission and 2.6% from epithermal component to the (n,f) spectrum at Fig.11.

The results for the ^{245}Cm isotope have been received with statistical uncertainty of the order of 0.9%. The systematic uncertainty mostly is defined by uncertainty in the g_f-factor for

^{245}Cm (3.5%). Our result overlaps within the error bars with the value adopted in the European (JEFF), Japanese (JENDL) and American (ENDF/B) neutron libraries [7].
These results were presented at FISSION 2009 Conference in May. This work is on the way.

4. Conclusions

- The current and future possibilities of measuring of nuclear data (ND) for MA in integral and micro data experiments at the SCK•CEN (Mol, Belgium) reactor installations are discussed,
- The possibilities of BR-1 reactor irradiation facilities to measure micro data neutron cross section are demonstrated by the results of currently have measured thermal neutron fission cross section of ^{245}Cm,
- The details of the design of reconstructed VENUS zero power installation are shown,
- The MA fission cross sections measurements and other details of soon coming GUINEVERE experimental program at VENUS-F facility are presented,
- Measurements of nuclear data of minor actinides as the part of proposed post-GUINEVERE experimental programme in support of Lead Fast Reactor development at VENUS-F installation in the frame of next FREYA FP7 project have been planed.

REFERENCES

[1] ALIBERTI, G., *et al*., Impact of Nuclear Data Uncertainties on Transmutation of Actinides in Accelerated-Driven Assemblies, Nucl. Sci. Eng. **146** (2004) 1-50.

[2] KOSCHEEV, V.N., *et al*., "Nuclear Data for Plutonium and Minor Actinides", Accelerator Driven Transmutation Technologies and Applications (Proc. 3rd Int. Conf. ADTTA'99), Praha, (1999), (CD-ROM file WE-1-15).

[3] D. B. PELOWITZ, "MCNPX user's manual, version 2.5.0", Technical report LACP-05-0369, Los Alamos National Laboratory, (April 2005).

[4] W.HAECK and B.VERBOOMEN, "MCNP neutron cross section library based on JEFF 3.1", NEA-1745 ZZ ALEPH-LIB-JEFF3.1 (2006) http://www.nea.fr/abs/html/nea-1745.html.

[5] W. HAECK and B. VERBOOMEN, "ALEPH-DLG 1.1.0 – Creating cross section libraries for MCNP(X) and ALEPH", Technical report NEA/JEFF/DOC-1125, OECD/NEA.

[6] W. HAECK and B. VERBOOMEN, "Verification and validation of a multi-temperature JEFF 3.1 library for MCNP(X)", Technical report NEA/JEFF/DOC-1099, OECD/NEA, (2005).

[7] K.D. ZHURAVLEV, N.I. KROSHKIN and A.P. CHETVERIKOV, At. Ener. **39** (1975) 285.

Integral Experiments in MINERVE Reactor Facility for Nuclear Data Validation

D. Bernard, P. Leconte

Commissariat à l'Energie Atomique,
CEA/DEN/CAD/DER/SPRC/LEPh Cadarache Bldg 230 FRANCE

Abstract. The CEA is deeply involved in a research program (Material Test Reactor and Zero Power Reactor) concerning the nuclear fuel advanced studies (actinides, plutonium), the waste management, the scientific and technical support of French PWR reactors and EPR reactor, and innovative systems. In this framework, specific neutron integral experiments have been carried out in the critical ZPR facilities of the CEA Cadarache such as MINERVE, EOLE and MASURCA. This paper deals with MINERVE Pool Reactor experiments. MINERVE is mainly devoted to neutronics studies of different reactor core types. The aim is to improve the knowledge of the integral absorption cross sections of actinides (OSMOSE program), of new absorbers (OCEAN program) and also for fission products (CBU program) in thermal, epithermal and fast neutron spectra.

Experimental Set Up

MINERVE is a pool type reactor operating at a maximum power of 100 watts. The core is submerged under 3 meter of water and is used as a driver zone for the different experiments located in a central [70cm x 70cm] square cavity (see Fig. 1) in which various UO_2 or MOx cladded fuel pins can be loaded.

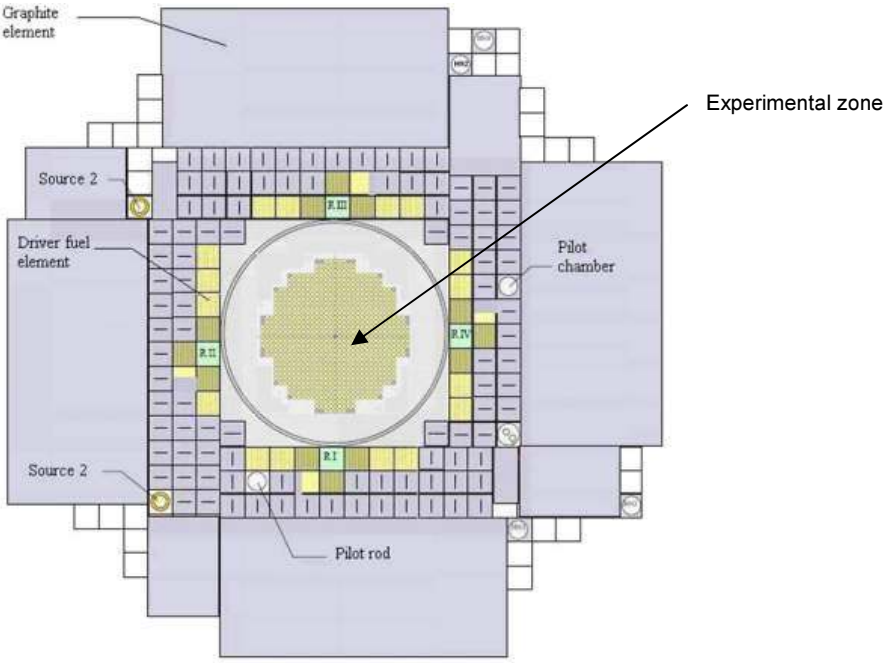

FIG.1. Scheme of the MINERVE reactor

The experimental technique consists in oscillating samples that contain the studied isotope in the center of the experimental lattice in order to measure their reactivity worth with an accuracy of around 1% (at 1σ). Each sample is placed into an oscillation rod and moved periodically and vertically between two positions located inside and outside the experimental core zone by the mean of an oscillator as shown in Fig. 2.

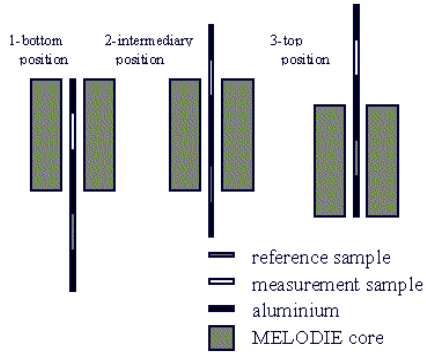

FIG.2. Movement of the oscillation sample inside the MINERVE facility

A compensated ionization boron chamber indicates the on-line local thermal neutron flux variation during the sample introduction at the center of the reactor (5sec). The delivered electronic signal involves rapidly (1μs) a mechanical movement to an "Automatic" Pilot Rod which total reactivity worth is about 10pcm (10^{-4} dk/k). The pilot rod is made of small glued cadmium sectors on a rotor and a stator (see Fig. 3). The neutronic shadow effect between the rotor and the stator is used to maintain criticality. The experimental signal is the angle between the rotor and the stator in Pilot Unit:

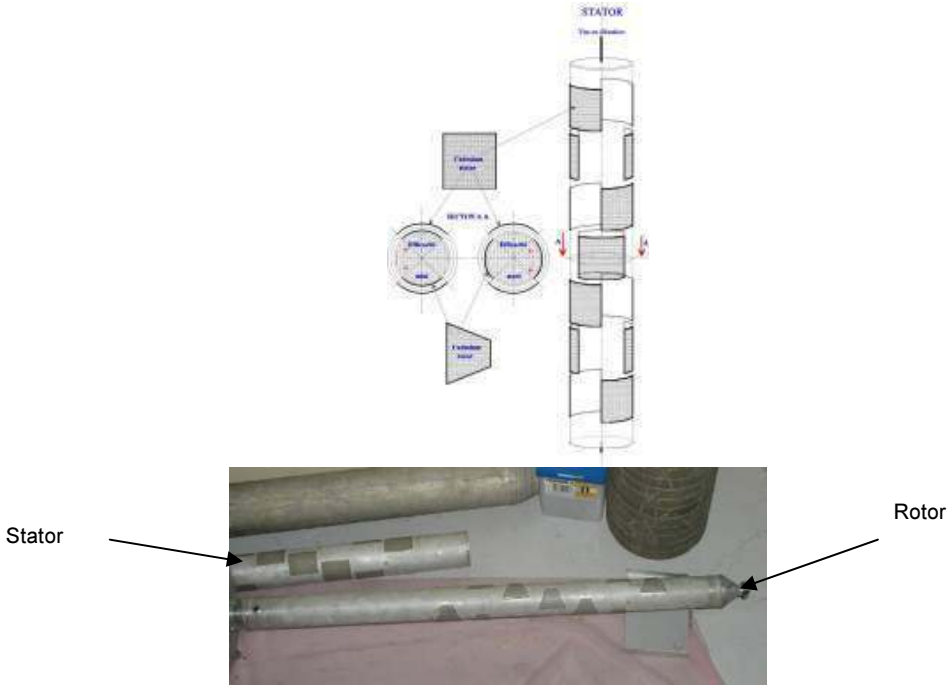

FIG.3. Automatic Pilot Rod with cadmium sectors

The reactor is supposed critical and the neutron precursors equilibrium is assumed during transients (samples insertion and extraction):

$$\frac{dC_i}{dt} = \frac{\beta_i}{\theta_c} n - \lambda_i C_i \approx 0 \qquad (1)$$

The on-line acquisition signal starts when the flux is constant in the pilot ionization chamber:

$$\left.\frac{dn}{dt}\right|_{Pilot\ chamber} = \frac{\rho - \beta}{\theta_c} n + \sum_i \lambda_i C_i \approx 0 \qquad (2)$$

Thus, the sample reactivity (ρ_{SAM}) is balanced by the reactivity inserted by the Automatic Pilot Rod (ρ_{APR}):

$$(1)+(2) \Rightarrow \frac{\rho}{\theta_c} n \approx 0 \Rightarrow \rho \approx 0$$

$$\rho = \rho_{SAM} + \rho_{APR} + o(\text{precursors} + \text{neutronic/electronic noises})$$

In term of Exact Perturbation Theory, the recorded angle between the stator and the rotor can be expressed as follow: (H represents the neutron Boltzmann transport operator, ϕ and ϕ^* the direct and adjoint flux)

$$\begin{aligned} \rho_{APR} &= 1/I_F < \phi^*_{APR}, \Delta H_{APR} \phi'_{APR} > \\ &= -\rho_{SAM} = -1/I_F < \phi^*_{SAM}, \Delta H_{SAM} \phi'_{SAM} > \end{aligned} \qquad (3)$$

The recorded angle as a function of time is represented by the gap between the two stationary positions as shown in Fig. 4.

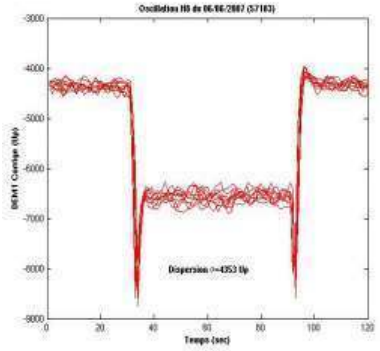

FIG.4. Acquisition Signal in Pilot Unit

Each sample is measured at least five times in order to improve the reproducibility of the measurement and to decrease significantly statistical errors on sample loading. A measurement corresponds to 10 oscillations of 120 s each, to improve the repeatability. Various lattices can be loaded in the experimental zone, ranging from thermal spectrum to fast range spectra (see Fig. 5).

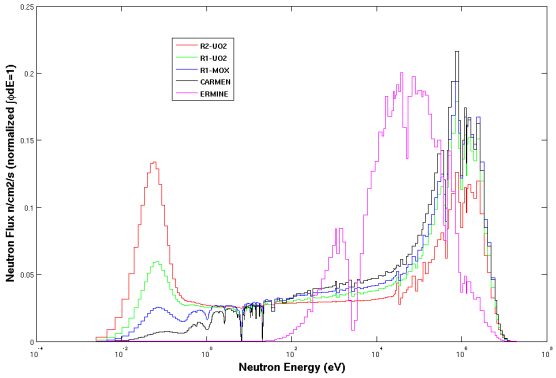

FIG.5. Various neutron spectra available in the MINERVE experimental zone thanks to different configurations

Hereafter are listed the main experimental programs performed last decade at the MINERVE Facility:

► **Fission Products : CBU (22 samples)**
→ ^{147,149,152,nat}Sm, ^{143,146,nat}Nd, ^{155}Gd, ^{153}Eu, ^{133}Cs (5 samples), ^{95,nat}Mo ^{99}Tc, ^{109,nat}Ag (3 samples), ^{nat}Ru, ^{103}Rh

► **Neutron Absorbers : OCEAN (19 samples)**
→ $^{166, 167, 168, 170}$Er, ^{160,161,162,163,164}Dy, ^{177,178,179,180}Hf, ^{151,153,nat}Eu, ^{155,157,nat}Gd

► **Actinides: OSMOSE (17 samples)**
→ ^{232}Th, UTh, ^{233,234}U, URE, ^{237}Np (2 samples),
→ ^{238,239,240,241,242}Pu, ^{241}Am (2 samples)
→ ^{243}Am, ^{244}Cm (2 samples)

In this paper we will focus on the OSMOSE program [1].

Signal Calibration and Uncertainties

The measured reactivity effects are lower than 10pcm. The neutron transport direct and adjoint equations cannot be solved on a 3D (or 2D) full core description by Monte Carlo or Deterministic transport codes. The interpretation is based on the 2D deterministic validated APOLLO2 code [2, 3] on a restricted geometry and uses the exact perturbation theory as shown in Eq. 3.

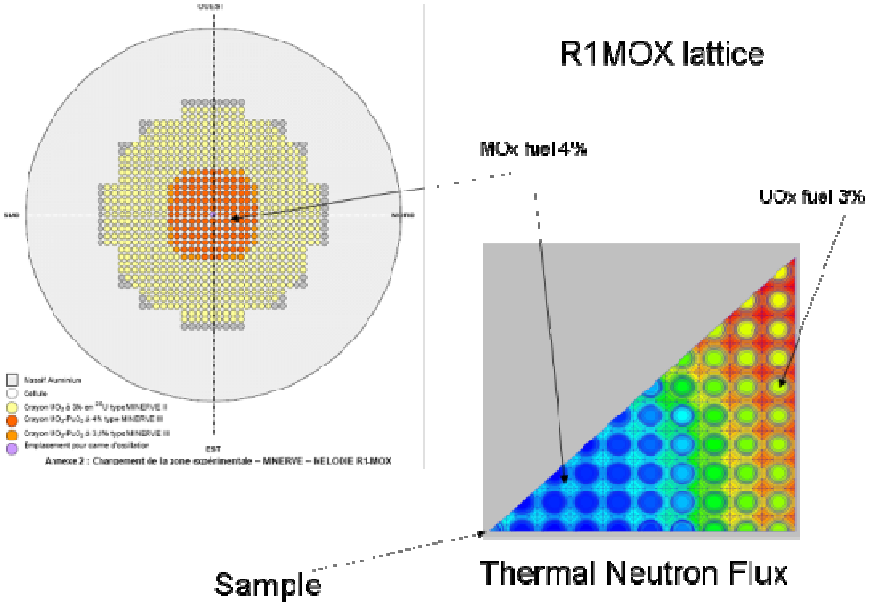

FIG.6. Thermal flux calculation with APOLLO2/JEFF-3.1.1

The calculation route is detailed below:

- The JEFF-3.1.1 nuclear data library is processed with up-to-date NJOY/CALENDF codes [4].
- The SHEM energy mesh (281goups) [5] is employed to avoid self-shielding calculation below 23eV. Probability Table description is used above for space-dependant actinides mutual & self-shielding calculations.
- The Method of Characteristics solver for direct and adjoint transport equations (flux calculation is qualified through spectral indices measurements such as total conversion ratio on lattice fuel pins).

The signal of the pilot rod has to be calibrated using samples containing well-know isotopes.

There are two series of calibration samples: a) one contains samples made of a UO_2 matrix with different uranium enrichments (0.25%, 0.5%, 0.72%, 1%, 2%, 3%, 4% and 4.95%) in ^{235}U, b) another contains samples made of a UO_2 matrix with a range of boron concentrations (0, 60, 100, 150, 200, 299, 333, 400, 419, 500 and 1062 ppm). The calibration curve (Fig. 7) shows the relation between the experimental signal (in Pilot Unit) and the calculated reactivity worth (in pcm given by the deterministic 2D model) of the ^{10}B and ^{235}U calibration samples.

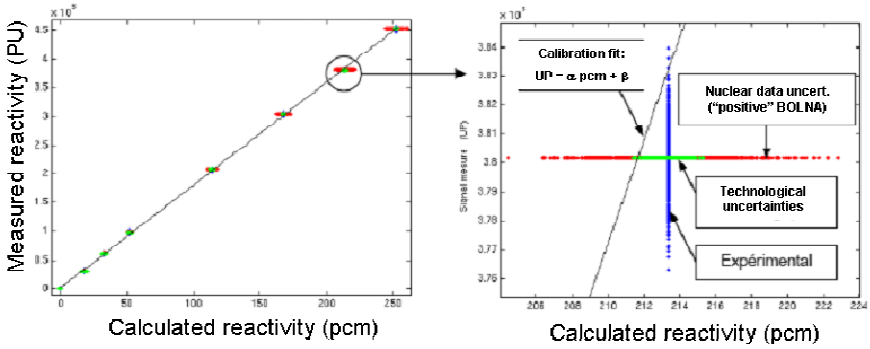

FIG.7. Calibration curve between calculated and measured reactivity

A unique calibration factor combines positive signals (^{235}U samples) and negative signals (^{10}B samples)

$$\alpha_{\text{lattice x}} = (4808 \pm 63) \text{ PU/pcm}$$

The fit accounts for the uncertainty on technological parameters (material balances, geometry), for the uncertainty on the experimental signals, and for the uncertainty on the nuclear data (BOLNA covariance matrix [6]).

OSMOSE Interpretation

The OSMOSE experimental program consists in measuring the reactivity worth of separated actinides from ^{232}Th to ^{244}Cm by the oscillation technique in several lattices. At the moment, oscillations have been performed in the LWR R1UO2 lattice (3%w/o ^{235}U; pitch: 1.26cm) and in the LWR R1MOX lattice (4% w/o Pu; pitch 1.26cm). Each oscillated sample is a double cladded column of 10 fuel pellets ($^{nat}UO_2$ sintered ceramic matrix doped with the separated isotope). High accurate chemical and isotopic analyses are performed for each sample during every step of the fabrication process [7]. Furthermore, for each sample, three additional fuel pellets are fabricated in parallel to perform destructive radio-chemical analysis. Finally, 1% (1σ) systematic error due to material balance knowledge can occur throughout the interpretation. Table 1 shows the target improvements in the quality of the nuclear data for the listed actinide isotopes that the OSMOSE program is hoping to achieve through the combination of more precise measurements and code assessment and validation efforts.

TABLE 1. Target Improvements in Nuclear Data from the OSMOSE Program.

Actinide	*Parameter*	*Current Uncertainty (at 1σ)*	*Target Uncertainty (at 1σ)*
U233	η_{therm} $\eta_{epitherm}$	± 2500 pcm ± 4000 pcm	± 1500 pcm ± 2500 pcm
U234	I_r σ_c^{th}	± 10 % ± 2 %	± 3 % ± 1.5 %
U236	I_r	± 5 %	± 3 %
Np237	I_r σ_c^{th}	± 7 % ± 3 %	± 2 % ± 1.5 %
Pu238	I_r σ_c^{th}	± 9 % ± 2 %	± 4 % ± 1.5 %
Pu239	η_{therm} $\eta_{epitherm}$	± 3000 pcm ± 4000 pcm	± 2000 pcm ± 2000 pcm
Pu240	I_r	± 3 %	± 1.5 %
Pu242	I_r	± 4 %	± 2 %
Am241	I_r σ_c^{th}	± 7 % ± 3 %	± 2 % ± 1.5 %
Am243	I_r	± 5 %	± 3 %
Cm244	I_r	± 5 %	± 3 %
Cm245	η_{therm}	± 4000 pcm	± 1500 pcm
Th232	I_r	± 4 %	± 2 %

Ir = resonance integral, σ_c^{th} = microscopic capture cross section, η = reproduction factor

The ongoing interpretation of OSMOSE program give the following preliminary results (see Table 2) in terms of discrepancy between calculation and experiment in %.

TABLE 2. (Calculation/Experiment – 1) values in %.

Lattices →	R1UO2	R1MOX
Samples ↓	JEFF-3.1.1	JEFF-3.1.1
TH232	5.0 ± 1.5	7.6 ± 4.5
UTH	-1.4 ± 5.3	9.0 ± 11.5
U233	0.9 ± 1.7	-3.9 ± 2.7
URE	-3.5 ± 1.5	-5.4 ± 4.4
NP237	0.8 ± 1.8	1.6 ± 4.1
PU238	-0.9 ± 1.8	-7.6 ± 4.5
PU239	-4.2 ± 1.9	-0.1 ± 3.5
PU240	3.4 ± 1.7	5.9 ± 6.7
AM241/1	-6.7 ± 2.6	-7.0 ± 6.2
AM241/2	-5.1 ± 1.6	-5.2 ± 2.5
AM243	4.4 ± 1.7	12.9 ± 2.5

Owing to exact perturbation formalism, the reactivity breakdown versus isotopes and energy ranges can be achieved as shown on Fig. 8.

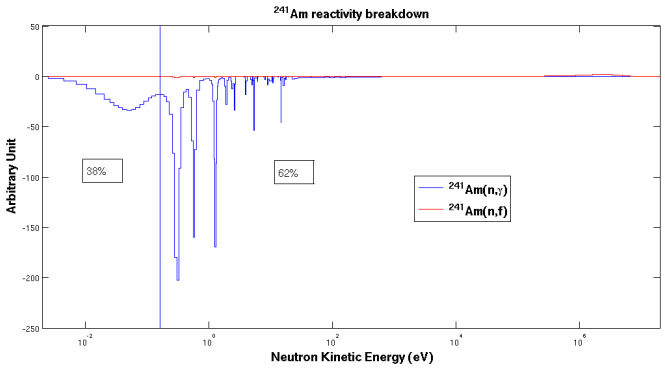

FIG.8. Reactivity breakdown for Americium targets

Then, we can underline a clear underestimation of the $^{241}Am(n,\gamma)$ JEFF-3.1.1 cross section ($\sigma_{\gamma 0}$ and/or γ resonance integral) by (5.3 ± 1.4)%.

Conclusion

Specific applications of Research Reactors such as pile oscillation in MINERVE provide high quality integral cross-sections (additional spectra can be loaded from pure thermal up to fast neutron range). A new experimental program on structural materials will be performed to ensure the nuclear data accuracy of C, H_2O, Be, Al, Zr, Pb, Mg, Fe, Cr, Ni, Mo, Cu, Ti, V, Cl, Co, Cd, Nb, Sn, Mn isotopes and elements.

REFERENCES

[1] J-P. HUDELOT *et al*., "OSMOSE: An Experimental Program for the Qualification of Integral Cross Sections of Actinides", Proc. Int. Conf. PHYSOR2004, Chicago (USA), April 25-29, 2004.

[2] R. SANCHEZ *et a*l., "APOLLO-II: A User-Oriented, Portable, Modular Code for Multigroup Transport Assembly Calculations", Proc. of Int. Conf. M&C, Paris (France), April 27-30 1987

[3] S. LOUBIÈRE *et al*., "APOLLO2, twelve years later", Proc. of Int. Conf. M&C, Reactor Physics and Environmental Analysis in Nuclear Applications, Madrid (Spain), 1999

[4] OECD/Nuclear Energy Agency, Nuclear Data Project: http://www.nea.fr/html/dbdata/projects

[5] N. HFAEIDH, A. SANTAMARINA, "Determination of the Optimized SHEM Mesh for Neutron Transport Calculation", Proc. of Int. Conf. M&C2005, Avignon, France, 2005.

[6] D. ROCHMAN *et al.*, "Preliminary Cross Section Covariance for WPEC Subgroup 26", BNL 77407-2007-IR, Brookhaven Natl Lab. (2007)

[7] F. JORION *et al*., "OSMOSE Program: Main Issues and R&D for Material Fabrication", ATALANTE2004 Conf., Nîmes (France), June 21-24 2004.

Benchmark analysis of the 2MW TRIGA MARK II Moroccan research reactor using the MCNP code and the latest nuclear data libraries

B. El Bakkari[a,b,2], B. Nacir[a], T. El Bardouni[b], C. El Younoussi[a,b], O. Merroun[b], A. Htet[c], Y. Boulaich[a,b], M. Chakir[d].

[a] Reactor Operating Unite (UCR), National Centre of Sciences, Energy and Nuclear Techniques (CNESTEN/CENM), POB 1382, Rabat Morocco.
[b] ERSN-LMR, Department of Physics, Faculty of Sciences, POB 2121, Tetuan, Morocco.
[c] Reactor Technology Unite (UTR), National Centre of Sciences, Energy and Nuclear Techniques (CNESTEN/CENM), POB 1382, Rabat Morocco.
[d] EPTN-LPMR, Faculty of sciences, Kenitra, Morocco.

Abstract. This study deals with the neutronic analysis of the 2MW TRIGA MARK II Moroccan research reactor. The reactor was commissioned at *Centre des Etudes Nucléaires de la Maâmora* (CENM) and it went critical on *May 2, 2007*. The 3-D continuous energy Monte Carlo code MCNP5 was used to develop a full model of the TRIGA reactor, using the maximum details allowed by the constructor General Atomics of USA. Continuous energy cross section data from the more recent nuclear data evaluations (ENDF/B-VI.8, ENDF/B-VII.0, JEFF-3.1, and JENDL-3.3) as well as S(α, β) thermal neutron scattering functions distributed with the MCNP code were used. The cross section libraries were generated by using the NJOY99 system updated to its more recent patch file "up259". The consistency and accuracy of both Monte Carlo simulation and neutron transport physics were established by benchmarking the TRIGA experiments.
Keywords: 2-MW TRIGA MARK II research reactor, MCNP5, ENDF/B-VI.8, ENDF/B-VII.0, JEFF-3.1, JENDL-3.3and NJOY99.

1. Introduction

A 2MW TRIGA MARK II research reactor was commissioned at the "Centre des etudes nucléaires de la Maâmora", Rabat, Morocco in 2006 and it went critical on 2 May 2007. The reactor was designed to effectively implement the various fields of basic nuclear research, manpower training and production of radioisotopes for its uses in agriculture, industry and medicine.

For the purpose of modelling the Moroccan TRIGA MARK II research reactor, the general purpose 3-D Monte Carlo N-Particle transport code MCNP (version 5C) was chosen because of its general modelling capability, correct representation of transport effects and continuous energy cross sections (X-5 Monte Carlo Team, 2003). The later is the most significant because this eliminates the need for collapsing multigroup cross sections for the reactor model and in core experiments. To reduce possible systematic errors due to inexact geometry simulation, a very thorough 3-D model of the TRIGA reactor was developed. All fresh fuel, control rod, and other in core elements (e. g., source elements, central thimble, and graphite elements) and outside core elements (e. g., neutrons beams, thermal column, etc.) were modelled using the maximum details allowed. The repeated structure capability of MCNP was used to create a full core, three dimensional model of TRIGA. The MCNP input was prepared in such a way that a very quick setup of any desired core configuration with an adequate position of all control rods is possible.

[2] Corresponding author. Tel: +21251235092; Fax:+21239994500; Email: bakkari@gmail.com

The accuracy of both the neutron transport physics as represented in MCNP and the user-defined model must be assessed. However, even though MCNP has been proven to simulate the physical interactions correctly. Since the Monte Carlo method simulates individual particle tracks through a given system, it can provide a very accurate probabilistic transport solution. That does not mean that the model of TRIGA will provide accurate answers. Therefore, to build confidence, the consistency and accuracy of both Monte Carlo simulation and neutron transport physics were established by benchmarking the TRIGA experiments.

2. MCNP modelling of TRIGA reactor

The reactor is a light water cooled, graphite-reflected one, designed for operation at a steady state power level of 2000 kW (thermal). An outstanding feature of the TRIGA reactor is its proven safety, which stems from the large prompt negative temperature coefficient of reactivity of its U-ZrH fuel moderator-material. The TRIGA core consists of 101 fuel elements, 17 graphite elements, central thimble, and a pneumatic transfer tube. The cross-sectional view of the present core configuration of the reactor is show in Figure 1, which was achieved on June 2007 during reactor start-up at full power operation. Elements are arranged in seven concentric rings and the spaces between the rods are filled with water that act as coolant and moderator.

The reactor was modelled in full 3-D detail to minimize the number of approximations. The repeated structure capability of MCNP was used to create a full core 3-D model of TRIGA.

The TRIGA lattice can be represented as a hexagonal prism, solids with eight faces. The fuel elements were modelled explicitly specifying the detailed structure of the rod to eliminate any homogenisation effects. The tapered end fixtures of the stainless steel were also modelled with a very little approximation. The power level of the reactor is controlled with five control rods: a regulating rod and four shim safety rods. The control rods were explicitly modelled along the active length containing three vertical sections of boron carbide, fuel follower and void region. The central thimble was considered to be filled with water and the pneumatic tube was considered to be void. The graphite dummy elements are of the same general dimensions and construction as the fuel-moderator elements, except these elements are filled entirely with graphite and are made of aluminium alloy.

The model was extended up radially containing the graphite reflector and lead shield. An annular well on the inside diameter in the top of the graphite reflector that provides for the rotary specimen rack was also modelled along with the radial and tangential beam ports that serve for experimentations around the TRIGA core. Modelling of the reactor was extended up to the thermal column; which is a 1219 mm squared assembly, located in the side of the reactor shield structure, which facilitates irradiation of large experimental specimens. It is located between beam ports NB1 and NB4; and the reactor tank that consists of an aluminium vessel installed in the reactor shield structure. All the geometric and material data are taken from the fabrication shipment documentation provided by the reactor manufacturer General Atomics of USA.

Figures 2 and 3 represent the radial and axial MCNP modelisation of the 2MW TRIGA MARK II research reactor at CENM.

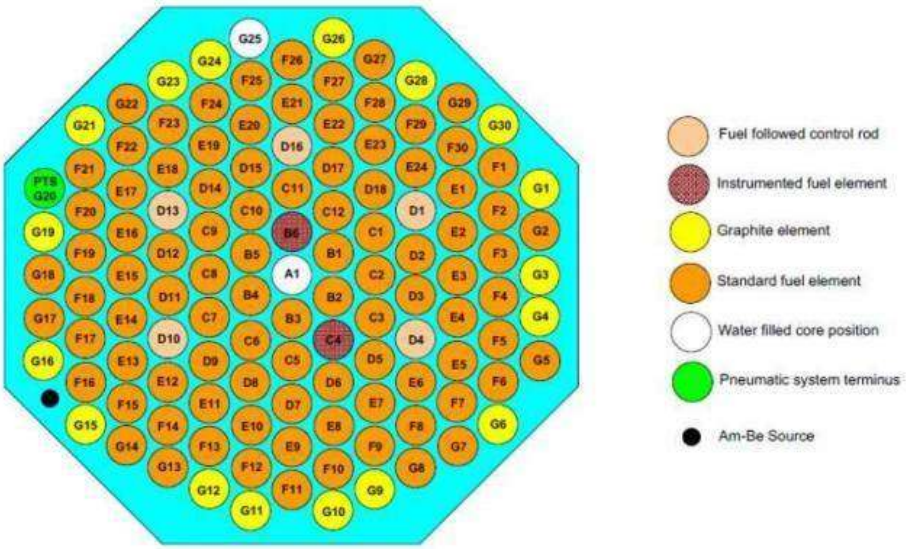

FIG.1. Present core configuration of the TRIGA reactor.

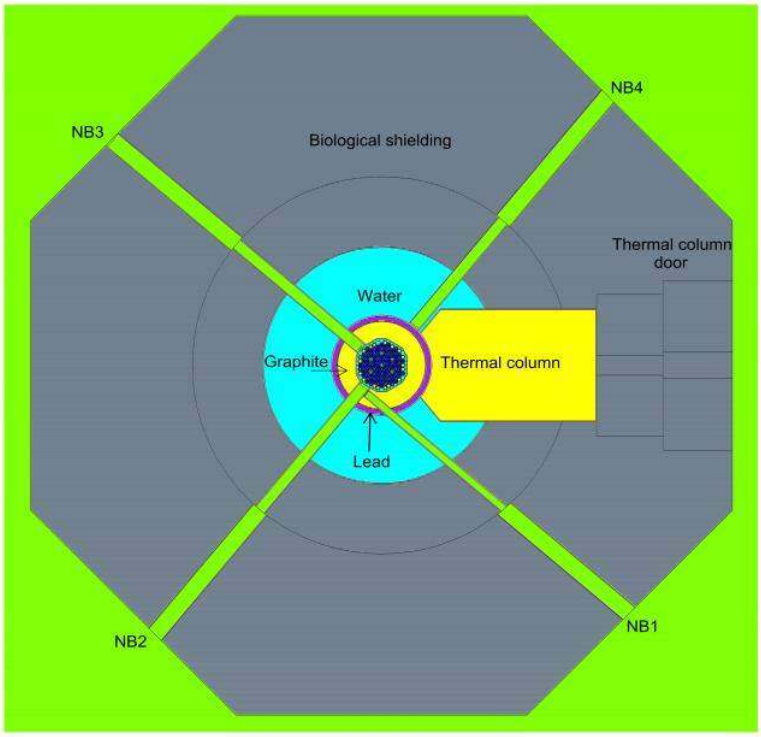

FIG.2. The radial view of the MCNP model of TRIGA reactor.

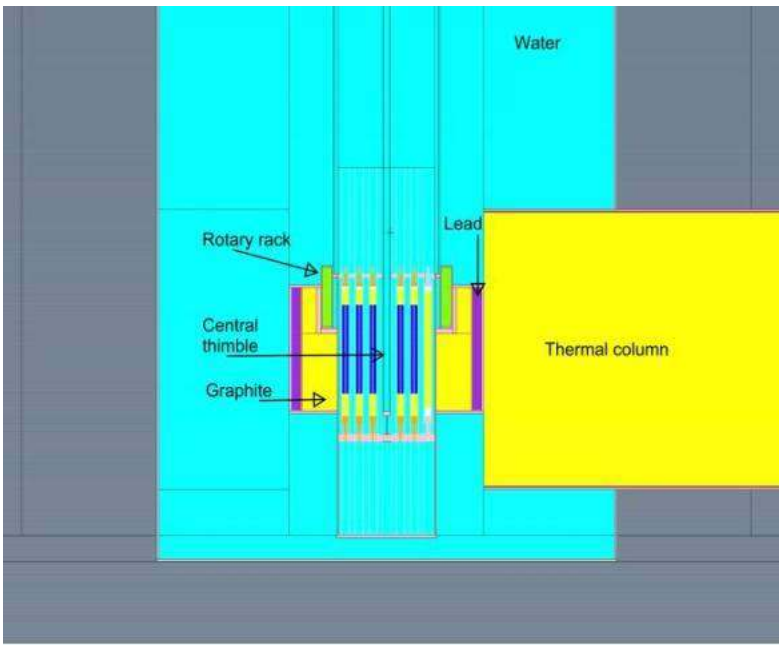

FIG.3. The axial view of the MCNP model of TRIGA reactor.

3. Continuous cross section library generation

Several continuous cross sections at various temperatures were generated for the MCNP code to cover the range of the TRIGA reactor temperature modelling. In general, the generation of such continuous cross sections begins with processing the evaluated nuclear data. In this research, we have used the more recent evaluated neutron data based on ENDF/B-VII (M. B. Chadwick, P. Oblozinsky, M. Herman at al., 2006), ENDF/B-VI.8 (P. F. Rose, 1991), JEFF-3.1 (A. Koning et al., 2006) and JENDL-3.3 (K. Shibata et al., 2002) as the data source. The process to construct the continuous cross section data libraries from the data source files is typically performed by the NJOY system code (R. E. MacFarlane, 1999). In this study, the NJOY99 system with its latest update file "up259" has been used to process the source evaluated nuclear data files into libraries suitable for use with the MCNP code. The procedure to process point-wise cross sections by each module of NJOY is show in Figure 4.

The principal advantage of NJOY is its most general-purpose applicability and comprehensive capability to process data in the recent ENDF format. It takes the basic data form the nuclear data library and converts them into forms needed for applications. Resonance cross-sections are constructed using a method of choosing the energy grid that incorporates control over the number of grid points generated for some materials. Summation cross sections are reconstructed from their parts. The resulting point wise cross-sections are written onto a "point-ENDF" (PENDF) file for future use. BROADR reads a PENDF file and Doppler-broadens the data. After broadening and thinning, the summation cross-sections are again reconstructed from their parts. The results are written onto a new PENDF file for future use. HEATR computes energy-balance heating and damage energy using reaction kinematics or applying conservation of energy. The ENDF photon production files can be used in this step, when available. GASPR module goes through all of the reactions given in an ENDF-format evaluation, determines which charged particles would be produced by the reaction, and adds up the particle yield times the reaction cross section to produce the desired gas production cross sections. THERMR produces pointwise cross-section in the thermal range Energy-to-energy incoherent inelastic scattering matrices can be computed for free-gas scattering or for bound scattering using a precomputed scattering law in ENDF file. PURR is used to prepare unresolved-region probability tables. ACER prepares cross-sections and scattering laws in

ACE format (a compact ENDF format) for the MCNP computer code. All the cross-secctions are represented on a union grid for linear interpolation by taking advantage of the representation used in RECONR and BROADR.

Finally, the S(α, β) thermal scattering cross sections of bound nuclei (i. e H in H2O, C in graphite, Zr in ZrH and H in HZr) were taken directly from the standard MCNP cross section library respecting the operation conditions of the TRIGA reactor. These thermal scattering data are essential to accurately model the neutron interactions at energies below ~ 4eV.

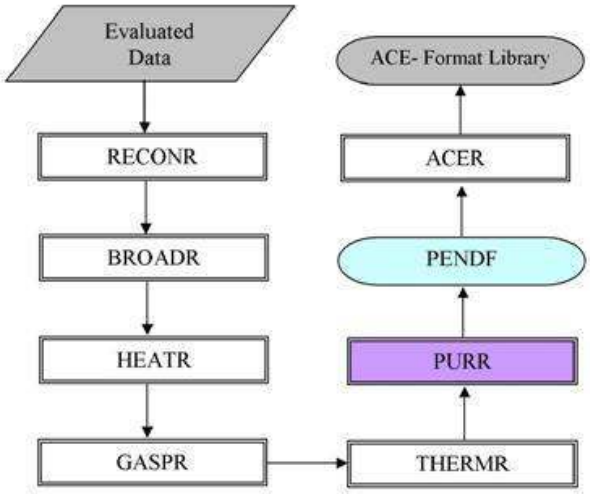

FIG.4. Flow diagram of NJOY99 processing for ACE format library construction.

4. Results and analysis

The calculations of the effective multiplication factor (k_{eff}) in the eigenvalue problem were performed with the "KCODE" option in the MCNP5 code. The initial source distribution for the keff calculations was given on the fuel meat points. The calculations were performed with 60000 cycles of iterations on a nominal source size of 60000 particles per cycle. In order to decrease statistical error estimates, initial number of 100 cycles were skipped. The estimated statistical errors (1σ) were reduced below 10 pcm for k_{eff} values and below 30 pcm for fission rates and neutron spectra calculations.

4.1. Core excess reactivity

Nuclear criticality, the ability to sustain a chain reaction by fission neutrons is characterized by keff, the eigenvalue of the neutron transport equation. The calculations of the effective multiplication factor (k_{eff}) in the eigenvalue problem for the fresh core were performed with the MCNP5 code using the ENDF/B-VII, ENDF/B-VI.8, JEFF-3.1 and JENDL-3.3 libraries. This was done because the core multiplication factor is an integral quantity and a criticality calculation is easy to perform. Also, any gross errors in the modelling should have been immediately apparent. The combined average of the absorption/collision/track-length estimator is quoted as the k_{eff} value in MCNP. Since we can not determine the value of k_{eff} experimentally, the calculated k_{eff} values obtained by MCNP were converted to reactivity values using the following equation:

$$\rho = \frac{keff - 1}{keff} \Big/ \beta_{eff} \qquad (1)$$

Where, ρ is the reactivity value in unite of dollar ($), and, β_{eff} is the fraction of effective delayed neutrons ($\beta_{eff} = 0.007$ for TRIGA fuel types).

The comparison between the experimental reactivity value and the MCNP ones is shown in Table 1.

TABLE 1. COMPARISON BETWEEN THE CALCULATED AND EXPERIMENTAL CORE EXCESS REACTIVITY.

	Reactivity value ($)	C/E
Experiment	10.27	–
ENDF/B-VII	10.55	1.027
ENDF/B-VI.8	10.14	0.987
JEFF-3.1	10.03	0.977
JENDL-3.3	10.02	0.975

According to the values in Table 1, we note that, generally, all the libraries produce results that are in very good agreement with the experiment. Since, deviations from the experiment are of the order of +2.7%, -1.3%, -2.3% and -2.5% for libraries ENDF/ B-VII, ENDF/B-VI.8, JEFF- 3.1 and JENDL-3.3, respectively.

4.2. Control rod worth

The calculation of the control rod worth simulated explicitly the experiment which was carried out by the positive period method (T. MATSUMOTO et al., 2000) for the shim and regulating rods. Using this method, the worth of one control rod was measured in the presence of other rods, used for compensating the excess reactivity. We started the simulation with the control rods critically positioned calculating the k_{eff0} of the core. Then one of the control rods was inserted at a certain position, calculating the new k_{eff}. The control rod worth for that position was determined by comparing k_{eff} and k_{eff0} as denoted Eq. (2) represented by reactivity ρ.

$$\rho = \rho_0 - \rho_1 = \left(1 - \frac{1}{keff_0}\right) - \left(1 - \frac{1}{keff}\right) = \frac{1}{keff} - \frac{1}{keff_0} \quad (2)$$

Table 2 shows the comparison results of MCNP calculations of the total rod worths using the four libraries to the experiment. Integral reactivity curves for all the five control rods were produced and are shown in Figures 5 to 9.

TABLE 2. COMPARISON BETWEEN THE MCNP CALCULATED CONTROL RODS WORTH OF TRIGA AND THE EXPERIMENT.

	C/E			
Control rod	ENDF/B-VII	ENDF/B-VI.8	JEFF-3.1	JENDL-3.3
Shim I	1.00	0.98	1.00	0.99
Shim II	0.93	0.92	0.94	0.95
Shim III	1.02	1.02	1.04	1.02
Shim IV	0.94	0.94	0.93	0.92
Regulating	0.96	0.95	0.94	0.97

The MCNP calculated control rod worths of TRIGA were found to be in very good agreement with the experiment. The maximum differences to experiment was found to be -7% for ENDF/B-VII with *Shim II*, -8% for ENDF/B-VI.8 with *Shim II*, -7% for JEFF-3.1 with *Shim IV* and -8% for JENDL-3.3 with *Shim IV*.
Also, according to the integral reactivity curves shown in Figures 5 to 9. We remark that, the agreement between the MCNP predicted values, for all the libraries studied, and the experimentally determined values are fairly good, with the difference between calculated versus experimental rod worths ranged from -8% to 4%. Also, it can be seen that for Shim II, Shim IV and Regulating rod, the largest differential reactivity worth occurred when the rods supposed fully withdrawn, which may be due to a small discrepancy between MCNP estimated and existent flux distribution around these rods.

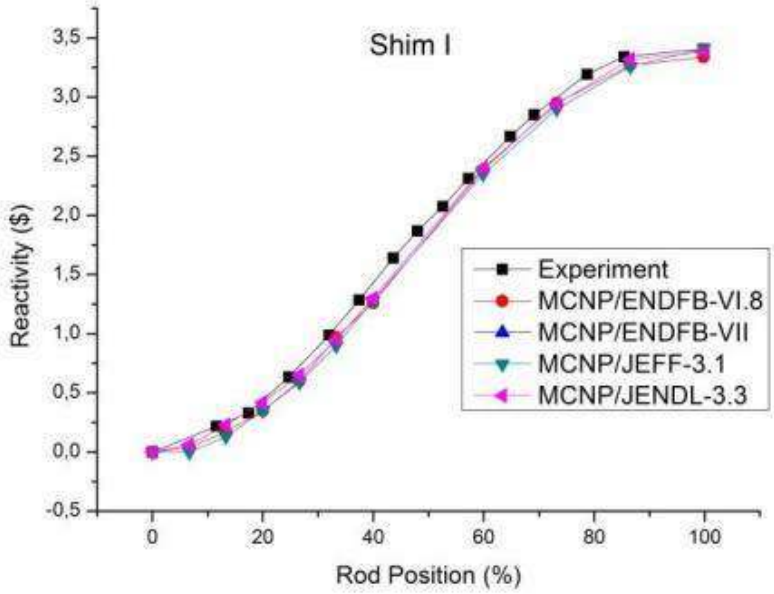

FIG.5. MCNP calculations and experimental integral rod worth for Shim I.

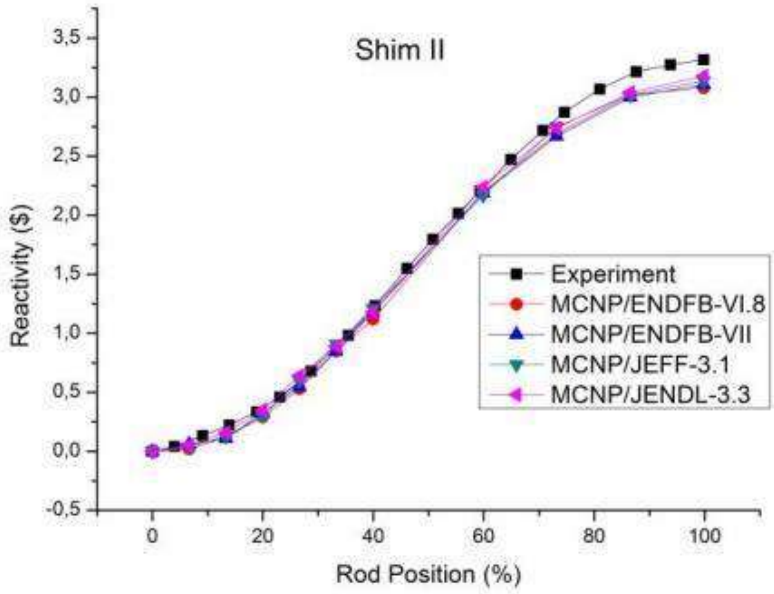

FIG.6. MCNP calculations and experimental integral rod worth for Shim II.

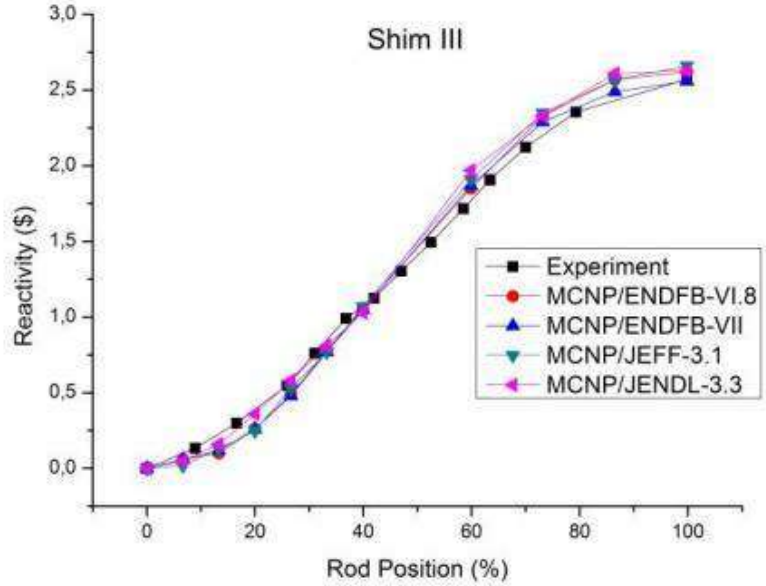

FIG.7. MCNP calculations and experimental integral rod worth for Shim III.

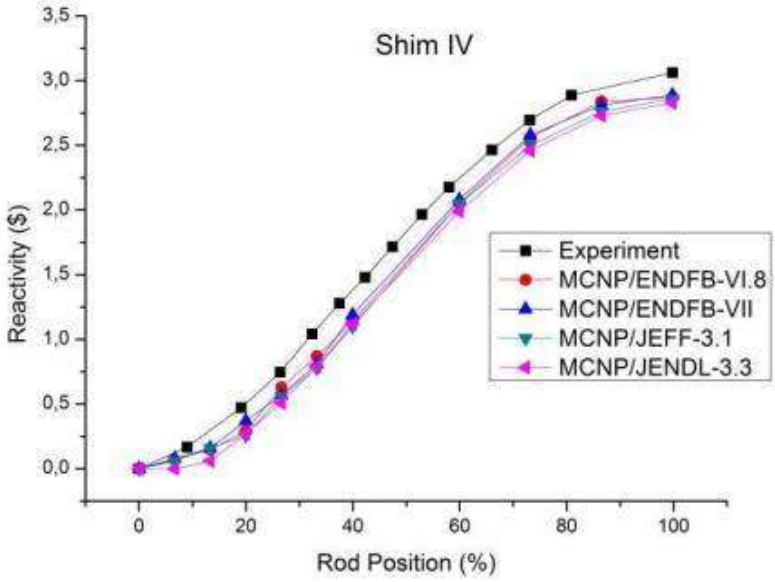

FIG.8. MCNP calculations and experimental integral rod worth for Shim IV.

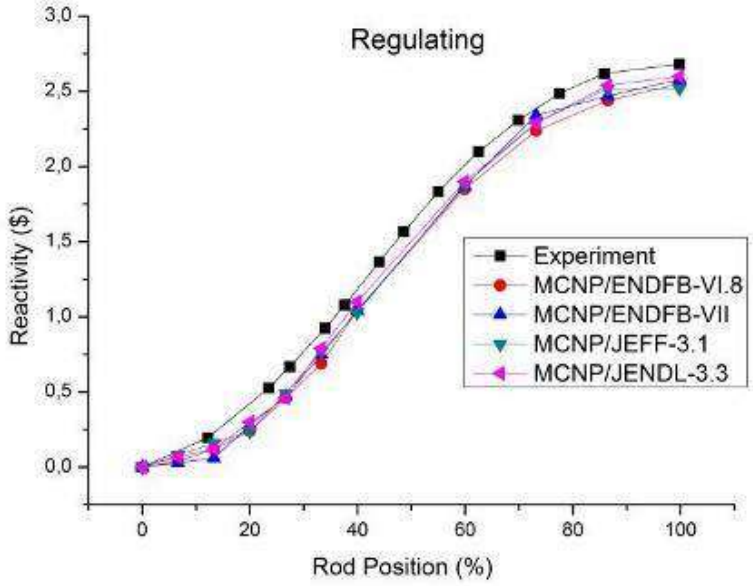

FIG.9. MCNP calculations and experimental integral rod worth for Regulating rod.

4.3. Power distribution and peaking factors

a) Power distribution

The total power produced within the fuel and fuel follower elements of the core was calculated by MCNP5 code using all the nuclear data libraries is shown in Figure 10. The fuel and fuel follower numbers are such that the fuel numbers from 1 to 6 represent the B ring of fuel elements TRIGA core arrangement (Fig. 1), and similarly from 7 to 18 represent the C ring, from 19 to 36 represent the D ring, from 37 to 60 represent the E ring, from 61 to 90 represent the F ring and from 91 to 101 represent the G ring.

From Figure 10, we remark that the maximum power production is 32.42 kW for ENDF/B-VII, 32.32 kW for ENDF/B-VI.8, 32.30 kW for JEFF-3.1 and 32.36 kW for JENDL-3.3. These values were observed within the fuel element designated by B3, B2, B2 and B3 (Fig. 3), respectively and they are assumed to be the hottest rod in TRIGA core corresponding to each of the libraries. Now the hot-rod factor in MCNP is determined for each of the libraries using the following component values:

$$\left[\overline{P}_{rod}/\overline{P}_{core}\right]_{\max} = \frac{\text{Average Power Produced in the hottest Fuel Element}}{\text{Average Power in the Core}}$$

= 1.62 [Obtained by ENDF/B-VII]
= 1.62 [Obtained by ENDF/B-VI.8]
= 1.61 [Obtained by JEFF-3.1]
= 1.62 [Obtained by JENDL-3.3]

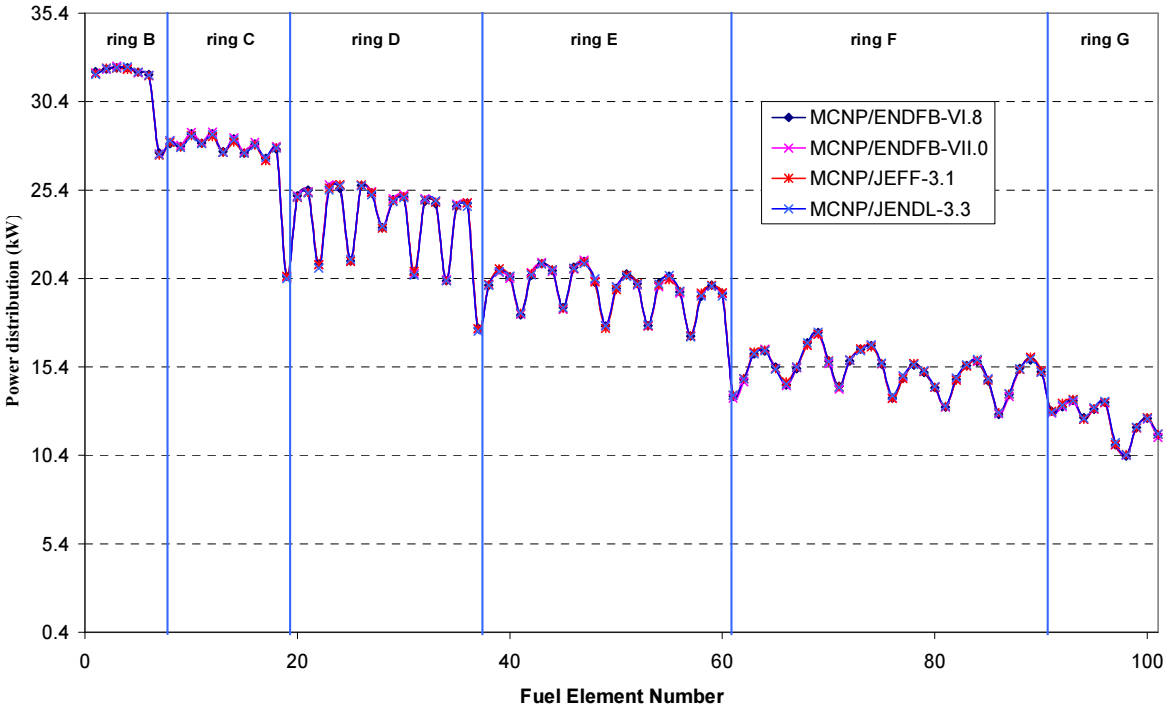

FIG.10. Power distribution within the fuel and fuel – follower elements of the TRIGA reactor.

These values are found to be in very good agreement with the proposed value in the FSAR. Also, on the basis of the thermal hydraulics analysis in the General Atomics safety analysis reports for other 2 MW TRIGA reactors it was concluded that maximum hot-rod factor from 1.6 and 1.7 is acceptable for 2 MW operation (M. Ravnik, 1995).

b) Axial peaking factor

The axial peaking factor f_z defined as $(P_{rod}/\overline{P}_{rod})_{axial}$ which is axial peak – to – average power ratio is calculated using the MCNP5 code and the axial power profiles for the hottest fuel element for all the nuclear data libraries are shown in Figure 11. The average volumetric values of power for each region were determined and the axial peak factors were found to be an almost analytical chopped cosine with a peak – to – average value of 1.28 for all the libraries. Note that the recommended value in the FSAR is 1.3 (maximum value) for the hot rod channel, which means that our calculated values are very good. One other thing to note is that the small increments shown in the left and right sides of the axial power profiles (Fig. 11) are due to the lower and upper reflectors of TRIGA fuel element.

c) Radial peak factor

Another peaking factor identified as radial peaking factor f_R is defined as $(P_{rod}/\overline{P}_{rod})_{radial}$, which is the peak – to – average power on a radial plane within a fuel rod, is also calculated for the hottest fuel element and the radial power profiles are shown in Figure 12. First of all, one can see that all the libraries produce similar results. The radial power factor increase when moving from the centre of fuel element to the outer region. This is principally done because more fission occurs in the radial outer portion of the fuel element due to radial volume weighting and self moderation. The maximum radial peaking factor obtained by all the libraries is 1.91.

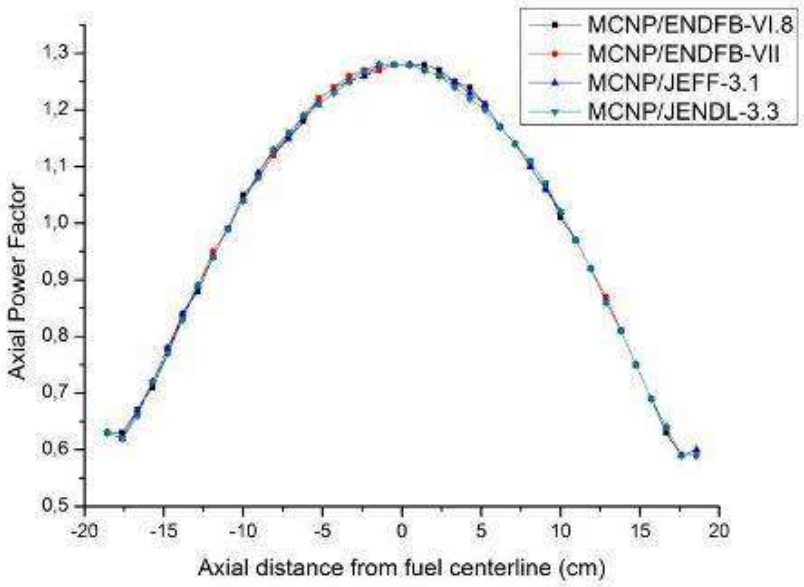

FIG.11. Hot Channel Fuel Axial Power Factor Profiles.

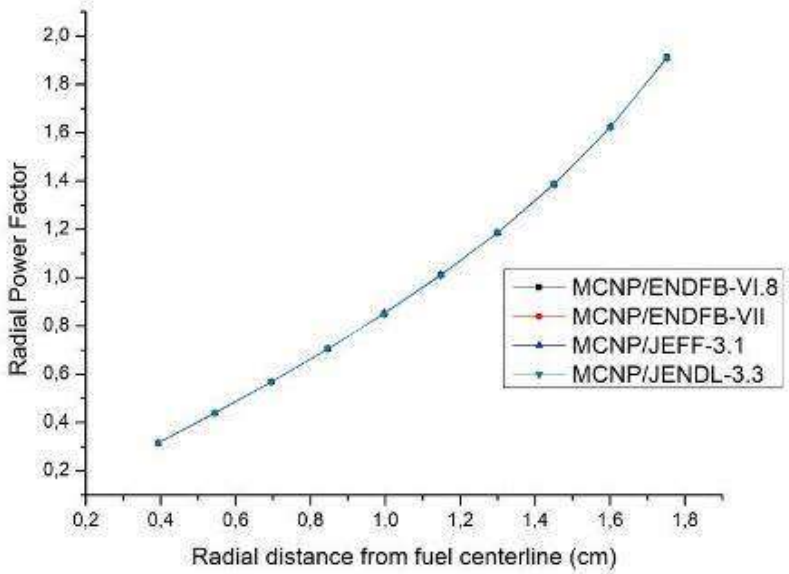

FIG.12. Hot Channel Fuel Radial Power Factor Profiles.

4.4. Temperature – dependent core modeling

TRIGA fuel was developed around the concept of inherent safety. A core composition was sought which had a large prompt negative temperature coefficient reactivity (α) such that if all the available excess reactivity were suddenly inserted into the core, the resulting fuel temperature would automatically cause power excursion to terminate before any core damage resulted. Experiments demonstrated that zirconium hybrid possesses a basic mechanism to produce the desired characteristic (M. T. SIMNAD, 1981).

The Moroccan TRIGA MARK II research reactor has a prompt negative temperature coefficient reactivity value of -0.01% ($\delta k / k / °C$) (Safety Comity, 2007). In this section, we studied the evolution of the core excess reactivity due to two different operating conditions. Cold conditions, means that the reactor temperature is 300 K. And, hot condition, means full

power operating conditions. Table 3 gives the prompt negative temperature coefficient reactivity calculated by MCNP using the four libraries for our TRIGA model.

$$\alpha = \frac{k_{eff,Hot} - k_{eff,Cold}}{T_{Hot} - T_{Cold}} \tag{3}$$

Where, $k_{eff,Hot}$ is the effective multiplication factor at hot conditions, $k_{eff,Cold}$ is the effective multiplication factor at cold conditions, T_{Hot} is the fuel temperature at hot conditions and T_{Cold} is the fuel temperature at cold conditions.

TABLE 3. THE PROMPT NEGATIVE TEMPERATURE COEFFICIENT REACTIVITY CALCULATED BY MCNP FOR TRIGA MODEL.

	ENDF/B-VI.8	ENDF/B-VII	JEFF-3.1	JENDL-3.3
$\alpha\ (\delta k/k/°C)$	-0.0096	-0.0097	-0.0095	-0.010

As it can be shown in Table 3, all the libraries produces results which are in very good agreement with the recommended FSAR value -0.01% ($\delta k/k/°C$), the *keff* of TRIGA reactor decreases as a function of temperature. Furthermore, the neutron flux spectra, for each of the libraries used in this study, are shown in Figure 13. So from the spectra figures, it can be noticed that the flux spectrum in the thermal range changes noticeably as a function of the average fuel temperature while the flux spectrum in the fast and epithermal ranges remains almost the same as the average fuel temperature increases. It is evident from the close-up plots of Figure 14 that the up-scattering rate by the bounded H in ZrH increases as the average fuel temperature increase. Increase in fuel temperature results in shift and deformation of the Maxwellian spectrum in fuel while the spectrum in water is slightly affected, because the water temperature remains almost constant. Consequently, the fuel reaction rate is decreased, while it remains constant in a nonfission part of the unit cell (the water and cladding). So the ratio between fission and the absorption reaction rate is reduced on the average over the entire unit cell. The multiplication factor is thus reduced, and the spectrum hardening effect is negative (S. I. Bhuiyan et al. 1991). This phenomenon causes the decreasing of the TRIGA core reactivity as observed by the calculations (Table 3). Although the up-scattering by the bounded H in ZrH is major effect that decreases the core excess reactivity in TRIGA core, the Doppler broadening has also an impact on the change in excess reactivity. Because, the absorption rate in the fuel meat increases with increasing average fuel temperature due to the Doppler broadening (C. Tippayakul et al., 2008). The excess reactivity generally decreases with the increasing absorption rate. Therefore, it is clearl that the Doppler effect is another phenomenon which decreases the excess reactivity of TRIGA reactor.

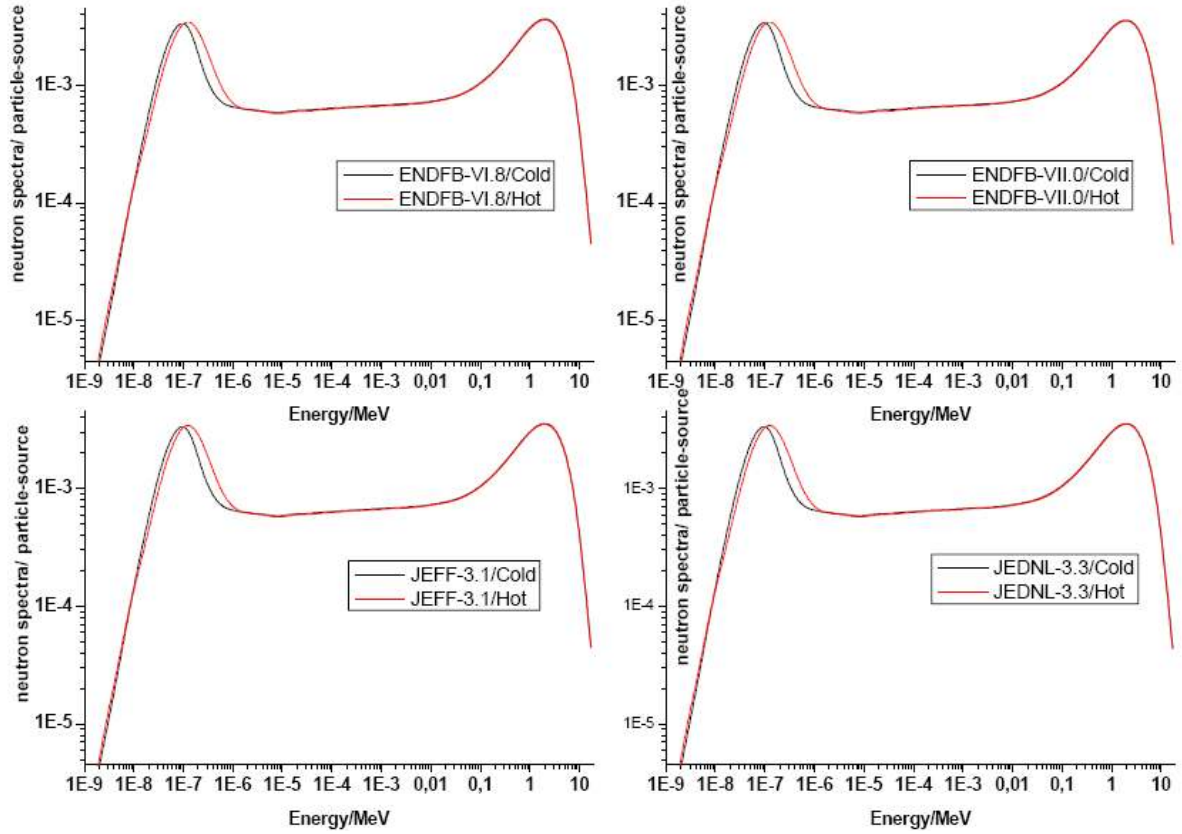

FIG.13. Neutron spectrum for the TRIGA fuel calculated by MCNP.

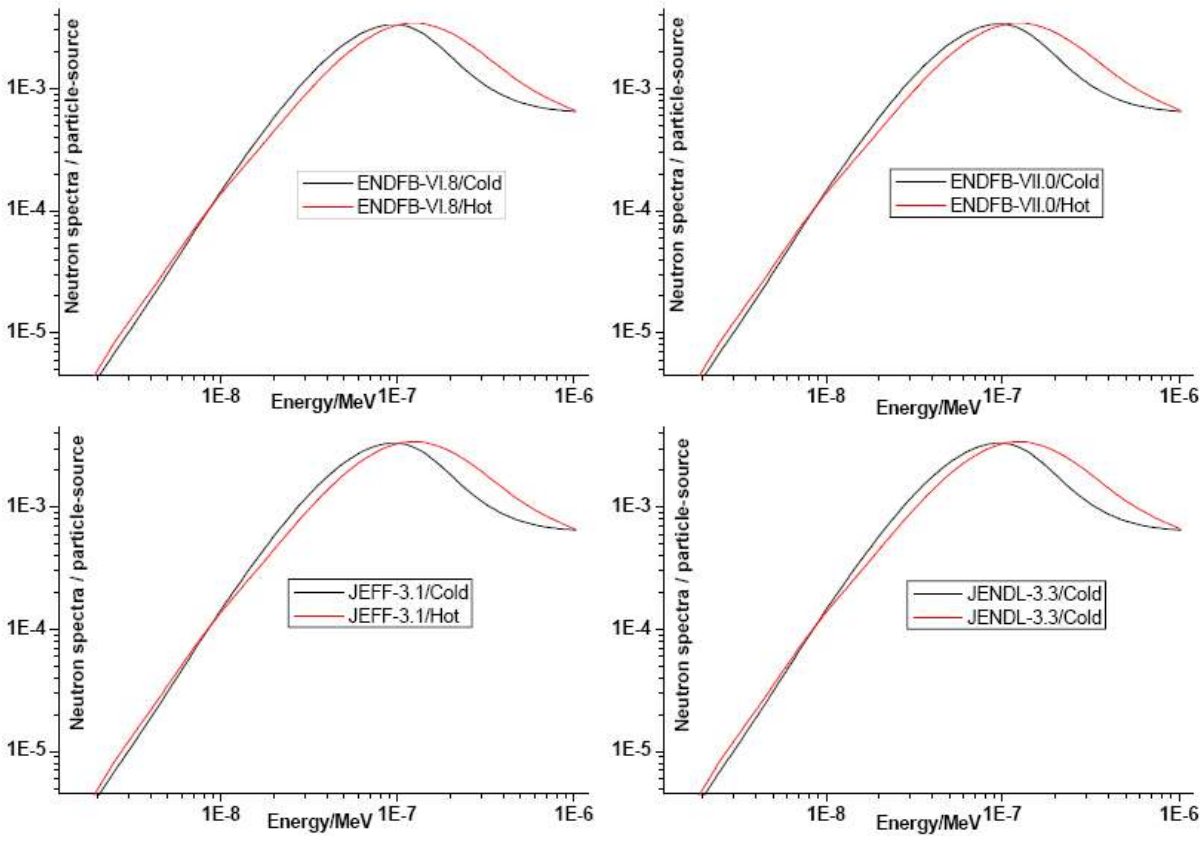

FIG.14. Close – up plots in thermal range.

4.5. Burnup calculation of the TRIGA reactor

The principal thrust of this section is on the burnup calculation of the 2MW TRIGA MARK II research reactor at CENM. By burnup we mean the following changes in the core: 1) depletion of U235, 2) fission products build-up, 3) spectral changes of flux, 4) negligible plutonium and 5) depletion of burnable poison.

a) Description of the burnup calculation

The criticality calculation gave confidence to perform a set of burnup calculations for the core loaded with fresh LEU fuel. Burnup calculations were performed for realistic operating conditions at a power of 2MW using our new elaborated burnup code BUCAL1 (B. El Bakkari et al., 2008; B. El Bakkari et al. 2009) and the latest nuclear data library ENDF/B-VII. The initial burnup steps in the calculation were taken smaller to consider the Xe and Sm build-up poisoning.

BUCAL1 is a FORTRAN computer code elaborated by "*Equipe de Radiation et Systèmes nucléaires (ERSN)*" at *University ABDELMALIK ESSAÄDI*, *Morocco*. The code is designed to aid in analysis, prediction, and optimization of fuel burnup performance in a nuclear reactor. It was developed to incorporate the neutron absorption tally/reaction information generated directly by MCNP5 code in the calculation of fissioned or neutron-transmuted isotopes for multi-fueled regions. The use of Monte Carlo method and punctual cross section data characterizing the MCNP code allows an accurate simulation of neutron life cycle in the reactor, and the integration of data on the entire energy spectrum, thus a more accurate estimation of results than deterministic code can do. The BUCAL1 strategy consists of using the nuclide inventory, MCNP tally information, power density, and other data to determine the new nuclide inventory for a given region of the core at a new time step. Then the new inventories are automatically placed back into MCNP input file and the case run for a new subsequent time step.

In order to optimize the MCNP calculation times, the fuel elements in the TRIGA core were separated into 7 different groups taken into account of the power distribution within the fuel and fuel-followed elements (Fig. 10). Thus burnup calculations were done for just 7 separate fuel elements instead of 101 fuel elements. Figure 15 gives the new fuel elements distribution within the core based on the separation technique already described.

b) TRIGA core life time estimation

The calculation of the k_{eff} and its relationship with core burnup is of primary importance to determine the core life time. First the excess reactivity for the beginning of the core life was calculated by MCNP at 2 MW reactor power and was found to be 6.77\$ (k_{eff} = 1.04975). Then burnup calculation was performed for the TRIGA core without changing the loading pattern to determine the core life of the primary fuel cycle and for the primary core configuration. The variation of k_{eff} as a function of total thermal power produced is presented in Figure 16.
At the initial burnup time a sharp loss of reactivity of 3.52\$ is observed which is particularly due to the build-up of ^{135}Xe and ^{149}Sm. The concentration of these fission products poisons strongly influence the reactivity and eventually reaches equilibrium at about 150 MWh and 1500MWh for Xe and Sm respectively, as can be seen from Figures 17 and 18. The excess reactivity becomes zero at 3360 MWh of reactor operating history which correspond to 70 days of continuum operation at full power which is the life time of primary fuel cycle for the actually core configuration.

The individual burnup (% ^{235}U depletion) of fuel and fuel-follower elements for each of the seven groups (Fig. 15) during the core life time is shown in Figure 19. The maximum value (~ 7 %) of ^{235}U depletion is observed for group K which correspond hottest fuel elements of B ring (Fig. 10). Then the ^{235}U depletion decreases when passing from the core centre to the core periphery until it reaches a value of 2.8 % for fuel elements of Q group. The core average burnup is found to be 4.54 %.

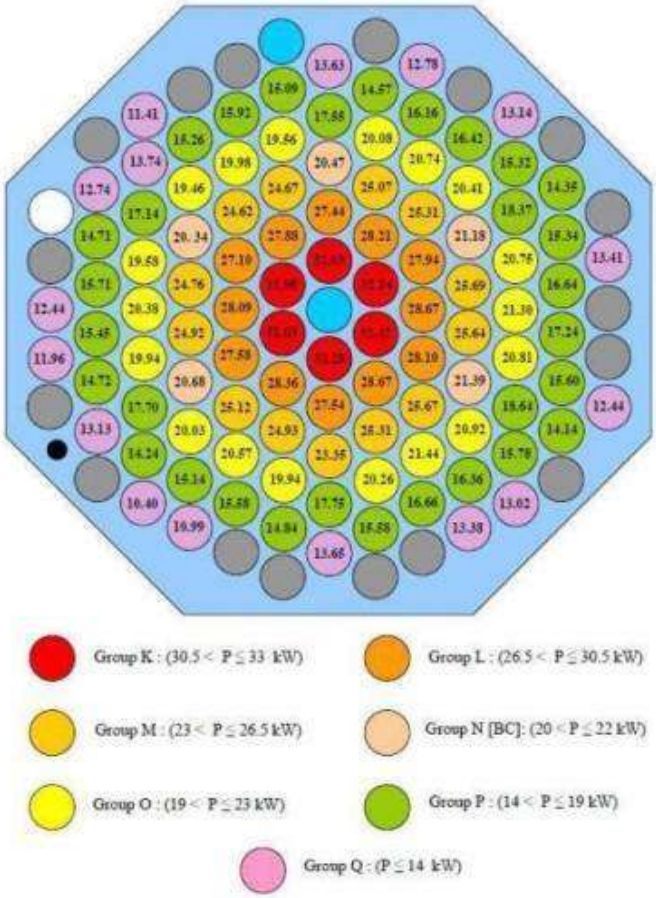

FIG.15. Fuel elements distribution for burnup calculation.

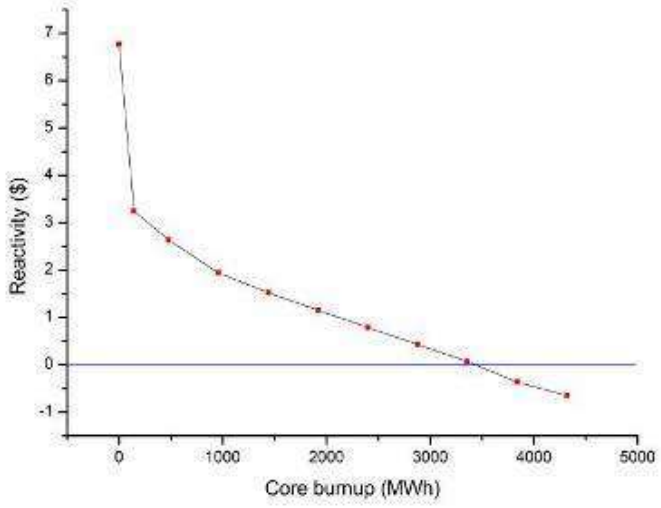

FIG.16. Excess reactivity ($) of TRIGA reactor as a function of burnup (MWh).

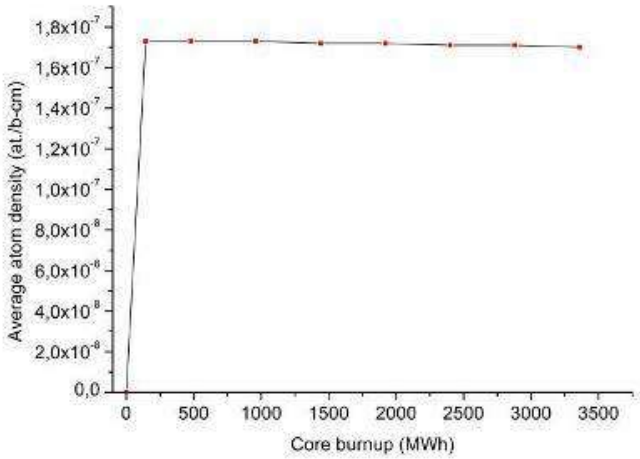

FIG.17. ^{135}Xe build-up as a function of core burnup.

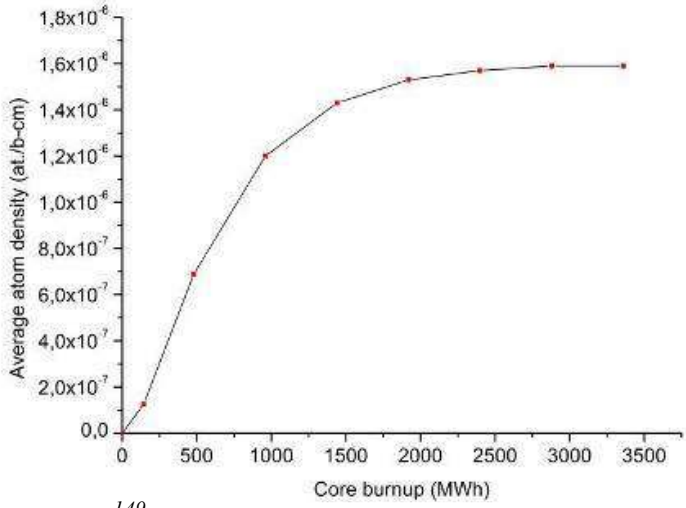

FIG.18. ^{149}Sm build-up as a function of core burnup.

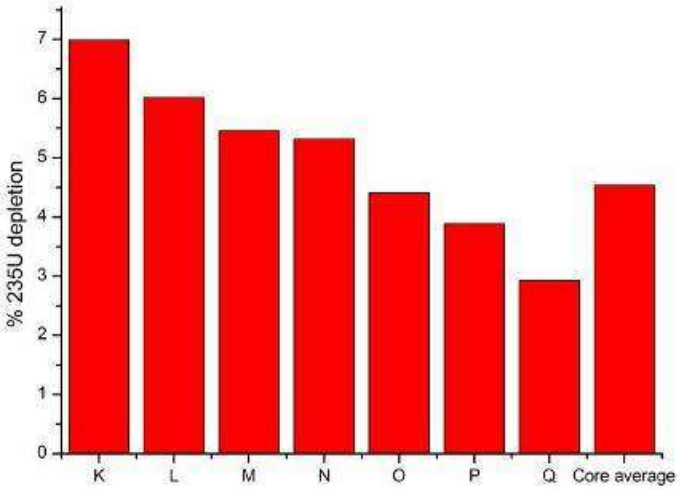

FIG.19. % ^{235}U depletion as a function of fuel groups.

5. Conclusion

The complete 3D MCNP model of the Moroccan TRIGA MARK II research reactor is presented. ENDF/B-VI.8, ENDF/B-VII, JEFF-3.1 and JENDL-3.3 neutron cross section evaluations were used for this study. Several continuous cross sections at various temperatures were proceeded for the MCNP code using the updated NJOY99 system. The consistency and accuracy of the MCNP model was established by comparing calculations to the experimental results of the benchmark experiments. Most of the steady – state experiments were simulated in the validation process of the physical model; effective multiplication factors, power distribution within the core, the power peaking factors, total and integral rods worth and the prompt negative temperature coefficient were performed and analysed. The MCNP calculated values were found to be in very good agreement with the experimental and the FSAR data within the estimated error of 8%. The burnup calculations made by our new elaborated burnup code BUCAL1 show that the averaged life time of the present core configuration is 3360 MWh and the core average burnup is found to be 4.54%.

ACKNOWLEDGMENT

The author wishes to thank the TRIGA reactor operators D. Riyach, S. Otmani and I. Marrhich for thier participation on the elaboration of this work.

REFERENCES

[1] X-5 Monte Carlo Team, 2003. - MCNP- A General Monte Carlo N-Particle Transport Code, Version5-, Los Alamos Natl Lab. (April 24, 2003).

[2] Safety Comity, 2007. *Final Safety Analysis report for the 2MW TRIGA MARK II research reactor (FSAR) at CENM, Rabat*, Morocco.

[3] M. B. CHADWICK, P. OBLOZINSKY, M. HERMAN *et al*., ENDF/B-VII.0: Next Generation Evaluated Nuclear Data Library for Nuclear Science and Technology, Nucl. Data Sheets **107** (2006) 2931-3060

[4] P. F. ROSE (Comp. and Ed.), 1991: "*ENDF-201, ENDF/B-VI Summary Documentation*," BNL-NCS-17541, 4th Edition (1991).

[5] A. KONING, R. FORREST, M. KELLETT, R. MILLS, H. HENRIKSSON and Y. RUGAMA, 2006. "The JEFF-3.1 Nuclear Data Library," JEFF Report 21.

[6] K. SHIBATA, T. KAWANO, T. NAKAGAWA, O. IWAMOTO, J. KATAKURA, T. FUKAHORI, S. CHIBA, A. HASEGAWA, T. MURATA, H. MATSUNOBU, T. OHSAWA, Y. NAKAJIMA, T. YOSHIDA, A. ZUKERAN, M. KAWAI, M. BABA, M. ISHIKAWA, T. ASAMI, T. WATANABE, Y. WATANABE, M. IGASHIRA, N. YAMAMURO, H. KITAZAWA, N. YAMANO and H. TAKANO, Japanese Evaluated Nuclear Data Library Version 3 Revision-3: JENDL-3.3, J. Nucl. Sci. Technol. **39** (2002) 1125.

[7] R. E. MACFARLANE, *NJOY-99 Nuclear Data Processing System*. [Online]. Available: http://t2.lanl.gov/codes/njoy99/index.html (update web site) (1999).

[8] TETSUO MATSUMOTO AND NOBUHIRO HAYAKAWA, Benchmark Analysis of TRIGA MARK II Reactivity Experiment Using a Continuous Energy Monte Carlo Code MCNP, J. Nucl. Sci. Technol. **37** (12) (2000) 1082 – 1087.

[9] M. Q. HUDA, M. RAHMAN, M. M. SARKER, S. I. BHUIYAN, Benchmark analysis of the TRIGA MARK II research reactor using Monte Carlo techniques, Ann. Nucl. Energy **31** (2004) 1299-1313.

[10] M. RAVNIK, *TRIGA Reactor Power Upgrading Analysis*. Nuclear Society of Slovenia, 2nd Regional Meeting: Nuclear Energy in Central Europe Portoroz, SLOVENIA, 11 – 14 September 1995 (1995).

[11] S. I. BHUIYAN *et al*., 1991. Generation of a library for reactor calculations and some applications in core and safety parameters of the 3-MW TRIGA MARK II research reactor. Fission reactors (accepted for Publication July 11, 1991).
[12] B. EL BAKKARI *et al*., Development of an MCNP-tally based burnup code and validation through PWR benchmark exercises, Ann. Nucl. Energy **36** (2009) 626-633.
[13] B. EL BAKKARI *et al*., Validation of a new continuous Monte Carlo burnup code using a MOX fuel assembly, Nucl. Eng. Des. **239** (2009) 1828–1838.

Validation of the ENDF/B-VII library for the WWR-M research reactor in Ukraine

Y. P. Mahlers

Institute for Nuclear Research
Prospect Nauki 47
Kiev 03680
Ukraine

Abstract. The initial release of the ENDF/B-VII nuclear data library is validated for the WWR-M research reactor in Ukraine using criticality experiments with various number of fuel assemblies in the core. For neutronics calculation, the MCNP code based on the 3-D Monte-Carlo method is applied. Continuous-energy cross-sections for use with MCNP are calculated with the NJOY code both for ENDF/B-VI and ENDF/B-VII data. Calculated criticality is compared to the corresponding experimental values. Calculation with ENDF/B-VI.8 mostly underestimates criticality while calculation with ENDF/B-VII.0 overestimates it. The main source of such the difference between ENDF/B-VII.0 and ENDF/B-VI.8 is revision of H_2O thermal scattering data and ^{27}Al cross-sections in the new evaluation. Nevertheless, for all the experiments, neutronics calculation is in good agreement with the measurement. Both for ENDF/B-VI and ENDF/B-VII, the maximum absolute deviation of the effective multiplication factor from the results of the measurement is about 0.4% and the root-mean-square deviation is about 0.2%.

1. INTRODUCTION

Recently, the new version of the ENDF/B nuclear data library was released [1]. It was shown [2-5] that ENDF/B-VII essentially differs from its precursor ENDF/B-VI and provides better agreement between calculation and measurement for most criticality benchmarks. In this paper, the initial release of ENDF/B-VII is verified for the WWR-M research reactor using criticality experiments at the WWR-M facility.

2. CRITICAL EXPERIMENTS

ENDF/B-VII can be validated for WWR-M neutronics calculation using the criticality measurement carried out at the WWR-M experimental facility [6]. The experimental parameters are listed in Table 1. The WWR-M2 fuel assembly design is depicted in Fig.1. The core layouts are shown in Fig.2-5. For all the layouts, experimental critical number of fuel assemblies was determined using calibration of control rods in terms of the number of additional fuel assemblies to be loaded to compensate their reactivity.

TABLE 1. EXPERIMENTAL PARAMETERS [6]

Type of fuel assemblies	WWR-M2
Fuel enrichment, %	36.3
Number of fuel elements in a fuel assembly	3
Average mass of ^{235}U in a fuel assembly, g	33.16
Fuel meat composition	U-Al
Pitch/flat-to-flat, mm	35/32
Element/clad/meat, mm	2.5/0.9/0.7
Length of fuel meat, cm	48.9
Moderator and reflector	Light water
Temperature, C	17.5

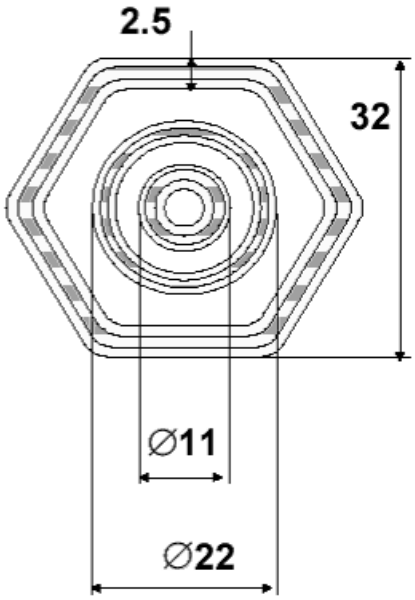

FIG.1. WWR-M2 Fuel Assembly Design

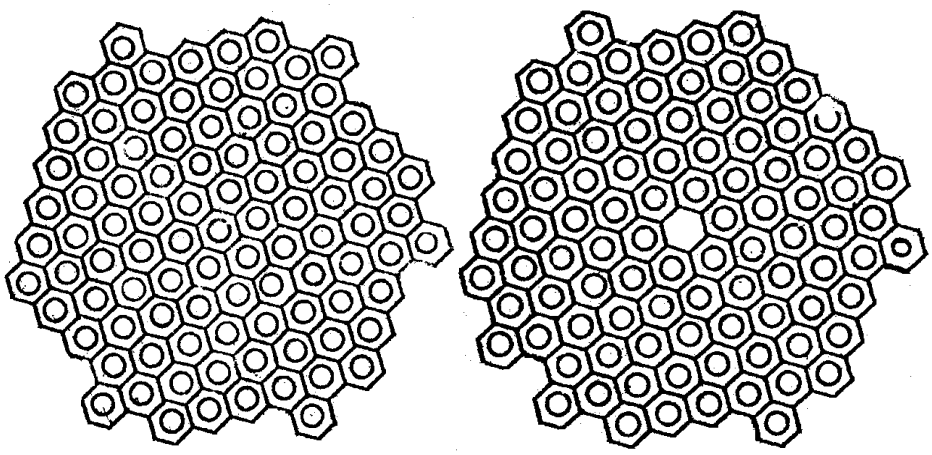

FIG.2. Left: Critical Experiment Layout 1, Right: Critical Experiment Layout 2

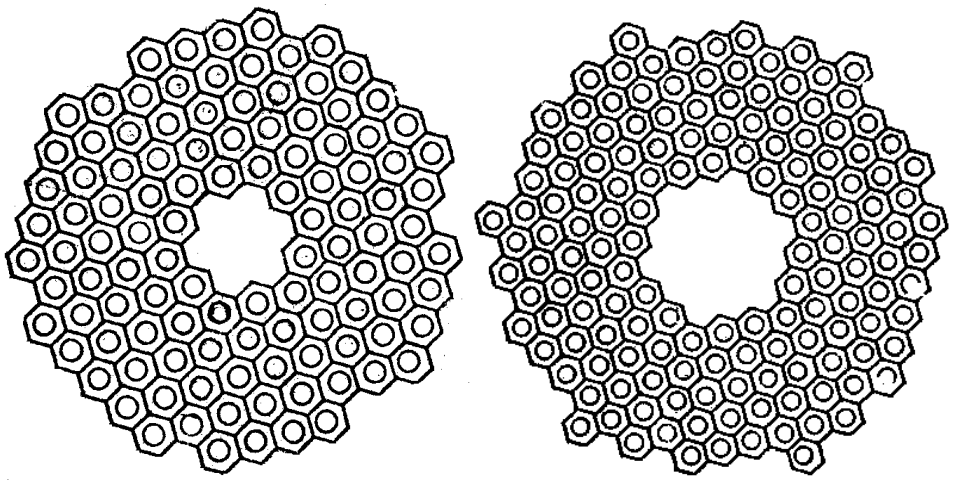

FIG.3. Left: Critical Experiment Layout 3, Right: Critical Experiment Layout 4

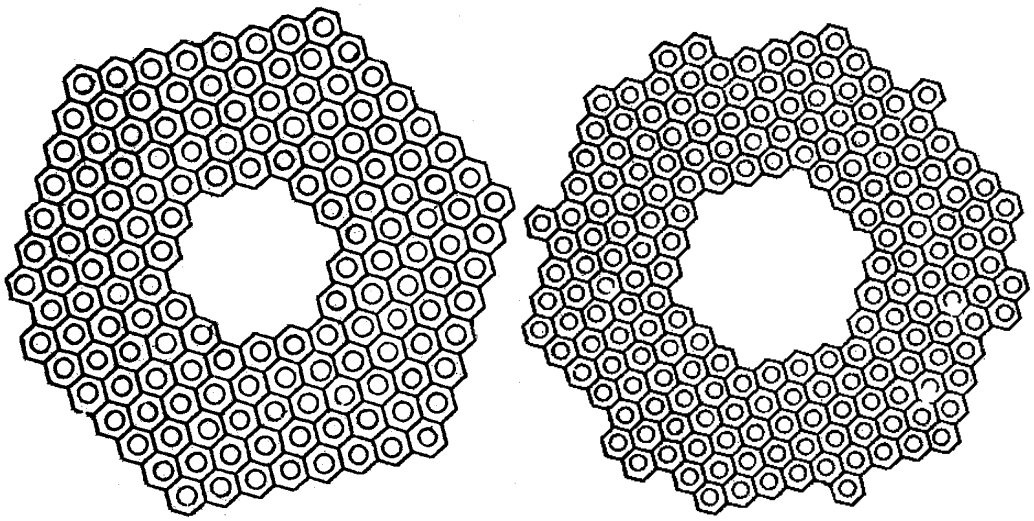

FIG.4. Left: Critical Experiment Layout 5, Right: Critical Experiment Layout 6

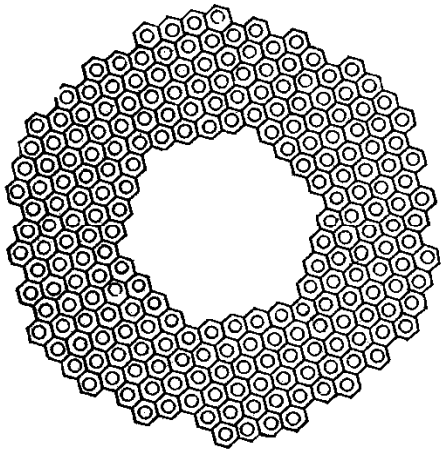

FIG.5. Critical Experiment Layout 7

3. NEUTRONICS MODEL

To verify ENDF/B-VII for WWR-M neutronics calculation, the MCNP code [7] based on the 3-D Monte-Carlo method was applied. Continuous-energy cross-sections for use with MCNP were calculated with the NJOY code [8] both for ENDF/B-VII.0 and ENDF/B-VI.8. Application of the 3-D Monte-Carlo method with continuous-energy cross-sections minimises errors of calculation because of the explicit and accurate modelling of the geometrical features and energy dependence in the WWR-M neutronics model. Statistical errors of calculation of the effective multiplication factor (k_{eff}) were less than 0.01%.

4. COMPARISON OF THE CALCULATION AND MEASUREMENT RESULTS

The results of the measurement and calculation are demonstrated in Table 2. The estimated measurement uncertainties for each layout are included in Table 2 also. For all the layouts, errors in k_{eff} corresponding to the estimated uncertainties in the experimental critical number of fuel assemblies shown in Table 2 are less than 0.1%. Statistical errors of calculation (standard deviations) are less than 0.01%.

TABLE 2. RESULTS OF THE MEASUREMENT AND CALCULATION

Layout	Experimental critical number of fuel assemblies [6]	Effective multiplication factor calculated by MCNP		Deviation from the measurement, %	
		ENDF/B-VII	ENDF/B-VI	ENDF/B-VII	ENDF/B-VI
1	94.1±0.2	1.0039	1.0019	0.39	0.19
2	93.5±0.2	1.0034	1.0011	0.34	0.11
3	108.8±0.3	1.0022	0.9988	0.22	–0.12
4	146.1±0.5	1.0005	0.9975	0.05	–0.25
5	147.8±0.5	1.0019	0.9984	0.19	–0.14
6	187.4±0.4	1.0008	0.9972	0.08	–0.28
7	225.1±0.4	1.0001	0.9968	0.01	–0.32

As we can see in Table 2, calculation with ENDF/B-VII.0 systematically overestimates criticality while calculation with ENDF/B-VI.8 mostly underestimates it. Average deviation of the effective multiplication factor calculated by MCNP from the results of the measurement is 0.18% for ENDF/B-VII.0 and –0.12% for ENDF/B-VI.8. The main source of such the difference between ENDF/B-VII.0 and ENDF/B-VI.8 is revision of H_2O thermal scattering data and ^{27}Al cross-sections in the new evaluation. Changes of the effective multiplication factor because of modification of ^{235}U and ^{238}U cross-sections were estimated to be less than 0.05%. Nevertheless, for all the experiments, neutronics calculation is in good agreement with the measurement. Maximum absolute deviation of the effective multiplication factor calculated by MCNP from the results of the measurement is 0.41% for ENDF/B-VII.0 and 0.32% for ENDF/B-VI.8. Root-mean-square deviation is 0.23% for ENDF/B-VII.0 and 0.22% for ENDF/B-VI.8.

Since the deviations of the calculated k_{eff} from the experimental values are very small for both ENDF/B-VII.0 and ENDF/B-VI.8, at this stage it is not possible to determine what library is better for WWR-M neutronics calculation. Moreover, about 0.3% of these deviations could be induced by the systematic uncertainty arising from the manufacturing tolerances in the dimensions of fuel assemblies, material impurities, etc. The main source of this systematic

uncertainty is estimated to be uncertainty of water fraction in the core because of high sensitivity of the effective multiplication factor to this value. The value of water fraction in fuel assemblies was measured during the experiment [6] but accuracy of this measurement was insufficient to get more reliable results.

As we can see in Fig. 2-5 and Table 2, both for ENDF/B-VII.0 and ENDF/B-VI.8, calculated k_{eff} decreases with increasing the number of fuel assemblies in the core. Reasons of this trend are not clear yet and should be analysed in future.

5. CONCLUSIONS

The initial release of the ENDF/B-VII nuclear data library was verified for the WWR-M research reactor in Ukraine using criticality experiments with various number of fuel assemblies in the core. For neutronics calculation, the MCNP code based on the 3-D Monte-Carlo method was applied. Continuous-energy cross-sections for use with MCNP were calculated with the NJOY code both for ENDF/B-VI and ENDF/B-VII data. Calculated criticality was compared to the corresponding experimental values.

Calculation with ENDF/B-VI.8 mostly underestimated criticality while calculation with ENDF/B-VII.0 systematically overestimated it. The main source of such the difference between ENDF/B-VII.0 and ENDF/B-VI.8 was revision of H_2O thermal scattering data and ^{27}Al cross-sections in the new evaluation. Nevertheless, for all the experiments, neutronics calculation was in good agreement with the measurement. The maximum absolute deviation of the effective multiplication factor from the results of the measurement was 0.41% for ENDF/B-VII.0 and 0.32% for ENDF/B-VI.8. The root-mean-square deviation was 0.23% for ENDF/B-VII.0 and 0.22% for ENDF/B-VI.8.

Thus, ENDF/B-VII is valid for WWR-M neutronics calculation.

REFERENCES

[1] CHADWICK, M.B., *et al*., ENDF/B-VII.0: Next generation evaluated nuclear data library for nuclear science and technology, Nucl. Data Sheets **107** (2006) 2931.

[2] VAN DER MARCK, S.C., Benchmarking ENDF/B-VII.0, Nucl. Data Sheets, **107** (2006) 3061.

[3] MOSTELLER R.D., Comparison of results for the MCNP criticality validation suite using ENDF/B-VII.0 and other nuclear data libraries, LA-UR-07, Los Alamos National Laboratory (2007).

[4] KOLBE, E., VASILIEVA, A., FERROUKHIA, H., ZIMMERMANN, M.A., Consistent evaluation of modern nuclear data libraries for criticality safety analyses of thermal compound low-enriched-uranium systems, Ann. Nucl. Energy, **35** (2008) 1831.

[5] MAHLERS, Y.P., VVER-1000 neutronics calculation with ENDF/B-VII data, Ann. Nucl. Energy **36** (2009) 1224.

[6] ASHRAPOV, T. B. *et al*., Critical masses for WWR-M fuel assemblies, Preprint No. 1343, Petersburg Nuclear Physics Institute, Gatchina (1987) (in Russian).

[7] BRIESMEISTER, J. F., Ed., MCNP – A general Monte Carlo N-Particle transport code, Version 4C, LA-13709-M, Los Alamos National Laboratory (2000).

[8] MACFARLANE, R. E., MUIR, D. W., BOICOURT, R. M., The NJOY nuclear data processing system, version 91, LA-12740-M, Los Alamos National Laboratory (1994).

[9] COURCELLE, A. *et al*., Nuclear data for improved LEU-LWR reactivity predictions, NEA/WPEC-22, Nuclear Energy Agency (2006).

Improvements in the Prediction Capability of Codes Used to Design Innovative Reactors

O. Cabellos[1,2], N. Garcia-Herranz[1,2], J. Sanz[2,3], E. González[4], F. Alvárez[4]

1) Department of Nuclear Engineering, Universidad Politécnica de Madrid, Spain
2) Instituto de Fusión Nuclear, Universidad Politécnica de Madrid, Spain
3) Department of Power Engineering, UNED, Spain
4) CIEMAT, Madrid, Spain

Abstract. In this paper, we assess the capability of codes to predict fuel cycle parameters for conceptual transmutation designs. The sensitivity/uncertainty and the Monte Carlo methodologies implemented in ACAB code will be described and the applicability to different nuclear fields is presented. We have studied the impact of activation cross-section uncertainties on relevant fuel cycle parameters, and the nuclear data requirements are evaluated so that such parameters can meet the assigned design target accuracies. We conclude with recommendations for future nuclear data measurement programs, beyond the specific results obtained with the present nuclear data files and the limited available covariance information.

1. Introduction

New nuclear systems and new nuclear fuel cycles are needed to improve the long term sustainability of nuclear energy. This long term option requires both better resource utilization (e.g. fast breeder reactors and fuel recycling) and less potential environmental impact and social acceptability (e.g. waste minimization including partitioning and transmutation). However, there is a lack of experimental and demonstration facilities to validate these concepts and to optimize their designs. In this sense, simulations might play more important place for the evaluation and extrapolation of performance, viability, cost and safety of innovative nuclear systems (e.g., new fast reactors, dedicated reactors for nuclear waste transmutation, accelerator driven systems, Gen-IV, etc.). Nevertheless, uncertainties (errors) in the nuclear data induce uncertainties in the simulation results, and methodologies to propagate this information are urgently needed both in terms of the reactor cores [1] and of the associated fuel cycles.

In this direction, an extensive work on nuclear data needs for innovative power reactors and fuel cycles is being performed. The sensitivity studies performed by a well-recognized expert group of OECD/NEA and by a work package of the NUDATRA domain IP-EUROTRANS have identified and independently corroborated a number of highest-priority isotopes/reactions for fast systems and waste minimization technologies.

Recently, the project entitled: “Accurate Nuclear Data for Nuclear Energy Sustainability” (ANDES), within Euratom Call FP7-Fission-2009, has been guided by these studies for the selection of the specific actions of nuclear developments. This project will cover three of the main aspects of nuclear data needs: i) improved differential measurements, ii) processing uncertainty/covariance information, and iii) validation with integral experiments. One of the objectives of ANDES proposal is to improve the inventory codes (ACAB code [2]) to handle the complete set of uncertainty/covariance data (i.e. those of nuclear reactions, radioactive decay and fission yield data) to illustrate the potential benefit of generalizing the assessment of simulation results with full uncertainties propagation. For this, capabilities will be

developed both to produce covariance data and to propagate the uncertainties through the inventory calculations.

In the present paper, we address the topic of the methodologies to be applied to estimate nuclear data uncertainty propagation to the isotopic inventory of the irradiated fuel and associated fuel cycle parameters, the activation cross section uncertainties and the list of parameters for the uncertainty evaluation and required target accuracies (section 2). In section 3, we present results of the use of the SU analysis in ADS-based nuclear waste burners: we study the effect of the covariance matrices and the priority list of required accuracies. Finally, in section 4, applications of the uncertainty methodology in other nuclear systems are presented.

2. Sensitivity and uncertainty methodology

This section describes the main features of the two proposed methodologies to be applied to propagate nuclear data uncertainties to the isotopic inventory and related parameters: sensitivity/uncertainty analysis (Section 2.1), and Monte Carlo uncertainty estimations (Section 2.2). These methodologies have been implemented into the inventory code ACAB [2] in order to assess the impact of cross section uncertainties.

2.1. Sensitivity/uncertainty analysis

Let $\mathbf{X}(t) = (X_1(t), X_2(t), \ldots, X_n(t))^T$ be the nuclide composition of a material at time t. The set of differential equations which describe the evolution of $\boldsymbol{X}$ in a neutron field may be written in matrix notation

$$\frac{d}{dt}\mathbf{X} = \mathbf{A}\mathbf{X} \tag{1}$$

where $\mathbf{A}$ is the n-by-n matrix involving the cross sections, fission yields and decay values. Given $\mathbf{X}_0 = \mathbf{X}(0)$ the initial nuclide density vector, the solution is $\mathbf{X}(t) = \exp(\mathbf{A}t)\mathbf{X}_0$.

Our goal is to analyse how cross section uncertainty is transmitted to the vector $\mathbf{X}$ and to other radiological quantities obtained as a function of $\mathbf{X}$. The *random* vector $\sigma = (\sigma_1, \sigma_2, \ldots, \sigma_m)$ contains all the cross sections involved in the problem. Let us assume that the other parameters (decay values, fission yields,...) are known and constant (not random), and that the analysis is carried out for a fixed time t. Each element X_i is a function of the random vector σ, $X_i = X_i(\sigma)$ where t will not be included for simplicity.

Let $\bar{\sigma}$ be the estimated cross section vector and $\mathbf{X}(\bar{\sigma}) = (\mu_1, \mu_2, \ldots, \mu_n)$ the solution of Equation (1) at this point. First order Taylor series provides a means of approximating $X_i(\sigma)$ about $\bar{\sigma}$,

$$X_i(\sigma) \approx X_i(\bar{\sigma}) + \sum_{j=1}^{m} \left[\frac{\partial X_i}{\partial \sigma_j}\right]_{\bar{\sigma}} (\sigma_j - \bar{\sigma}_j) \tag{2}$$

which can be written as

$$\frac{X_i(\sigma) - \mu_i}{\mu_i} \approx \sum_{j=1}^{m} \frac{\bar{\sigma}_j}{\mu_i}\left[\frac{\partial X_i}{\partial \sigma_j}\right]_{\bar{\sigma}} \frac{(\sigma_j - \bar{\sigma}_j)}{\bar{\sigma}_j} \tag{3}$$

$$\text{where : } \rho_{ij} = \frac{\bar{\sigma}_j}{\mu_i}\left[\frac{\partial X_i}{\partial \sigma_j}\right]_{\bar{\sigma}} \tag{4}$$

is known as the *sensitivity coefficient*. The value $e_i = \frac{X_i(\sigma) - \mu_i}{\mu_i}$ denotes **the relative change (error) in the amount of nuclide** *i* due to relative changes (errors) in cross sections equal to $\varepsilon_j = \frac{\sigma_j - \overline{\sigma}_j}{\overline{\sigma}_j}$.

The partial derivatives in Eq. (2) can be obtained efficiently; the computer implementation only implies a slight modification of the readily available routines to compute the exponential of a matrix.

The random variable ε_j is the **relative error in cross section** and a measure of its uncertainty is the *Mean Square Error* (MSE) defined by $E[\varepsilon_j^2]$, where E means expectation. When for all j, $E[\varepsilon_j] = 0$, then the MSE is the variance of ε_j. For the random vector $\varepsilon = [\varepsilon_1, \varepsilon_2, \ldots, \varepsilon_m]^T$ the m-by-m **variance matrix** is $M=E[\varepsilon\varepsilon^T]$.

Equation (3) gives a natural method for obtaining an approximation for the mean vector and variance matrix of $e = (e_1, e_2, \ldots, e_q)^T$. Let *S* be the q-by-m matrix containing the sensitivity coefficients, i.e.,

$$S = \begin{bmatrix} \rho_{11} & \rho_{12} & \cdots & \rho_{1m} \\ \rho_{21} & \rho_{22} & \cdots & \rho_{2m} \\ \vdots & \vdots & \ddots & \vdots \\ \rho_{q1} & \rho_{q2} & \cdots & \rho_{qm} \end{bmatrix}$$

then $e \approx S\varepsilon$ and taking expectations on both sides $E[e] \approx S\,E[\varepsilon]$ and the q-by-q variance matrix of e is

$$M_e \approx SMS^T$$

In the sensitivity/uncertainty formulation σ_j can stand for the cross section in a given group or for the total/effective *spectrum-averaged* cross section. When the effective spectrum-averaged cross section is used in the formulation, we should previously compute the uncertainty for this effective cross section starting from the values provided in the multi-group uncertainty library.

For a given neutron environment, we can define the corresponding *spectrum-averaged* cross section. Let $[\phi_1, \phi_2, ..., \phi_G]$ be the values of the flux corresponding to each energy group, the *spectrum-averaged* cross section is obtained as

$$\sigma_i = \frac{\phi_1\sigma_i^1 + \phi_2\sigma_i^2 + \cdots + \phi_G\sigma_i^G}{\phi_1 + \phi_2 + \cdots + \phi_G} \tag{5}$$

Given V_i the *G*-by-*G* variance matrix of the *relative* cross sections vector, the variance Δ_i^2 of the *relative spectrum-averaged* cross section is then: $\Delta_i^2 = \omega^T V_i \omega$

with $\omega = [\frac{\phi_1}{\overline{\phi}}\frac{\sigma_i^1}{\sigma_i}, \frac{\phi_2}{\overline{\phi}}\frac{\sigma_i^2}{\sigma_i}, \cdots, \frac{\phi_G}{\overline{\phi}}\frac{\sigma_i^G}{\sigma_i}]^T$ and $\overline{\phi} = \phi_1 + \phi_2 + \cdots + \phi_G$ the total flux. In inventory calculations, this procedure to derive one-group covariance data guaranties that the uncertainty using different group structure remains constant [3].

The V_i matrix is the relative covariance matrix or fractional error matrix used for representing uncertainties in evaluated nuclear data files, such as the Evaluated Nuclear Data File (ENDF). It is worthwhile noting that a key point to implement the proposed approach is the availability of reliable uncertainty data, and the appropriate processing of the cross-section uncertainty

data included in the corresponding libraries. To deal with response functions directly dependent on the isotopic inventory the sensitivity/uncertainty formalism is straightforward.

2.2 Monte Carlo method

Other possible methodology to perform uncertainty analysis is random simulation or Monte Carlo method. To apply this methodology it is necessary information about the probability distribution of the cross section errors. Different assumptions can be made about the probability distribution of the cross section. The simplest and more usual (in many other areas) is the normal distribution. When the variance is large, this distribution can generate negative values for the cross sections. To avoid this drawback an alternative distribution is the log normal, that is: $\log\left(\frac{\sigma_i}{\overline{\sigma}_i}\right) \rightarrow N(0,\Delta_i^2)$

There are quite a few important reasons to recommend this well known distribution. For instance, taking into account that $\log\left(\frac{\sigma_i}{\overline{\sigma}_i}\right) = \log\left(1+\frac{\sigma_i-\overline{\sigma}_i}{\overline{\sigma}_i}\right) \approx \frac{\sigma_i-\overline{\sigma}_i}{\overline{\sigma}_i}$, when $\frac{\sigma_i-\overline{\sigma}_i}{\overline{\sigma}_i}$ is small (that is, when Δ_i is small), the log normal assumption is practically equivalent to the normality.

The above distribution can be applied to the cross-sections of individual energy groups or to the spectrum-averaged cross section. In this section we are going to explain the first one. The results are almost the same when the uncertainties are low. For the reaction *i*, we assume that the joint probability distribution of the cross sections is given by:

$$\log\begin{bmatrix} \sigma_i^1/\overline{\sigma}_i^1 \\ \sigma_i^2/\overline{\sigma}_i^2 \\ \vdots \\ \sigma_i^G/\overline{\sigma}_i^G \end{bmatrix} \rightarrow N(0,V_i) \qquad (6)$$

where V_i is the *G*-by-*G* variance matrix and let P_i be the *G*-by-G matrix that verify $V_i = P_i P_i^T$.

It can be proven that the values obtained as follow have the joint probability distribution given above:

- Generate $Z = (Z_1, Z_2, ..., Z_G)^T$ independent $N(0,1)$ random variables
- $Y = P_i Z$, $Y = (Y_1, Y_2, ..., Y_G)^T$
- For every group *k*: $\sigma_i^k = \overline{\sigma}_i^k \exp(Y_k)$, $k = 1,2,...,G$

The three former steps and the Eq. (5) can be applied to get a sample of the random vector $\sigma = (\sigma_1, \sigma_2, ...,\sigma_m)$ of cross-sections. From this vector, the matrix **A** is computed and the vector of nuclide quantities at time t is obtained as $X(t) = exp(\mathbf{A}t)\mathbf{X}_0$. Repeating the sequence explained before it is possible to get a sample of *N* vectors $\{X^1(t), X^2(t), ..., X^N(t)\}$ and from the sample it is possible to estimate the mean, variance and of the distribution of $X(t)$. It is worth noting that the computational algorithm to estimate by the Monte Carlo approach uncertainties of isotopic inventory-dependent quantities due to the whole set of cross section, is similar to the one already implemented to estimate uncertainties in the number of atoms of the different nuclides.

2.3 Cross-section uncertainties

To study the impact of nuclear data uncertainties on the performance parameters, such as the irradiated fuel isotopic composition, it is necessary to establish a realistic ‘‘compilation’’ of nuclear data uncertainties and their correlation (variance-covariance matrices). A wide review

of uncertainties from the most recent activation data files, general-purpose evaluated nuclear data files and bibliography proposals has been performed in Ref. [4]. The following summarises present situation and our adopted strategy:

i) For activation data files, in particular EAF2005-7/UN [5, 6], no more than three values for energy below 20 MeV are given, neglecting all type of correlations (in energy, between different isotopes, among reactions, etc.), the multigroup covariance matrices that can be obtained have the off-diagonal values set to zero.
ii) For general-purpose evaluated nuclear data files the standard computational processing tools available are used (NJOY, ERRORRJ). We can obtain multigroup covariance matrices with energy correlations, and multigroup covariance matrices correlating different isotopes and reaction types [7].
iii) Regarding bibliography proposals for nuclear data multigroup covariance matrices, the 15-energy-group structure ANL [8] and BOLNA [9] proposals have been considered. It can be said that concerning to actinide reactions they are very likely the most reliable data at present. These uncertainties (diagonal values) are based as much as possible on the nuclear data performance in the analysis of selected, clean integral experiments (irradiated fuel and sample analysis, criticality and fission rates in zero-power critical facilities). Regarding energy correlations, the ANL correlations were said to be a first guess, and BOLNA appears as the more recent contribution to the correlation question.
iv) Finally, as correlations data are at present not well known, we have generated several matrices corresponding to different covariance structures associated to simple correlation models that we have proposed [4,10,11]. This allows us to study the effect of the covariance structure in the actinide inventory using the existing variance/diagonal data. Let us assume that the energy range are divided in G groups and let $[E_1, E_2, \ldots, E_G]$ be the energy mean values or center points of each group. The correlation among the groups with energies E_i and E_j is defined by the equation

$$c_{ij} = \exp[-\theta|\log E_i - \log E_j|] \qquad (7)$$

where θ is a positive parameter between 0 and ∞, that can be considered as a correlation range parameter. When θ is large, the correlations are low and *vice versa*, when θ is small, the correlations are high.

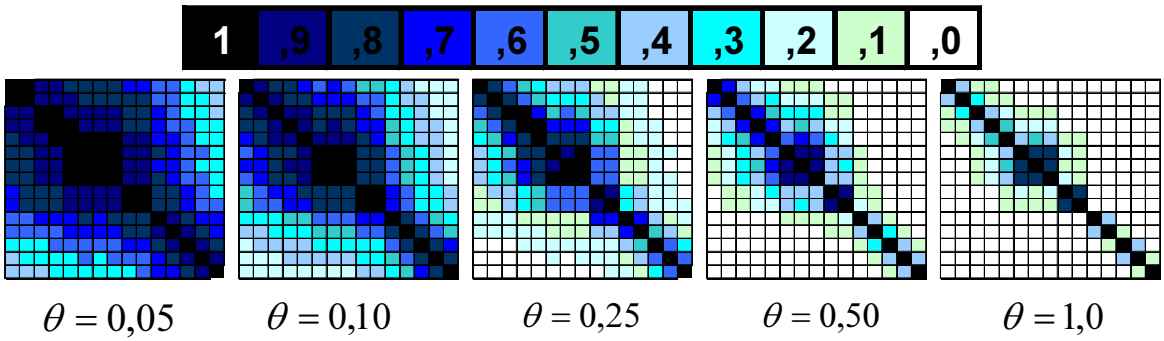

FIG.1. Correlation matrices obtained following the Equation (7) with different values of the parameter θ

2.4 List of parameters and suggestions for target accuracies

Here, we propose a list of selected topics and parameters of the fuel cycle and the repository for the ADS-based scenario to be analyzed. In this case study, characteristic storage and cooling times, and mass flows were defined. Briefly, the established list includes:

i) Transmutation potential: At the end of irradiation
ii) Reprocessing: Decay heat at t=0, 2 years after discharge
iii) Fabrication: Neutron source at t=2, 3 years after discharge (1 year storage)
iv) Waste conditioning: Decay heat and neutron emission after reprocessing and t=50 years after last irradiation
v) Waste in the final repository: Decay heat and dose/radiotoxicity t=0, 200, 500, 1000, 10 000, 100 000, 300 000 years after storage

Finally, the target accuracies are (these values are in agreement with those proposed in the recent bibliography [12] and [13]): i) for the transmutation potential, i.e., nuclide concentrations at end of irradiation, the assigned value is 5%; and ii) for all the other fuel cycle related parameters (i.e., decay heat, neutron source, and dose) the fixed value is 10%.

3. Application of SU analysis in ADS-based burners

3.1 First problem: Effect of the covariance matrices

The system used in the analysis it is one of the two ADS-based nuclear waste burners considered in the RED-IMPACT project [14]. The basic ADS characteristics are: fuel (TRU-Zr) N, core cooled by lead-bismuth eutectic in forced convection, total fuel burn-up 150 GWd/THM, thermal power 850 MW. The initial isotopic composition for actinides is shown in the second column of Table I. The given composition corresponds to an initial mass of actinides of 16.6 kg.

For the reference 500-day irradiation problem, different set of results have been obtained using the Monte Carlo approach, and are provided in Table I. In the first set, only the "diagonal" values of the ANL covariance matrices are used (any kind of correlations is neglected). The results obtained are given in column 4 of Table I. In the second set, the full ANL covariance matrices are considered, i.e., including the energy correlation assigned in [3]. The results are provided in column 11. The third set uses a series of correlation parametric matrices, generated according with eq. (1) for the following values of θ: $\theta = 1$, $\theta = 0.5$, $\theta = 0.25$, $\theta = 0.1$, $\theta = 0.05$ and $\theta = 0$. The results are provided in columns 5-10.

Results given in columns 4-11 show that: i) most of the nuclides exhibit concentration uncertainties below the target value of 5%; ii) there are a few nuclides with uncertainty values a little higher than 5% (in this group the nuclide with a higher uncertainty in the concentration is Am-242m); and iii) there are two nuclides, namely Cm-243 and Cm-245, that clearly show a concentration uncertainty far above 5%.

It is also found that generally, the uncertainties for the concentrations of all nuclides increase with the irradiation time. Yet there are three exceptions: Pu-243, Pu-244 and Cm-242. In Figure 2 it is shown the uncertainty evolution as a function of the irradiation time for the concentration of Cm isotopes. The mean value of the concentration is represented by the red line, and the uncertainties results (curves in blue) are given as the mean ±2 standard deviations. As far as Cm-242 is concerned, it is the nuclide exhibiting the highest decrease in the uncertainty from 250 to 1000 days of irradiation. On the contrary, in Figure 2 we also show the uncertainty evolution as a function of the irradiation time for Cm-243, Cm-244, and Cm-245, as examples of those nuclides for which the uncertainty increases with the irradiation time.

TABLE I. UNCERTAINTY EVALUATION USING ANL UNCERTAINTIES (DIAGONAL VALUES, COLUMN 4) AND DIFFERENT CORRELATION MATRICES (ANL PARTIAL ENERGY CORRELATION, COLUMN 11, AND PARAMETRIC CORRELATIONS, COLUMNS 5-10). THE RELATIVE ERRORS (RATIO BETWEEN STANDARD DEVIATION AND THE MEAN, IN %) ARE CALCULATED BY THE MONTE CARLO APPROACH. RESULTS USING EAF2005 UNCERTAINTIES ARE ALSO GIVEN (COLUMN 12). RESULTS ARE REFERRED AT THE END OF 500-DAY IRRADIATION.

Isotope	Initial (10^{23} at.)	Final (10^{23} at.)	Relative error of the final concentrations (%)								
			ANL No correl.	Theta (θ)						ANL correl	EAF 2005
				1	0.5	0.25	0.1	0.05	0		
^{234}U	4.30	3.74	1.13	1.52	1.73	2.01	2.19	2.36	2.50	1.69	4.47
^{235}U	1.08	0.99	2.30	3.11	3.72	4.71	5.19	5.69	5.93	3.52	13.05
^{236}U	1.50	1.45	0.90	1.24	1.55	1.79	2.04	2.22	2.27	1.47	1.94
^{238}U	0.01	0.009	0.49	0.67	0.83	0.96	1.15	1.23	1.26	0.81	1.69
^{237}Np	17.95	10.84	1.87	2.53	3.00	3.54	4.18	4.18	4.51	3.01	7.10
^{238}Pu	32.10	28.73	1.96	2.63	3.13	3.86	4.44	4.57	5.10	2.93	4.89
^{239}Pu	46.77	29.41	1.30	1.73	2.09	2.51	2.88	2.99	3.20	1.98	5.47
^{240}Pu	137.40	113.53	0.81	1.09	1.40	1.69	1.92	2.04	2.21	1.34	2.31
^{241}Pu	28.12	24.21	3.07	4.10	5.14	6.16	7.26	7.87	8.36	4.85	9.90
^{242}Pu	61.44	55.35	0.81	1.04	1.25	1.49	1.79	1.89	1.94	1.24	2.44
^{243}Pu	-	0.0005	3.80	4.89	6.20	7.34	8.96	9.75	9.56	5.83	12.18
^{244}Pu	-	0.0004	3.48	4.25	5.74	6.49	7.91	8.16	8.66	5.22	14.09
^{242}Am	26.55	16.09	1.89	2.55	3.16	3.60	4.15	4.31	4.86	2.91	7.52
^{242m}Am	1.49	0.98	4.27	5.74	7.49	8.58	9.49	10.07	10.85	6.04	14.72
^{243}Am	24.39	21.37	1.98	2.50	3.26	3.66	4.43	4.74	4.96	3.00	7.46
^{242}Cm	0.02	2.87	3.20	4.26	5.22	5.86	6.81	7.12	7.68	4.87	11.17
^{243}Cm	**0.22**	**0.32**	**14.78**	**19.00**	**24.21**	**27.13**	**32.09**	**35.24**	**35.95**	**22.91**	**28.30**
^{244}Cm	20.59	23.12	3.72	4.48	5.54	6.65	7.49	7.73	8.22	5.43	6.89
^{245}Cm	**5.92**	**5.52**	**11.62**	**14.17**	**18.35**	**21.59**	**25.51**	**26.18**	**28.45**	**16.68**	**15.06**
^{246}Cm	3.82	3.81	3.38	4.36	5.73	7.05	7.53	8.38	8.90	5.40	7.71
^{247}Cm	1.05	0.90	0.88	1.15	1.50	1.84	1.97	2.20	2.33	1.43	15.58
^{248}Cm	-	0.14	0.31	0.41	0.53	0.64	0.69	0.77	0.82	0.50	31.27
^{249}Bk	-	0.0004	0.18	0.24	0.31	0.38	0.41	0.46	0.49	0.30	39.78
^{250}Cf	-	0.00005	0.11	0.14	0.18	0.22	0.24	0.26	0.28	0.17	50.33

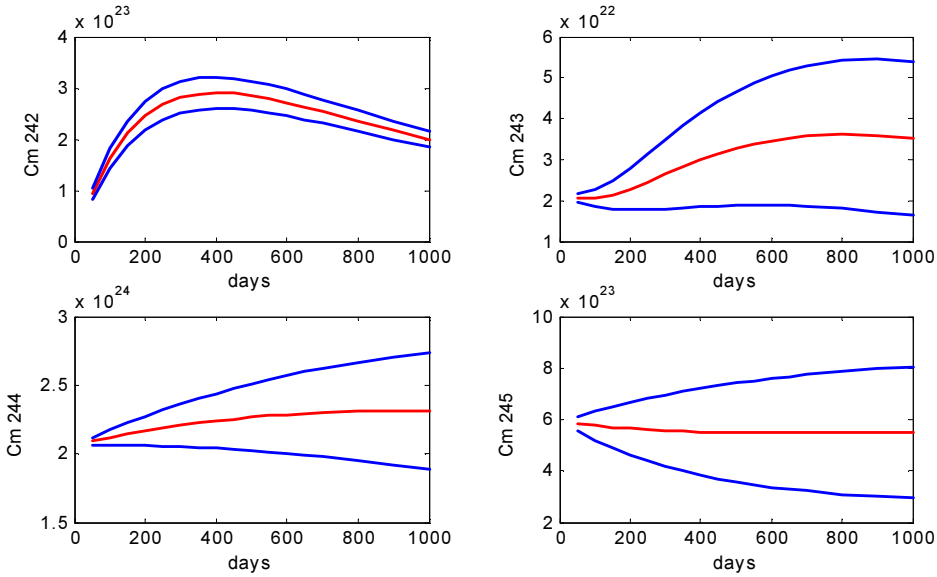

FIG.2. Prediction of the concentration of Cm isotopes as a function of the irradiation time. Mean values are represented by the red curve. Uncertainties, represented by the graphs in blue, are given as the mean ±2 standard deviations

3.2 Second Problem: identification of critical XS and priority list of required accuracies

In this section the prototype selected is the *European Facility for Industrial Transmutation* (EFIT). The basic ADS characteristics are: core cooled by pure lead, thermal power 400 MW, initial total mass of actinides 2.074 tonnes, and 150 GWd/tHM discharge burn-up corresponding to an equilibrium cycle (~778 irradiation days) [15].

Multiple recycling of the fuel in ADS is required to achieve the desired radiotoxicity reduction. The uncertainty of the radionuclide content in the initial fuel rises in each cycle since a high amount of the new fresh fuel is the result of previous irradiations with its corresponding uncertainty. To take into account the impact of such scenario on the fuel, consecutive irradiation cycles inside ADS should be simulated. However, in our analysis, this effect is investigated considering a single longer irradiation period, corresponding to a discharge burn-up of 500 GWd/tHM (equivalent to 3-4 consecutive irradiation cycles).

For these calculations, the neutron environment given above is assumed, since the fuel would be irradiated in the same reactor, characterised by a similar initial isotopic composition after having reached the equilibrium cycle.

The objective of the present study is to provide a confident set of uncertainty estimates for EFIT. The neutron cross-section uncertainty data have been taken from the EAF-2007/UN library [6], which contains uncertainty information for all the actinides potentially present in the irradiated fuel. The associated best-estimated/nominal cross-section values have been taken from the EAF-2007 library. On the other hand, the required data to calculate the decay heat, radiotoxicity and neutron emission have been obtained processing different EAF-2007 basic libraries: decay data basic library, differential ranges for α-particles library, cross-section library for (α,n) reactions and commitment effective dose equivalent library.

For the EFIT prototype analyzed in this report, 21 nuclides of interest have been identified, either by their transmutation potential (T) or by their impact in the response functions (DH: decay heat, N: neutron emission, R: radiotoxicity).

TABLE II. MOST RELEVANT NUCLIDES AND UNCERTAINTIES IN ITS CONCENTRATION.

Nuclide	Uncertainty in concentration (%)		Relevant in:			
	Burn-up (GWd/tHM)					
	150	500				
U-234	4.6	16.1	T	DH		
U-235	13.1	18.4	T			
U-236	1.8	7.6	T			
Np-237	6.3	23.7	T			
Pu-238	4.3	10.8	T	DH		R
Pu-239	4.6	12.9	T	DH		R
Pu-240	2.0	7.0	T	DH		R
Pu-241	8.2	14.7	T			
Pu-242	2.1	7.9	T	DH		R
Am-241	7.2	20.7	T	DH		R
Am-242m	12.8	28.6	T			
Am-243	6.6	15.6	T	DH		R
Cm-242	10.7	7.7	T	DH	N	R
Cm-243	23.3	32.6	T			
Cm-244	6.0	13.3	T	DH	N	R
Cm-245	13.3	18.8	T			
Cm-246	7.5	21.7	T		N	
Cm-247	15.4	27.2	T			
Cm-248	6.4	19.8			N	
Cf-250	31.9	28.9			N	
Cf-252	52.4	46.1			N	

To determine the reduction in the cross section uncertainties and establish priorities, we have used a methodology based on the minimization of the so called objective function. The objective function is constrained to the maximum uncertainty of 10% in the response functions (decay heat, neutron emission, radiotoxicity by ingestion, radiotoxicity by inhalation) for a relevant set of cooling time were selected.

The uncertainties included in the EAF_UN-2007 library for these critical cross sections should be reduced in a factor specified in Table III to fulfil the target uncertainty of 10% in the response functions. Notice that this table of required accuracies is the necessary uncertainty reduction for the current energy correlation structure implicit in the EAF_UN-2007 library. Taking into account the large impact of correlations on uncertainty results, it can be concluded that, if this library is to be used, it could be necessary a better evaluation of the correlation energy structure of the cross sections in addition to a reduction of the relative errors.

TABLE III. TABLE OF REQUIRED ACCURACIES: UNCERTAINTY REDUCTION OF CRITICAL CROSS SECTIONS, NECESSARY TO SATISFY THE TARGET ACCURACY OF 10% IN RESPONSE FUNCTIONS. CALCULATIONS CORRESPOND TO A BURN-UP OF 500 GWD/THM.

Isotope	Cross Section	Uncertainty (Δ%)		EAF2007 / Target	Isotope	Cross Section	Uncertainty (Δ%)		EAF2007 / Target
		EAF2007	Target				EAF2007	Target	
U234	(n,γ)	38.9	-		CM242	(n,γ)	30.0	-	
U234	(n,γ-M)	38.9	-		CM243	(n,fission)	16.0	-	
U235	(n,fission)	12.9	-		CM243	(n,γ)	32.0	-	
NP237	(n,γ)	14.3	-		CM244	(n,γ)	24.6	14.7	2
PU238	(n,fission)	12.3	-		CM245	(n,fission)	9.7	-	
PU238	(n,γ)	14.5	-		CM245	(n,γ)	32.7	18.9	2
PU239	(n,fission)	9.6	-		CM246	(n,γ)	28.2	15.1	2
PU240	(n,γ)	9.3	-		CM247	(n,fission)	16.5	-	
PU241	(n,fission)	15.6	13.5	1.2	CM247	(n,γ)	32.1	12.6	3
PU242	(n,γ)	12.6	-		CM248	(n,γ)	19.2	6.6	3
AM241	(n,γ)	15.8	-		BK249	(n,γ)	31.7	8.7	4
AM241	(n,γ-M)	15.8	-		CF249	(n,γ)	32.4	11.3	3
AM242M	(n,fission)	24.0	-		CF250	(n,fission)	33.0	17.5	2
AM242M	(n,γ)	32.8	-		CF250	(n,γ)	29.3	7.7	4
AM243	(n,γ-M)	15.3	-		CF251	(n,fission)	31.6	11.5	3
					CF251	(n,γ)	29.9	7.6	4

4. Other applications of the uncertainty methodology

4.1 Application in IFMIF/DEMO/IFE: Prediction of H, He, Tritium

The effect of the activation cross section uncertainties in the assessment of both solid transmutants and hydrogen and helium production has been analyzed in Ref. [17]. We conclude that in the case of the iron element the maximum uncertainty for H- and He- gas production is below 5%. The transmutation performance of the Eurofer steel is predicted. We observed that the transmutation of the main constituents of Eurofer, Fe and Cr, is not significant. However, the prediction of minor constituents of Eurofer, such as Ti, V and Mn increase in all cases, except for the soft neutron environment IFE/HYLIFEII. In addition, new elements are generated during the irradiation time in the vicinity of the initial elements. In general, the concentration of newly generated elements is insignificant. In the case of rhenium and osmium, the higher generation occurs in IFE/HYLIFEII due to a soft neutron environment. The evolution of the elemental composition during irradiation shows a linear dependence on the irradiation time. There are a few exceptions such as B, Co and Ni.

We have also studied the prediction of the tritium production required for handling procedures of samples, safety & maintenance and licensing of the International Fusion Materials Irradiation Facility (IFMIF). We have addressed an uncertainty analysis to draw conclusions on the reliability of the tritium prediction under the potential impact of activation cross section uncertainties. Relative errors up to 51% in tritium prediction can be found. We conclude that there is no sufficient experimental validation of the evaluated tritium production cross sections, especially for iron and sodium. Therefore a dedicated experimental validation program for those elements should be proposed and launched [18].

TABLE IV. GAS PRODUCTION RATES FOR HYDROGEN AND HELIUM (APPM) AND REL. ERR. (ε, IN %) OF TYPICAL EXPECTED AND IMPURITIES ELEMENTS IN REDUCED ACTIVATION STEELS AFTER 1 YEAR OF IRRADIATION. [17]

		HFTM/IFMIF				DEMO				HYLIFEII			
Z	Element	H	ε%	He	ε%	H	ε%	He	ε%	H	ε%	He	ε%
5	B	806	7	3474	7	739	10	54250	6	38	12	64376	5
6	C	423	16	3431	39	3	7	3964	56	0	6	108	48
7	N	2683	12	2468	12	3831	19	1829	27	355	7	137	6
8	O	359	10	1397	8	412	5	1200	7	8	4	70	7
13	Al	1084	9	703	10	1425	9	962	14	45	5	33	16
14	Si	2309	4	1202	4	2487	2	1472	3	85	2	58	3
15	P	3936	17	880	14	5596	26	1087	10	187	19	45	4
16	S	4281	8	2662	13	4056	13	2873	22	206	6	185	13
22	Ti	986	8	415	32	795	6	274	5	25	3	7	6
23	V	659	10	81	7	738	2	105	2	22	2	2	2
24	Cr	1143	6	300	12	1167	4	235	13	35	3	8	23
25	Mn	844	17	197	31	713	20	163	5	18	15	4	5
26	Fe	1445	7	293	5	1452	2	318	2	47	2	10	3
27	Co	1249	17	259	27	1827	16	241	8	43	15	7	4
28	Ni	5787	6	1808	29	7118	5	1290	11	830	12	500	22
29	Cu	2030	17	317	5	2170	26	331	6	97	21	10	7
39	Y	789	16	52	8	898	26	37	5	27	27	1	5
41	Nb	738	15	120	17	520	8	113	4	13	7	3	4
42	Mo	1120	12	104	9	1241	25	94	7	28	19	2	6
73	Ta	193	24	19	26	31	7	4	6	1	13	0	12
74	W	224	10	26	12	42	10	343	30	2	9	965	29

4.2 Fission Chambers

The selection of the fissile material for the inner coating of the fission chamber (FC) plays the most crucial role in order to assess the pertinence of sub-miniature fission chambers [19]. Calculations concerning the isotopic composition and the fission rates as a function of the neutron energy and fluence are necessary to assure the suitability of the chosen material. A study based on the estimate the burn-up of different fissile deposits as a function of the neutron fluence showed that the relative error in fission rate due to activation cross-section uncertainty data is significant [19].

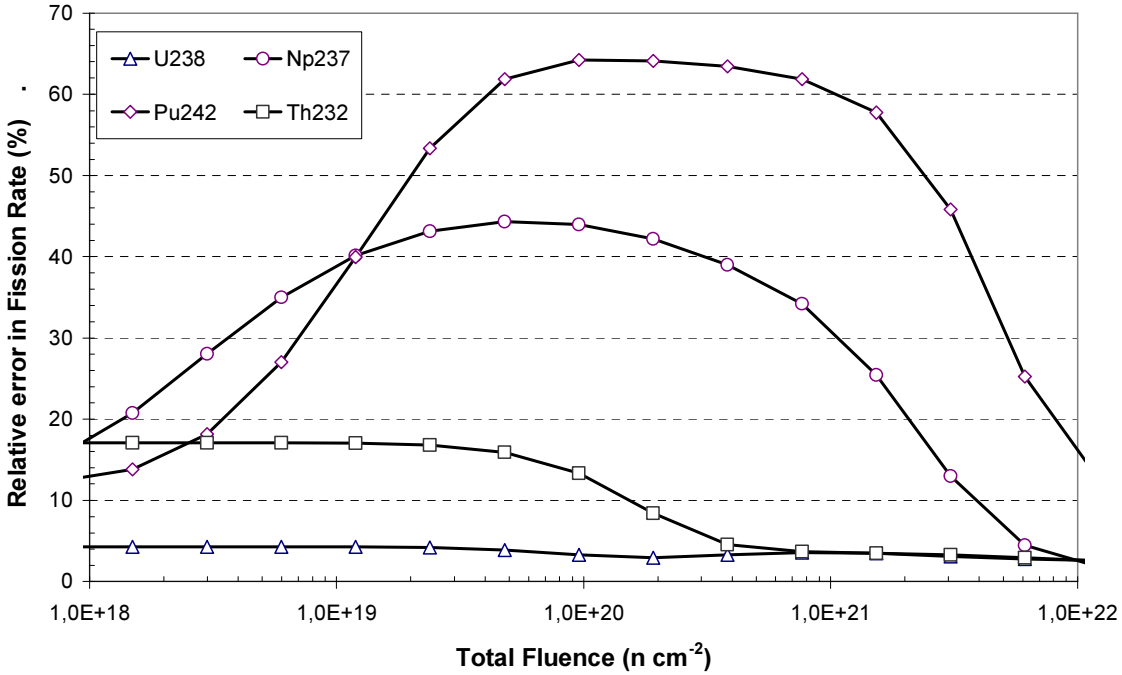

FIG.3. Relative error (in %) in fission rates for different fissionable pure deposits calculated with a typical neutron flux of the BR2 reactor.

5. Conclusions

Once uncertainty information is provided (point-wise or multi-group structure) in the different kind of nuclear data libraries, processing tools are available to convert this information into the form of multi-group covariance matrices for extensive use in inventory codes. We have developed and implemented a methodology in ACAB code to estimate the impact of neutron cross-section uncertainties using two uncertainty propagation techniques: sensitivity/uncertainty and Monte Carlo.

This code is able to deal with multi-group covariance matrices in any arbitrary group structure correlation (extension to deal with reaction and isotope correlations are to be done within ANDES project). In addition, the Monte Carlo technique is recommended when computing the overall/global effect of the complete set of uncertainties. Sensitivity/uncertainty methodology is recommended for analysis of the uncertainty results obtained by the Monte Carlo method.

We have illustrated the potential benefit of generalizing the assessment of simulation results with full uncertainties propagation to estimate their impact on reactor and fuel cycle and repository parameters in different nuclear systems. In this respect, we are able to establish a priority list of nuclear data improvements after a detailed calculation of the specific system(s).

REFERENCES

[1] G. ALIBERTI *et al*., Nuclear data sensitivity uncertainty and target accuracy assessment for future nuclear systems, Ann. Nucl. Energy **33** 700-733 (2006).

[2] J. SANZ, O. CABELLOS, N. GARCÍA-HERRANZ, *ACAB-2008, ACtivation ABacus Code V2008,* NEA Data Bank (NEA-1839), February 2000.

[3] H. HIRUTA, G. PALMIOTTI, M. SALVATORES, R. ARCILLA JR., P. OBLOZINSKY, R.D. MCKNIGHT, *Few Group Collapsing of Covariance Matrix Data Based on a Conservation Principle*, Nucl. Data Sheets **109** (2008) 2801-2801.

[4] J. SANZ (responsible of the deliverable), *Interim Report on the description of selected nuclear data sensitivity methodologies for the fuel cycle and the repository parameters*, Deliverable D5.10, Domain DM5 NUDATRA, Workpackage 5.1 (May, 2006). Authors of the referenced sections: J. Sanz, O. Cabellos, N. García-Herranz, J. Juan, P. Sauvan, F. Ogando, E. González, P. T. León, F. Alvarez-Velarde.

[5] R.A. FORREST, J. KOPECKY and J-CH. SUBLET, *The European Activation File: EAF-2005 cross section library*, UKAEA FUS 515 (2005).

[6] *The European Activation System: EASY-2007 overview*. R.A. Forrest, UKAEA FUS 533, 2007.

[7] I. KODELI, E. SARTORI, *ZZ-COV-15GROUP-2006, NEA1730 Package OECD/NEA Data Bank*.

[8] G. PALMIOTTI, M. SALVATORES, *Proposal for Nuclear Data Covariance Matrix*, *JEFDOC 1063 Rev.1* (January 20, 2005).

[9] SALVATORES M. *et al*., "*OECD/NEA WPEC Subgroup 26 Final Report: Uncertainty and Target Accuracy Assessment for Innovative Systems Using Recent Covariance Data Evaluations*" 2008.

[10] J. SANZ, J. JUAN, O. CABELLOS, N. GARCIA, F. ALVAREZ, E. GONZALEZ, *Application of Monte Carlo techniques for propagation of cross section uncertainties to actinide inventory in ADS transmuters: comparison with sensitivity analysis*, in Proceedings of the International Conference on Nuclear Data for Science and Technology, April 22-27, 2007, Nice, France, editors O.Bersillon, F.Gunsing, E.Bauge, R.Jacqmin, and S.Leray, EDP Sciences, 2008, pp 285-288.

[11] N. GARCÍA-HERRANZ, O. CABELLOS, J. SANZ, J. JUAN, *Impact of different correlation structures in cross-section covariance matrices on the inventory and inventory-related parameters*, International Conference on the Physics of Reactors "Nuclear Power: A Sustainable Resource", PHYSOR'08, Interlaken, Switzerland, September 14-19, 2008.

[12] G. ALIBERTI, G. PALMIOTTI, M. SALVATORES, C. G. STENBERG, *Transmutation Dedicated Systems: An assessment of Nuclear Data Uncertainty Impact*, Nucl. Sci. Eng. **146** (2004) 13-50.

[13] G. ALIBERTI, G. PALMIOTTI, M. SALVATORES, T.K. KIM, T.A. TAIWO, M. ANITESCU, I. KODELI, E. SARTORI, J.C. BOSQ, J. TOMMASI, *Nuclear data sensitivity, uncertainty and target accuracy assessment for future nuclear systems,* Ann. Nucl. Energy **33** (2006) 700–733

[14] L. BOUCHER (responsible of deliverable), *Detailed description of selected fuel cycle scenarios*. FP6 RED-IMPACT Deliverable 1.4. Contract nº FI6W-CT-2004-002408. Draft version. November 2004.

[15] J. SANZ (responsible of the deliverable), *Report of the numerical results from the evaluation of the nuclear data sensitivities, priority list and table of required accuracies for nuclear data*, Deliverable D5.11, Domain DM5 NUDATRA, Workpackage 5.1 (Feb, 2009). Authors of the referenced sections: J. Sanz, O. Cabellos, N. García-Herranz, J. Juan, P. Sauvan, F. Ogando, E. González, P. T. León, F. Alvarez-Velarde.

[16] O. CABELLOS, J. SANZ, N. GARCÍA-HERRANZ, *Effect of activation cross-section*

uncertainties in the assessment of primary damage for MFE/IFE structural materials, The fifth International Conference on Inertial Fusion Sciences and Applications (IFSA2007), J. Phys.: Conf. Ser. 112 Volume 112 (2008) 032046 (4pp)

[17] O. CABELLOS, A. KLIX, U. FISCHER, N. GARCIA-HERRANZ, J. SANZ, S. SIMAKOV, *Impact of activation cross section uncertainties on the tritium production in the HFTM specimen cells*, 14th International Conference on Fusion Reactor Materials, September 6-11, 2009.

[18] O. CABELLOS, B. CABELLOS, N. GARCÍA-HERRANZ, J. SANZ, P. ORTEGO, C. TORE, *Sensitivity/uncertainty Analysis Applied to the Phase VII Benchmark*. International Workshop on Advances in Applications of Burnup Credit for Spent Fuel Storage, Transport, Reprocessing, and Disposition to be held in cooperation with the IAEA, 27-30 October 2009, Cordoba, Spain.

[19] O. CABELLOS, P. FERNÁNDEZ, D. RAPISARDA, N. GARCÍA-HERRANZ, Assessment of fissionable material behaviour in fission chambers, (accepted to be published in Nucl. Instr. Meth. A, 2010)

The TAPIRO Fast-Neutron Source Reactor as a support to Nuclear Data Assessment

M. Carta, O. Fiorani, R. Rosa, A. Santagata

ENEA – Via Anguillarese, 301 – 00123 Rome – Italy

Abstract. TAPIRO is a fast neutron source reactor operating at CASACCIA Research Center since 1971. The project, entirely developed by ENEA's staff, is based on the general concept of AFSR (Argonne Fast Source Reactor - Idaho Falls).
The reactor is equipped with a homogeneous cylindrical core having 6.29 cm as radius and 10.87 cm as height; cladding is provided by stainless steel (0.5 mm thickness) placed on a cylindrical copper reflector having (30 cm as thickness). All components assembled in a stainless steel tank, are placed inside a near spherical borated concrete shielding system having 1.75 m as thickness. Channels of various dimension and with different neutron spectra are distributed around the core. A large thermal column is manufactured by graphite blocks, suitable to be removed and replaced with experimental assemblies for any research purpose.
The TAPIRO possibilities for reactor experiments with energies up to 1.35 MeV will be illustrated.

1. Reactor layout

The TAPIRO reactor, located in the ENEA Casaccia Centre near Rome, is a highly enriched uranium-235 fast neutron facility. Since 1971, it has been used for fast reactor shielding experiments, biological effects of fast neutrons, etc. A sketch of the reactor is shown in Figures 1 and 2. The nominal power is 5 kW (thermal) and the core (with central neutron fluence rate of 4×10^{12} n · cm^{-2} · s^{-1}) is cooled by helium. The reactor cylindrical core (12.58 cm diameter and 10.87 cm height) is made of 93.5 % enriched uranium metal in a uranium-molybdenum alloy (98.5 % U, 1.5 % Mo in weight) and is totally reflected by copper; it is made by two overlapped cylindrical blocks: the upper one is fixed to the reactor structure whereas the lower one is movable and can drop in order to rapidly shut-down the system. The reactivity control is achieved by adjustment of the core neutron leakage from the reflector.

The copper reflector (cylindrical-shaped) is divided into two concentric zones: the inner zone, up to 17.4 cm radius, and the outer zone up to 40.0 cm. radius. The height of the reflector is 72.0 cm. A 60° sector of the external copper reflector is removable allowing insertion of fissile spectral conversion zones feeding the thermal column.

The reactor is surrounded by borate concrete shielding about 170 cm thick. Four experimental channels take place within the system: three different channels at the reactor midplane and one tangential (to the top edge of the core) channel. One midplane channel crosses over the core allowing measures of small samples (internal diameter of the channel in correspondence of the core ≈ 1 cm) in an almost pure U-235 fission spectrum.

A large experimental cavity, labeled thermal column (parallelepiped 110 × 110 × 160 cm), is present within the shield zone. The maximum depth available for the epithermal column is 160 cm (distance from the external surface of the reflector), reserved for filter/moderator materials.

2. Neutronics

At the full nominal reactor power, the total core integrated neutron source strength is of ≈ 3×10^{14} n/s. Such an integrated neutron source strength provides a total neutron fluence rate of ≈ 4×10^{12} $n \cdot cm^{-2} \cdot s^{-1}$ at the core center (≈ 8×10^{11} $n \cdot cm^{-2} \cdot s^{-1}$ > 1.35 MeV estimated by calculation) and a total neutron fluence rate of ≈ 1.5×10^{10} $n \cdot cm^{-2} \cdot s^{-1}$ (≈ 4×10^{7} $n \cdot cm^{-2} \cdot s^{-1}$ > 1.35 MeV estimated by calculation) at the entrance of the thermal column.
A large array of spectral shapes is available throughout the system.

3. Activities in Progress up-today

Actually, the reactor team (1 Director + 1 Supervisors + 1 trainee Operator + 1 Technician) drives the TAPIRO reactor in order to support R&D activities in the following fields:

- Materials: Characterization of N-16 counters devoted to monitoring functions in eastern Europe power plants. Neutron radiation damage on lead tungstate single crystals, APD's (Avalanche Photo Diodes) and optical flats in the frame of the ECOLE electromagnetic calorimeter design (CERN LHC-Large Hadron Collider Project). Neutron radiation influence on airspace electronic components (silicon based). Radiography and sectional radiography in the field of non-destructive analysis techniques.
- Radiology: BNCT (Boron Neutron Capture Therapy) and, in general, neutron radiation effects on cancerous cells [1].

4. Future Activities

4.1. Support to Accelerator-Driven System R&D

The TAPIRO source reactor provides a rich variety of relevant reference neutron spectra, with reasonably high neutron fluence rate (ranging from 10^{12} $n \cdot cm^{-2} \cdot s^{-1}$ at the core center to 10^{10} $n \cdot cm^{-2} \cdot s^{-1}$ within the thermal column). The natural capabilities of the system, conceived as a neutron source producer, consider its application in the field of the neutronic characterization of neutron source fed components.

- Different patterns of neutron field available in the system allow investigations of selected phenomena (like radiation damage) under a large variety of fluence and spectrum conditions.
- Static and dynamic neutron flux regimes may be employed in order to perform parametric studies on ADS prototypical fuel components inserted within the reactor thermal column (eventually fed by an auxiliary spectral converter zone).
- Steady neutron flux conditions may be employed to analyze, for example, the influence of fuel/Pb ratio on neutronic behavior of fuel-lead matrices.
- Dynamic neutron flux conditions, achievable by dropping the lower movable portion of the TAPIRO core, may reproduce absolute reactivity measurement conditions relative to source-jerk techniques.

4.2. Blanket Experiments

Benchmark experiments are possible on the fast source reactor TAPIRO in order to validate the neutronic codes for studying systems characterized by significant spectral changes within the core and blanket, as is the case for HTGR and fast systems. The experiments would consist in detection traverses in graphite and lead columns, starting from near external reflector boundary, where a sector of the outer copper reflector can be removed obtaining a very hard neutron spectrum. In experiments along the graphite column the spectrum gradually softens up to thermal values, whereas in experiments along the lead column the spectrum softens from hard to epithermal ones. Different materials would be interposed, such as U-nat, Pb, Fe, etc. to reproduce spectrum transition conditions at interface points between regions

with different compositions. Activation foils would be used for analysis with threshold energies in the fast, intermediate and epithermal regions. The activity measurement performed by quantitative gamma spectrometry will allow the detection of the neutron flux and spectral properties in a suitable number of energy groups for each of the given sets of control points. Other detection techniques, such as those utilizing fission chambers, would also be considered.

Analogous experiments on TAPIRO were performed in the early 70's for studying the propagation of neutrons along the axis of a large sodium tank inserted in place of the graphite column. It was a measurement campaign made in collaboration with CEA Cadarache within the fast reactor program and had a similar purpose, i.e., that of testing the ability of neutronic codes to reproduce the measured quantities. Those experimental data are now included in the NEA documentation within the International Reactor Physics Experiment Evaluation Project (IRPhEP [2]).

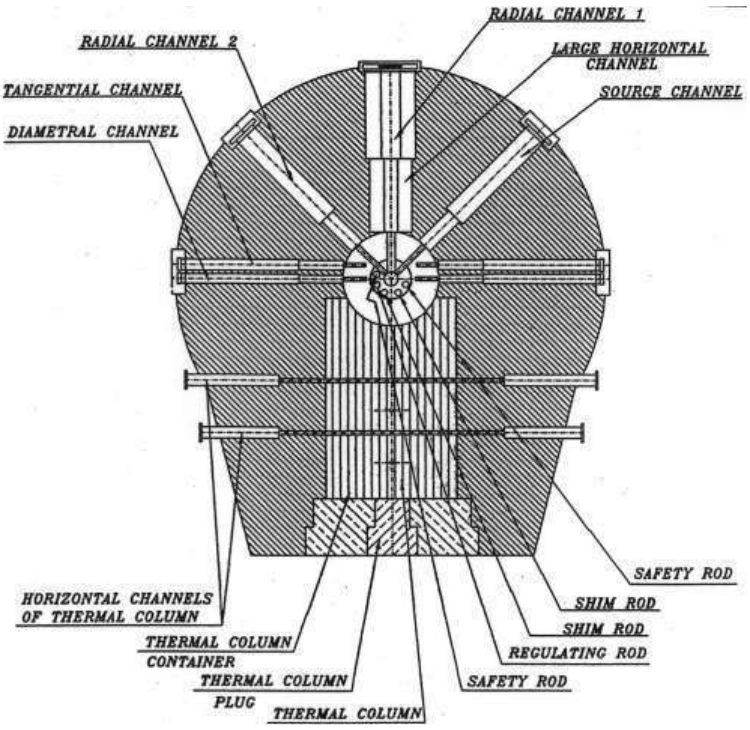

FIG.1. TAPIRO Horizontal Section

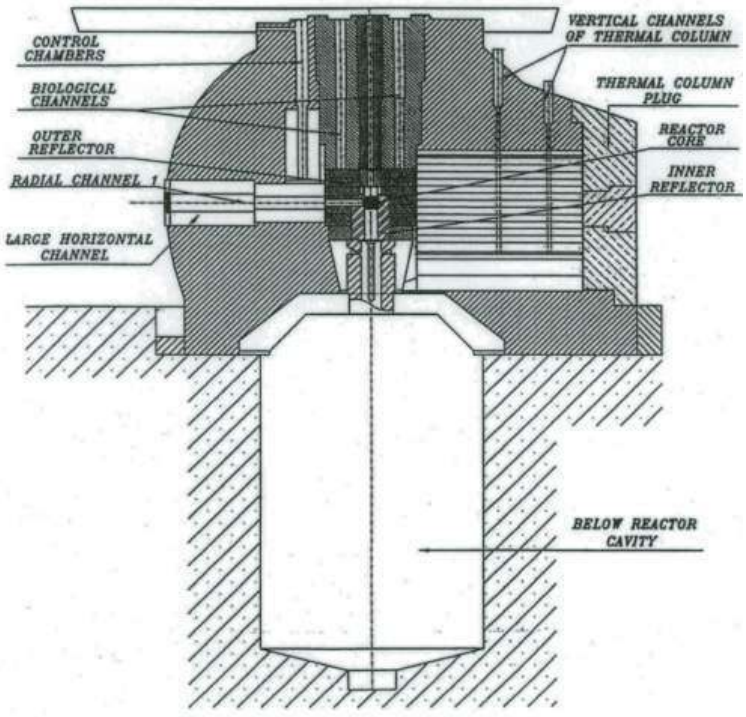

FIG.2. TAPIRO Vertical Section

5. Conclusion

The TAPIRO reactor, with its particular features in terms of neutron energy spectra, large thermal column cave and availability of irradiation channels in contact with the core combined with the flexibility in reflector material allowing can provide a valid experimental support to the nuclear data assessment.

A significant contribution may be given by the TAPIRO reactor in the validation of cross-section and codes in the fast neutron range. Integral experiments may be performed in different irradiation channels; especially, the large thermal column cave allows assembling of representative systems. An update of the neutronic characterization of the reactor, executed in the early 70's, is fundamental for the future activities.

REFERENCES

[1] R. ROSA, S. AGOSTEO, K.W. BURN, F. CASALI, A. FESTINESI, G. GAMBARINI, E. NAVA, G. ROSI, R. TINTI: ENEA's TAPIRO Fast Reactor: Epithermal Neutron Column for Boron Neutron Capture Therapy Experimental Program. Proceedings of the Villa Vigoni Workshop on Experimental Relating to Treatment of Tumors with Adrons, Menaggio (CO-I), September, 1-4, 1998, pp. 42-46.

[2] Evaluation Guide for the International Reactor Physics Experiments Evaluation Project (IRPhEP) NEA/NSC/DOC(2005)2.

Research potential of the McMaster nuclear reactor

Adriaan Buijs, Simon E. Day, Chris J. Heysel

McMaster University, Hamilton, Canada

Abstract. This presentation introduces the McMaster Nuclear Reactor (MNR): its design parameters, past and current use and possible future use as a research reactor for nuclear cross section measurements. MNR began operating in April 1959, as the first university-based research reactor in the Commonwealth of Nations, and remains the highest-flux reactor in a university environment in Canada to this day and the only research reactor in Canada with a full containment structure. The reactor is fuelled with low enrichment uranium (19.75% enriched, MTR-type plate fuel), and is cooled and moderated with light water. Current operation is 14 hours per day, five days per week at a thermal power of 3MW. Potential 24-hour operation at a thermal power of 5MW is being investigated.

1. Introduction

This report describes the McMaster Nuclear Reactor, its current use as a commercial and a scientific instrument, and its possible use in providing relevant nuclear data in the future. In order to provide some perspective, the code validation effort undertaken in the design of the next generation CANDU reactors is described as well.

2. The McMaster Nuclear Reactor

The McMaster Nuclear Reactor (MNR) is a swimming-pool design, MTR-type reactor located on the campus of McMaster University. MNR began operating in April 1959, as the first university-based research reactor in the Commonwealth of Nations, and remains the highest-flux reactor in a university environment in Canada, and the only research reactor in Canada with a full containment structure [1]. MNR continues to be operated for a variety of educational, research and commercial purposes.

The core is located near the bottom of the 10 metre-deep swimming pool. Coolant flow is either via natural circulation (for low power operation) or gravity-head driven down-flow. Forced flow make-up is accomplished via the primary pump. The MNR system is shown schematically in FIG..

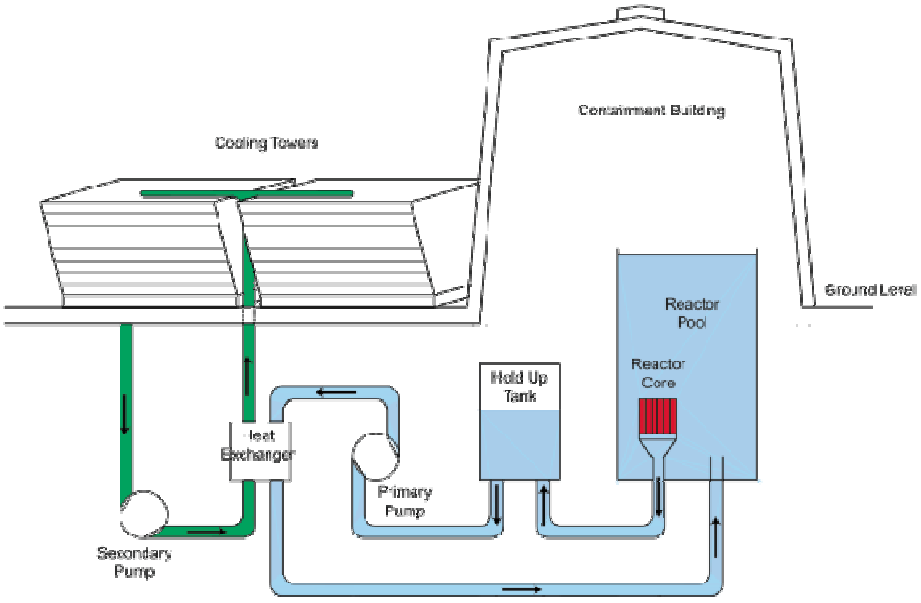

FIG.1. MNR Schematic

MNR is fuelled with LEU (19.75% enriched) plate fuel, having completed conversion via burnup in May 2008 under the guidance of the Reduced Enrichment for Research and Test Reactors (RERTR) program. A standard fuel assembly contains 18 curved plates, the inner 16 containing fuel. Control fuel assemblies are similar, containing nine (9) fuelled plates and an absorber rod guide. A schematic of a standard fuel assembly is shown in FIG.2.

The core is defined by a nine by six grid plate. A typical core contains on the order of 30 standard fuel assemblies and six (6) control fuel assemblies. Control is via a set of five (5) gang-operated Ag-In-Cd shim-safety rods and a single stainless-steel regulating rod. The Reference Core configuration (an analysis tool) is shown in
FIG.3.

The core is light-water cooled and -moderated with additional reflection provided by a row of graphite reflector assemblies. Irradiation facilities include both in-core and out-of-core positions, a pneumatic sample system for NAA, and a set of six radial beam-tubes, see Fig. 4. Current operation is 14 hours-per-day, five days-per-week, at a thermal power of 3MW. The peak flux in the central irradiation position at this power is 6 x 10^{13} n/cm^2/s. Lower flux positions are located on the edge of the core, in the graphite reflector and beyond the reflector. A single beryllium reflector assembly (in-core) can also accommodate irradiation samples.

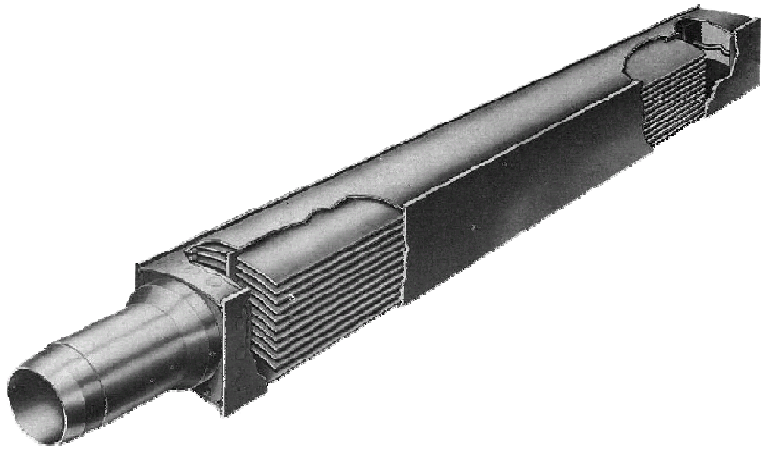

FIG.2. Cut-away schematic of an MTR-type fuel assembly

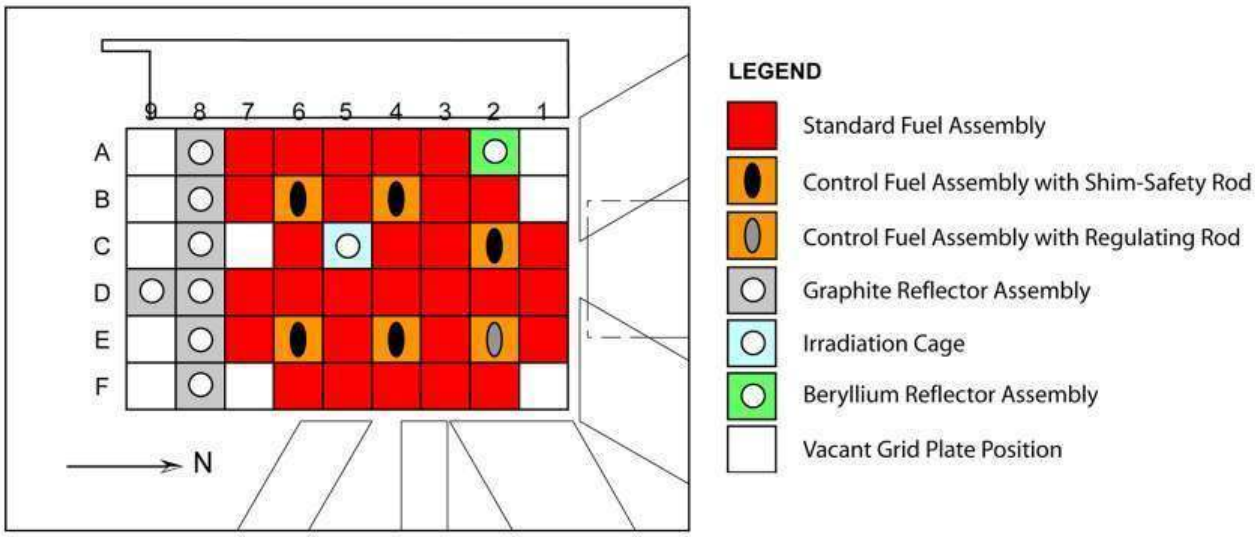

FIG.3. MNR Reference Core Configuration

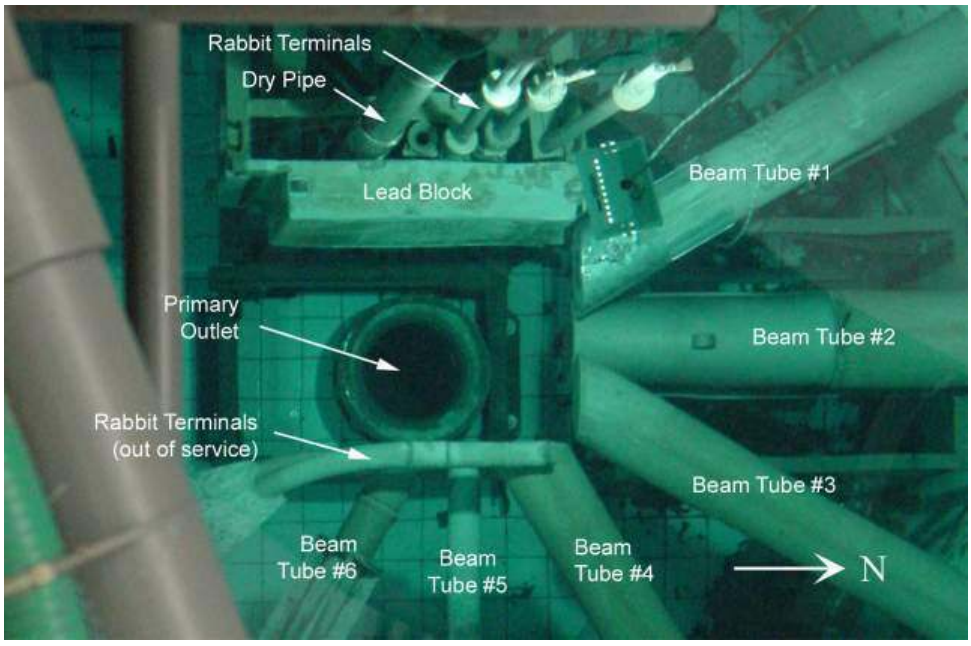

FIG.4. MNR Experimental Facilities

MNR is complemented by a set of high-level laboratories, including the Centre for Neutron Activation Analysis (CNAA), located in the adjoining Nuclear Research Building.

2.1 Commercial Use of MNR

The commercial use of the MNR has two main components:

1. The radiography of rotor blades for airplane engines; Two beam ports are dedicated to this activity. The radiographic scans of the rotor blades reveal possible defects in the blades;

2. The reactor currently produces I-125 which is used in the treatment of prostate cancer. It supplies enough I-125 to treat over 45,000 patients annually. The irradiation targets are in-core.

Other activities include the analytical services:

1. A prompt gamma activation analysis (dedicated beam port);
2. Delayed-neutron counting for the determination of low levels of uranium in samples;
3. Activation analysis of short-lived isotopes: Ca, Cl, Dy, F, I, In, K, Mg, Mn, Na, Rh, Se, Ti, V.

The services 2 and 3 use the pneumatic "rabbit" system. The channels available to these services are summarized in Table 1.

TABLE 1. SITE DESCRIPTION FOR ANALYTICAL SERVICES.

Site	Length, mm	Diameter, mm	Number of Sites	Flux n/cm^2s
CAPSULES	40	18	9	4×10^{13}
RIFLS	750	60	2	5×10^{12}
LVR	750	125	1	3×10^{11}
DRY TUBE	750	60	1	1×10^{12}
RABBITS	50	13	5	3×10^{12}

2.2 Current Research at MNR

In addition to activities related to commercial operation mentioned above, the MNR group is involved in research projects associated with a variety of groups external to McMaster, as well as internal:

- Currently producing the following medical isotopes
  - Na-24, Mn-56, Ir-192, Sc-46, Sb-124: for well-logging and other applications in the oil and gas industry;
  - Na-24, Cu-64, K-42: for biological studies (fish and plants);
  - Au-198, I-125: for cancer treatment.
- Others in small quantities for various one-of-a-kind applications;
- Reactor physics and safety analysis specific to MNR;
- NAA: Medical physics and other users inside McMaster;
- Real-time neutron radiography: installed on beam port number 3;
- Condensed Matter Physics: installed on beam port number 6;
- Archaeometry (the branch of archaeology that deals with dating of archaeological specimens through specific radio-isotope techniques) and NAA for archaeology (rabbit- as well as hot-cell based)

With all these applications, full-time use of MNR is ensured. With them, the reactor provides a service which is appreciated by users -- internal and external -- and indispensable for the

success of their research. The purely commercial activities of the reactor ensure a level of funding that supports operation and maintenance of the reactor.

2.3 Potential Future Research at MNR

As part of ongoing efforts to develop a diverse research program, MNR is currently involved in various R&D initiatives. Some of those are extensions of the research already being undertaken at MNR. They are:

- Reactor applications, activities related to:
  - Medical isotope production;
  - Material irradiation and Post Irradiation Examination (PIE);
  - An approved positron beam-line project.

Other activities are new and would need to be initiated:

- Potential Nuclear Data Research:
  - Code benchmarking for validation of methods and data libraries;
  - Beam-line chopper experiments for education and cross section measurement. A beam-line chopper has been built for educational purposes, but is not currently being used;
  - A mono-crystal-based energy selector may be built to provide a narrow thermal-energy beam for cross-section measurements;
  - NAA reactor-specific cross section determination for absolute value analysis & optimization.

2.4 Conclusions on the Research Potential of MNR

- MNR was designed as, and has been an excellent tool for fundamental research in nuclear physics and reactor physics.
- MNR is currently a facility of choice for many interdisciplinary research activities, both inside and outside the McMaster community.
- MNR is expertly operated and provides a flexible and co-operative research and development environment. Given the goal of developing a diverse research platform, the Reactor Group in collaboration with external faculty groups, are accepting of new opportunities.

2.5 The Use of Nuclear Data in the Design of the Advanced CANDU Reactor[3]

Canada is one of a few countries that is currently developing and marketing a new-generation (III+) power reactor. This reactor, the ACR-1000 is based on the classic design of the CANDU-6, and shares the following main attributes with it:

- Horizontal pressure tubes in a low-pressure moderator;
- On-power refuelling;
- A Heavy water moderator.

Features that set it apart from classic CANDUs are:

- Low enriched fuel, including absorbers such as Dy, Gd, and Hf as an impurity;
- Light-water coolant;

[3] Advanced CANDU Reactor, ACR and ACR-1000 are registered trademarks of Atomic Energy of Canada, Limited.

- Reduced lattice pitch;

These features ensure a more economical operation of the reactor in terms of burnup, lower capital costs as a result of a lower heavy-water inventory, and an increase of intrinsic safety features; For example a negative full-core void-reactivity and a distinctively negative power coefficient [2].

For the design of the ACR, no prototype is available (though existing CANDU reactors should be considered prototypes for the features that they have in common). The features beyond CANDU reactors are being designed on the basis of computer codes [3]. These codes have been successfully applied to CANDU reactors and were extended for applications that are new to ACR (WIMS 3.1, RFSP). Also, the Monte Carlo code MCNP has been used extensively. The codes include 2D and 3D transport codes for multi-group lattice calculations, and a 3-D, 2-group diffusion code for full-core calculations of dynamic effects and transients.

The validation of these codes is based on the following principles:

- The codes are validated **together** with their appropriate nuclear data libraries for the specific application of the ACR.
- The validation of the codes and libraries is provided by a **test reactor** (as opposed to a research reactor), ZED-2 at the Chalk River Laboratory in Ontario. The conditions in this test reactor are made to be similar to the ACR conditions as far as neutronics is concerned.
- The validation addresses a well-defined set of nuclear data libraries that were derived by AECL from the ENDF/B-VI data. The libraries were derived with the ACR-design in mind, both for MCNP and for the multigroup (89 groups) library for WIMS-AECL.
- At the test reactor, the relevant phenomena, such as the coolant void reactivity were measured, and biases and uncertainties were extracted.
- A methodology based on the TSUNAMI formalism was employed to extend this validation from the ZED-2 reactor to the ACR conditions. As part of this formalism, the following steps were taken:
    - Sensitivities to the nuclear data were established both for the ZED-2 reactor and the ACR design;
    - A quantification of the similarity of the ZED-2 and ACR reactor was established on the basis of the sensitivities, justifying the application of ZED-2 results to ACR design.
    - Nuclear data were adjusted (in terms of their uncertainties) to yield a k_{eff}=1 for the simulated ZED-2 experiments. The adjusted cross sections provided the code bias in the modelling of the ACR properties.
- Additional verification of the codes and libraries was performed using data from the proto-type reactor FUGEN in Japan, which is similar to the ACR design.

Finally, a completely independent effort is undertaken to verify the ACR parameters, with carefully selected **independent** codes (WIMS-9, PANTHER and MONK), and independently derived libraries (JEFF).

The validation scheme described here is self-consistent; on the basis of the current knowledge of nuclear data, with the use of test reactors and data from similar reactors such as FUGEN, the properties of the Advanced CANDU Reactor can be established to a level sufficient for licensing, construction and operation of the reactor.

While current data libraries provide a good modelling of test measurements, an increased accuracy of the nuclear data does reduce the need to rely on test reactors. The recent issuing of ENDF/B-VII, which has improved the modelling of critical systems considerably, serves as an example. Of course, this is being demonstrated with test reactor data.

3. Conclusion

- MNR was designed as, and has been an excellent tool for fundamental research in nuclear physics and reactor physics.
- MNR is currently a facility of choice for many interdisciplinary research activities, both inside and outside the McMaster community.
- MNR is expertly operated and provides a flexible and co-operative research and development environment. Given the goal of developing a diverse research platform, the Reactor Group in collaboration with external faculty groups, are accepting of new opportunities.
- This paper also described the Canadian effort in designing the next generation CANDU reactor, and the role that nuclear data play in this design.

REFERENCES

[1] A.E. PIDRUCZNY, M.P. BUTLER, P.C. ERNST, M.F. COLLINS and J.M. AVELAR, The McMaster University Nuclear Reactor (MNR) Research Facilities, J. Radioanal. Nucl. Chem. **180** (2) (1994) 313-318.

[2] A. BUIJS *et al*., "The Physics Design of the Advanced CANDU Reactor", International Conference on Reactor Physics, Nuclear Power: A Sustainable Resource, Casino-Kursaal Conference Center, Interlaken, Switzerland, September 14-19, 2008

[3] A. BUIJS, "The Design Process and Simulation Tools Used in the Neutronic Design of the ACR-1000 Core", CNS 23rd Nuclear Simulation Symposium, Ottawa Nov 2-4, 2008.

Provision of Nuclear Data by Experiments at the High Flux Reactor of the Institut Laue Langevin

Ulli Köster , Michael Jentschel

[a] Institut Laue Langevin, 6 rue Jules Horowitz, 38042 Grenoble Cedex 9, France

Abstract. The Institut Laue Langevin in Grenoble hosts about forty instruments that are served with neutrons by a 58 MW high flux reactor. In-pile positions with neutron fluxes up to 1.5×10^{15} $cm^{-2}s^{-1}$ are available. Most instruments use extracted neutron beams with neutron energies ranging from few neV to about 1 eV, reaching capture fluxes up to 2×10^{10} $cm^{-2}s^{-1}$. Optionally these neutron beams can be spin polarized to >99%, rendered monochromatic by crystal diffraction or velocity selectors or chopped for time-of-flight measurements. An overview on provision of nuclear data by ILL instruments is given. In particular we discuss how some established instruments that traditionally served specific purposes can be temporarily converted to serve new applications. Examples are the use of the fission fragment separator LOHENGRIN for high resolution measurements of rare (n,α) and (n,p) reactions and the use of the crystal spectrometers GAMS for (n_{th},γ) cross-section measurements on in-situ bred radioactive isotopes.

Introduction

The 58 MW high flux reactor of the Institut Laue Langevin in Grenoble provides slow neutrons for about 40 different instruments. Most of these instruments use extracted neutron beams for neutron scattering applications, but some of these instruments can be used for nuclear data measurements. This covers nuclear data in a wide sense: cross-sections, branching ratios, half-lives, fission yields, fission product properties, gamma ray energies, binding energies, scattering lengths, etc.
An extensive review of such applications of ILL instruments was given recently [1]. In the present contribution we focus the discussion on some specific examples and show how some established instruments that traditionally served specific purposes can be temporarily converted to serve new applications.

The fission fragment separator LOHENGRIN

The recoil separator LOHENGRIN [2] at ILL provides mass- and energy-separated fission fragment beams. A fissile or fertile actinide target is placed in an in-pile position at a thermal neutron flux of 5.5×10^{14} $cm^{-2}s^{-1}$, see Fig. 1. The fission products are emitted into 4π solid angle. When leaving the target with kinetic energies of typically 0.3 to 1.3 MeV per nucleon, several electrons are stripped off and the ions acquire an average equilibrium charge state between 18+ and 25+. Ions emitted into a small solid angle of about 3×10^{-5} sterad reach, after 8 m flight through an evacuated beam tube, a 45° dipole magnet that will deflect and analyze them according to their momentum over ionic charge ratio. Subsequently the ions are deflected vertically by a 35.5° cylindrical condensator. This electrostatic deflector performs an analysis according to kinetic energy over ionic charge. The combination of both magnetic and electric fields results in a separation according to mass over ionic charge and a separation according to kinetic energy in perpendicular direction. For a usual target size of 7x0.5 cm^2 the mass resolving power is 600 and the energy resolution about 1%. If needed, both values can be further improved by using smaller targets.

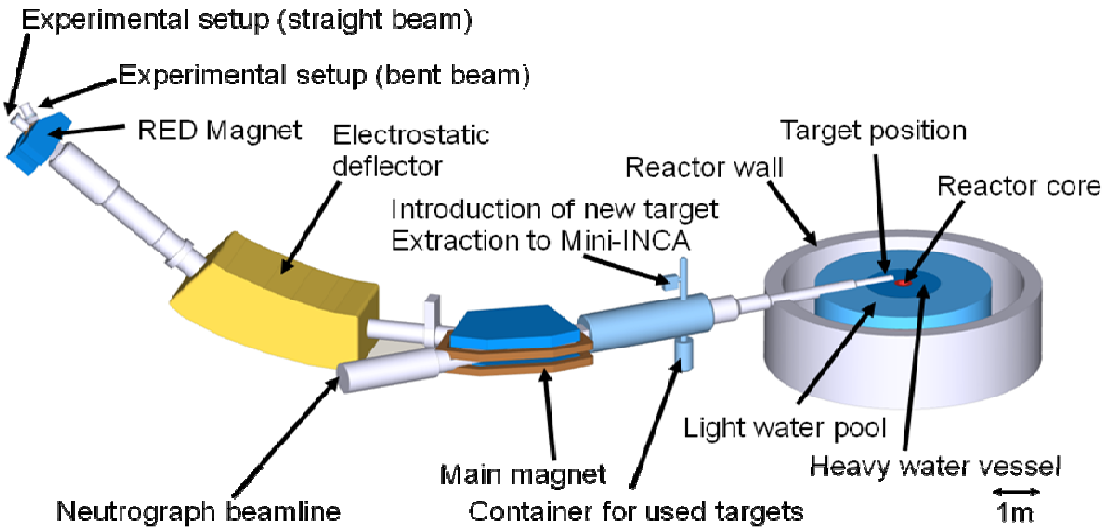

FIG.1. Set-up of the LOHENGRIN recoil separator.

Fission yield measurements

Yields and kinetic energy distributions of fission fragments are determined by scanning mass by mass the distributions in ionic charge state and kinetic energy and counting the ions in the focal plane. The mass yields are readily obtained by integrating over ionic charge and kinetic energy. For light elements ($Z<40$) an ionization chamber with split anode allows identifying isobars by their specific energy loss. Thus, isotopic yields of light binary and of ternary fission fragments are directly measured by ion counting.

Fission yields and kinetic energy distributions of light binary fission fragments and of ternary particles were determined at LOHENGRIN for many fission systems ranging from ^{229}Th(n,f) to ^{251}Cf(n,f) [1]. Even very exotic ternary fission fragments like the halo nuclei ^{11}Li and ^{14}Be could be clearly identified with yields as low as 10^{-10} per fission [3].

When the ultimate energy resolution is not needed, the so-called RED (reverse energy dispersion) magnet [33] focuses up to 40 cm of the energy dispersed beam (i.e. $\Delta E/E=5.5\%$) from the focal plane onto a few cm length. This area can be surrounded by an efficient array of radiation detectors. Usually two fourfold clover Ge detectors and one coaxial Ge detector are used for gamma detection. Occasionally additional Ge detectors provided by the users are installed.

Gamma spectroscopy allows identifying isobars also for heavier elements ($Z>40$). Combining the electro-magnetic mass separation of LOHENGRIN with gamma spectrometry it became recently possible to measure the isotopic fission yields of heavy fragments in ^{239}Pu(n,f) [4]. Similar measurements of heavy fission fragments and in the valley of symmetry are planned for other fission systems to complement the existing yield data that is mostly limited to the light fission peak.

Interesting fission studies could be performed in various mass regions once suitable target material consisting of ^{229}Th, ^{231}Pa, ^{232}U or ^{236}Np became available.

Nuclear spectroscopy

Apart from fission yield measurements the mass-separated radioactive ion beams can also be used for decay spectroscopy. The setup is particularly efficient for the study of microsecond

isomers. Due to the short transport time through the separator (1-2 μs) even the decay of isomeric states with half-lives down to 0.5 μs can be studied [5]. Isomers in very neutron-rich isotopes (e.g. in ^{136}Sb with N/Z = 1.67 [6]) and with excitation energies up to 6.6 MeV (17^- isomer in ^{98}Zr [5]) have been studied. A review of some LOHENGRIN experiments on microsecond isomers can be found in ref. [7,8].

For conversion electron spectroscopy a LN_2 cooled Si detector is available and for ultrafast timing measurements several $LaBr_3$:Ce detectors. Beta-detection for beta-gamma spectroscopy is performed with plastic scintillation detectors. Beta-delayed neutrons are detected with an array of 18 ^{3}He tubes embedded in a polyethylene matrix [9].

An electrostatic beam chopper allows modulating the continuous fission fragment beam to beam-on/beam-off periods from few milli-seconds to hours. Thus longer-lived isomers and isotopes can be identified by following the grow-in and decay of the respective gamma rays. A tape system serves for removal of long-lived activity.

Fission of the standard actinide isotopes ^{233}U, ^{235}U, ^{239}Pu and ^{241}Pu is well suited for population of neutron-rich isotopes and isomers in the mass ranges 79 to 113 and 127 to 156. The remaining valley of symmetry (mass 114 to 126) and very neutron-rich lanthanide isotopes would be best populated by fission of higher Z targets. Cm and Cf targets of sufficient mass would allow pushing nuclear spectroscopy in the little explored regions of mass 114 to 126 and beyond mass 156. Such targets do not necessarily require isotopically separated material since the non-fissile even mass isotopes will eventually be bred to the fissile odd mass isotopes and contribute to the fission rate. Thus, a perfect target for this purpose would consist of a mixture of various Cm or Cf isotopes that is sufficiently “old” so that the short-lived isotopes (^{243,244}Cm and ^{250,252}Cf respectively) are somewhat depleted to limit the total alpha activity.

High-resolution (n,α) and (n,p) spectroscopy

Usually considered as fission fragment separator, LOHENGRIN is also very suitable for high-resolution spectroscopy of alphas, protons and corresponding recoil nuclei produced in (n,α) and (n,p) reactions respectively. The high neutron flux at the target position enables to breed radioactive nuclei, which in turn undergo (n,α) or (n,p) reactions. Examples are ^{58}Ni(n,γ)^{59}Ni(n,α) [see Fig. 2], ^{58}Ni(n,γ)^{59}Ni(n,p) [see Fig. 3], ^{151}Eu(n,γ)^{152}Eu(n,p) or ^{151}Eu(n,γ)^{152}Eu(β$^-$)^{152}Gd(n,γ)^{153}Gd(n,α). Due to the electro-magnetic separation protons and alphas do not interfere in the detector. Therefore, weak proton lines are detectable even for strong (n,α) emitters.

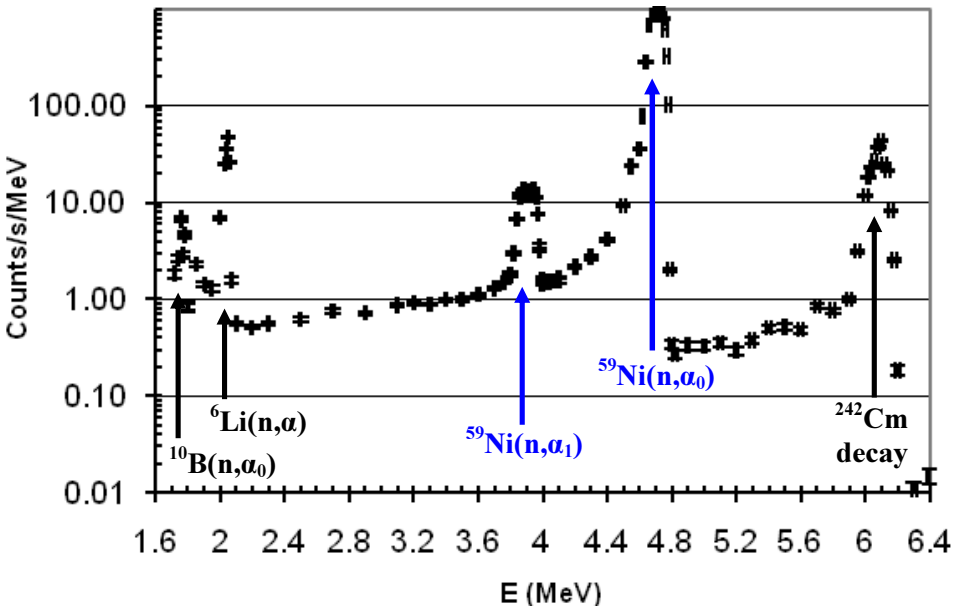

FIG.2. Alpha spectrum measured with a 0.25 µm thick nickel foil with originally natural isotopic composition that had been exposed to a thermal neutron fluence of 6×10^{21} cm^{-2}. Specific background lines are discussed in the text.

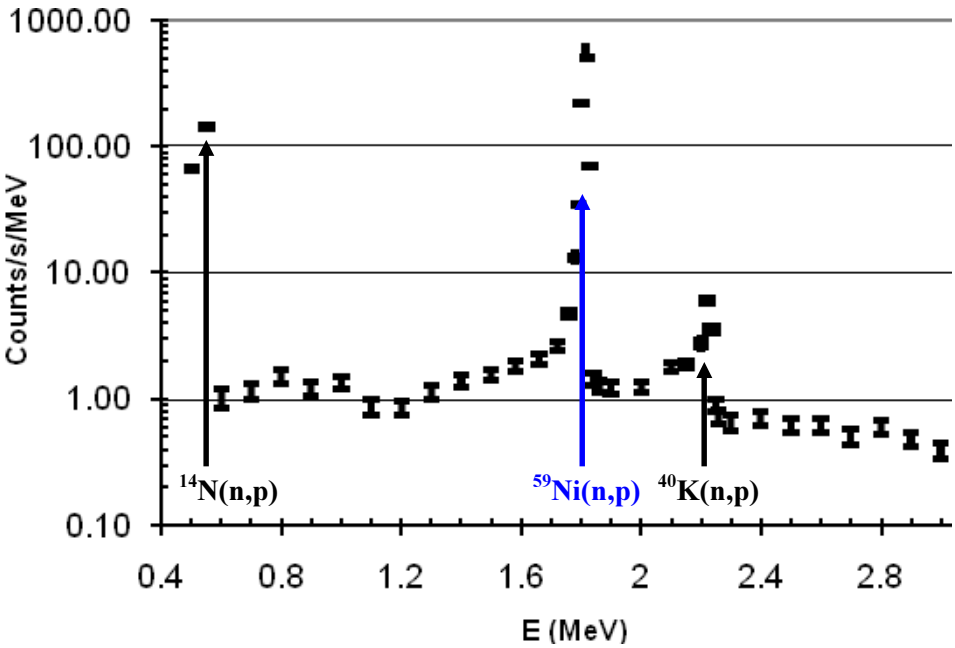

FIG.3. Proton spectrum measured with a 0.25 µm thick nickel foil with originally natural isotopic composition that had been exposed to a thermal neutron fluence of 6×10^{21} cm^{-2}. Specific background lines are discussed in the text.

Compared to direct measurements at external neutron beams the presence of some LOHENGRIN specific background has to be considered: 6.1 MeV alphas stem from ^{242}Cm decay. The latter was produced by transmutation of ^{241}Am targets from which a small amount has been sputtered off by the fission products and deposited on the target holder. ^{10}B(n,α) background is due to boron diaphragms in the beam tube. Also ^{6}Li(n,α) may occur from residues of LiF that were self-sputtered on the target holder from LiF targets used to tune the spectrometer. Finally ^{40}K(n,α) and ^{40}K(n,p) background occurs which is bred from traces of natural potassium ("finger prints") on the target holder. Such background can cover weak lines that fall exactly at the same energies. Protons below 0.6 MeV cannot be detected due to background from ^{14}N(n,p) in the rest gas of the beam tube.

The GAMS crystal spectrometers

The instrument GAMS has a tangential through-going beam tube, see Fig. 4. Samples are placed in a thermal neutron flux of 5×10^{14} $cm^{-2}s^{-1}$. Emitted prompt or delayed capture gamma rays are tightly collimated onto two crystal spectrometers placed at 17 and 21 m respectively from the target. After Bragg diffraction on one or two perfect Si or Ge crystals the gamma ray intensity is monitored with a Ge detector. Scanning the angle of the diffracting crystal allows measuring with high resolution the energy of the gamma rays. The rotation angle is measured absolutely by laser interferometers providing excellent accuracy for the deduced gamma ray energies. Therefore, most reference energies that are today commonly used in gamma-ray spectroscopy are based on measurements at GAMS. Summing all measured energies of a gamma-ray cascade after thermal neutron capture allows measuring the neutron binding energy [10]. Such measurements provide precision data on nuclear masses, complementary to Penning trap measurements [11]. The flat crystal spectrometer GAMS4 [12] is presently being upgraded to GAMS6 [13] with even higher accuracy.

Not only the centre of a measured gamma-ray energy distribution carries physics information, but also its width: a detailed analysis of the Doppler broadening of the energy distribution of secondary gamma-rays allows deducing the lifetime of intermediate levels in the range of femtoseconds to picoseconds. This so-called GRID (Gamma Ray Induced Doppler broadening) method [14] has provided important information on transition strengths; see e.g. ref. [15]. Also neutrino-induced Doppler-broadening has been observed [16].

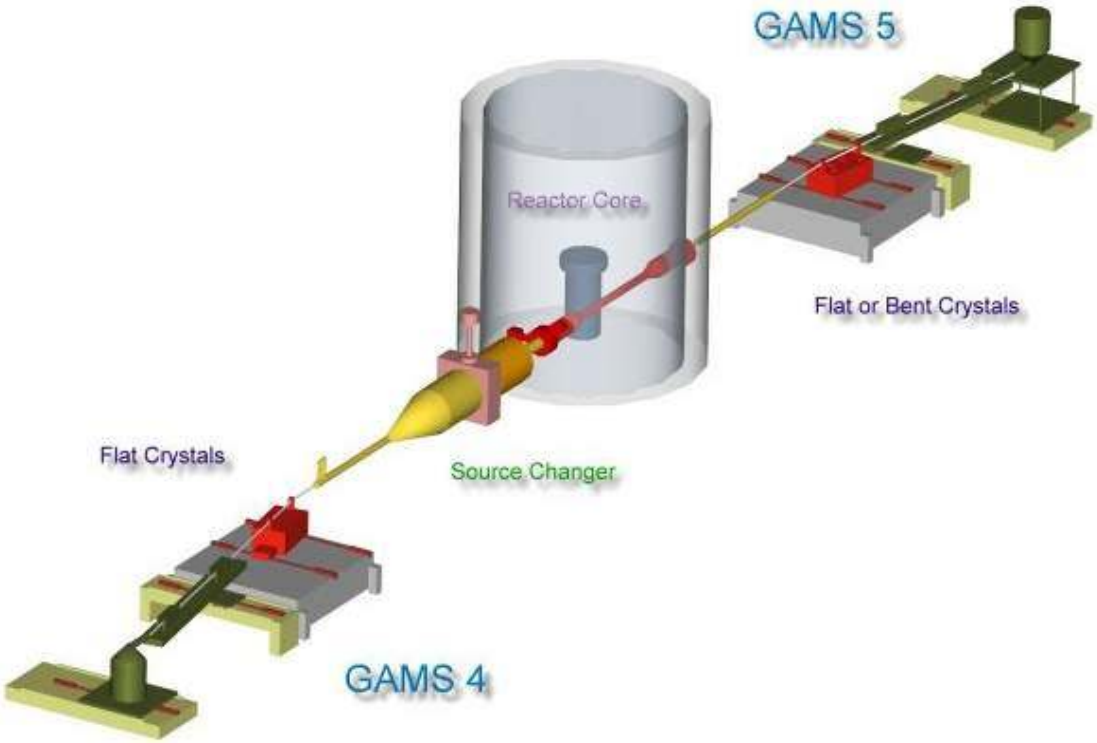

FIG.4. Set-up of the GAMS crystal spectrometers for high resolution spectroscopy of capture and decay gamma-rays.

Bent crystal spectrometer

Flat crystal spectrometers provide the highest possible resolution, but they suffer from an intrinsically low solid angle acceptance. Therefore, samples of several grams are needed and, only relatively strong gamma transitions can be used for spectroscopy. An alternative are bent

crystal spectrometers in DuMond geometry with a three to four orders of magnitude higher angular acceptance [17]. The GAMS5 spectrometer can be used alternatively with flat or bent crystals [18]. With bent crystals the amount of sample material can be reduced to some ten milligrams, i.e. rare, highly enriched sample material can be used for nuclear spectroscopy. Also radioactive samples can be used, e.g. enriched targets of ^{40}K [19], ^{99}Tc [20], ^{129}I [21], ^{226}Ra [22, 23], ^{230}Th [22, 24], ^{232}Th [22, 25], ^{234}U [26, 27], ^{238}U [27, 28], 237Np [29], ^{240}Pu [30], ^{244}Pu [22], ^{241}Am [31], ^{243}Am [32], ^{248}Cm [33] have been used. While lower compared to flat crystals, the energy resolution of bent crystals still exceeds by far that of Ge detectors, in particular for low gamma ray energies of some ten to hundred keV. At 100 keV gamma ray energy the resolution in first order is about 30 eV, for higher diffraction orders the resolution improves proportional to the order. Depending on the energy and intensity of the line, measurements are possible till about fifth order. Thus, doublets or multiplets are usually fully resolved. Due to the high energy resolution, excitation schemes can often be built solely based on the Ritz principle.

For energies above 1 MeV the resolution of bent crystal spectrometers drops below that of a good Ge detector. Still, the fact that other gamma-ray energies are physically separated from the beam by diffraction into a different direction assures an excellent peak to background separation. The dynamic range is basically only limited by the source strength. Often five orders of magnitude are accessible, which is far better than any Compton suppressed Ge detector could achieve.

Multi-neutron capture reactions

The neutron flux at the GAMS target position is nearly as high as at the LOHENGRIN target position. Therefore also here multi-neutron-capture reactions can be used to populate nuclei further from stability and nuclear spectroscopy has been performed for neutron-rich nuclei that are several neutrons away from stability. Examples are ^{192}Os(n,γ)^{193}Os(n,γ)^{194}Os [34], ^{153}Eu(n,γ)^{154}Eu(n,γ)^{155}Eu(n,γ)^{156}Eu [35] or ^{226}Ra(n,γ)^{227}Ra(β$^-$)^{227}Ac(n,γ)^{228}Ac(β$^-$)^{228}Th [22].

The capture cross-sections on intermediate unstable isotopes can be deduced from the time dependence of the intensities of the different capture and decay gamma-rays. Thus, in addition to nuclear spectroscopy results new cross-sections could as well be derived from several GAMS measurements, e.g. for ^{75}Se(n,γ) [36].

Finely collimated, the gamma-ray beam can also be used for direct spectroscopy with a Ge detector. Complemented by surrounding NaI detectors the Ge detector serves either as pair spectrometer for high energy gamma-rays or as Compton suppressed Ge detector for lower energy gamma-rays. Such an arrangement was previously used at the R1 reactor in Stockholm [37], but at present GAMS at ILL seems to be the sole research reactor equipped with a through-going beam tube and an in-pile target for gamma-ray spectroscopy.

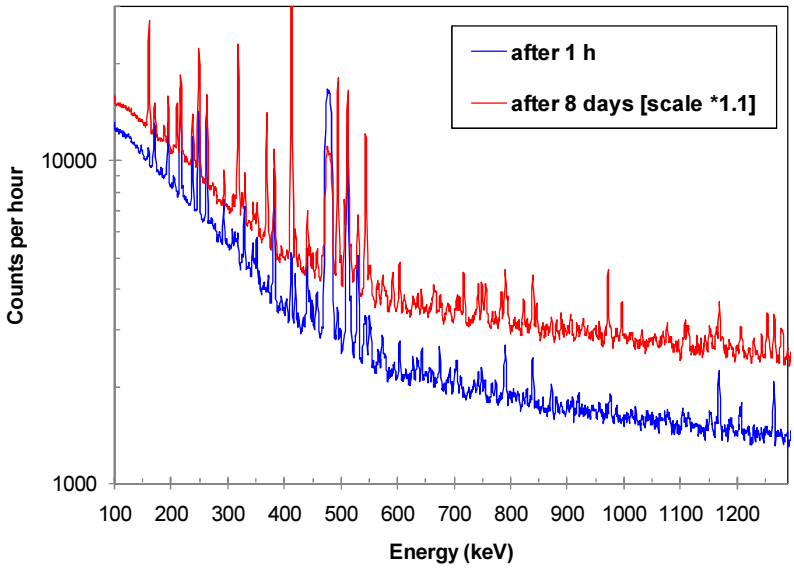

FIG.5. Direct gamma-ray spectra of a gold foil in the GAMS in-pile target position exposed to the neutron flux for one hour and eight days, respectively.

Figure 5 shows direct gamma-ray spectra taken from a thin Au target in the GAMS target position. The observed gamma lines are initially prompt lines of ^{197}Au(n,γ), later are growing-in the decay line of ^{197}Au as well as prompt and delayed lines of ^{198}Au(n,γ), ^{199}Au(n,γ), ^{199}Hg(n,γ). Background lines are mainly from ^{27}Al(n,γ) (since the Au foil is enclosed in a Al foil wrapping), ^{23}Na(n,γ) and ^{35}Cl(n.γ) (due to traces of NaCl on the target holder). The 511 keV peak stems principally from high energy gamma rays from the reactor core that undergo pair creation and annihilation in the target and target environment, respectively. The broad 478 keV peak originates from ^{10}B(n,αγ) in boron diaphragms in the beam tube. Crystal spectrometers have intrinsically a smaller solid angle acceptance than the direct observation with Ge detectors. Hence, the background lines that are emitted from the area around the target are correspondingly reduced when using crystal spectrometers.

The V4 high flux irradiation position

A still higher neutron flux compared to the LOHENGRIN and GAMS in-pile positions is available in the V4 vertical beam tube. Its irradiation position at only 15 cm distance from the reactor core provides at full reactor power a flux of about 1.5×10^{15} cm^{-2}s^{-1} thermal neutrons, 3×10^{14} cm^{-2}s^{-1} epithermal neutrons (0.625 eV < E < 0.82 MeV) and 2×10^{13} cm^{-2}s^{-1} fast neutrons (E>0.82 MeV). This maximum neutron flux is available close to the bottom of the beam tube. Higher up the flux drops and the ratio of thermal to epithermal neutrons increases. Samples are enclosed in quartz ampoules and Al capsules and irradiated in an irradiation shuttle up to many weeks. After decay for some days the irradiation shuttle is opened in a hot cell and the samples can be retrieved for nuclear spectroscopy or other investigations.

Miniature fission ionization chambers with on-line current measurement allow following the evolution of the fission rate during an irradiation over several weeks [38]. See ref. [39] for a detailed discussion of transmutation experiments with actinide samples in V4.

At present V4 is being used for production of radioisotopes for medical applications [40]. In a test irradiation of various $^{186}WO_3$ samples specific ^{188}W activities up to 126 GBq/g were obtained after a 49 day irradiation at 90% of nominal reactor power. This thick target result is only about one fifth of the specific activity expected for a thin target with the published cross-

sections: 37 b for ^{186}W(n,γ), 70 b for ^{187}W(n,γ) and 12 b for ^{188}W(n,γ). A similar discrepancy was already observed previously in ^{188}W production at other reactors [41, 42]. Obviously the ^{187}W(n,γ) cross-section is in reality significantly smaller or/and the ^{188}W(n,γ) destruction cross-section significantly larger than the published ones. New cross-section measurements are under way at ILL to solve this discrepancy. The magnitude of the ^{188}W(n,γ) cross-section is decisive for the ultimately reachable specific activity. If this cross-section is sufficiently small, the specific activity could be further increased by irradiating longer, e.g. for two consecutive reactor cycles of 50 days each.

Due to its long lifetime ^{188}W is ideally suited for production runs in a full reactor cycle of 50 days. After decay of ^{187}W for at least 7 days, the activated ^{186}W target can be removed from the irradiation position, packed and shipped to ITG (Isotope Technologies Garching) for radiochemical processing. The present ILL authorization permits irradiation of up to 10 grams of ^{186}W per irradiation shuttle. Thus about 5 TBq (135 Ci) ^{188}W can be produced per year. In combination with the high quality ITG ^{188}W/^{188}Re generators this assures the required isotope supply for a large-scale application of endovascular brachytherapy with ^{188}Re [43] and of therapy with ^{188}Re labelled radiopharmaceuticals.

Successful test irradiations have also been performed with enriched $^{176}Yb_2O_3$ targets to produce non-carrier-added ^{177g}Lu. This indirect way of producing the therapeutic isotope ^{177g}Lu (e.g. used for peptide receptor radioisotope therapy of gastrointestinal tumors) via beta-decay of ^{177}Yb followed by a chemical Lu/Yb separation provides pure ^{177g}Lu with very high specific activities, above 3000 TBq/g of lanthanide [44]. Compared to the standard production via ^{176}Lu(n,γ), it moreover avoids producing the disturbing long-lived isomer ^{177m}Lu. The latter may cause a waste handling problem for hospitals that are using ^{177}Lu for therapy [45]. The only drawback of the indirect method is the cross-section for ^{176}Yb(n,γ) that is nearly three orders of magnitude lower compared to the ^{176}Lu(n,γ) cross-section. Therefore, irradiation positions with high neutron flux are required to compensate the low cross-section and make best use of the rare enriched ^{176}Yb targets.

When producing ^{99}Mo by thermal neutron capture on ^{98}Mo one is confronted with an even lower cross-section for thermal neutron capture of only 0.14 b. A test irradiation in the V4 beam tube has shown that despite this low cross-section saturation activities above 1 TBq ^{99}Mo per g of ^{98}Mo are possible (due to the significant resonance integral of 7 b the epithermal component contributes, too). This is sufficiently high to use standard generator technology (acidic alumina columns) to produce high quality ^{99}Mo/^{99m}Tc generators.

Instruments using extracted neutron beams

Most instruments at ILL are devoted to neutron scattering. They can be classified as [46]:

a) two-axis diffractometers with one- or two-dimensional neutron detectors,
b) three-axis spectrometers with an energy analyzing crystal between sample and neutron detector to study inelastic processes,
c) time-of-flight spectrometers with a chopped neutron beam.

All these instruments use monochromatic neutron beams that are provided by Bragg diffraction on a monochromator crystal. Some monochromators focus the neutron beam horizontally and/or vertically onto the sample to increase the flux.

Hot neutrons

The beam tubes of some of these instruments are pointing at the "hot neutron source" of the ILL reactor, a thermally insulated graphite cylinder (20 cm diameter and 30 cm height) placed at about 20 cm from the fuel element that is heated by gamma radiation from the reactor core to about 2000 °C. Thus, the neutron spectrum is shifted towards higher energies and shorter wavelengths compared to thermal neutrons. After crystal diffraction monochromatic "hot" neutrons are available for experiments. At 0.1 eV neutron energy a flux of 4×10^{7} $cm^{-2}s^{-1}$ is available, dropping to 10^{6} $cm^{-2}s^{-1}$ at 1 eV. In principle one could temporarily convert such a scattering instrument for measurements of cross-sections with monochromatic hot neutron beams by placing a suitable detector downstream or besides of the sample.

Cold neutrons

The thermal neutron energy spectrum of the reactor can also be shifted to lower energies and longer wavelengths by down-moderation in one of ILL's two cold sources. These are in-pile vessels filled with 25 K cold liquid deuterium. Neutron guides pointing at a cold source will extract a spectrum of cold neutrons. Several instruments are served by these neutron guides, thereof one instrument that is dedicated to applications in nuclear and neutron physics: PF1B.

The PF1B intense cold neutron beam with polarization option

PF1B is a multipurpose beam port where an intense beam of cold neutrons with a capture flux of 2×10^{10} $cm^{-2}s^{-1}$ on a 20×6 cm^{2} area is available. The cold neutrons are transported from the cold source by a 72 m long ballistic supermirror neutron guide [47] with little losses to the experimental area while eliminating background of gamma rays or fast neutrons from the reactor completely. Remaining background of fast neutrons (approx. 10^{-6} of the slow neutron flux [48]) and gamma rays is mainly generated locally by the neutron beam collimation system. The average neutron energy of the PF1B beam is 5.4 meV corresponding to a Maxwellian spectrum at 62 K. With the use of super-mirror polarizers, the PF1B neutron beam can be polarized up to 99.7%. For a fully polarized beam the capture flux is still 3×10^{9} $cm^{-2}s^{-1}$.

The most frequent application of the polarized PF1B beam is for studies of the free neutron decay. Various standard model parameters can be extracted from a precise measurement of angular distributions and correlations of the electrons and protons emitted in neutron decay, see e.g. [49]. Parity violating asymmetry was also observed in neutron-induced reactions, namely for the tritons emitted in $^{6}Li(n,\alpha)t$ and the gamma rays emitted in $^{10}B(n,\alpha\gamma)^{7}Li$ reactions induced by polarized cold neutrons [50]. Surprisingly, neutron polarization affects the angular distribution of ternary particles emitted in cold-neutron induced fission of ^{235}U, too [51].

Unpolarized, the intense cold neutron beam serves for cross-section measurements. For example the $^{39}Ar(n,\alpha)$ reaction was studied at PF1B [52]. Measurements of fission cross-sections and of yields and energy distributions of ternary fission fragments [53] at PF1B are reviewed in ref. [4]. Due to the excellent stability of the neutron beam intensity it is possible to deduce absolute cross-sections from subsequently performed relative measurements with the sample and a reference sample, respectively.

The large area experimental zone ($3\times10\times3$ m^{3}) permits the installation of complex setups. Fission targets can be surrounded by an array of Ge detectors for spectroscopy of prompt and delayed gamma transitions. The discovery of nanosecond-isomers in fission fragments with such a setup is discussed in ref. [54].

While many experiments use the entire spectrum of the white neutron beam, it is also possible to select individual energies. A Dornier/Astrium velocity selector rotating at up to 28300 rpm allows selecting neutron energies from 0.02 to 13 meV with a transmission above 80% and a velocity resolution of about 10% FWHM [55].

Very cold and ultracold neutrons at PF2

Still lower neutron energies compared to PF1B are available at the PF2 beam lines [56]. A vertical beam tube extracts neutrons from the vertical cold source. The progressive curvature of the neutron guide eliminates all neutrons but those with the lowest energies. This results in a beam of very cold neutrons with a flux of 4×10^6 $cm^{-2}s^{-1}$ at 8 μeV over an area of 7×3.4 cm^2. Very cold neutrons (VCNs) can be "cooled" even further by collisions with a neutron turbine. The produced ultracold neutrons (UCNs) with energies between 0 and 250 neV are totally reflected under all angles from suitable surfaces (e.g. nickel, diamond-like-carbon, beryllium, etc.) and can thus be stored for several minutes in so-called neutron bottles.

A flux of 3×10^4 $cm^{-2}s^{-1}$ UCNs is available over an area up to 14×10 cm^2. Due to the 1/v behaviour the cross-sections for VCNs and UCNs are huge, making it possible to achieve significant absorption even for very thin samples, e.g. made from rare enriched or highly radioactive isotopes. For extremely high cross-sections of several ten Mbarn even deviations from the exponential attenuation law are expected [57].

Actinide samples

Actinide targets can be routinely used at most ILL instruments. At instruments in the neutron guide halls actinide samples with a radiotoxicity equivalent to 20 MBq ^{239}Pu (as unspecified compound with 1 μm granularity) can be used. This corresponds to 0.3 g ^{233}U, 1.5 g ^{235}U, 8 mg ^{239}Pu, 0.3 mg ^{241}Pu, 3 mg ^{245}Cm, 0.2 mg ^{251}Cf, etc. Due to the high neutron flux such sample quantities are usually sufficient for most applications. For target compounds with smaller dose conversion factor for inhalation h_{inh}, (e.g. less volatile oxides with large granularity) correspondingly higher activities are allowed. Still higher activities (equivalent to 370 MBq ^{239}Pu) can be handled at instruments situated in the reactor hall, i.e. at Neutrograph, PF2, the hot neutron instruments, etc. At LOHENGRIN and Mini-INCA samples with activities up to 3.7 GBq activity can be used.

Conclusion and Outlook

The high flux reactor of ILL is equipped with several unique instruments for nuclear data measurements. LOHENGRIN is the world-leading spectrometer for precise studies of thermal neutron induced fission and competes well for nuclear spectroscopy of isomers and isotopes with lifetimes ranging from microseconds to seconds. Many interesting fission studies and nuclear spectroscopy studies would benefit from the availability of suitable fission targets made from lighter actinides and Cm, Cf isotopes, respectively.

The GAMS crystal spectrometers provide on one hand excellent resolution and accuracy for the determination of absolute gamma ray energies; on the other hand they can be used to perform general nuclear spectroscopy or to measure capture cross-sections of in-situ bred isotopes.

Another strong point of ILL is the availability of a multitude of external neutron beams with neutron energies ranging from few neV up to about 1 eV. Even after monochromatization by Bragg diffraction on crystals or velocity selectors, the neutron fluxes are sufficiently high for

most types of cross-section measurements. There is large potential to use such neutron beams of different energies for solving discrepancies of previous cross-section measurements that might be caused by low-lying resonances or measurements in an imperfect Maxwellian neutron spectrum.

Many possible applications of ILL instruments have been presented. It should be reminded that ILL is a user facility. Thus, the physics performed on these instruments depends on the experiments proposed by the user community. You are very welcome to propose experiments similar to those presented above or even completely different ones, if they can profit of the ILL instruments' characteristics.

REFERENCES

[1] U. KÖSTER, Proc. of the EFNUDAT Workshop on Nuclear Data Measurements, Theory and Applications, Budapest, 23-25 September 2009.
[2] P. ARMBRUSTER, *et al*., Nucl. Instr. Meth. **139** (1976) 213.
[3] U. KÖSTER*, et al*., Nucl. Phys. **A652** (1999) 371.
[4] O. SEROT, Proc. of the IAEA Technical Meeting on Specific Applications of Research Reactors: Provision of Nuclear Data, Vienna, 2009.
[5] G.S. SIMPSON, *et al.,* Phys. Rev. **C76** (2007) 041303(R).
[6] G.S. SIMPSON, *et a*l., Phys. Rev. **C74** (2006) 064308.
[7] J.A. PINSTON and J. GENEVEY, J. Phys. **G30** (2004) R57.
[8] W. URBAN, *et al.*, AIP Conf. Proc. 1090 (2009) 494.
[9] L. MATHIEu, *et al*., AIP Conf. Proc. 1175 (2009) 285.
[10] M.S. DEWEY, *et al.,* Phys. Rev. **C73** (2006) 044303.
[11] S. RAINVILLE, *et al.,* Nature **438** (2005) 1096.
[12] E.G. KESSLER, *et al*., Nucl. Instr. Meth. **A457** (2001) 187.
[13] J. KREMPEL, *et al.,* CPEM2008 Conf. Digest (2008) 634.
[14] H. BÖRNER and J. JOLIe, J. Phys. **G19** (1993) 217.
[15] H.G. BÖRNER, *et al*., Phys. Rev. Lett. **66** (1991) 691.
[16] N. STRITT, *et al*., Phys. Rev. Lett. **78** (1997) 2592.
[17] H.R. KOCH, *et al*., Nucl. Instr. Meth. **175** (1980) 401.
[18] C. DOLL, *et al*., J. Res. Natl. Inst. Stand. Technol. **105** (2000) 167.
[19] B. KRUSCHE, *et al*., Nucl. Phys. **A417** (1984) 231.
[20] J.A. PINSTON, *et al*., Nucl. Phys. **A321** (1979) 25.
[21] S.L. SAKHAROV, *et al*., Nucl. Phys. **A494** (1989) 36.
[22] H.G. BÖRNER, *et al*., Nucl. Instr. Meth. **166** (1979) 251.
[23] T. von EGIDY, *et al*., Nucl. Phys. **A365** (1981) 26.
[24] D.H. WHITE, *et al.,* in Neutron Capture Gamma-Ray Spectroscopy, eds. R.E. Chrien and W.R. Kane, Plenum Press (1979) 802.
[25] P. JEUCH, *et al*., Nucl. Phys. **A317** (1979) 363.
[26] J. ALMEIDA, *et al.,* Nucl. Phys. **A31**5 (1979) 71.
[27] H.G. BÖRNER, *et al*., Nucl. Instr. Meth. **164** (1979) 579.
[28] H.G. BÖRNER, *et al*., Z. Phys. **A286** (1978) 31.
[29] R.W. HOFF, *et al*., Phys. Rev. **C41** (1990) 484.
[30] D.H. WHITE, *et al.,* Phys. Rev. **C57** (1998) 1112.
[31] J.L. SALICIO, *et al*., Phys. Rev. **C37 (**1988) 2371.
[32] R.W. HOFF, *et al*., Phys. Rev. **C29 (**1984) 618.
[33] R.W. HOFF, *et al*., Phys. Rev. **C25** (1982) 2232.
[34] R.F. CASTEN, *et al.*, Phys. Lett. **76B** (1978) 280.

[35] M.K. BALODIS, *et a*l., Nucl. Phys. **A523** (1991) 261.
[36] Y. TOKUNAGA, *et al*., Nucl. Phys. **A411** (1983) 209.
[37] S.E. ARNELL, *et al*., Nucl. Instr. Meth. **54** (1967) 165.
[38] S. CHABOD, *et al.,* Nucl. Instr. Meth. **A566** (2006) 633.
[39] A. LETOURNEAU, et al., Proc. of the IAEA Technical Meeting on Specific Applications of Research Reactors: Provision of Nuclear Data, Vienna, 2009.
[40] U. KÖSTER, *et al*., Eur. J. Nucl. Med. Mol. Imaging **36** (2009) S400.
[41] S. MIRZADEH, *et al*., Report ORNL TM-12010 (1992).
[42] F.F. KNAPP Jr., *et al*., Appl. Radiat. Isot. **45** (1994) 1123.
[43] W.A. WOHLGEMUTH, *et al*., Cardiovascular and Interv. Radiology 31 (2008) 698.
[44] C. BARKHAUSEN, *et al*., Eur. J. Nucl. Med. Mol. Imaging **36** (2009) S399.
[45] R. HENKELMANN, *et al*., Eur. J. Nucl. Med. Mol. Imaging **36** (2009) S267.
[46] The Yellow Book, Guide to Neutron Research Facilities, see: http://www.ill.eu/
[47] H. ABELE, *et al*., Nucl. Instr. Meth. **A562** (2006) 407.
[48] M.A. LONE, *et al*., Nucl. Instr. Meth. **174** (1980) 521.
[49] M. SCHUMANN, *et al.,* Phys. Rev. Lett. **99** (2007) 191803.
[50] V.A. VESNA, *et al*., Nucl. Phys. **A827** (2009) 425c.
[51] F. GÖNNENWEIN, *et al*., Phys. Lett. **B652** (2007) 13.
[52] G. GOEMINNE, *et al*., Nucl. Instr. Meth. **A489** (2002) 577.
[53] S. VERMOTE, *et al*., Nucl. Phys. **A806** (2008) 1.
[54] I. TSEKHANOVICH, *et al*., Phys. Rev. **C78** (2008) 011301.
[55] V. WAGNER, *et al*., Physica **B180/181** (1992) 938.
[56] A. STEYERL, *et al*., Phys. Lett. **A116** (1986) 347.
[57] H. RAUCH, *et al*., Phys. Rev. Lett. **83** (1999) 4955.

The updated version of Chinese Evaluated Nuclear Data Library (CENDL-3.1) and China nuclear data evaluation activities

Zhigang Ge[1], Hongwei Yu[1], Youxiang Zhuang [1], Tingjin Liu [1], Jingshang Zhang [1], Ping Liu[1], Haicheng Wu[1], Zhao.Zhixiang[2], Haihong Xia[3]

(1) China Nuclear Data Center,
China Institute of Atomic Energy (CIAE),
Beijing 102413, P.R.China
(2) China Committee of Nuclear Data,
China Institute of Atomic Energy (CIAE),
Beijing 102413, P.R.China
(3) The Department of Nuclear Physics,
China Institute of Atomic Energy (CIAE),
Beijing 102413, P.R.China

Abstract. The updated Chinese Evaluated Nuclear Data Library CENDL-3.1 is a fruit based on the nuclear data evaluated works in recent years, at China Nuclear Data Center (CNDC) in cooperation with China Nuclear Data Coordination Network (CNDCN). CENDL-3.1 contains the evaluated data for reactions with incident neutrons on about 210 nuclides (from ^{3}H to ^{249}Cf) in energy region of 10^{-5} eV-20MeV. All data obtained according to the evaluations of experimental data and theory predictions. For most important nuclei of this library, the benchmark testing and validations have been performed; the comparisons with other nuclear data libraries (ENDF/B, JENDL, BROND, JEF, et al.) have been done. The testing version of CENDL-3.1 is CENDL-3.0, which has been provided for China domestic users. Follow the using back feed of CENDL-3.0, a lot of improvement has been done. The CENDL3.1 will be provided for all users by ENDF format and released to the world this year. In the past several years, CNDC and CNDCN also have got a lot of progress in the fields of nuclear data theory study, model and code developments, and nuclear database establishment etc. These progresses will be introduced in this presentation.

1. CENDL-3.1 Library

1.1. The view of CENDL-3.1

CENDL-3.1 is a general purpose evaluated nuclear data file, which contains the fruits of the nuclear data evaluation and measurement works in recent years in China. CENDL-3.1 contains the evaluated data files for reactions with incident neutrons on almost 210 nuclides (see Table 1), among them, 173 nuclides are newly evaluated, and 37 nuclides are taken from CENDL-2.1. During the evaluation processes, the newest experimental information included new measurements made by Chinese scientists in China domestically, are collected, evaluated carefully and corrected by using the new standard cross sections and decay data et al.

TABLE 1. THE NUCLIDES OF CENDL-3.1

Nucl.	Content
Light Elements	^{1,2,3}H,^{3,4}He,^{6,7}Li,^{9}Be,^{10,11}B,^{12}C,^{14}N,^{16}O,^{19}F
Structural Materials	^{23}Na,^{24,25,26}Mg,^{27}Al,^{28}Si,^{31}P,^{nat}S,^{nat}Cl,^{nat}K,^{nat}Ca,$^{46-50}$Ti,^{nat}V,^{50,52,53,54}Cr,^{55}Mn,^{54,56,57,58,nat}Fe,^{59}Co,^{nat}Ni,^{63,65}Cu,^{nat}Zn,^{nat}Mo,$^{174,176-180,nat}$Hf,^{nat}W,^{197}Au,^{nat}Pb,^{209}Bi
Fission Products & Medium Elements	^{69,71,nat}Ga,^{83,84,85,86}Kr,^{85,87,nat}Rb,^{88,89,90}Sr,^{89,91}Y,^{93,95}Zr,^{93,95}Nb,^{95,97,98,100,99}Tc,^{99,100,101,102,103,104,105}Ru,^{103,105}Rh,^{105,108}Pd,^{107,109,nat}Ag,^{113,nat}Cd,^{115,nat}In,^{nat}Sn,^{121,123,125,nat}Sb,^{130}Te,^{127,129,135}I,^{123,124,131,132,134,135,136}Xe,^{133,134,135,137}Cs,^{130,132,134,135,136,137,138,nat}Ba,^{139}La,^{136,138,140,141,142,144}Ce,^{141}Pr,^{142,143,144,145,146,147,148,150,nat}Nd,^{147,148,148m,149}Pm,^{144,147,148,149,150,151,152,154,nat}Sm,^{151,153,154,155,nat}Eu,^{152,154,155,156,157,158,160,nat}Gd,^{164}Dy,^{175,176,nat}Lu,^{181}Ta,^{nat}Hg,^{nat}Ti
Actinides	^{232}Th,^{232,233,234,235,236,237,238,239,240,241}U,^{236,237,238,239}Np,^{236,237,238,239,240,241,242,243,244,245,246}Pu,^{240,241,242,242m,243,244}Am,^{249}Bk,^{249}Cf

UNF [1] series cods LUNF, UNF, FUNF [2] were used in the model calculations for the light elements, structural materials, fission products & medium elements, heavy elements and actinides, respectively. Most of the input model parameters are taken from the RIPL [3] library and were adjusted based on the experimental information. APMN [4] and APOM94 [5] programs are used for optimal optical potential parameters automatically searching. ECIS95 [6] is also involved for some model calculations.

For important nuclides, the evaluated reaction cross sections, angular distributions, energy-angle distributions et al. are presented and some covariance files also are included in CENDL-3.1. All new evaluated data files obtained according to the evaluations of experimental data and theory predictions. For most important light elements, structural materials and actinide nuclei of this library, the validations with hundreds of benchmarks have been performed; the comparisons with other nuclear data libraries (ENDF/B, JENDL, BROND, JEFF, et al.) have been done.

The testing version of CENDL-3.1 is CENDL-3.0 which has been provided for China domestic users and used in many relevant fields, for example, in projects of China Experimental Fast Reactor and HI-13 Tandem Accelerator Upgrading *et al*. Based on the using back feed of CENDL-3.0, a lot of improvement has been done for CENDL3.1. The CENDL3.1 will be released in 2009 and provided for all users by ENDF format.

1.2. The evaluation of CENDL-3.1

1.2.1. Light elements

Based on the updated experimental information, a series codes (LUNF) are developed for model calculations of ^{6,7}Li,^{9}Be,^{10,11}B, ^{12}C,^{14}N and ^{16}O, mainly for double differential cross sections (MF-6) [7]. The full sets of neutron data, i.e. cross sections of all reactions, energy and angular distribution of secondary neutrons and differential cross sections, etc. were provided. Fig. 1 shows the calculated results of the total inelastic scattering reactions of ^{6}Li(n, n'g) compared with experimental data [8, 9]. The results of the ^{6}Li (n, nd) ^{4}He reaction cross section are showed in Fig. 2 [10-13]. Fig. 3 is the MF-6 of n+^{16}O comparison with exp. data of M. Baba, *et al*. [14].

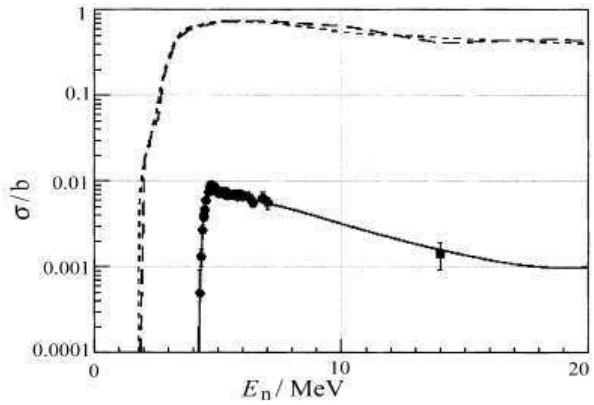

FIG.1. ^{6}Li(n, n'γ) ^{6}Li total inelastic scattering reaction

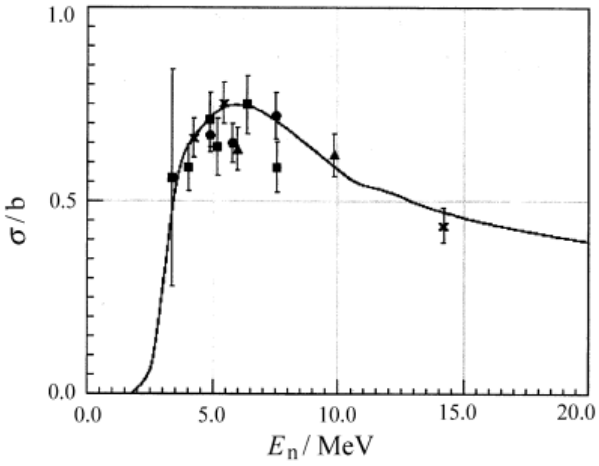

FIG.2. ^{6}Li (n, nd) ^{4}He reaction cross section

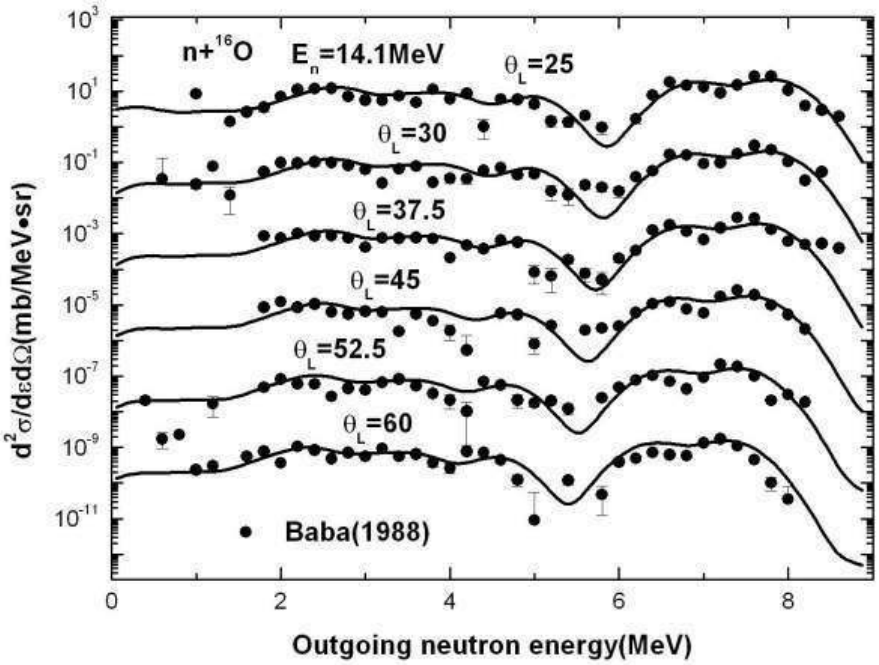

FIG.3. The double differential cross sections (MF-6) of n+^{16}O comparison with exp. data

1.2.2. Structural materials

According to the MUP[8] code used in the CENDL-2 evaluations and the new results of nuclear reaction theoretical studies, a new code UNF used for structural material and medium nuclides calculation was development. With the UNF code calculations and evaluation of new

experimental data, the full neutron data set (γ-production data including for some nuclei) are provided in ENDF6 format.

Comparing to CENDL-2, the main development of CENDL-3.1 for the structured materials is that in addition to the data of natural elements, the data of their isotopes are also included, and the data consistent between the natural elements and their isotopes are made. As examples, evaluated total cross sections of n+$^{46\sim50,nat}$Ti and $n+^{90}Zr$ are showed in Figures 4 and 5.

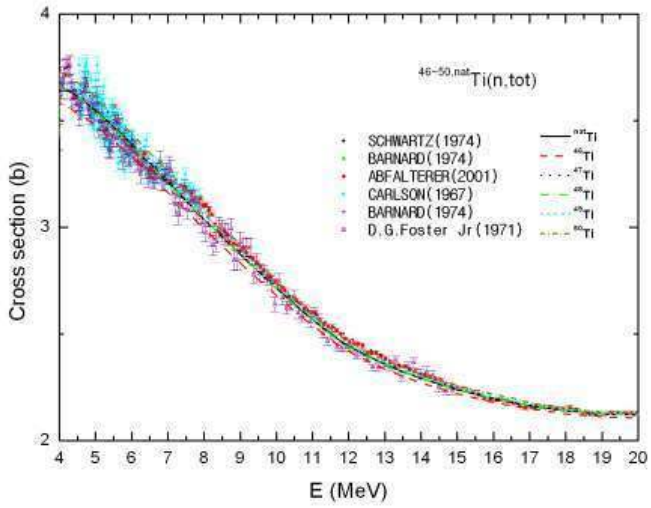

FIG.4. $^{46\sim50,nat}Ti$ (n,tot) comparison with exp. Data[Ref 15-19]

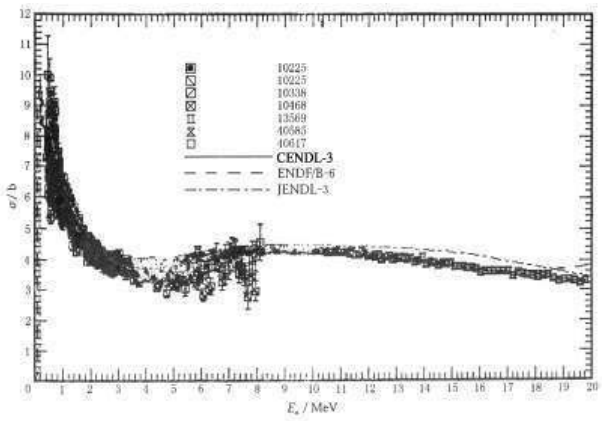

FIG.5. The evaluated total cross section of $n+^{90}Zr$ comparison with exp. data [Ref 20-25] *and JENDL3.2, ENDF/B6*

1.2.3. Fission products

From MF-1 to MF-5 are provided in CENDL-3.1 for most fission products nuclides, MF-1 to MF-6 are variable for others. A code SUNF, the simple version of UNF, is developed for the model calculations of fission products nuclides. The data of 101 fission products nuclides are sent to join in the international comparison of FP and coordinated by WPEC Subgroup 21, and some of them are selected as the data file of ENDF/B-VII. Fig. 6 and Fig. 7 show the evaluated results compared with exp. data for ^{140}Ce(n,2n) and Sn(n, γ) respectively.

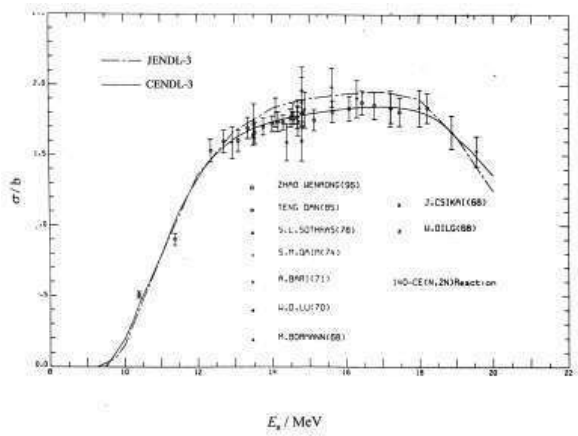

FIG.6. The evaluated (n,2n) reaction cross section of n+^{140}Ce[Exp. data Ref.26-34]

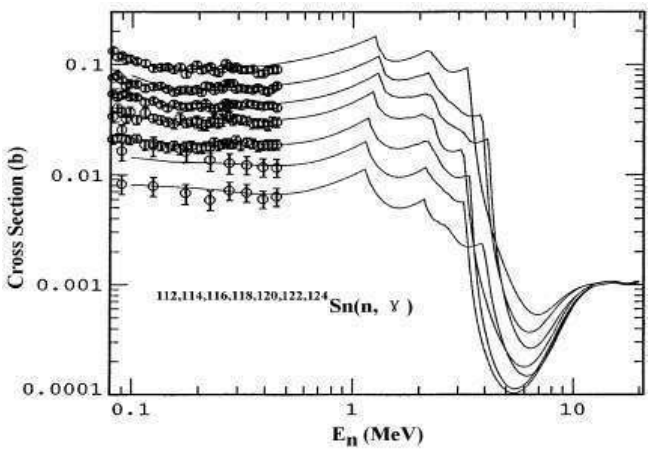

FIG.7. Sn (n, γ) reactions evaluations comparisons with exp. data[Ref. 35]

1.2.4. Actinides

On the basis of the model calculations with the code FUNF and adjusting the model parameters carefully, the new experimental data, 32 actinides are evaluated or re-evaluated. MF-1~6, 12~15 are included for important actinides (e.g., U, Pu isotopes), and MF-1~5 for others. The file number and nuclides were extended comparing with the pervious version of CENDL, and the results of the benchmark testing have been considered during the evaluation process. Figures 8-10 show the new evaluations for n+^{240}Pu.

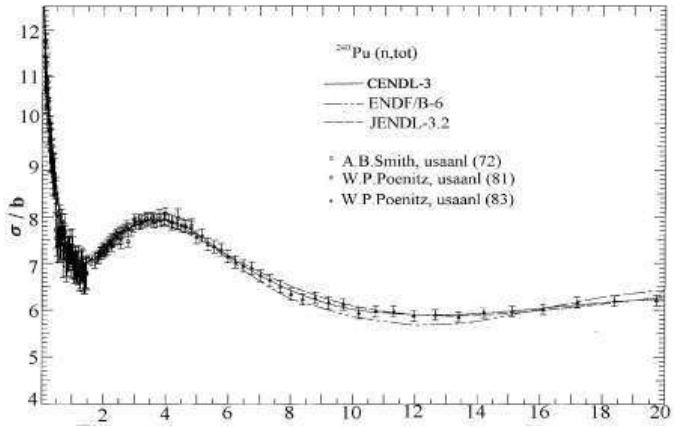

FIG.8. ^{240}Pu (n, tot) evaluations comparisons with exp. data [Ref. 36-38] *and other libraries*

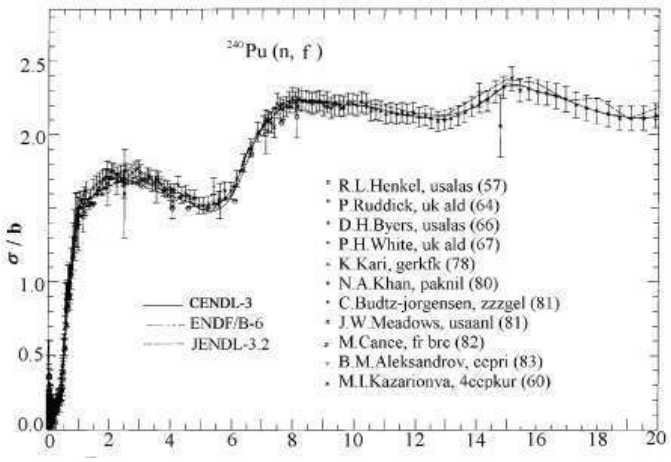

FIG.9. ^{240}Pu (n, f) evaluations comparisons with exp. data [Ref. 39-49] *and other libraries*

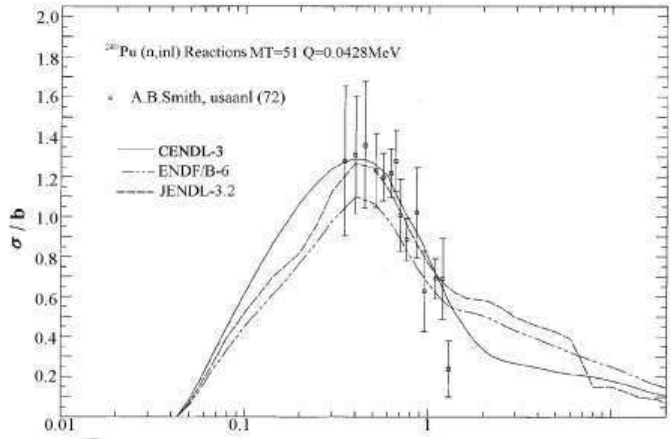

FIG.10. ^{240}Pu (n, inl) (MT=51) evaluations comparisons with exp. data [Ref. 36] *and other libraries*

1.2. The benchmark testing of CENDL-3.1

In order to test the reliability of the data from CENDL-3.1 the benchmark testing for some light, medium-heavy nuclides and actinides of CENDL-3.1 has been performed; the calculations and analyses of benchmarks are done with Monte Carlo code MCNP-4C and transformation codes. The data processing is carried out by using the internationally used code system NJOY94. These benchmarks are based on IAEA specifications [50] for the FNS (Fusion Neutronics Source) experiments [51] and OKTAVIAN experiments [52] in Japan. Some results are compared ENDF/B-VII, JENDL-3.3 and JEF-2.2 validated CENDL-3.1 to identify the source of the discrepancies with the experimental results.

1.2.1. Light nuclides

FNS experiments are used to validate Be, C, N, O and Li evaluations. For C, as shown in Fig. 11, good achievements are obtained in general, except discrepancy at 66.8 degree. For LiO_2, good agreement with the benchmark values is achieved. Only a little under prediction around 0.3MeV is observed in Fig. 12, which is caused by ^{16}O evaluation obviously.

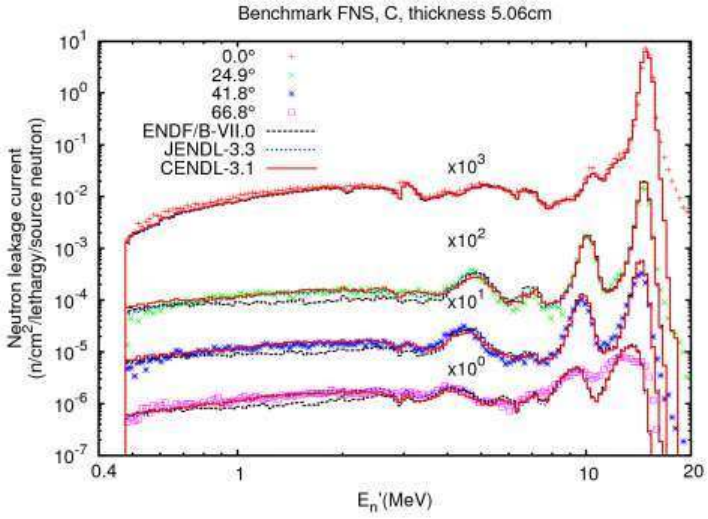

FIG.11. Comparison of angular neutron leakage current from 5cm-thick graphite slab calculated with CENDL-3.1, ENDF/B-VII.0 and JENDL-3.3.

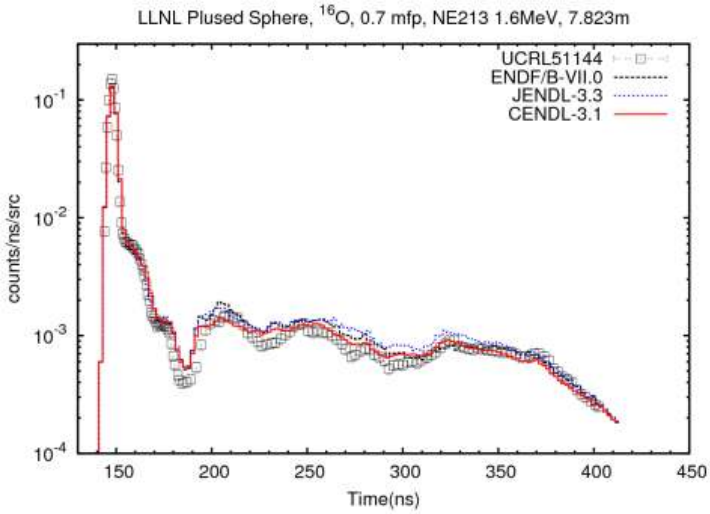

FIG.12. Comparison of neutron leakage spectrum from LLNL pulse sphere benchmark.

1.2.2. Medium-heavy nuclides

Ti, Mn and Mo evaluations for CENDL-3.1 are tested with benchmark OKTAVIAN. From the comparison of neutron leakage current gives in Fig. 13, good agreement with the measurement above 0.8 MeV is obtained for Ti. However, from the beginning to 0.8MeV, the prediction is higher than the benchmark values. Since the evaluator of Ti confirmed (n,2n) cross section of ^{48}Ti is low enough, this discrepancy still can not be explained. For ^{55}Mn in Fig. 14, an obvious under prediction of neutron leakage around 10 MeV is occurred, it is doubtable that direct reaction part of the inelastic cross section is missing. This problem should be corrected in future. For Mo, the calculated neutron leakage spectrum is lower than the measurement, especially from 6 to 13 MeV. Again, the contribution from inelastic scattering reaction is under estimated.

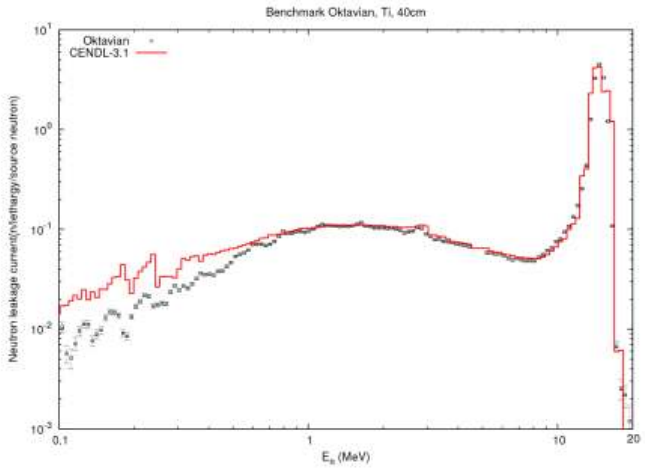

FIG.13. Results for the neutron spectrum for the OKTAVIAN Ti benchmark.

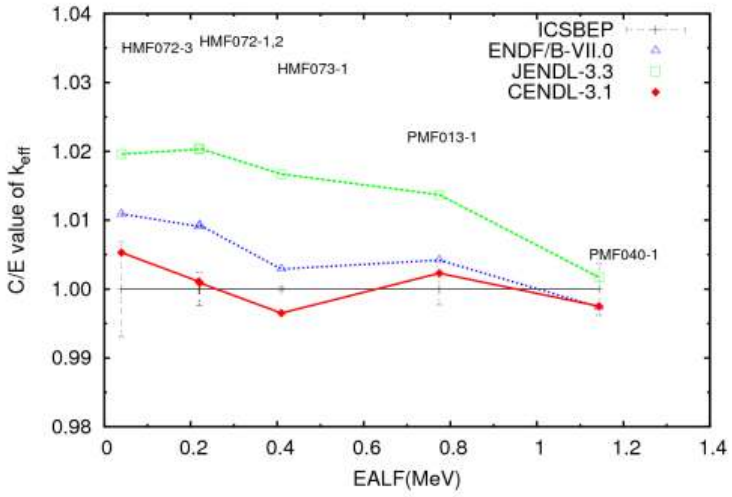

FIG.14. Comparison of copper-reflected benchmark C/E values of k_{eff} calculated with CENDL-3.1, ENDF/B-VII.0 and JENDL-3.3.

1.2.3. Actinides

Many kinds of experimental benchmark are used to validate the actinides. A large number of criticality benchmarks from International Handbook of Criticality Safety Benchmark Experiments (ICSBEP) were selected, including fast and thermal spectrum. Fig. 15-17 show the calculation results of ^{235}U of CENDL-3.1 and ENDF/B-VII.0 for different kind fast and thermal system. One can see that the ^{235}U data of CENDL-3 are good agreement with the measurement for some system in some energy region.

1.3. Conclusion

CENDL-3.1 was completed in 2005, and it has been improved. CENDL-3.1 was released on Dec. 24, 2009. Nuclides and data files of CENDL-3.1 are increased and extended compared with CENDL-2.1. All evaluations performed based on the new experimental data and new model calculations carefully. They are improved compared with CENDL-2.1. The data of the most important nuclides are validated by the benchmark testing. Some of them are better than other evaluated libraries according to the results of the benchmark testing.

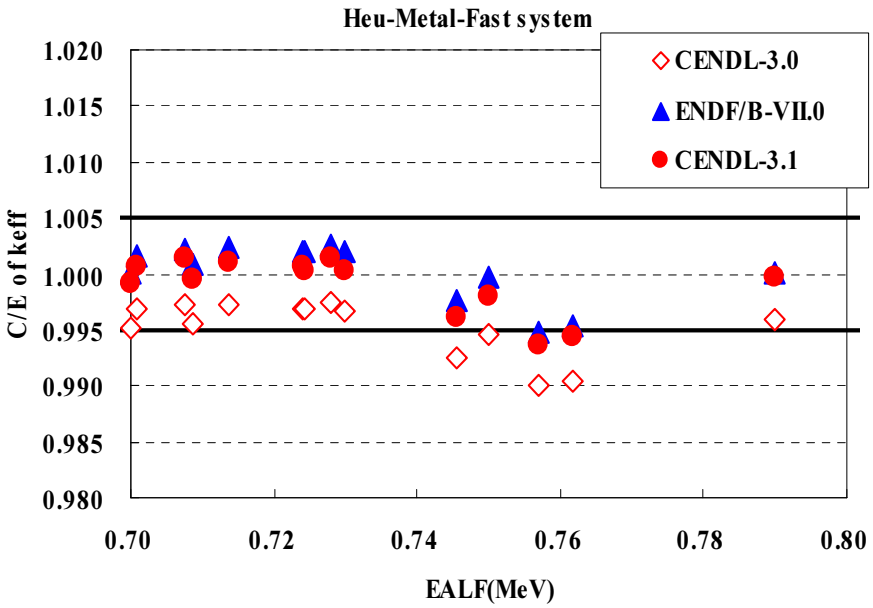

FIG.15 Comparison of HEU unmoderated benchmark C/E values of k_{eff} calculated with CENDL-3.0, 3.1 and ENDF/B-VII.0.

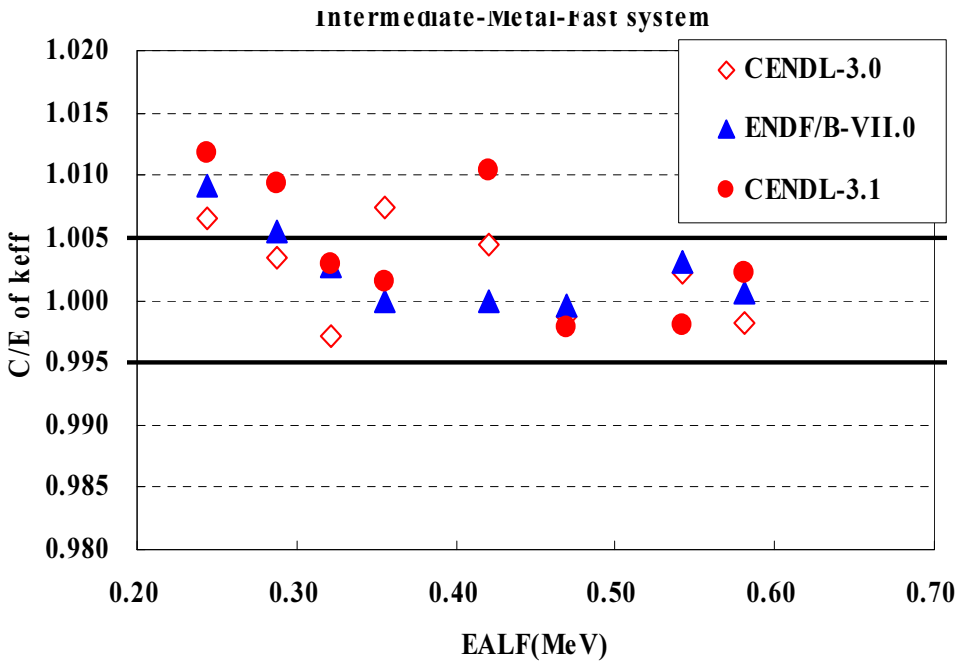

FIG.16 Comparison of IEU-Metal-Fast system benchmark C/E values of k_{eff} calculated with CENDL-3.0, 3.1 and ENDF/B-VII.0.

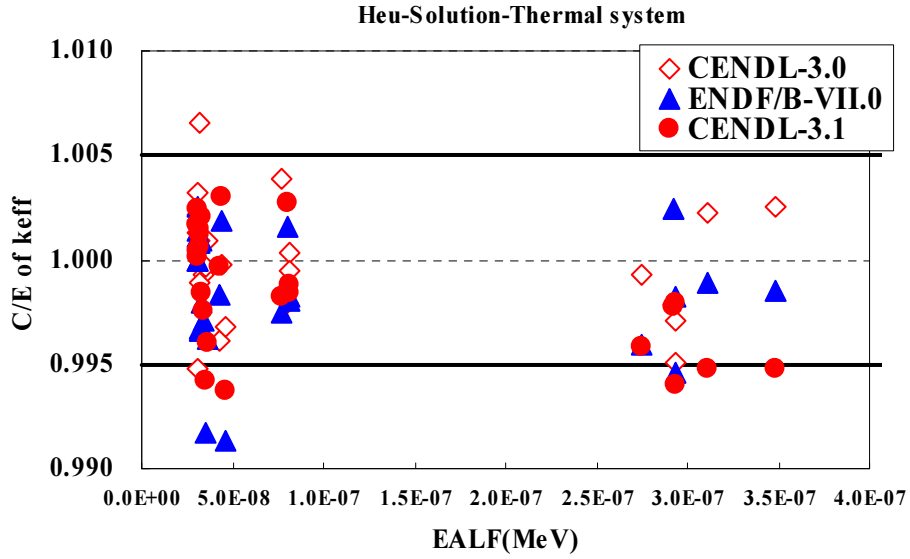

FIG.17 Comparison of HEU-Solution-Thermal system benchmark C/E values of k_{eff} calculated with CENDL-3.0, 3.1 and ENDF/B-VII.0.

2. Other progresses on nuclear data evaluations

2.1 Nuclear reaction model study

The models are improved and completed for light nuclides of 1p shell, which contains the dynamics and kinematics of nuclear reactions.

A method to set up file-6 of light nuclei for evaluated neutron data in ENDF6 format below 20 MeV has been established and the energy balance is strictly considered. This method has been used in the calculation of ^{6,7}Li, ^{9}Be, ^{10,11}B, ^{12}C,^{14}N and ^{16}O in CENDL-3.1.

2.2 Covariance study

A code EXPOV for evaluating the covariance matrix of experimental data is developed. The covariance data are output in ENDF6 format. The code together with the spline fitting code SPC for multi-sets of correlative data are used to practically evaluate the covariance data for ^{58,60,61,62,64,nat}Ni, ^{63,65,nat}Cu and ^{27}Al and the reasonable results have been got.

A program RAC based on the R matrix theory for calculating covariance data of light nuclide is developed. The program has been tentatively used to calculate the covariance data for ^{6,7}Li and ^{10,11}B, ^{16}O the reasonable results have been got for the cross sections up to 5 MeV. The calculated data and their covariance data for ^{6}Li, ^{10}B have been accepted internationally as standard data of light nuclide.

Also a code has been developed for calculating the covariance data of structural material nuclides based on the statistical theory, including optical model, Hauser-Feshbach and preequilibrium emission model. The code has been used to calculate the covariance data of Ni, Cu and their isotopes in ENDF6 format.

2.3 The systematic study of fission yield data

Based on the mass distribution data up to 200 MeV measured by Zoller [Ref. 53], the systematic on dependence of chain yield on incident neutron energy for each mass number A is studied. And also the systematic of mass distribution on mass A and incident neutron energy is investigated by using 5 (or 3) Gaussian model. The calculated results could reproduce the

experimental data used well. The investigation also shows that the correlation between the parameters of the systematic and the yields calculated with the systematic is quite complicated and, in general, is quite strong.

2.4 The study on the dependence of yield on energy

Taken some typical important fission products from $^{235, 238}$U fission, and the dependences of fission yield on incident neutron energy are studied. The covariance data are also evaluated based on each set of experimental data and the correlation among the data due to the systematical error, such as fission rate (or normalization), detector efficiency, decay data etc., is taken into account in the fitting and the covariance matrix is obtained as a fit result. The results show that the data for most of product nuclides can be fitted with a linear function. But for some special product nuclides the data have to be fitted with a spline function.

2.5 Nuclear structure and decay data

CNDC has taken permanent responsibility for evaluating and updating NSDD for A=51, and 195-198 mass chain. The data have been revised using available experimental decay and reaction data for mass chain A=197, and are being updated for mass chain A=196. Updated evaluation of A=197 has been sent to NNDC, USA. The evaluations of mass chain A=52-56 are being updated at Jilin University. The decay data of ^{233}U are being evaluated on the basis of the new measured data.

3. Conclusion

In the recently years, a lot of progress on nuclear data evaluation and related fields has been obtained.

A new evaluated neutron data librariy CENDL-3.1, which contains about 210 nuclei, has been finished and is released on 24 December 2009.

A series mode codes used for the calculation of 1p shell light nuclei has been development, which contained the MF6 calculation.

Some evaluation tools of nuclear data evaluation have been developed and used in the nuclear data activities.

REFERENCES

[1] ZHANG JINGSHANG, Nucl.Sci.Eng. **142** (2002) 207.
[2] ZHANG JINGSHAN，inter report (2003).
[3] RIPL http://www-nds.iaea.org/RIPL-2/.
[4] SHEN QINGBIAO, CNDP (INDC(CRP)-053/L) 25 (2001)19.
[5] SHEN QINGBIAO, CNDP (INDC(CRP)-027/L) 7 (1992)19.
[6] J. RAYNAL, CEN-N2772, 1994.
[7] ZHANG JINGSHAN，Commun. Theor. Phys. (China) **39** (2003) 433.
[8] G. PRESSER, *et al*., Nucl. Phys. **A131** (1969) 679.
[9] BESOTOSNYJ, *et al*., Yadernye Konstanty **19** (1975) 77.
[10] R. BATCHELOR, *et al*., Nucl. Phys. **47** (1963) 385.
[11] J. C. HOPKINS, *et al*., Nucl. Phys. **A107** (1968) 139.
[12] P. W. LISOWSKI, *et al*., Los Alamos Scientific Lab. Reports, 8342(1980).
[13] S. CHIBA, *et al*., J. Nucl. Sci. and Tech. **22** (1985) 771.
[14] M. BABA, *et al*., Conf. on Nuclear Data for Basic and Applied Science, Santa Fe 1, 223

(1985).
[15] R.B. SCHWARTZ, *et al*., NBS-MONO-138(1974).
[16] E. BARNARD, *et al*., Nucl. Phys. **A229** (1974) 189.
[17] W.P. ABFALTERER, *et al*., Phys. Rev. **C63** (2001) 044608.
[18] A.D. CARLSON, *et al*., Phys. Rev. **158** (1967) 1142.
[19] D.G. FOSTERJR, *et al*., Phys. Rev. **C3** (1971) 576.
[20] L. GREEN, *et al*., WAPD-TM-1073(1973).
[21] R. W. STOOKSBERRY, *et al*., Nucl. Sci. Eng. **51** (1973) 235.
[22] P. GUENTHER, *et al*., Phys. Rev. **C12** 7(1975) 179.
[23] R.W. FINLAY, *et al*., Phys. Rev. **C47** (1993) 237.
[24] A.N. DJUMIN, *et al*., 77KIEV, 2 (1977) 74.
[25] M.V. PASECHNIK, *et al*., 80KIEV, 1 (1980) 304.
[26] KONG XIANGZHONG, *et al*., Comm. Nucl. Data Progr. **14** (1995) 5.
[27] TENG DAN, *et al*., Chin. J. Nucl. Phys. **7** (4) (1985) 307.
[28] S.L. SOTHRAS, *et al*., J. Inor. Nucl. Chem. **40** (1978) 585.
[29] S.M. QAIM, Nucl. Phys. **A224** (1974) 319.
[30] A. BARI, BARI (1971).
[31] W.D. LU, *et al*., Phys. Rev. **1** (1970) 350.
[32] M. BORMANN, *et al*., Nucl. Phys. **A115** (1968) 309.
[33] J. CSIKAI, *et al*., Acta Phys. Hung. **24** (1968) 233.
[34] W. DILG, *et al*., Nucl. Phys. **A118** (1968) 9.
[35] V.M. TIMOKHOV, *et al*., Fiz.-Energ Institut, Obninsk Reports, 1921(1988).
[36] A.B. SMITH, *et al*., Nucl. Sci. Eng. **47** (1972) 19.
[37] W.P. POENITZ, *et al*., ANL-NDM-80 (1983).
[38] W.P. POENITZ, *et al*., Nucl. Sci. Eng. **78** (1981) 333.
[39] R.L. HENKEL, *et al*., AECD-4256 (1957).
[40] P. RUDDICK, *et al*., JNE/AB **18** (1964) 561.
[41] D.H. BYERS, *et al*., 66WASH, 2, (1966) 903.
[42] P.H. WHITE, *et al*., JNE **21** (1967) 671.
[43] K. KARI, *et al*., Kernforschungszentrum Karlsruhe Reports, 2673 (1978).
[44] N.A. KHAN, *et al*., Nuclear Instrum. Meth. Physics Res. **173** (1980) 137.
[45] C. BUDTZ-JORGENSEN, *et al*., Nucl. Sci. Eng. **79** (4) (1981) 380.
[46] J.W. MEADOWS, Nucl. Sci. Eng. **79** (1981) 233.
[47] M. CANCE, *et al*., 82ANTWER, 51 (1982).
[48] B.M. ALEKSANDROV, *et al.*, Yad. Konst. **1**/50 (1983) 3.
[49] M.I. KAZARINOVA, *et al*., At. Energ. **8** (1960) 139.
[50] Fusion Evaluated Nuclear Data Library CDROM, IAEA-NDS-CD-6
[51] Y. OYAMA, *et.al*., JAERI-M 94-014, (1994) 126.
[52] C. ICHIHARA, *et.al*., JAERI-M 94-014, (1994) 125.
[53] C.M. ZOLLER, Ph.D. thesis, TH Darmstadt, 1995.

Data processing and validation needs of group-wise working cross section libraries for nuclear fission reactor shielding and radiation damage applications

M. Pescarini

ENEA
Agenzia Nazionale per le Nuove Tecnologie,
l'Energia e lo Sviluppo Economico Sostenibile
Dipartimento Fusione, Tecnologie e Presidio Nucleare
Sezione Sistemi Nucleari Innovativi e Chiusura Ciclo Nucleare
Bologna, Italy

Abstract. The generation of broad-group working cross section libraries for nuclear fission reactor shielding and radiation damage applications in different spectral environments (LWR, SFR, LFR, HTR, etc.) is recommended in order to permit the use, in particular, of the three-dimensional (3D) deterministic transport codes in the data validation activities. 3D deterministic transport analyses could be performed, in parallel with similar 3D Monte Carlo analyses, on single-material and engineering neutron shielding benchmark experiments, included in the SINBAD (ORNL/RSICC – OECD/NEA Data Bank) international database. This action, mainly performed by the national research institutes, would be very useful not only for the reactor physicist and nuclear engineer data validation interests but also for the nuclear safety authorities and the industrial organizations.

1. Introduction

The nuclear data validation on integral benchmark experiments can be strictly intended as a scientific activity addressed to obtain an information feed-back dedicated to correct or modify the evaluated nuclear data files contained in the nuclear data libraries (JEFF, ENDF/B, JENDL, BROND, CENDL, etc.). It is evident that the three-dimensional (3D) Monte Carlo codes using continuous-energy (point-wise) cross sections play a central role in the validation of the evaluated nuclear data libraries since these processed point-wise cross section libraries effectively assure a best agreement to the original evaluated nuclear data files from which these libraries were derived.

On the other hand, if the nuclear data validation is intended in a more general sense, i.e., an activity addressed to test any kind of processed cross section used in the transport calculations performed by research or industry, it is necessary to take into account also the validation of the group-wise working cross section libraries needed to run the deterministic transport codes. This wider approach offers to nuclear data validation two independent ways for nuclear data processing and transport calculation thus increasing the reliability of the processed cross sections (point-wise and group-wise) in support of nuclear safety. This additional contribution to nuclear data validation, provided by using the group-wise working cross section libraries and deterministic transport codes, is particularly appreciated by the nuclear reactor physicists and nuclear engineers involved in the transport analyses dedicated to research and power reactor shielding problems. In this more complete and recommendable nuclear data validation, it is necessary to test not only the evaluated data files but also the neutron and photon energy discretizations of the working library group structures and the self-shielding of the group-wise cross sections, used in deterministic transport calculations. Differently from the 3D Monte Carlo codes using a single processed point-wise cross section library to treat the different spectral environments of interest, when the 3D deterministic transport codes are employed it is not practically possible to use only one broad-group spectrum-independent

working cross section library for any kind of application treated with these codes. In fact, despite the formidable increase of the calculation power, these codes could have convergence problems when fine-group spectrum-independent multi-purpose libraries are used together with hundreds of thousands of volumetric spatial meshes, possibly needed to describe accurately the geometry of many neutron shielding benchmark experiments or used to perform shielding analyses for commercial nuclear power reactors.

Consequently several broad-group working libraries should be generated through problem-dependent collapsing of fine-group pseudo-problem-independent cross section libraries, based on the most recent evaluated nuclear data libraries (JEFF-3.1.1, ENDF/B-VII.0, JENDL-3.3, etc.), using reactor zone-weighted spectra for the specific reactor types (LWR, SFR, LFR, HTR, etc.) of current interest, i.e., the Generation III and IV nuclear fission reactors.

2. Group cross section libraries and 3D deterministic transport codes for shielding applications

Since many years, at the international level, a decrease of activity was observed for debating production, features and performances of group-wise working cross section libraries for nuclear reactor shielding and radiation damage applications. These libraries are necessary to run the deterministic transport codes which are, e.g., included in the US packages DOORS [1], DANTSYS [2], PARTISN [3], etc., distributed by OECD/NEA Data Bank and ORNL/RSICC. On the other hand these packages, unlike those which include Monte Carlo codes (e.g. MCNP [4]), do not contain any working cross section library. The production of fine-group (150-200 neutron groups + 30-50 photon groups) coupled (neutron and photon) pseudo-problem-independent cross section libraries, based on the Bondarenko [5] self-shielding method (e.g. of the type similar to the ORNL VITAMIN-B6 [6] general-purpose library in AMPX format, with 199 neutron groups and 42 photon groups) continues in several research institutes (ENEA, ORNL, KAERI, etc.). On the other hand, the generation of derived broad-group working libraries of collapsed and self-shielded cross sections for free distribution (e.g. of the type similar to the ORNL BUGLE-96 [6] broad-group working library in FIDO-ANISN format, with 47 neutron groups and 20 photon groups for LWR applications) is practically absent.

The current situation is unjustified, taking into account the actual increased performances of computers and 3D deterministic transport codes, the potential availability of collapsed and self-shielded group-wise cross section libraries for different spectral, temperature and compositional conditions and, finally, the requirements of the nuclear safety authorities.

Concerning the 3D deterministic transport codes (e.g., TORT [7] in the DOORS package, THREEDANT in the DANTSYS package, PARTISN, etc.) which necessarily use the group-wise cross section libraries, they increased, in recent years, their calculation performances in an impressive way and expanded their applicability to handle complex geometries, reaching in many cases the detail offered by the 3D Monte Carlo codes (e.g., MCNP). This result was achieved through the use of pre/post-processor systems of ancillary programs (e.g., ENEA-Bologna BOT3P [8] distributed by OECD/NEA Data Bank and ORNL/RSICC), dedicated to the 2D and 3D deterministic transport codes. In particular, with the support of BOT3P, based on combinatorial geometry algorithms, it is now easily possible to generate automatically detailed spatial mesh grids not only for the 2D and 3D transport codes of the DOORS and DANTSYS systems but also for any other possible transport code (through simple interfaces dedicated to manage the BOT3P binary output files), together with the graphical verification of the input data of the geometrical model.

During the last 10-15 years, the 3D discrete ordinates (S_N) transport codes increased their competitiveness with respect to the corresponding 3D Monte Carlo stochastic codes, obtaining comparable or even more convenient performances in terms of CPU times, with the same calculation precision, similar description capability of complex geometries and suitable simulation of different neutron and photon spectral conditions. Moreover 3D discrete ordinates commercial codes (e.g., ATTILA US code system) with unstructured spatial grids (finite elements) can now treat not only the neutral but also the charged particle transport as the more conventional classic 1D, 2D and 3D discrete ordinates codes (respectively ROZ, KASKAD and KATRIN) of the CNCSN Russian system of deterministic codes.

Since deterministic transport codes are going to be employed in the analysis of the Generation IV nuclear reactor projects within the European Union activities, it would be highly recommended that a specific interest dedicated to the generation of group-wise working cross section libraries should be promoted. Finally, it is very important to underline that the deterministic transport codes permit reliable and effective sensitivity and uncertainty analyses, particularly recommended in the data validation activity.

About the availability of innovative multi-group libraries, for example, the interesting features of the VITAMIN-B6 (ORNL, ENDF/B.VI.3 [9] data) library must be underlined. Unlike similar previous libraries as VITAMIN-C [10] (ORNL, ENDF/B-IV data), VITAMIN-E [11] (ORNL, ENDF/B-V data) or VITAMIN-J [12] (OECD/NEA Data Bank, JEF-1 data), VITAMIN-B6 introduced a fine-group discretization (more than 30 neutron groups) in the thermal neutron energy region below 5 eV, including upscatter cross sections. This has the potential of treating with precision, together with the fast neutron spectrum calculation performances, problems where a rigorous description of the thermal neutron spectrum is essential. This is specifically requested, for example, in the case of the boron neutron capture therapy (BNCT) medical applications [13] or when it is necessary to calculate the thermal neutron and photon radiation damage, as emerged for some material testing reactors (MTRs) [14] and light water reactors (ABWRs) [15] [16]. In particular the ENEA-Bologna Nuclear Data Group, in co-operation with specialists of a State Scientific Center of the Russian Federation, the Institute for Physics and Power Engineering of Obninsk (SSC RF IPPE), contributed in this field various libraries in the VITAMIN-B6 energy group structure, freely distributed by OECD/NEA Data Bank. The JEFF-2.2 [17] based VITJEF22.BOLIB [18] and MATJEF22.BOLIB [19] libraries, respectively in AMPX and MATXS format, and the JEFF-3.1 [20] based VITJEFF31.BOLIB [21] and MATJEFF31.BOLIB [22] libraries, respectively in AMPX and MATXS format, were generated. All these libraries were obtained through versions of the NJOY [23] (LANL) nuclear data processing system with the additional use, for the libraries in AMPX format, of the SCAMPI [24] (ORNL) nuclear data processing system, a development of the AMPX-77 [25] (ORNL) nuclear data processing system. To generate VITJEFF31.BOLIB, in particular, it was necessary to develop an updated and corrected version of SCAMPI, the ENEA-Bologna Revision 2007 [26] of SCAMPI in free distribution at the OECD/NEA Data Bank, to process the recent evaluated data libraries (JEFF-3.1, ENDF/B-VII.0, etc.) in double-precision. More recently the VITJEFF311.BOLIB library in AMPX format, based on JEFF-3.1.1 [27] data, and the similar VITENDF70.BOLIB library, based on ENDF/B-VII.0 [28] data, were produced but not yet made generally available. From these two libraries two broad-group working libraries of self-shielded cross sections for LWR shielding and radiation damage applications were generated through cross section collapsing[4]. These libraries, named BUGJEFF311.BOLIB and BUGENDF70.BOLIB, were generated in the FIDO-ANISN format in the BUGLE-96 energy group structure, include the whole set of the IRDF-2002 [29] [30] dosimetry cross sections processed in the BUGLE-

[4] Not yet freely available

96 47 neutron group structure and, finally, are available also in versions which contain upscatter cross sections.

During the last years, the ENEA-Bologna Nuclear Data Group has performed several actions addressed to generate practical tools to increase, in particular, the performance and competitiveness of the 2D and 3D deterministic transport codes:

1) several group-wise cross section libraries [18] [19] [21] [22];
2) a pre/post-processor system [8] dedicated to the 2D and 3D deterministic transport codes;
3) transport analyses dedicated to reactor shielding benchmark experiments [31] [32] [33] [34] [35] [36];
4) the whole set of the IRDF-2002 [29] [30] dosimetry cross sections processed in the 47 neutron group structure of the BUGLE-96 cross section library.

At the same time, this work was developed following the standard recommendations proposed by the OECD/NEA Data Bank.

With respect to the nuclear safety authority requirements it is noted that the use of the deterministic transport codes is often preferred by the industrial organizations that must fulfil quality assurance procedures in nuclear reactor safety calculations. In fact there is no need, as in the case of the Monte Carlo codes, to justify the validity of the statistics adopted since the deterministic codes are based on rigorous analytical solutions of the neutral particle transport equations. Moreover, despite the free availability of systems which permit the problem-dependent nuclear data processing (NJOY/TRANSX [37], AMPX-77, SCAMPI, SCALE [38], etc.) to obtain broad-group working libraries of collapsed and self-shielded cross sections from fine-group general-purpose cross section libraries, the expertise about nuclear data processing systems and methods is not generally widespread at the industrial level. This implies that, also for quality assurance purposes, in order to reduce the probability of errors in the data entry during the problem-dependent data processing phase, it is often preferred using of already processed working libraries, with parameterized sets of self-shielded cross section libraries for a specific type of application and nuclear reactor (e.g., BUGLE-96 library for LWR shielding). In any case, to follow the quality assurance approach, working cross section libraries with parameterized sets of self-shielded cross section libraries, like BUGLE-96, are necessary to perform the validation of the problem-dependent working cross section libraries, possibly directly processed by the industrial organizations for a specific model of fission reactor.

3. Proposals

1) It would be highly recommendable to restart the generation of broad-group coupled neutron and photon working cross section libraries for nuclear reactor shielding and radiation damage applications with self-shielded neutron cross sections, obtained through problem-dependent cross section collapsing from fine-group general-purpose cross section libraries. In particular, to face also the project needs of the Generation IV nuclear fission reactors, it should be recommended to produce new working libraries, based on updated evaluated data (JEFF-3.1.1, ENDF/B-VII.0, etc,) and individually conceived for a definite type of reactor (LWR, SFR, LFR, HTR, etc.) with similar spectral, temperature, compositional and geometrical specifications.

2) With the possible involvement of IAEA and OECD/NEA, it would be highly recommendable to organize, at the international level, an influential and qualified forum of experts in nuclear and reactor physics in order to suggest and to propose to the national

nuclear data processing working groups, specific energy group structures of interest for the working cross section libraries dedicated to the various reactor types (LWR, SFR, LFR, HTR, etc.). In parallel, the forum of experts should verify and promote the availability of the research institutes and industrial organizations to release the needed data for the various reactors types: the temperature, compositional and geometrical data to permit the problem-dependent cross section collapsing and self-shielding, dedicated to obtaining the broad-group working library cross sections. It is underlined that, in particular, the availability of these data is a crucial point to produce, through problem-dependent collapsing, the specific correct self-shielding of the broad-group working library neutron cross sections. This action would also permit, in particular, parallel and independent nuclear safety analyses on the commercial nuclear power reactors, at the national level, addressed to improve the reliability of the nuclear safety calculation procedures.

3) To test the new working libraries, it should be important to extend the availability of neutron shielding benchmark experiments with new single-material and engineering experiments, dedicated to the various types of Generation III and Generation IV fission reactors. The relative compositional and geometrical data could be properly included, for example, in the SINBAD (ORNL/RSICC - OECD/NEA Data Bank) database, dedicated to fission reactor shielding benchmark experiments. At the same time it would be recommendable an increasing availability, within the SINBAD database, of 3D shielding calculation examples with deterministic transport codes, dedicated to the analysis of the fission reactor shielding benchmark experiments. This would contribute, promote and facilitate the use of the 3D deterministic transport codes and related group-wise working cross section libraries.

4. Conclusion

An initiative to promote the generation of broad-group working cross section libraries should be initiated at international level, possibly involving IAEA and OECD/NEA. The working libraries should be generated through problem-dependent collapsing of fine-group pseudo-problem-independent cross section libraries, based on the most recent evaluated nuclear data libraries (JEFF-3.1.1, ENDF/B-VII.0, JENDL-3.3, etc.), using reactor zone-weighted spectra for the specific reactor types (LWR, SFR, LFR, HTR, etc.) of current interest, i.e., the Generation III and IV nuclear fission reactors.

The neutron and photon energy group structures of the working libraries should be proposed by an international forum of specialists in nuclear and reactor physics in order to address the national nuclear data processing working groups to a reliable and qualified work of group-wise cross section libraries processing. IAEA and OECD/NEA could play an important role in organizing the international forum of specialists that would also verify the availability of the research institutes and industrial organizations in releasing the needed data for the various reactors types: the specific temperature, compositional and geometrical data to best match the problem-dependent cross section collapsing and self-shielding, leading to the broad-group working library cross sections.

The generation of broad-group working cross section libraries would permit their validation with the 3D deterministic transport codes, for various different spectral environments, on the single-material and engineering shielding benchmark experiments contained, e.g., in the SINBAD (ORNL/RSICC – OECD/NEA Data Bank) international database of fission reactor neutron shielding benchmark experiments.

The validation of the broad-group working cross section libraries, mainly performed by the national research institutes, would permit adding to the corresponding results that might be available with the 3D Monte Carlo codes, the complementary results obtained with the 3D deterministic transport codes, adopting a common consistent 3D geometrical approach. This would meet the increasing need, at the industrial and nuclear reactor safety level, of qualified validations of group-wise cross section libraries together with neutral particle deterministic transport codes. In fact these codes can offer accurate analytical solutions of the transport equations and do not require justifying the validity of the statistics adopted, as requested in the Monte Carlo analyses, towards the nuclear safety authorities.

REFERENCES

[1] DOORS3.1: One-, Two- and Three-Dimensional Discrete Ordinates Neutron/Photon Transport Code System, ORNL, RSIC Computer Code Collection CCC-650, August 1996. Available from OECD/NEA Data Bank as CCC-0650/04 DOORS-3.2A.

[2] DANTSYS 3.0: One-, Two-, and Three-Dimensional, Multigroup, Discrete Ordinates Transport Code System, ORNL, RSIC Computer Code Collection CCC-547, August 1995.

[3] R.E. ALCOUFFE, R.S. BAKER, J.A. DAHL, S.A. TURNER, R. WARD, PARTISN: A Time-Dependent, Parallel Neutral Particle Transport Code System, LA-UR-05-3925, May 2005. Available from OECD/NEA Data Bank as CCC-0707/02 PARTISN-4.00.

[4] J.F. BRIESMEISTER Ed., MCNP - A General Monte Carlo N-Particle Transport Code, Version 4C, LANL, LA-13709-M, April 2000.

[5] I.I. BONDARENKO, M.N. NIKOLAEV, L.P. ABAGYAN, N.O. BAZAZIANTS, Group Constants for Nuclear Reactors Calculations, Consultants Bureau, New York, 1964.

[6] J.E. WHITE, D.T. INGERSOLL, R.Q. WRIGHT, H.T. HUNTER, C.O. SLATER, N.M. GREENE, R.E. MACFARLANE, R.W. ROUSSIN, Production and Testing of the Revised VITAMIN-B6 Fine-Group and the BUGLE-96 Broad-Group Neutron/Photon Cross-Section Libraries Derived from ENDF/B-VI.3 Nuclear Data, Oak Ridge National Laboratory, NUREG/CR-6214, Revision 1, ORNL-6795/R1, 1996. Available from OECD/NEA Data Bank as DLC-0184/ ZZ VITAMIN-B6.

[7] W.A. RHOADES, D.B. SIMPSON, The TORT Three-Dimensional Discrete Ordinates Neutron/Photon Transport Code (TORT Version 3), ORNL, ORNL/TM-13221, October 1997.

[8] R. ORSI, BOT3P Version 5.3: A Pre/Post-Processor System for Transport Analysis, ENEA FPN-P9H6-011, October 22, 2008. Available from OECD/NEA Data Bank as NEA-1678/09 BOT3P5.3.

[9] P.F. ROSE, ENDF/B-VI Summary Documentation, Brookhaven National Laboratory, BNL-NCS-17541 (ENDF-201) 4th Edition, October 1991.

[10] R.W. ROUSSIN, C.R. WEISBIN, J.E. WHITE, N.M. GREENE, R.Q. WRIGHT, J.B. WRIGHT, VITAMIN-C: The CTR Processed Multigroup Cross Section Library for Neutronics Studies, Oak Ridge National Laboratory, ORNL/RSIC-37, 1980. Available from OECD/NEA Data Bank as DLC-0041/VITAMIN-C.

[11] C.R. WEISBIN, R.W. ROUSSIN, J.J. WAGSCHAL, J.E. WHITE, R.Q. WRIGHT, VITAMIN-E: An ENDF/B-V Multigroup Cross-Section Library for LMFBR Core and Shield, LWR Shield, Dosimetry and Fusion Blanket Technology, Oak Ridge National Laboratory, ORNL-5505 (ENDF-274), February 1979. Available from OECD/NEA Data Bank as DLC-0113/VITAMIN-E.

[12] E. SARTORI, VITAMIN-J, a 175 group Neutron Cross Section Library Based on JEF-1 for Shielding Benchmark Calculations, OECD/NEA Data Bank, JEF/DOC-100 Preliminary, October 1985.
[13] D.W. NIGG, P.D. RANDOLPH, F.J. WHEELER, Demonstration of Three-Dimensional Deterministic Radiation Transport Theory Dose Distribution Analysis for Boron Neutron Capture Therapy, Medical Physics, Volume 18, No. 1, January/February 1991.
[14] I. REMEC, J.A. WANG, F.B.K. KAM, K. FARREL, Effects of Gamma-Induced Displacements on HFIR Pressure Vessel Materials, Journal of Nuclear Materials, Volume 217, pp. 258-268, 1994.
[15] D.E. ALEXANDER, L.E. REHN, The Role of Gamma Rays and Freely-Migrating Defects in Reactor Pressure Vessel Embrittlement, Proceedings of the 9th International Symposium on Reactor Dosimetry, Prague, Czech Republic, 2-6 September 1996, World Scientific, pp. 508-515, 1998.
[16] D.E. ALEXANDER, L.E. REHN, The Contribution of High Energy Gamma Rays to Displacement Damage in LWR Pressure Vessels, Letter to the Editors, Journal of Nuclear Materials, Volume 209, pp. 212-214, 1994.
[17] The JEF-2.2 Nuclear Data Library, JEFF Report 17, OECD/NEA Data Bank, April 2000.
[18] M. PESCARINI, R. ORSI, T. MARTINELLI, A.I. BLOKHIN, V. SINITSA, VITJEF22.BOLIB – A JEF-2.2 Multigroup Coupled (199 n + 42 γ) Cross Section Library in AMPX Format for Nuclear Fission Applications, ENEA FIS-P815-001, April 16, 2003. Available from OECD/NEA Data Bank as NEA-1699/01 ZZ VITJEF22.BOLIB.
[19] M. PESCARINI, R. ORSI, T. MARTINELLI, A.I. BLOKHIN, V. SINITSA, MATJEF22.BOLIB – A JEF-2.2 Multigroup Coupled (199 n + 42 γ) Cross Section Library in MATXS Format for Nuclear Fission Applications, ENEA FIS-P815-007, June 6, 2004. Available from OECD/NEA Data Bank as NEA-1740/01 ZZ MATJEF22.BOLIB.
[20] The JEFF-3.1 Nuclear Data Library, JEFF Report 21, OECD/NEA Data Bank, 2006.
[21] M. PESCARINI, V. SINITSA, R. ORSI, VITJEFF31.BOLIB – A JEFF-3.1 Multigroup Coupled (199 n + 42 γ) Cross Section Library in AMPX Format for Nuclear Fission Applications, ENEA FPN-P9H6-007, February 18, 2008. Available from OECD/NEA Data Bank as NEA-1801/01 ZZ VITJEFF31.BOLIB.
[22] M. PESCARINI, V. SINITSA, R. ORSI, MATJEFF31.BOLIB – A JEFF-3.1 Multigroup Coupled (199 n + 42 γ) Cross Section Library in MATXS Format for Nuclear Fission Applications, ENEA FPN-P9H6-014, May 5, 2009. Available from OECD/NEA Data Bank as NEA-1847/01 ZZ MATJEFF31.BOLIB.
[23] R.E. MACFARLANE, NJOY-99, "README0", PSR-0480/02, December 31, 1999.
[24] SCAMPI: Collection of Codes for Manipulating Multigroup Cross Section Libraries in AMPX Format, Oak Ridge National Laboratory, RSIC Peripheral Shielding Routine Collection PSR-352, September 1995. Available from OECD/NEA Data Bank as PSR-0352 SCAMPI.
[25] N.M. GREENE, W.E. FORD III, L.M. PETRIE, J.W. ARWOOD, AMPX-77: A Modular Code System for Generating Coupled Multigroup Neutron-Gamma Cross-Section Libraries from ENDF/B-IV and/or ENDF/B-V, ORNL/CSD/TM-283, October 1992. Available from OECD/NEA Data Bank as PSR-0315 AMPX-77.
[26] V. SINITSA, M. PESCARINI, ENEA-Bologna 2007 Revision of the SCAMPI (ORNL) Nuclear Data Processing System, ENEA FPN-P9H6-006, September 13, 2007. Available from OECD/NEA Data Bank as PSR-0352/05 SCAMPI.
[27] The JEFF-3.1.1 Nuclear Data Library, JEFF Report 22, OECD/NEA Data Bank, 2009.

[28] M.B. CHADWICK *et al*., ENDF/B-VII.0: Next Generation Evaluated Nuclear Data Library for Nuclear Science and Technology, Nuclear Data Sheets, Volume 107, Number 12, December 2006.
[29] O. BERSILLON, L.R. GREENWOOD, P.J. GRIFFIN, W. MANNHART, H.J. NOLTHENIUS, R. PAVIOTTI-CORCUERA, K.I. ZOLOTAREV, E.M. ZSOLNAY, "International Reactor Dosimetry File 2002.
(IRDF-2002)", International Atomic Energy Agency, Vienna (A), Technical Report Series No.452, 2006.
[30] R. ORSI, M. PESCARINI, Dosimetry Cross Section Processing from IRDF-2002 in the BUGLE-96 (47 n) Neutron Group Structure, ENEA FPN-P9H6-015, September 22, 2009.
[31] Prediction of Neutron Embrittlement in the Reactor Pressure Vessel: VENUS-1 and VENUS-3 Benchmarks, NEA/NSC/DOC(2000)5, OECD/NEA NSC, 2000.
[32] M. PESCARINI, M.G. BORGIA, R. ORSI, VENUS-1 Benchmark Experiment Details and Results of the ENEA-Bologna Calculations, Second Meeting of the OECD/NEA Nuclear Science Committee Task Force on Computing Radiation Dose and Modelling of Radiation-Induced Degradation of Reactor Components (TFRDD), Paris, France, March 3-4, 1998.
[33] M. PESCARINI, M.G. BORGIA, R. ORSI, T. MARTINELLI, ENEA-Bologna Validation of the BUGLE-96 ENDF/B-VI Library on the VENUS-1 Neutron Shielding Benchmark Experiment - A Synthesis of the Final Results, ENEA Bologna, ENEA SIEC KT-SCG-00005, 1999. JEF/DOC-778, JEFF Working Group Meeting on Benchmark Testing, Data Processing and Evaluations, OECD/NEA Data Bank, Issy-les-Moulineaux, France, April 12-14, 1999.
[34] M. PESCARINI, R. ORSI, M.G. BORGIA, T. MARTINELLI, ENEA Nuclear Data Centre Neutron Transport Analysis of the VENUS-3 Shielding Benchmark Experiment, ENEA Bologna, ENEA SIEC KT-SCG-00013, March 19, 2001. PDF electronic version included in the NEA-1517 SINBAD REACTOR (ORNL/RSICC - OECD/NEA Data Bank) international data base of fission reactor shielding benchmark experiments.
[35] M. PESCARINI, R. ORSI, T. MARTINELLI, Automatic Generation of 3D Fine Mesh Geometries for the Analysis of the VENUS-3 Shielding Benchmark Experiment with the TORT Code, Proceedings of the International Conference on Supercomputing in Nuclear Applications, SNA-2003, Paris, France, September 22-24, 2003. ENEA FIS-P815-004, October 22, 2003.
[36] M. PESCARINI, V. SINITSA, R. ORSI, Generation and Preliminary Testing of ENEA–Bologna BUGLE-Type Group Libraries Based on JEFF-3.1 and ENDF/B-VII.0 Nuclear Data for LWR Shielding and Pressure Vessel Dosimetry, Proceedings of the International Conference on the Physics of Reactors "Nuclear Power: A Sustainable Resource", Interlaken, Switzerland, September 14-19, 2008. ENEA FPN-P9H6-012, October 3, 2008.
[37] TRANSX 2.15: Code System to Produce Neutron, Photon, and Particle Transport Tables for Discrete –Ordinates and Diffusion Codes from Cross Sections in MATXS Format, RSIC Peripheral Shielding Routine Collection PSR-317, February 1995. Available from OECD/NEA Data Bank as PSR-0317 TRANSX 2.15.
[38] SCALE: A Modular Code System for Performing Standardized Computer Analyses for Licensing Evaluation, ORNL/TM-2005/39, Version 6.0, Vols. I-III, January 2009. Available from OECD/NEA Data Bank as CCC-0750 SCALE 6.

ANNEX I. RECOMMENDED MEASUREMENTS OF NUCLEAR DATA AT RR FACILITIES

In order to stimulate the continuation or installation of new nuclear data measurement programmes at RR facilities, the following list of present nuclear data needs is given in this Annex. This list is primarily based on the OECD/NEA high priority list accessible via the following weblink: *www.nea.fr/html/dbdata/hprl/hprl.pl* (also see Annex II). Furthermore, the measurements of fission fragment yields and integral measurements for nuclear data validation are equally recommended. In particular, the efforts on optimization of neutron beams in terms of intensity and spectral shape as well as developing dedicated associated instrumentation should be continued.

The meeting participants recommend the following measurements to be performed at RR facilities as the 1st priority, where H. and G. refer to the list given in Annex II:

- Measurements of capture cross sections for ^{239,241}Pu (H.32 and H.33)
- Measurements of important inelastic cross sections, e.g., ^{56}Fe (integral measurement of neutron flux and shape as well as gamma heating in the moderating media with a fission neutron spectrum as source; H.34), ^{238}U (k_{eff} in conjunction with follow-up measurements as H.18), ^{23}Na (void reactivity coefficient and H.29), ^{28}Si (H.40), ^{206,207}Pb (H.41, H.42) and ^{nat}Zr. Alternative methods based on filtered beams and fission converters may contribute to the list of measurement techniques, but need dedicated investigation
- Measurements of prompt neutron-photon multiplicities and energy spectra both with thermal and fast fission neutron energy spectra
    - Neutrons: ^{243}Am (G.16, spectrum), ^{244}Cm (G.17, spectrum), ^{233}U (G.9, nubar) and ^{240}Pu (H.38, nubar). Both integral and differential measurements are recommended, also as a function of incident neutron energy provided by velocity selected or filtered beams. Both types of methods should be applied in the same measurement environment to eventually remove existing discrepancies. A crucial point to improve the existing data will be to arrive at a detection technique covering the full energy range of fission neutrons
    - Photons: ^{235}U (H.4) and ^{239}Pu (H.3). Thermo or optical luminescence dosimetry, giving the integrated prompt and delayed dose; methods are insensitive to the neutron component but do not provide spectral information; spectral measurements of prompt gamma emission require separation of gamma-rays from neutrons by, for example, TOF or pulse shape discrimination
- Correlated pre- and post-neutron fission fragment yield measurements for ^{233,235}U and ^{239,241}Pu with thermal and fast fission spectrum neutron beams and for ^{232}Th and ^{238}U using a fast fission spectrum. Here, increased efforts to develop high-resolution fission fragment spectrometers with sufficient detection efficiency are paramount.

- Fission cross section measurements for ^{232}Pa and ^{238}Np, and also for other minor actinides (e.g., ^{245}Cm), at well-defined incident neutron energies

- Dedicated integral experiments for reaction rates and cross section validation in well-defined and variable neutron energy spectra, cf. contributed papers from El Bakkari, Bernard, Kochetkov and Mahlers

- Measurements of capture cross sections and decay data relevant to production of certain radioisotopes relevant for nuclear medicine applications (e.g., ^{99}Mo, ^{177}Lu, ^{188}Re) and requiring very intense thermal fluxes

- Experimental and evaluation efforts towards the establishment or improvement of covariance matrices relevant to reaction cross sections and propagation of associated uncertainties in reaction rates and decay data, in particular those of material evolution and transmutation calculations

ANNEX II. OECD/NEA NUCLEAR DATA HIGH PRIORITY LIST

Note: more detailed information on specific reaction, neutron energy range, precision required, etc., is available from the official OECD/NEA web site at http://www.nea.fr/html/dbdata/hprl/hprl.pl, which should be checked regularly for updates. The below snapshot gives the status of high priority nuclear data needs as of May 2010.

Req.	ID	View	Target	Reaction	Quantity	Energy range	Sec.E/Angle	Accuracy	Cov	Field	Date
G	1		14-SI-28	(n,np)	SIG	Threshold-20 MeV	4 pi	20	Y	Fusion	21-SEP-05
H	2		8-O-16	(n,a),(n,abs)	SIG	2 MeV-20 MeV		See details	Y	Fission	21-SEP-05
H	3		94-PU-239	(n,f)	Prompt g-prod	Thermal-Fast	Eg=0-10MeV	7.5	Y	Fission	28-APR-06
H	4		92-U-235	(n,f)	prompt g-prod	Thermal-Fast	Eg=0-10MeV	7.5	Y	Fission	10-MAY-06
H	5		72-HF-0	(n,g)	SIG	0.5-5.0 keV		4	Y	Fission	28-APR-06
G	6		92-U-233	(n,g)	SIG	10 keV-1.0 MeV		9	Y	Fission	28-APR-06
G	7		26-FE-56	(n,xn)	SIG,DDX	7 MeV-20 MeV	1MeV-20MeV	30		Fission,ADS	13-JUL-06
H	8		1-H-2	(n,ela)	dA/dE	0.1 MeV-1 MeV	0-180 Deg	5	Y	Fission	25-JUL-06
G	9		92-U-233	(n,g)	nubar, SIG	Thermal-10 keV		.5	Y	Fission	19-APR-07
G	10		79-AU-197	(n,tot)	SIG	5 keV-200 keV		5		Science,Fusion	18-MAY-07
G	11		94-PU-239	(n,f), (n,g)	SIG,eta, alpha	1 meV-1 eV		1	Y	Fission	09-MAY-07
H	12		92-U-235	(n,g)	SIG, RP	100 eV-1 MeV		3	Y	Fission	29-AUG-07
G	13		24-CR-52	(n,xd), (n,xt)	SIG	Threshold-65 MeV		20	Y	Fusion	23-OCT-07
G	14		94-PU-242	(n,g), (n,tot)	SIG	0.5 eV-2.0 keV		8	Y	Fission	06-JUL-07
H	15		95-AM-241	(n,g), (n,tot)	SIG	Thermal		See details		Fission	08-NOV-07
G	16		95-AM-243	(n,f)	n spectrum	Eth-10 MeV		10		ADS	08-NOV-07
G	17		96-CM-244	(n,f)	n spectrum	Eth-10 MeV		10		ADS	08-NOV-07
H	18		92-U-238	(n,inl)	SIG	65 keV-20 MeV	Emis spec.	See details	Y	Fission	28-MAR-08
H	19		94-PU-238	(n,f)	SIG	9 keV-6 MeV		See details	Y	Fission	31-MAR-08
H	21		95-AM-241	(n,f)	SIG	180 keV-20 MeV		See details	Y	Fission	31-MAR-08
H	22		95-AM-242	(n,f)	SIG	0.5 keV-6 MeV		See details	Y	Fission	31-MAR-08
H	25		96-CM-244	(n,f)	SIG	65 keV-6 MeV		See details	Y	Fission	04-APR-08
H	27		96-CM-245	(n,f)	SIG	0.5 keV-6 MeV		See details	Y	Fission	04-APR-08
H	29		11-NA-23	(n,inl)	SIG	0.5 MeV-1.3 MeV	Emis spec.	See details	Y	Fission	04-APR-08
H	32		94-PU-239	(n,g)	SIG	0.1 eV-1.35 MeV		See details	Y	Fission	04-APR-08
H	33		94-PU-241	(n,g)	SIG	0.1 eV-1.35 MeV		See details	Y	Fission	04-APR-08
H	34		26-FE-56	(n,n')	SIG	0.5 MeV-20 MeV	Emis spec.	See details	Y	Fission	04-APR-08
H	35		94-PU-241	(n,f)	SIG	0.5 eV-1.35 MeV		See details	Y	Fission	04-APR-08
H	36		92-U-238	(n,g)	SIG	20 eV-25 keV		See details	Y	Fission	15-SEP-08
H	37		94-PU-240	(n,f)	SIG	0.5 keV-5 MeV		See details	Y	Fission	15-SEP-08
H	38		94-PU-240	(n,f)	nubar	200 keV-2 MeV		See details	Y	Fission	15-SEP-08
H	39		94-PU-242	(n,f)	SIG	200 keV-20 MeV		See details	Y	Fission	15-SEP-08
H	40		14-SI-28	(n,inl)	SIG	1.4 MeV-6 MeV		See details	Y	Fission	15-SEP-08
H	41		82-PB-206	(n,inl)	SIG	0.5 MeV-6 MeV		See details	Y	Fission	15-SEP-08
H	42		82-PB-207	(n,inl)	SIG	0.5 MeV-6 MeV		See details	Y	Fission	15-SEP-08

ANNEX III. LIST OF RR FACILITIES PROVIDING NUCLEAR DATA MEASUREMENTS

Source: IAEA RR Data Base available at http://www.iaea.org/worldatom/rrdb/, May 2010.

Country	Reactor Name	Thermal Power (kW)	Type	Thermal Flux, n/cm^2/s	Fast flux, n/cm^2/s	Criticality Date	Facility web link
Bangladesh	TRIGA MARK II	3,000.00	TRIGA MARK II	7.5 E13	3.8 E13	1986/09/14	AERE
Brazil	IPEN/MB-01	0.10	Crit Assembly	1.0 E09	6.0 E09	1988/11/09	IPEN
Belgium	VENUS	0.50	Crit Assembly	5.0 E09		1964/04/30	SCK/CEN
Belgium	BR-1	4000.00	Graphite	2.0 E12	2.0E11	1956/05/11	SCK/CEN
China	MNSR IAE	27.00	MNSR	1.0 E12	1.0 E12	1984/03/10	CIAE
China	HWRR-II	15000.00	Heavy Water	2.4 E14	5.2 E12	1958/09/01	CIAE
China	SPR IAE	3500.00	Pool	4.0 E13	1.1 E13	1964/12/20	CIAE
France	MASURCA	5.00	Fast Critical Assembly		3.0 E09	1966/12/01	CEA Cadarche
France	EOLE	0.10	Tank in Pool	1.0 E09		1965/12/02	CEA Cadarache
France	HFR	58300.00	Heavy Water	1.5 E15		1971/07/01	ILL
France	SILENE	1.00	Homogeneous	1.0 E16	2.0 E16	1974/01/01	CEA Valduc
France	MINERVE	0.10	Pool	1.0 E09		1959/09/29	CEA Cadarache
Ghana	GHARR-1	30.00	MNSR	1.0 E12	1.2 E12	1994/12/17	NNRI
Hungary	BUDAPEST RES. REACTOR	10000.00	Tank WWR	2.5 E14	1.0 E14	1959/03/25	KFKI AEKI
India	APSARA	1000.00	Pool	1.3 E13	1.0 E12	1956/08/04	BARC
Israel	IRR-2	26000.00	Heavy Water			1963/12/01	NRCN
Italy	RSV TAPIRO	5.00	Fast Source		4.0 E12	1971/04/04	ENEA
Japan	FCA	2.00	Fast Critical Assembly		5.0 E09	1967/04/29	JAEA
Japan	KUR	5000.00	Tank	6.0 E13	6.5 E13	1964/06/25	KURRI
Japan	JRR-4	3500.00	Pool	7.0 E13	8.7 E13	1965/01/28	JAEA
Japan	KUCA	0.10	Critical Assembly	1.0 E09	1.0 E09	1974/08/06	KURRI
Japan	JRR-3M	20000.00	Pool	2.7 E14	1.4 E14	1990/03/22	JAEA
Korea, Republic of	HANARO	3000.00	Pool	4.5 E14	3.0E14	1995/02/08	KAERI
Morocco	MA-R1	2000.00	TRIGA Mark II	4.4 E13	1.8 E13	2007/05/02	CNESTEN
Nigeria	NIRR-0001	30.00	MNSR	1.0 E12	5.0 E12	2004/02/03	CERT
Russian Federation	BFS-1	0.20	Critical Assembly			1961/01/01	IPPE
Russian Federation	BFS-2	1.00	Critical Assembly			1969/01/01	IPPE
Russian Federation	IBR-2M	1500.00	Fast Burst	1.0 E13	1.5 E14	1977/11/30	JINR
Russian Federation	SM-3	100000.00	Pressure Vessel	5.0 E15	2.0 E15	1961/01/10	RIAR

Switzerland	PROTEUS	1.00	Critical Assembly	5.0 E09	5.0 E09	1968/01/01	PSI
Ukraine	WWR-M KIEV	10000.00	Tank WWR	1.2 E14	0.7 E14	1960/12/02	INR Kiev
United States of America	AGN-201 TEXAS A&M UNIV.	0.01	Homogeneous	2.0 E08	1.0 E08	1957/01/01	AGN-201M NRL
United States of America	KSU TRIGA MK II	250.00	TRIGA Mark II	1.0 E13	1.2 E13	1962/10/16	KSU MNE
United States of America	NSCR TEXAS A&M UNIV.	1000.00	Converted TRIGA	2.0 E13	2.0 E11	1962/01/01	NSC
United States of America	OSTR, OREGON STATE UNIV.	1100.00	TRIGA Mark III	1.0 E13	5.0 E13	1967/03/08	OSURC
United States of America	OSURR OHIO ST. UNIV.	500.00	Pool	1.5 E13	1.0 E13	1961/03/16	OSU NRL
United States of America	UMLR UNIV. MASS. LOWELL	1000.00	Pool	1.4 E13	9.2 E12	1975/01/02	UMLRL
United States of America	HFIR	85000.00	Tank	2.5 E15	1.0 E15	1965/08/01	ORNL
United States of America	UMRR	200.00	Pool MTR	2.0 E12	1.0 E12	1961/12/11	MUST NE
Vietnam	DALAT RESEARCH REACTOR	500.00	Pool	2.1 E13	6.0 E12	1963/02/26	DNRI

ANNEX IV. MONITOR REACTIONS AND MATERIALS FOR NEUTRON SPECTRUM CHARACTERIZATION

Source: Mr Mark A. Kellett, NDS/NAPC-IAEA, M.A.Kellett@iaea.org; November 2009
Recommendations by Frans De Corte (Ghent University, Belgium) for other candidate materials that have suitable capture and threshold reactions
• Au, Zr and Lu; standard materials available as components of k_0-IAEA.
Requests should be addressed to: Mr M. Haji-Saeid, IAEA, Head of Industrial Applications and Chemistry Section, NAPC-IAEA
• Additionally recommended:

1) $^{115}In(n,n')^{115m}In$ [T½ = 4.486 h; Eγ = 336.2 keV, 45.9 %]
~ 0.025 MBq /mg, φ_f (= $1x10^{11}$ n/(s cm^2)) × t_{irr} (=5 h)
~ 12000 γ ·s^{-1} / mg, φ_f (= $1x10^{11}$ n/(s cm^2)) × t_{irr} (=5 h)
Notes: a) to be used under Cd-cover; b) not to be used for (n, γ) activation, because of neutron self-shielding problems.

2) $^{64}Zn(n,p)^{64}Cu$ [T½ = 12.70 h; Eγ = 511.0 keV, 35.7 %]
~ 0.0033 MBq /mg, φ_f (= $1x10^{11}$ n/(s cm^2))×t_{irr} (=5 h)
~ 1200 γ·s^{-1} / mg, φ_f (= $1x10^{11}$ n/(s cm^2)) × t_{irr} (=5 h)
Notes: a) to be used under Cd-cover; b) low Cu-content = 15 ppm.

3) $^{64}Zn(n,\gamma)^{65}Zn$ [T½ = 244.3 d; Eγ = 1115.5 keV, 50.6 %]
~ 0.0038 MBq /mg, φ_{th} (= $2x10^{12}$ n/(s cm^2)) × t_{irr} (=5 h)
~ 0.00038 MBq /mg, φ_{epi} (= $1x10^{11}$ n/(s cm^2)) × t_{irr} (=5 h)
~ 1900 γ·s^{-1} / mg, φ_{th} (= $2x10^{12}$ n/(s cm^2)) × t_{irr} (=5 h)
~ 190 γ·s^{-1} / mg, φ_{epi} (= $1x10^{11}$ n/(s cm^2)) × t_{irr} (=5 h)

4) $^{68}Zn(n,\gamma)^{69m}Zn$ [T½ = 13.76 h; Eγ = 438.6 keV, 94.8 %]
~ 0.054 MBq /mg, φ_{th} (= $2x10^{12}$ n/(s cm^2)) × t_{irr} (=5 h)
~ 0.0086 MBq /mg, φ_{epi} (= $1x10^{11}$ n/(s cm^2)) × t_{irr} (=5 h)
~ 51000 γ·s^{-1} / mg, φ_{th} (= $2x10^{12}$ n/(s cm^2)) × t_{irr} (=5 h)
~ 8100 γ·s^{-1} / mg, φ_{epi} (= $1x10^{11}$ n/(s cm^2)) × t_{irr} (=5 h)

5) $^{58}Ni(n,p)^{58}Co$ [T½ = 70.86 d; Eγ = 810.8 keV, 99.5 %]
~ 0.00016 MBq /mg,φ_f (= $1x10^{11}$ n/(s cm^2)) × t_{irr} (=5 h)
~ 160 γ·s^{-1} / mg, φ_f (= $1x10^{11}$ n/(s cm^2)) × t_{irr} (=5 h)
Note: preferably to be used under Cd-cover.

6) $^{54}Fe(n,p)^{54}Mn$ [T½ = 312.1 d; Eγ = 834.8 keV, 99.98 %]
~ 0.0000024 MBq /mg, φ_f (= $1x10^{11}$ n/(s cm^2)) × t_{irr} (=5 h)
~ 2.4 γ·s^{-1} / mg, φ_f (= $1x10^{11}$ n/(s cm^2)) × t_{irr} (=5 h)
Note: preferably to be used under Cd-cover.

7) $^{58}Fe(n,\gamma)^{59}Fe$ [T½ = 44.50 d; Eγ = 1099.3 keV, 56.5 %; Eγ = 1291.6 keV, 43.2 %]
~ 0.00026 MBq /mg, φ_{th} (= $2x10^{12}$ n/(s cm^2)) × t_{irr} (=5 h)
~ 0.000013 MBq /mg,φ_{epi} (= $1x10^{11}$ n/(s cm^2)) × t_{irr} (=5 h)
~ 150 γ·s^{-1} / mg, φ_{th} (= $2x10^{12}$ n/(s cm^2)) × t_{irr} (=5 h); [1099.3 keV]
~ 7.5 γ ·s^{-1} / mg, φ_{epi} (= $1x10^{11}$ n/(s cm^2)) × t_{irr} (=5 h); [1099.3 keV]

8) $^{98}Mo(n,\gamma)^{99}Mo$ [T½ = 65.94 h; Eγ = 140.5 keV (^{99m}Tc; T½ = 6.01 h), 89.06 %]
~ 0.02 MBq /mg, φ_{th} (= $2x10^{12}$ n/(s cm^2)) × t_{irr} (=5 h)
~ 0.05 MBq /mg, φ_{epi} (= $1x10^{11}$ n/(s cm^2)) × t_{irr} (=5 h)
~ 18000 γ·s^{-1} / mg, φ_{th} (= $2x10^{12}$ n/(s cm^2)) × t_{irr} (=5 h)
~ 45000 γ ·s^{-1} / mg, φ_{epi} (= $1x10^{11}$ n/(s cm^2)) × t_{irr} (=5 h)

9) $^{100}Mo(n,\gamma)^{101}Mo$ [T½ = 14.61 min; Eγ = 306.8 keV (^{101}Tc; T½ = 14.2 min), 88.7 %]
~ 0.24 MBq /mg, φ_{th} (= $2x10^{12}$ n/(s cm^2)) × t_{irr} (=5 h)
~ 0.23 MBq /mg, φ_{epi} (= $1x10^{11}$ n/(s cm^2)) × t_{irr} (=5 h)
~ 200000 γ·s^{-1} / mg, φ_{th} (= $2x10^{12}$ n/(s cm^2)) ×t_{irr} (=5 h)

$\sim 200000\ \gamma \cdot s^{-1}$ / mg, φ_{epi} (= $1x10^{11}$ n/(s cm^2)) × t_{irr} (=5 h)

Availability of synthetic multi-element standard materials (SMELS)

Peter Vermaercke (SCK, Mol) was contacted during 2006 and reported that SMELS material is available for use in validating the implementation of the k_0 method in a given laboratory and/or research reactor. SMELS material can, in principle, be made available upon written request, but that no new production of the SMELS material is envisaged in the near future.

ANNEX V. LIST OF PARTICIPANTS

Bangladesh	Hossain S.M.	Bangladesh Atomic Energy Commission Institute of Nuclear Science & Technology (INST) Atomic Energy Research Establishment (AERE) G.P.O. Box No.-3787 Dhaka 1000, Bangladesh Tel: 880 2 7788249 Fax: 880 2 7701337 E-mail: Syed9495@yahoo.com
Belgium	Kochetkov A.	SCK.CEN Boererang 200 BE-2400 Mol Belgium Tel.: 32 14332193 Fax: 32 14321529 E-mail: anatoly.kochetkov@sckcen.be
Canada	Buijs A.	McMaster University 1280 Main Street Hamilton L8S 4L7 Canada Tel: 1 905 525 9140 ext. 24925 Fax: 1905 5278409 E-mail buijsa@mcmaster.ca
China	Ge Zhigang	China Nuclear Data Center P.O.Box 275-41 Beijing 102413 P.R.China Tel: 86-10-69357275 Fax: 86-10-69358119 E-mail gezg@ciae.ac.cn
EU	Oberstedt S.	European Commission Joint Research Centre IRMM Retieseweg 111 B-2440 Geel Belgium Tel.: +32 14571361 Fax: +32 14571376 E-mail: Stephan.Oberstedt@ec.europa.eu
France	Bernard D.	Commissariat a l'Energie Atomique CEA Bâtiment 230 F- 13108 Saint Paul lez Durance France Tel: (+33) 4 42 25 49 13 Fax: (+33) 4 42 25 70 09 E-mail: david.bernard@cea.fr
France	Köster U.	Institut Laue Langevin 6 rue Jules Horowitz F-38042 Grenoble Cedex 9 France Tel: 33 47620 7154 Fax: 33 47620 7777 E-mail koester@ill.fr

France	Letourneau A.	Commissariat a l'Energie Atomique CEA/Saclay Bâtiment 703 91191 Gif sur Ivette Cedex France Tel: 33 1 69 08 76 01 Fax: 33 1 69 08 75 84 E-mail aletourneau@cea.fr
France	Serot O	Commissariat a l'Energie Atomique CEA Bâtiment 230 F- 13108 Saint Paul lez Durance France Tel: 33 442257630 Fax: 33 442257009 E-mail olivier.serot@cea.fr
Ghana	Nyarko B.J.B.	National Nuclear Research Institute Ghana Atomic Energy Commission P.O. Box LG 80 Legon-Accra - Ghana Tel: 233 277406076 Fax: 233 21 400807 E-mail b.nyarko@gaecgh.org
India	Rasheed K.K.	Bhabha Atomic Research Centre Reactor Physics Design Division Engg. Hall # 1 BARC, Mumbai-400085 India Tel: 91 22 25593623 Fax: 91 22 25505151 E-mail krasheed@barc.gov.in
Italy	Pescarini M.	ENEA Via Martiri di Monte Sole 40129 Bologna - Italy Tel: 39 051 6098233 Fax: 39 051 6098705 E-mail massimo.pescarini@enea.it
Italy	Rosa R.	ENEA Via Anguillarese 301 00123 Roma - Italy Tel: 39 063 0484883 Fax: 39 063 0484874 E-mail roberto.rosa@enea.it
Italy	Santagata A.	ENEA Via Anguillarese 301 00123 Roma - Italy Tel: 39 063 0484258 Fax: 39 063 0486436 E-mail alfonso.santaga@enea.it
Japan	Oshima M.	Japan Atomic Energy Agency (JAEA) 2-4 Shirakata-Shirane TOKAI, Naka-gun Ibaraki-ken 319-1195, Japan Tel: +81 29 282 5458 Fax: +81 29 282 5458 E-mail oshima.masumi@jaea.go.jp

Korea, Rep. of	Kim Myong-Seop	Korea Atomic Energy Research Institute 1045 Daedeok-daero Yuseong, 305-353, Daejeon Korea, Rep. of Tel: +82 42 868 8666 Fax: +82 42 861 0209 E-mail mskim@kaeri.re.kr
Morocco	EL Bakkari B.	Centre d'Etudes Nucléaires de la Maâmora CNESTEN/CENM Centre d'Etudes Nucléaires de la Maâmora B.P.1382 R.P. Rabat 10001 P.O. Box 1382 Rabat, Morocco Tel: 212 651235092 Fax: 212 537803277 E-mail bakkari@cnesten.org.ma
Nigeria	Jonah S.	Nigeria Atomic Energy Commission 9 Kwame Nkrumah Crescent Asokoro, P.M.B. 646, Garki, Abuja, Nigeria Tel: 234 93146512 Fax: 234 93146516 E-mail jonahsa2001@yahoo.com
Spain	Cabellos O.	Universidad Politecnica de Madrid Department of Nuclear Engineering C/Jose Gutierrez Abascal 2 Madrid, 28006, Spain Tel: 34 913363108 Fax: 34 913363002 E-mail cabellos@din.upm.es
Ukraine	Gritzay O.	Institute for Nuclear Research of National Academy of Sciences of Ukraine Prospekt Nauky 47 Kyiv, Ukraine, 03680 Tel: 380 44 525 3987 Fax: 380 44 525 4463 E-mail ogritzay@kinr.kiev.ua
Ukraine	Mahlers Y.	Institute for Nuclear Research 47 Prospect Nauki Kiev 03680 Ukraine Tel: 380 44525-5105 Fax: 380 44 525 5105 E-mail mahlers@gluk.org
OECD/NEA	Rugama Y.	OECD/NEA, Nuclear Science 12 Bd des Iles 92130 Issy-les-Moulineaux France Tel: 33 14 5241099 Fax: 33 45 241128 E-mail rugama@nea.fr

IAEA	Pronyaev V.	International Atomic Energy Agency Department of Nuclear Sciences and Applications Division of Physical and Chemical Sciences Nuclear Data Section Vienna International Centre P.O. Box 100 1400 WIEN, AUSTRIA Tel.: +43-1-2600-21717 Fax: 0043 1 26007 EMail: V.Pronyaev@iaea.org
IAEA	Capote Noy, R. M.	International Atomic Energy Agency Department of Nuclear Sciences and Applications Division of Physical and Chemical Sciences Nuclear Data Section Vienna International Centre P.O. Box 100 1400 WIEN, AUSTRIA Tel.: +43-1-2600-21713 Fax: 0043 1 26007 EMail: R.CapoteNoy@iaea.org
IAEA	Ridikas D. (Scientific Secretary)	International Atomic Energy Agency Department of Nuclear Sciences and Applications Division of Physical and Chemical Sciences Physics Section Vienna International Centre P.O. Box 100 1400 WIEN, AUSTRIA Tel.: 0043 1 2600 21751 Fax: 0043 1 26007 EMail: D.Ridikas@iaea.org

ANNEX VI. MEETING AGENDA

Monday, 12 October 2009

08:30-09:30	**Registration, Gate 1**
09:30-10:30	**Welcome & Opening Remarks** *Mr G. Mank (Section Head, Physics Section, NAPC)* *Mr. D. Abriola (Acting Section Head, Nuclear Data Section, NAPC)* *Ms Y. Rugama (Member of SAC, Nuclear Science Section, NEA)* *Mr V. Pronyaev (Member of SAC, Nuclear Data Section, NAPC)* *Mr D. Ridikas (IAEA Scientific Secretary & Member of SAC, Physics Section, NAPC)* Self introduction of the participants, Election of Chairperson and *Rapporteur* Discussion and Approval of the Agenda, Administrative Arrangements
10:30-11:00	**Objectives of the Meeting (within the IAEA project Enhancement of Utilization and Applications of Research Reactors)** *Mr D. Ridikas*, IAEA
11:00-11:30	Coffee break
11:30-12:15	**Precision Neutron Cross Section Measurements at Reactor Neutron Filtered Beams** *Ms O. Gritzay, INR, Ukraine*
12:15-13:00	**Neutron capture cross-section measurements by high-resolution γ-ray spectroscopy** *Mr M. Oshima, JAEA, Japan*
13:00-14:00	Lunch break
14:00-14:45	**The Out-of-core Neutron Irradiation Facility of HANARO for Measurement of Neutron Cross-section** *Mr M.S. Kim, KAERI, Korea*
14:45-15:30	**Experimental Determination of Neutron Capture Cross Sections at a Rare Thermal Energy Using the BAEC TRIGA Reactor** *Mr S.M. Hossain*, BAEC, Bangladesh
15:30-16:00	Coffee break
16:00-17:00	**Discussion on "RR based neutron beam capabilities for cross section measurements"** All

Tuesday, 13 October 2009

09:00-09:45	**The Use of Miniature Neutron Source Reactor Facility for the Determination of Neutron-induced Cross section Data** *Mr S.A. Jonah, CERT, Nigeria*
09:45-10:30	**Cross Section Determination of Short-to-Medium Lived Nuclides in a Low Power RR and Am-Be Neutron Source** *Mr B.J.B. Nyarko, GAEC, Ghana*
10:30-11:00	Coffee break
11:00-11:45	**Cross section measurements for thermal neutron-induced reaction on actinides at the ILL reactor** Mr A. Letourneau, CEA Saclay, France
11:45-12:45	**Discussion on "RR activation and other methods for cross section measurements"** All
12:45-14:00	Lunch break
14:00-14:45	**Prompt γ-ray emission in nuclear fission** *Mr S. Oberstedt, IRMM-JRC, Belgium/EU*
14:45-15:30	**Binary and Ternary Fission Yield Measurements at the Institut Laue-Langevin** *Mr O. Serot, CEA Cadarache, France*
15:30-16:00	Coffee break
16:00-17:00	**Discussion on "Fission studies and fission fragment measurements at RRs"** All

18:00-	**Hospitality Event** *All*

Wednesday, 14 October 2009

09:00-09:45	**Fast Reactor Integral Experiments at BARC for Cross-section Evaluation** *Mr K.K. Rasheed, BARC, India*
09:45-10:30	**Measurements of Nuclear Data for MA at VENUS-F and BR-1 reactors** *Mr A. Kochetkov, SCK*Mol, Belgium*
10:30-11:00	Coffee break
11:00-11:45	**Integral Experiments in Minerve Reactor Facility for Nuclear Data Validation** Mr D. Bernard, CEA Cadarache, France
11:45-12:45	**Discussion on "Integral RR experiments for Nuclear Data Validation"** All
12:45-14:00	Lunch break
14:00-14:45	**Benchmark analysis of the 2MW TRIGA MARK II Moroccan research reactor using the MCNP code and the latest nuclear data libraries** *Mr B. Bakkari, NSC, Morocco*
14:45-15:30	**Validation of the ENDF/B-VII library for the WWR-M research reactor in Ukraine** *Mr Y.P. Mahlers, INR, Ukraine*
15:30-16:00	Coffee break
16:00-16:45	**Improvements in the Prediction Capability of Codes Used to Design Innovative Reactors** *Mr O. Cabellos, Univ. Polit. Madrid, Spain*
16:45-17:45	**Discussion on "Validation of Different Evaluated Data Files against experimental data originating from RRs"** All

Thursday, 15 October 2009

09:00-09:45	**The TAPIRO Fast-Neutron Source Reactor as a support to Nuclear Data Assessment** *Mr R. Rosa, ENEA, Italy*
09:45-10:30	**Research Potential of the McMaster Nuclear Reactor** *Mr A. Buijs, McMaster Univ., Canada*
10:30-11:00	Coffee break
11:00-11:45	**Measurement of thermal neutron capture cross-sections of unstable isotopes with the GAMS spectrometer at ILL** *Mr U. Koester, ILL, France*
11:45-12:45	**Discussion on "Potential of RRs for provision of Nuclear Data for various applications"** All
12:45-14:00	Lunch break
14:00-14:45	**The Updated Progress of Chinese Evaluated Nuclear Data Library (CENDL-3.1) and nuclear data evaluation activities in China** *Mr Ge Zhigang, CIAE, China*
14:45-15:30	**Nuclear Data Activities at NEA: Potential Role of RRs** *Ms Y. Rugama, NEA, France*
15:30-16:00	Coffee break
16:00-16:45	**Nuclear Data Activities at IAEA: Potential Role of RRs** *Mr V. Pronyaev, IAEA, Austria*
16:45-17:45	**Discussion on "Potential of RRs for provision of Nuclear Data for various applications"** All

Friday, 16 October 2009

09:00-12:30	**Discussion** • **Identify future needs of Nuclear Data and the role RR could play in this respect** • **Identify common issue areas on nuclear data needs, provision, validation by RRs** • **Suggest collaborative research activities in this area that the IAEA could promote and facilitate** *All*
12:45-14:00	Lunch break
14:00-15:30	**Discussion:** • **Formulation of conclusions and recommendations** • **Drafting of the meeting report** *All*
15:30-16:00	Coffee break
16:00-17:00	**Drafting and Finalizing meeting report** **Closing of the meeting** *All*
17:00	End of the meeting

Nuclear Data Section
International Atomic Energy Agency
Vienna International Centre, P.O. Box 100
A-1400 Vienna
Austria

e-mail: services@iaeand.iaea.org
fax: (43-1) 26007
telephone: (43-1) 2600-21710
Web: http://www-nds.iaea.org